SSC-386

SHIP MAINTENANCE PROJECT

Volume 1

Fatigue Damage Evaluation

SHIP STRUCTURE COMMITTEE

1995

I-C-1

SSC-386   SHIP MAINTENANCE PROJECT Volume 1

Ship Structure Committee   1995

I SPINE

COMMITTEE ON MARINE STRUCTURES

Commission on Engineering and Technical Systems

National Academy of Sciences – National Research Council

The COMMITTEE ON MARINE STRUCTURES has technical cognizance over the interagency Ship Structure Committee's research program.

John Landes, University of Tennessee, Knoxville, TN
Howard M. Bunch, University of Michigan, Ann Arbor, MI
Bruce G. Collipp, Marine Engineering Consultant, Houston, TX
Dale G. Karr, University of Michigan, Ann Arbor, MI
Andrew Kendrick, NKF Services, Montreal, Quebec
John Niedzwecki, Texas A & M University, College Station, TX
Barbara A. Shaw, Chairman, Pennsylvania State University, University Park, PA
Robert Sielski, National Research Council, Washington, DC
Stephen E. Sharpe, Ship Structure Committee, Washington, DC

DESIGN WORK GROUP
John Niedzwecki, Chairman, Texas A&M University, College Station, TX
Bilal Ayyub, University of Maryland, College Park, MD
Ovide J. Davis, Pascagoula, MS
Maria Celia Ximenes, Chevron Shipping Co., San Francisco, CA

MATERIALS WORK GROUP
Barbara A. Shaw, Chairman, Pennsylvania State University, University Park, PA
David P. Edmonds, Edison Welding Institute, Columbus, OH
John F. McIntyre, Advanced Polymer Sciences, Avon, OH
Harold S. Reemsnyder, Bethlehem Steel Corp., Bethlehem, PA
Bruce R. Somers, Lehigh University, Bethlehem, PA

RECENT SHIP STRUCTURE COMMITTEE PUBLICATIONS

Ship Structure Committee Publications – A Special Bibliography

SSC–384 Post–Yield Strength of Icebreaking Ship Structural Members C. DesRochers, J. Crocker, R. Kumar, D. Brennan, B. Dick, S. Lantos 1995

SSC–383 Optimum Weld–Metal Strength for High Strength Steel Structures R. Dexter and M. Ferrell 1995

SSC–382 Reexamination of Design Criteria for Stiffened Plate Panels by D. Ghose and N. Nappi 1995

SSC–381 Residual Strength of Damaged Marine Structures by C. Wiernicki, D. Ghose, N. Nappi 1995

SSC–380 Ship Structural Integrity Information System by R. Schulte–Strathaus, B. Bea 1995

SSC–379 Improved Ship Hull Structural Details Relative to Fatigue by K. Stambaugh, F. Lawrence and S. Dimitriakis 1994

SSC–378 The Role of Human Error in Design, Construction and Reliability of Marine Structures by R. Bea 1994

SSC–377 Hull Structural Concepts For Improved Producibility by J. Daidola, J. Parente, and W. Robinson 1994

SSC–376 Ice Load Impact Study on the NSF R/V Nathanial B. Palmer by J. St. John and P. Minnick 1995

SSC–375 Uncertainty in Strength Models for Marine Structures by O. Hughes, E. Nikolaidis, B. Ayyub, G. White, P. Hess 1994

SSC–374 Effect of High Strength Steels on Strength Consdierations of Design and Construction Details of Ships by R. Heyburn and D. Riker 1994

SSC–373 Loads and Load Combinations by A. Mansour and A. Thayamballi 1994

SSC–372 Maintenance of Marine Structures: A State of the Art Summary by S. Hutchinson and R. Bea 1993

SSC–371 Establishment of a Uniform Format for Data Reporting of Structural Material Properties for Reliability Analysis by N. Pussegoda, L. Malik, and A. Dinovitzer 1993

SSC–370 Underwater Repair Procedures for Ship Hulls (Fatigue and Ductility of Underwater Wet Welds) by K. Grubbs and C. Zanis 1993

SSC–369 Reduction of S–N Curves for Ship Structural Details by K. Stambaugh, D. Lesson, F. Lawrence, C–Y. Hou, and G. Banas 1993

SSC–368 Probability Based Ship Design Procedures: A Demonstration by A. Mansour, M. Lin, L. Hovem, A. Thayamballi 1993

SSC–367 Fatigue Technology Assessment and Strategies for Fatigue Avoidance in Marine Structures by C. C. Capanoglu 1993

I - C -4

SHIP MAINTENANCE PROJECT

This report summarizes the results of a joint industry-government sponsored cooperative research project that focused on the development of engineering technology that could lead to improvements in structural maintenance for new and existing tankers. The project was a milestone in that it was conducted on behalf of 22 sponsoring and participating organizations representing government regulatory bodies, classification societies, new-build and repair yards, and ship owners and operators. In these times of fiscal austerity, future joint industry projects will continue to be essential for leveraging our industry wide research needs.

The report has been divided into four volumes; Fatigue Damage Evaluation, Corrosion Damage Evaluation, Repairs and Maintenance, and Durability Considerations. These studies developed and verified engineering guidelines for the evaluation of fatigue damage and corrosion to critical structural components of exisiting ships. A Repair Management System is developed to aid in the diagnosis of ship structural failures and the evaluation of repair alternatives. Finally, engineering and maintenance measures to improve the durability of critical structural details in tankers are proposed. A glossary of terms used is provided and recommendations are presented for future research.

J. C. CARD
Rear Admiral, U.S. Coast Guard
Chairman, Ship Structure Committee

1. Report No. SSC-386	2. Government Accession No. PB96-113683	3. Recipient's Catalog No.
4. Title and Subtitle Structural Maintenance Project Volume 1 Fatigue Damage Evaluation Software Theory Documentation and Verification		5. Report Date September 1992
		6. Performing Organization Code SMP Vol. 1(1-3,5,8)
7. Author(s) Cramer, E.H., Schulte-Strauthaus, R., Bea, R.G.		8. Performing Organization Report No. SR1340
9. Performing Agency Name and Address University of California at Berkeley Department of Naval Architecture Berkeley, CA 94720		10. Work Unit No. (TRAIS)
		11. Contract or Grant No. 59275-SSC
		13. Type of Report and Period Covered
12. Sponsoring Agency Name and Address Ship Structure Committee U.S. Coast Guard (G-MMS/SSC) 2100 Second St. S.W. Washington D.C. 20593-0001		Final Report
		14. Sponsoring Agency Code G-M

15. Supplementary Notes
Sponsored by the Ship Structure Committee. Jointly funded by other organizations as a joint industry project. See inside the report for further details.

16. Abstract

This report is one in a series of reports conducted as part of a two year Joint Industry Research Project "Structural Maintenance for New and Existing Ships" initiated in June 1990 by the Department of Naval Architecture and Offshore Engineering of the University of California at Berkeley to both develop practical tools and procedures for the analysis of proposed ship structural repairs and to prepare guidelines for the cost effective design and construction of lower-maintenance ship structures. This project was organized into six studies. This report is based on the results of Study 1 -- Fatigue Damage Evaluations whose objective is to develop and verify engineering guidelines for the evaluation of fatigue damage to critical structural components of existing ships. There are three reports. The first report addresses the fatigue reliability of welded details in tanker structures having multiple fatigue crack initiation sites. The second report includes a summary of the general fatigue life evaluation and fracture mechanics procedures, a description of the long-term loading, a description of the uncertainties, and a description of the probabilistic and deterministic calculation procedures. The fatigue reliability model is extended to include the effect of inspection updating where not necessarily the whole structure considered is inspected in each inspection. The third report uses for two ship classes the integrated software package to analyze the fatigue damage for selected details and to compare the results with fatigue failure rate statistics obtained from data analyses of actual failure data.

17. Key Words Fatigue Failure Fracture Mechanics	18. Distribution Statement Distribution unlimited, available from: National Technical Information Service, Springfield, VA 22161 (703) 487-4650		
19. Security Classif. (of this report) Unclassified	20. SECURITY CLASSIF.(of this page) Unclassified	21. No. of Pages 338	22. Price $44.50

Form DOT F 1700.7 (8/72)   Reproduction of form and completed page is authorized.

NIST

United States Department of Commerce
Technology Administration
National Institute of Standards and Technology
Metric Program, Gaithersburg, MD 20899

METRIC CONVERSION CARD

Approximate Conversions to Metric Measures

Symbol	When You Know	Multiply by	To Find	Symbol
LENGTH				
in	inches	2.5	centimeters	cm
ft	feet	30	centimeters	cm
yd	yards	0.9	meters	m
mi	miles	1.6	kilometers	km
AREA				
in^2	square inches	6.5	square centimeters	cm^2
ft^2	square feet	0.09	square meters	m^2
yd^2	square yards	0.8	square meters	m^2
mi^2	square miles	2.6	square kilometers	km^2
	acres	0.4	hectares	ha
MASS (weight)				
oz	ounces	28	grams	g
lb	pounds	0.45	kilograms	kg
	short tons (2000 lb)	0.9	metric ton	t
VOLUME				
tsp	teaspoons	5	milliliters	mL
Tbsp	tablespoons	15	milliliters	mL
in^3	cubic inches	16	milliliters	mL
fl oz	fluid ounces	30	milliliters	mL
c	cups	0.24	liters	L
pt	pints	0.47	liters	L
qt	quarts	0.95	liters	L
gal	gallons	3.8	liters	L
ft^3	cubic feet	0.03	cubic meters	m^3
yd^3	cubic yards	0.76	cubic meters	m^3
TEMPERATURE (exact)				
°F	degrees Fahrenheit	subtract 32, multiply by 5/9	degrees Celsius	°C

Approximate Conversions from Metric Measures

Symbol	When You Know	Multiply by	To Find	Symbol
LENGTH				
mm	millimeters	0.04	inches	in
cm	centimeters	0.4	inches	in
m	meters	3.3	feet	ft
m	meters	1.1	yards	yd
km	kilometers	0.6	miles	mi
AREA				
cm^2	square centimeters	0.16	square inches	in^2
m^2	square meters	1.2	square yards	yd^2
km^2	square kilometers	0.4	square miles	mi^2
ha	hectares (10,000 m^2)	2.5	acres	
MASS (weight)				
g	grams	0.035	ounces	oz
kg	kilograms	2.2	pounds	lb
t	metric ton (1,000 kg)	1.1	short tons	
VOLUME				
mL	milliliters	0.03	fluid ounces	fl oz
mL	milliliters	0.06	cubic inches	in^3
L	liters	2.1	pints	pt
L	liters	1.06	quarts	qt
L	liters	0.26	gallons	gal
m^3	cubic meters	35	cubic feet	ft^3
m^3	cubic meters	1.3	cubic yards	yd^3
TEMPERATURE (exact)				
°C	degrees Celsius	multiply by 9/5, add 32	degrees Fahrenheit	°F

°C	-40	-20	0	20	37	60	80	100
°F	-40		0	32	80 98.6	160		212

water freezes   body temperature   water boils
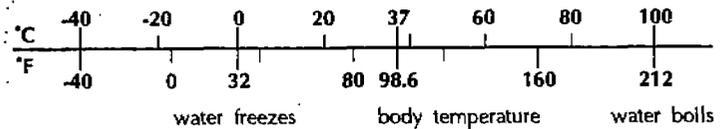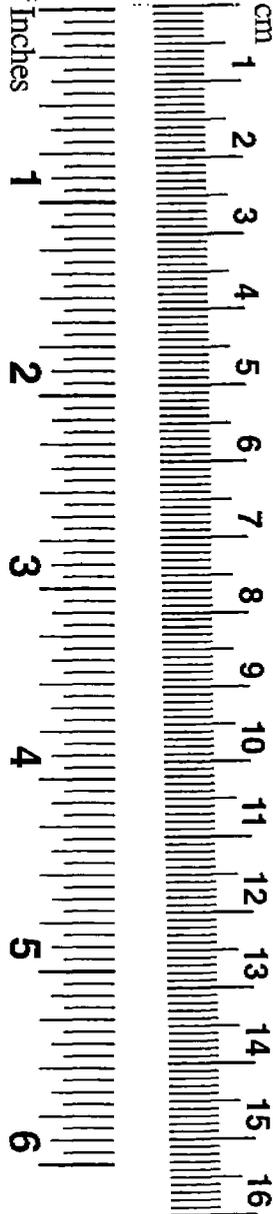
Structural Maintenance Project
Volume 1 : Fatigue Damage Evaluation

CONTENTS

5,6 X   /X

Cross Reference List for Reports under the Ship Maintenance Project

University of California, Berkeley		SSC	NTIS
Number	Title	Report #	Accession #
	−SSC Published Reports		
SMP 1–3	Fatigue Reliability of Welded Joints in Tanker Structures	SSC–386–Vol 1	PB96–113683
SMP 1–5	Fatigue Damage Evaluation Software : Theory Documentation	SSC–386–Vol 1	PB96–113683
SMP 1–8	Fatigue Damage Evaluation Software : Verification Analysis	SSC–386–Vol 1	PB96–113683
SMP II–1	The Development of a Rational Basis for Defining Corrosion Limits in Tankers	SSC–386–Vol 2	PB96–113691
SMP 4–1	RMS – Repair Management System	SSC–386–Vol 3	PB96–113709
SMP 5–1	Durability Considerations for New and Existing Ships	SSC–386–Vol 4	PB96–113717
SMP 5–2	Advancements in Tankship Internal Strucutral Inspection Techniques	SSC–386–Vol 4	PB96–113717
−The below reports are available from NTIS but were not published by the SSC			
SMP 1–6	Fatigue Damage Evaluations: User Manual	SSC–386–1–6	PB95–261608
SMP 1–7	Fatigue Damage Evaluations: Program Documentation	SSC–386–1–7	PB95–261780
SMP 1–9	Fatigue Damage Evaluations: Structural Maintenance Project Tanker Database	SSC–386–1–9	PB95–261772
SMP 1–10	Fatigue Damage Evaluations: PROSHIP– User Manual	SSC–386–1–10	PB95–261590
SMP 1–11	Fatigue Damage Evaluations: PROSHIP– Program Documentation	SSC–386–1–11	PB95–261582
SMP 2–1	Evaluation of Corrosion Damage in Crude and Product Carriers	SSC–386–2–1	PB95–261798
SMP 2–2	Corrosion Margins for Oil Tankers	SSC–386–2–2	PB95–261806
SMP 2–3	Ship Maintenance Information System	SSC–386–2–3	PB95–264016
SMP 2–4	Corrosion Damage Evaluations	SSC–386–2–4	PB95–264024
SMP 3–1	Structural Analysis and Loadings: Modeling & Analysis Strategy Development	SSC–386–3–1	PB95–264057
SMP 3–1A	Structural Analysis and Loadings: Loadings Strategy Development	SSC–386–3–1A	PB95–264065
SMP 3–2	Study of Critical Structural Details	SSC–386–3–2	PB95–264032

The Ship Structural Maintenance Projects 1990 - 1995

By

Professor Robert Bea

Department of Naval Architecture & Offshore Engineering
University of California at Berkeley

ABSTRACT

This paper summarizes the objectives, approach, organization, and results of a series of joint industry - government sponsored cooperative research projects that focused on development of engineering technology that could lead to improvements in structural maintenance for new and existing tankers.

The first phase of the Structural Maintenance for New and Existing Ships Project (SMP I) was conducted by the Department of Naval Architecture and Offshore Engineering at the University of California at Berkeley (UCB) during the 3-year period 1990 through 1992. The project was conducted in behalf of 22 sponsoring and participating organizations representing government regulatory bodies, classification societies, new-build and repair yards, and ship owners and operators.

The second and third phases of the SMP were conducted during the period 1993 through 1995. These phases of the research addressed high priority problems identified during SMP I.

INTRODUCTION

The *Structural Maintenance for New and Existing Ships Project* (SMP I) had two primary technical goals:

To develop practical tools and procedures for analysis of proposed ship structural repairs in order to minimize time and materials within the constraints of regulatory and class requirements and prudent engineering practices, and

To prepare guidelines for the cost-effective design and construction of lower-maintenance ship structures which also facilitate future inspections and repairs.

9

SMP I focused on two primary aspects of structural maintenance:

Fatigue effects on the performance of critical internal structural components of existing and new ship hulls (including high strength steel, reduced scantling designs), and

Corrosion effects on the critical internal structures of existing and new ship hulls.

In addition to its technical objectives, SMP I had important organization objectives. The project was intended to provide a common, neutral ground for the constructive interaction between ship owners and operators, ship classification societies, governmental agencies and ship building and repair yards. The development of informed consensus approaches to the problems associated with structural maintenance of existing ships and design of new ship hull structures provided significant benefits to the ship industry.

SMP I ORGANIZATION

There were four major organizational components in SMP I. The first component was the project sponsors and participants. There were 22 national and international organizations including ship owners and operators, ship construction and repair yards, classification societies and government agencies that comprised the first component (Table 1).

The second organization component was the Project Technical Committee (PTC). Each of the project sponsors and participants were represented on the PTC. The PTC was chaired by Mr. John Conlon of the American Bureau of Shipping (ABS). The purpose of the PTC was to provide the project investigators with directions on technical goals and objectives, with information and data to assist the project, and to monitor the project budget and schedule.

The third organization component was the Office of Research Services and Sponsored Projects Office at the University of California at Berkeley. This component was responsible for the project contracting, invoicing, and accounting.

The fourth organization component was the project researchers and consultants. Table 2 summarizes the names and responsibilities of the project researchers and consultants.

SMP I RESEARCH STUDIES

Six inter-related studies comprised SMP I. The fatigue and corrosion damage evaluations constituted the basic studies in the project (Studies 1 and 2). These evaluations, however, could not be completed without defining the boundary loading and fixity conditions of the local details where damage has occurred. Such boundary loads and conditions were developed in Study 3.

Based on results from Studies 1 - 3, repair strategies and guidelines were developed in Studies 4 and 5. Finally, software packages for personal computers with documentation were developed in Study 6. The following paragraphs describe in more detail the content of each of these studies. The reports developed during each of the studies are cited in the list of references.

Study 1 - Fatigue Damage Evaluations

The objective of this study was to develop and verify engineering approaches to assess fatigue effects on the performance characteristics of Critical Structural Details (CSD) in tanker hulls, including the effects of inspection, maintenance and repair. This study addressed both mild steel and HTS/LS steel hull structural elements and systems.

This study developed a database on fatigue cracking in tankers and developed simplified approaches for evaluating the fatigue durability of CSD, including a long-term hot-spot stress range - number of cycles (S-N) approach and a fracture mechanics based approach [4, 24-29]. Both deterministic and probabilistic fatigue analysis approaches were developed including software to perform the long-term stress range calculations [4,8,9,12,13]. The S-N approach was validated by comparing the computed and database based probabilities of fatigue failure in two types of CSD in a fleet of tankers [3, 28]. A reliability based evaluation was developed to provide insight into fatigue of groups of CSD [7]. A probability based inspection and repair analysis process that recognized realistic occurrences of weld flaws and probabilities of crack detection was developed and illustrated [7].

Study 2 - Corrosion Damage Evaluations

The objective of this study was to develop and verify engineering approaches to evaluate internal corrosion effects (general and pitting) on the structural strength and leak integrity characteristics of critical (to strength and leak integrity) components comprising existing ship hulls and new builds.

The principal developments from this study were a database on general corrosion in tankers that could be interfaced with the fatigue cracking database [22], an evaluation of the statistical characteristics of the corrosion rates for various elements and locations in tankers [5], and the development of an approach to evaluate conditions in which plate renewals were implicated [22, 6].

Study 3 - Interaction of Details with Adjacent Structure

This study played a key role in that it provided input and support to the fatigue and corrosion damage effects parts of the project . The over all objective was to develop a reliable but simplified and practical analytical tool that could enable engineers to make the necessary structural system performance evaluations rapidly and with accuracy sufficient to make good decisions on repairs and maintenance strategies.

The analysis of the interaction between critical internal structural details, e.g., brackets, and adjacent structural components, e.g., webs and stiffened plate panels, provided: (a) an accurate and efficient model of the load-displacement behavior of the detail in conjunction with the adjacent structural components, and (b) the stress distributions at the element level for the fatigue, corrosion and repair evaluations. The study was organized into two principal tasks (Table 3). The first task was focused on structural analysis and the second task was focused on evaluation of loading characteristics.

The successful completion of Task 1 and Task 2 provided the foundation for the development of: (a) a library of typical generic structural detail modules consisting of the detail and the adjacent structure of sufficient extent to model the detail's boundary conditions, (b) a corresponding library of module loadings, and (c) the Personal Computer (PC) software necessary to implement the analysis [32,33, 34].

This study was focused on two general classes of tankers: a fleet of 165,000 dwt single-hull tankers and a fleet of 190,000 dwt double-bottom tankers [3,28]. The study resulted in development of global and local loading transfer functions that could be utilized in the long-term sea-state, heading, speed, and cargo or ballast condition dependent characterization of mid-ship hull loadings [32,9]. A global to local procedure based on linear beam theory was developed and studied using detailed finite element models [32]. Given the local primary loadings acting on the boundaries of a given CSD, detailed Finite Element Models (FEM) were developed to define the crack-opening hot-spot stresses at pre-defined locations on the CSD [33,34].

Study 4 - Fatigue and Corrosion Repair Assessments

The objective of this study was to develop and verify with ship service data engineering guidelines for the evaluation of fatigue and corrosion repairs to critical structural components of existing ships, and to develop general guidelines for new builds to help maximize inspectability and minimize repairs.

The work of the Tanker Structural Co-operative Forum (TSCF) provided a valuable starting point for this effort. As well, the special reports developed by Committee V.3 (Service Experience - Ships), of the International Ship & Offshore Structures Congress (ISSC) provided important direction for this effort. In particular, the TSCF and ISSC have documented frequently occurring fatigue damage, and strategies to repair that damage. An objective of this study was to continue and extend the TSCF and ISSC developments. The study resulted in development of a simplified procedure and computer program that could be used to rapidly determine the comparative fatigue performance characteristics of alternative repairs to CSD [14].

Study 5 - Durability Guidelines for New Ships

The Ship Structures Committee (SSC) initiated a research project that was conducted in parallel with SMP I on the topic of development of Marine Structural Integrity Programs (*MSIP*) for ships [2]. The project addressed new build ship life-cycle phases, structural and non-structural (operational) aspects, inspections and

quality control, and inter-relationships of design of new VLCCs and ULCCs and MSIP.

In addition to a practical approach that could used to develop life-cycle MSIP for new builds, the project was intended to define a general purpose computer based information and evaluation system to assist in the life-cycle management of the structural integrity of ships. As a basis for the development of MSIP, the study reviewed the U.S. Air Force's Airframe Structural Integrity Program and the comparable program of the Federal Aviation Administration. Results from the Ship Structures Committee sponsored research project were incorporated into Study 5.

This study resulted in development of a handbook for naval architects and repair engineers that provides practical information on development of durable CSD in ships, repairs of these CSD, and software to guide repair engineers in the evaluation of alternative repairs [17].

Another parallel study was sponsored by the U. S. Coast Guard on the topic of inspections of CSD in tankers. Existing techniques and procedures were reviewed and recommendations developed to facilitate data gathering and analyses [15].

Study 6 - Development of Software and Applications Examples

This study, unlike the other technical studies, was focused at providing the background, standards and support so that the computer codes developed by the various researchers could be of uniform quality, would facilitate modification and be user friendly. As such, this study provided a uniform foundation and standard interfaces which served as a reference for all of the studies.

The software was intended to be of "Beta" grade, sufficiently "debugged" to allow initial applications. It was left to future industry efforts to develop the software to be of industrial grade and quality. The programs were written in the FORTRAN language for IBM PC and PC compatible equipment.

A major contribution of this study was the development of a front-end windows based input system that would provide information and data files for the integration of the other software components developed during the study [23]. This input system allows a user to define a wide variety of CSD in the classes of ships included in the loadings and structural analysis data files. Extensive 'help' screens were provided to assist the user in developing and validating the input.

SMP II RESEARCH STUDIES

The SMP II studies were conducted during the period 1992 - 1994. During SMP II, four additional research studies were conducted. These studies addressed high priority problems identified during SMP I. The studies were sponsored individually by various members of the SMP I project.

13

The SMP II studies were: 1) Fatigue Classifications of CSD in Tankers, 2) Study of the Fatigue of Proposed CSD in Double-Hull Tankers, 3) Development of a Rational Basis to Define Corrosion Limits in Tankers, and 4) Repair Management System (RMS) for CSD in Tankers.

Study 1 - Fatigue Classifications

The objective of this study was to develop methods that could assist naval architects in the performance of fatigue life evaluations for CSD in large oil tankers. This study focused on two topics: 1) fatigue classifications, and 2) development of a management system for selection of S-N curves.

This study resulted in development of a procedure to use the stresses at the hot spots (areas of high stress concentrations) of proposed CSD [30]. These hot spots are identified based on the results from detailed finite element analyses of a CSD and observations of fatigue cracking in ship CSD. This approach makes it necessary to define the way the hot spot stresses are obtained from the finite element analyses and to use S-N curves which are calibrated for this procedure.

The specific geometry and testing conditions associated with the details used to define S-N curves was obtained for 6 generic CSD. Different finite element analysis methods (e.g. plate and shell elements), mesh sizing procedures (e.g. equal to half the plate thickness), and hot spot "extrapolation" techniques were explored to define a method that would give consistent results for the variety of details. Simple details for which there are well defined stress concentration factors also were studied (e.g. plates with holes, formed boundaries) to define a consistent procedure to define the hot spot stresses.

The results from this study indicated that one could 'collapse' the wide variety of S-N curves based on nominal stresses to two 'fundamental' S-N curves: one for welds, and one for plate edges [30]. The crack opening stress (normal to the direction of cracking) was identified as the fundamental stress for use with these 'fundamental' S-N curves.

The second part of this study resulted in the development of a computer based management system to assist naval architects in choosing appropriate S-N curves for given CSD. This management system and the hot spot extrapolation procedure developed in the first part of the study was used in a repetition of the fatigue calibration / verification study performed during SMP I. Unlike the experience in SMP I based on a traditional nominal stress S-N approach, it was found in SMP II that the revised procedure developed results that were not in good agreement with the observed fatigue behavior in the class of ships studied. The revised procedure under estimated the probabilities and frequencies of fatigue cracking in the CSD [30].

This study theorized that the observed under estimate of the fatigue cracking frequency was due to an under estimating of the cyclic stress ranges and due to unconservative damage accumulation developed by the linear damage accumulation model, S-N curves based on in-air testing, and ignoring mean stress effects. The under estimate of the cyclic stress ranges was attributed to the lack of recognition of

'second order' effects such as those due to green water on the decks, slamming and whipping.

Study 2 - Fatigue of Proposed CSD

The objective of this study was to conduct analytical studies of proposed CSD for new double hull tankers to assure that they have desirable durability and robustness (defect / damage tolerance) characteristics.

Fatigue analyses were performed on important CSD from two structural systems that were proposed for the next-generation of double-hull tankers [35,36, 37]. The objective of the analyses was to determine if the proposed CSD possess desirable degrees of durability. Alternative configurations of the CSD were studied to define effective means of increasing the durability characteristics.

The CSD that were studied were defined and provided by the study participants. Several innovative CSD that were proposed for the next-generation of tankers were analyzed [36]. One of these did not utilize cutouts in the side shell longitudinal - transverse webframe or bulkhead intersections.

Results from this study indicated that there is an extremely wide range in the expected durability characteristics of the proposed CSD. Modifications to the CSD designs were explored to determine how best to increase the fatigue lives. Comparisons of the results from this study with those performed by the ship designer have highlighted the importance of several parts of the analysis procedure and the needs for a consistent procedure to perform such analyses [3, 35]. In more than one case, the initial comparisons of predicted fatigue lives have differed by factors of 10 to over 50. Once the sources of the differences in the procedures were located and modifications introduced to make the procedures directly comparable, then the differences are much smaller.

Study 3 - Rational Corrosion Limits

The objective of this study was to evaluate the effects of internal corrosion on the strength of tanker structures and to provide a rational basis for determination of wastage limits. During SMP I, corrosion margins and allowable wastage as presently defined by the different classification societies were studied [6, 22]. This study documented the extremely large differences in design corrosion allowances and permissible wastage allowances for CSD in tankers. This study highlighted the need for a rational process to define corrosion margins and permissible wastage.

The structural capacity of a tanker is related to plating thickness which, in turn, is related to time through projected corrosion rates. An extensive corrosion rates database was developed during SMP I [5, 22]. Routines were written to statistically analyze the variability in the corrosion rates for various structural details, tank types, and locations [5]. This database was utilized to determine how corrosion might be distributed through the ship primary structure as a function of time, service, and protective measures [21]. The two classes of tankers studied

15

during SMP I (165,000 dwt single hull and 190,000 dwt double bottom) were used as the study examples.

As corrosion progresses through the ship structure as a function of time, the time varying capacity (local and global) due to corrosion was determined. A series of parametric studies were performed to define how different rates and locations of corrosion affect the local leak integrity and global capacity of the ship hull structure. It is this inclusion of the time dimension that makes it possible to predict life cycle costs of steel maintenance and renewal and that can ultimately provide a rational basis for optimizing initial design and maintenance strategies [3,21].

Due to the multitude of uncertainties involved in this type of evaluation, reliability analysis methods were used evaluate the implications of the uncertainties. Reliability analysis also provided a convenient framework for the consideration of both ultimate and serviceability (e.g. leak integrity) limit states. Procedures were developed to evaluate the effects of general corrosion on the strength characteristics (flexure, buckling, etc.) of components and these procedures linked with the corrosion database. Simplified procedures were developed to evaluate the limit state characteristics of the ship hull structure [21]. Verification of the process was demonstrated by application to a tanker that had experienced hull girder failure during an unloading process. Good agreement between the simplified method and the observed failure were achieved.

Study 4 - Repair Management System

The objective of this study was to further develop the computer based Repair Management System (RMS) developed during SMP I to assist tanker maintenance engineers in defining more efficient and effective steel repairs []. The RMS incorporated the guidelines on fracture and corrosion repairs and inspections developed during SMP I.

The approach taken in development of RMS was to provide intelligent front-end access to the information required to make repair decisions. The RMS approach combined the use of experience-based knowledge of fatigue of and repairs to CSD and simplified analytical procedures in order to rank repair alternatives according to the expected life and cost of the repair. The user must select the most appropriate alternative from knowledge of the economics of the ship. Depending on the economic goals of the owner, a different repair alternative can be selected [18].

The RMS study developed two primary contributions during SMP II. The first was a procedure to estimate the long-term cyclic stress range characteristics for a particular ship [19]. This procedure was based on the observed time to cracking of a particular CSD and a Weibull long-term stress range distribution. The two free parameters in the long-term stress range distribution were demonstrated to be relatively stable for the purposes of the simplified fatigue analysis [19].

The second contribution was development of stress reduction (or modification) factors that could be used to define how proposed modifications to CSD would change

8

the stress concentration factors. These stress reduction factors were developed from an extensive finite element study of alternative CSD [18, 19, 20].

The RMS was incorporated into a highly interactive PC windows based program that made extensive use of graphical inputs and outputs. Extensive help windows were provided to guide repair engineers through the analyses and evaluations. Example applications were provided to illustrate how this system might be applied in repair yards [18].

SMP III RESEARCH STUDIES

SMP III was conducted during the period 1993 - 1995. During SMP III, four additional research studies were initiated. These studies addressed high priority problems identified during SMP II. The studies were sponsored individually by various members of the SMP I and II projects.

The SMP III studies were: 1) Fitness for Purpose of Cracked CSD in Tankers, 2) Development of a Ship Structural Integrity Information System - SSIIS, 3) Maintenance of Marine Structures: A State-of-the-Art Summary, and 4) Inspection of Marine Structures.

Study 1 - Fitness for Purpose of Cracked CSD

One of the most hotly debated topics that surfaced during SMP I was that of cracked CSD [3]. One community insisted that ships should not sail with cracks in their primary structure. Another community insisted that their ships did not sail with cracks in their primary structure. The MSIP study had clearly indicated that all structures could be expected to have cracks in their primary structure; it was a case of where, how big they were, and how they might affect the capacity and serviceability of the ship [2].

During SMP I, the possibility of developing S-N curves that reflected or incorporated different sizes of flaws was investigated [26]. Linear fracture mechanics formed the basis for such a development. Given the discovery of a crack in a CSD, these 'equivalent S-N' curves could be used with traditional fatigue methods to determine what the remaining life (time to reach critical crack size) might be. During SMP II, this concept was further explored and developed [39-46].

The first portion of the study resulted in development of S-N curves for welds that reflected the presence of different lengths of through-thickness cracks based on the results from linear fracture mechanics [39]. A computer program was written to facilitate performing the necessary fracture mechanics computations [40].

The second portion of the study explored the problems associated with 'load shedding' or load redistribution due to boundaries of the CSD or intersections of the propagating cracks with other structural elements. A first-generation analytical approach was developed to address load shedding effects [42, 43].

In the third portion of the study, the applications of the results from the previous two portions of the study were integrated into an example application that involved one of the classes of ships studied during SMP I. A probability based inspection and repair methodology was developed and programmed based on the earlier developments in SMP I [7] and the developments in SMP III [41].

Study 2 - Ship Structural Integrity Information System

The SSIIS project had two main objectives. The first objective was development and documentation of standards for development of a computerized ship structural integrity information system for tank ships with a focus on the inspection and fatigue durability characteristics of CSD. The second objective was demonstration of the application of these standards with a prototype PC based database and reporting system. This prototype database and reporting system was focused on the U. S. Coast Guard requirement for a Critical Area Inspection Plan (CAIP).

The background for the SSIIS was developed in the previous MSIP study [2]. The SSIIS was identified as one of several primary components in a comprehensive ship quality information system [31]. Other components addressed ship equipment and facilities, ship operations, and human and organization factors involved in ship operations and maintenance. SSIIS was one part of a comprehensive life-cycle, full-scope information and communications system intended to help improve the management and quality of commercial ships.

The project reviewed a variety of commercial, classification society, government agency, and owner / operator databases with the objective of identifying the advantages and disadvantages of these databases as they might be adopted into the framework of a comprehensive SSIIS. The study also reviewed a variety of CAIP reports that had been submitted to the U. S. Coast Guard with the objective of identifying the strong and weak points of these reports and defining how the generation of and formats for the reports might be improved in the SSIIS.

The study identified how advanced database technology and the availability of powerful and economic computer systems and storage capacity might be utilized to develop an integrated database system for ships [31]. A modular based system was defined that would allow components of SSIIS to be developed in an incremental fashion. An 'alpha' version of a SSIIS CAIP was developed.

In the second stage of this study, particular attention was given to how the process of ship surveys and inspections might be 're-engineered' so that the overall efficiency of the process of gathering , analyzing, reporting, and communicating information might be improved and made more efficient [11]. Such a process could provide positive incentives to develop and implement the SSIIS. Without this process, SSIIS was seen by most ship owners and operators as representing a 'cost' that could be avoided. Also, the advantages of interfacing the development of the SSIIS with the operations related components were explored for the same reasons: to provide positive incentives and to free available resources to develop and implement a comprehensive ship quality information system that could lead to safer and more

10

efficient ship operations. A 'beta' version of a SSIIS CAIP was developed and its application illustrated [11].

Study 3 - Maintenance of Marine Structures

The objective of this study was to provide an overview of the current state of the art of maintaining marine structures as documented by Ship Structure Committee reports over the past four decades. The study documentation was intended to help provide a readily accessible and updatable database for development of future research planning [16]. Each part of the database and the associated report related to the strategic plan for SSC research developed by the Committee on Marine Structures of the National Academy of Engineering. The database was developed in Microsoft FoxPro for Windows.

The topics in the project report addressed included design for durability, maintenance, and repair; probability based design; steel structure assembly and welding; structural fastenings; vibration control; fatigue; structure fractures; corrosion protection and rates; corrosion surveys; inspections; non-destructive testing; in-service monitoring and instrumentation systems; database systems; and the SSC report database [16].

Study 4 - Inspection of Marine Structures

The objective of this study was to develop a better understanding of the probability of detection of fatigue cracks in tanker CSD [8, 15]. This factor exerts a major influence on the timing, effectiveness, and utility of probability based inspection and repair results [8, 41].

Based on a review of the literature and interviews with inspectors and ship surveyors, a model of the factors that influence the probability of detection of fatigue cracks was developed [10]. This study included a review of the treatment of the probability of detection of fatigue cracks in aviation, nuclear power, manufacturing equipment, and other marine structures (e.g. offshore platforms).

Four approaches to analyzing inspection performance were identified and evaluated for application to tanker inspections and surveys [10]. These included expert judgment, laboratory experiments, in situ experiments, and benchmarked inspection data. The results of the study suggested that in situ experiments, benchmarked inspection data, and a hybrid (in situ test on an out-of-service vessel) are potentially useful approaches to further develop inspection probability of detection characterizations [10].

An example of the use of benchmarked inspection data was developed during this study, demonstrating the feasibility of the approach. This exploratory study showed that inspection performance can vary greatly in different regions in the same vessel. Most importantly, this study revealed that the 'readily detected' crack is significantly larger than that estimated by most inspectors and analysts (e.g. a 90 % probability of detecting cracks with through thickness lengths in the range of 300 to 400 mm using traditional visual techniques [10].

/9

CONCLUSIONS AND OBSERVATIONS

After six years of research, what was accomplished? The answer to this question depends on who is answering it. The following answers and observations are those of the author.

The original vision of developing practical tools and procedures for analyses of proposed ship structural repairs clearly were reached. In addition, the original vision of preparing guidelines for the cost-effective design and construction of lower maintenance ship structures which could also facilitate inspections and repairs clearly was realized. The products from this effort summarized in the list of references are an example of the results that can be developed from an intensive, coordinated and applied research program performed by a university for industry.

As a result of these efforts, it is contended that ship maintenance technology has been significantly advanced and made more practical for engineering use. The research studies have significantly advanced the technology of durability analysis, design, and repair (corrosion, fatigue cracking); inspections; and ship maintenance information and communication systems. In the author's opinion, one of the most important products of this research have been the students that have been educated and graduated to government and industry positions. These students represent the long-term potential of industrialization and application of the technology and understanding developed during the SMP.

Perhaps as important as any of the technology developments was the industry - classification society - owner / operator - builder / repairer - government technical forum that was developed and exercised. This forum repeatedly provided an open and neutral ground upon which debates of old and new ideas could be conducted. The organization acted to help disseminate the collective and impressive experience and wisdom of the participants. This forum acted to help develop important insights into what might be done in the future to improve the quality and efficiency of the durability and maintenance of commercial ships.

Were the tools and technology developed by the SMP perfect or complete? Were they without limitations? Did all of the studies reach all of their original objectives? The answer to these questions must be no. The products of this series of efforts represents the best that could be developed by a university, with the resources and objectives of a university, by dedicated students and faculty, within the available time, money, experience, and information provided to perform the studies. Perhaps, all those involved in this series of projects should appreciate what they were able to accomplish, not what they were not able to accomplish.

What was not accomplished? In the author's opinion, the primary shortfall was in the industrialization and application of the technology developed during the SMP. The potential for this shortfall was clearly recognized by the researchers and sponsors / participants during the SMP. However, the means for addressing this shortfall were not developed, and in most cases, have not been developed.

Many of the sponsors and participants and their engineering service contractors and consultants face very significant 'barriers' to being able to industrialize and apply this technology. Down-sizing, out-sourcing, cost-cutting, and 'early retirements' that have invaded all segments of this industry have exacerbated the situation. Unless and until these barriers are surmounted, the technology will not be applied and further developed. There must be equitable and long-term positive incentives and resources to further develop, industrialize, and utilize the technology. Wise industrialization and application of the SMP technology represents the next important challenge to enable the true long-term goals of this research to be reached.

ACKNOWLEDGMENTS

REFERENCES

1. Bea, R. G., Pollard, R.,, Schulte-Strathaus, R., and Baker, R. (1991). *"Maintenance for New and Existing Ships,"* Proceedings of the Marine Structural Inspection, Maintenance and Monitoring Symposium, Ship Structure Committee and Society of Naval Architects and Marine Engineers, Arlington, VA.

2. Bea, R. G. (1992). *Marine Structural Integrity Programs - MSIP*, Ship Structure Committee, Report SSC-365, 1992, Washington, D. C.

3. Bea, R. G. (1993). *Ship Structural Maintenance: Recent Research Results and Experience*, Proceedings, The Institute of Marine Engineers.

4. Chen, Y-k. (1992a). *Fatigue Classification of Ship Structural Details,* Structural Maintenance for New and Existing Ships, Report SMP 1-4.

5. Chen, Y-k (1992b). *Analysis of Oil Tanker Corrosion Data,* Structural Maintenance for New and Existing Ships, Report SMP 2-3.

6. Chen, Y-k (1992c). *Corrosion Margins for Oil Tankers.* Structural Maintenance for New and Existing Ships, Report SMP 2-2.

7. Cramer, E. H. and Bea, R. G. (1992). Fatigue Reliability of Welded Joints in Tanker Structures, Structural Maintenance for New and Existing Ships, Report SMP 1-3.

8. Cramer, E. H., Schulte-Strathaus, R., and Bea, R. G. (1992). *Fatigue Life Evaluation Software: Theory Documentation,* Structural Maintenance for New and Existing Ships, Report SMP 1-5.

9. Cramer, E. H., Friis-Hansen, P., and Schulte-Strathaus, R. (1992). *PROSHIP: User Manual,* Structural Maintenance for New and Existing Ships, Report SMP 1-10.

10. Demsetz, L. A., Cario, R., and Schulte-Strathaus, R. (1995). Inspection of Marine Structures, Report to Maritime Administration, Project No. DTMA91-93-G-00040, SSC Project SR-1365.

11. Dry, M. and Bea, R. G. (1995). Ship Structural Integrity Information System - Phase II: SSIIS II, Report to Department of Transportation, Maritime Administration, Maritime Enhancement Institute, University of California at Berkeley.

12. Friis-Hansen, P., and Schulte-Strathaus, R. (1992). *PROSHIP: Program Documentation,* Structural Maintenance for New and Existing Ships, Report SMP 1-11.

13. Friis-Hansen, P. (1993). "On Combination of Slamming and Wave Induced Responses," Journal of Ship Research, April.

14. Gallion, K. A., and Bea, R. G. (1992). *RMS - Repair Management System: A System to Aid in the Diagnosis of Ship Structural Failures and the Evaluation of Repair Alternatives,* Structural Maintenance of New and Existing Ships, Report SMP 4-1.

15. Holtzman, R. S., and Demsetz, L. (1992). *Advancements in Tankship Internal Structural Inspection,* structural Maintenance for New and Existing Ships, Report SMP 5-2.

16. Hutchison, S. C., and Bea, R. G. (1993). *Maintenance of Marine Structures: A State of the Art Summary,* Report to Department of Transportation, Maritime Administration, Maritime Enhancement Institute, University of California at Berkeley, and Report to Ship Structure Committee, SSC 372, NTIS # PB94-121951, Washington, D. C.

17. Ma, Kai-tung, and Bea, R. G. (1992). *Engineering Guidelines for the Inspections and Repairs of Tankers,* Structural Maintenance for New and Existing Ships, Report SMP 5-1.

24

18. Ma, Kai-tung, and Bea, R. G. (1993).*RMS - Repair Management System - Further Development,* Structural Maintenance for New and Existing Ships, Report SMP 4-2.

19. Ma, Kai-tung, and Bea, R. G. (1995a). *Fatigue Life Estimation for Repaired Ship Critical Structural Details,* Proceedings of the Offshore Mechanics and Arctic Engineering Conference, OMAE Paper No. 95-731M, Copenhagen, Denmark.

20. Ma, Kai-tung, and Bea, R. G. (1995b). *"Repair Management System for Fatigue Cracks in Ships,"* Proceedings of the Annual Meeting of the Society of Naval Architects and Marine Engineers, Washington, DC.

21. Mayoss, R., and Bea, R. G. (1992). *Corrosion Damage Evaluation,* Structural Maintenance for New and Existing Ships, Report SMP 2-4.

22. Pollard, R. R., and Bea, R. G. (1991). *Evaluation of Corrosion Damage in Crude & Product Carriers,* Structural Maintenance for New and Existing Ships, Report SMP 2-1.

23. Reed, J., and Webster, W. C. (1992). *Front End for Ship Maintenance Project Analysis,* Structural Maintenance for New and Existing Ships, Report SMP 6-2.

24. Schulte-Strathaus, R. (1993). "Effective Fatigue Damage Control for Critical Structural Details in Oil Tankers," Paper Presented to the Northern California Section, Society of Naval Architects and Marine Engineers, May 6.

25. Schulte-Strathaus R., and Bea, R. G. (1991). *Fatigue Database Development and Analysis,* Structural Maintenance for New and Existing Ships, Report SMP 1-1.

26. Schulte-Strathaus, R., and R. G. Bea (1992a). *Fatigue Life Evaluation Software: User Manual,* Structural Maintenance for New and Existing Ships, Report SMP 1-6.

27. Schulte-Strathaus, R. and Bea, R. G. (1992b) *Fatigue Life Evaluation Software: Program Documentation,* Structural Maintenance for New and Existing Ships, Report SMP 1-7.

28. Schulte-Strathaus, R., and Bea, R. G. (1992c) *Verification Study for Tanker CSD Evaluation Software,* Structural Maintenance for New and Existing Ships, Report SMP 1-8.

29. Schulte-Strathaus R., and Bea, R. G. (1992d). *SMP Tanker Database: Documentation,* Structural Maintenance for New and Existing Ships, Report SMP 1-9.

30. Schulte-Strathaus, R., and Bea, R. G. (1994a). *Development of Calibrated S-N Curves and System for the selection of S-N Curves,* Report to Joint Industry Project Fatigue Classification of critical Structural Details in Tankers, Report No.

23

FACTS-1-1, Dept. of Naval Architecture & Offshore Engineering, University of California Berkeley.

31. Schulte-Strathaus R., and Bea, R. G. (1994b). *Ship Structural Integrity Information System - SSIIS,* Report to Department of Transportation, Maritime Administration, MAR-382, Maritime Enhancement Institute, University of California at Berkeley, and SSC Report 380 Washington, D. C.

32. Stear, J. and Paulling, R. (1992). *Structural Analysis and Loading,* Structural Maintenance for New and Existing Ships, Report SMP 3-1.

33. Xu, T., Paulling, R., and Bea, R. G. (1992). *Study of Critical Structural Details,* Structural Maintenance for New and Existing Ships, Report SMP 3-2.

34. Xu, T., and Bea, R. G. (1992). *Study of Critical Structural Details,* Structural Maintenance for New and Existing Ships, Report SMP 3-2.

35. Xu, T., and Bea R. G. (1993a). *Fatigue Analysis of Critical Structural Details in a 150,000 DWT Double-Hull Tanker,* Research Report SMP II-1 Dept. of Naval Architecture & Offshore Engineering, University of California at Berkeley.

36. Xu, T., and Bea R. G. (1993b). *Fatigue Analysis of Critical Structural Details in a 190,000 DWT Double-Bottom Tanker,* Research Report SMP II-2 Dept. of Naval Architecture & Offshore Engineering, University of California at Berkeley.

37. Xu, T., and Bea R. G. (1993c). *CSD Library and Finite Element Analysis,* Research Report SMP II-3, Dept. of Naval Architecture & Offshore Engineering, University of California at Berkeley.

38. Xu, T. (1995). *"Fatigue and Fracture of Critical Structural Details in Tankers, Part I - Technical Developments, Part II - Numerical Illustrations",* Papers Presented to the Northern California SNAME Section, Submitted for Publication in the Journal of Marine Technology, Society of Naval Architects and Marine Engineers, New York, NY.

39. Xu, T., and Bea R. G. (1995a). *Fitness for Purpose Analysis of Cracked Critical Structural Details (CSD) in Tankers,* Research Report SMP III-1 Dept. of Naval Architecture & Offshore Engineering, University of California at Berkeley.

40. Xu, T., and Bea R. G. (1995b). *Fracture- A Computer Code for Crack Growth Analysis of Cracked Critical Structural Details (CSD) in Tankers,* Research Report SMP III-3 Dept. of Naval Architecture & Offshore Engineering, University of California at Berkeley.

41. Xu, T., and Bea R. G. (1995c). *Pro-IMR A Computer Code for Probability-Based Inspection Planning,* Research Report SMP III-5 Dept. of Naval Architecture & Offshore Engineering, University of California at Berkeley.

24

42. Xu, T., and Bea R. G. (1995d). *Load Shedding Analysis for Cracked Critical Structural Details (CSD) in Tankers*, Research Report SMP III-2 Dept. of Naval Architecture & Offshore Engineering, University of California at Berkeley.

43. Xu, T., and Bea R. G. (1995e). *"Load Shedding of Fatigue Fractures in Ship Structures,"* Submitted for Publication in the Journal of Marine Structures.

44. Xu, T., and Bea R. G. (1995f). *"Fitness for Purpose Analysis of Cracked Critical Structural Details (CSD) in Oil Tankers,"* Submitted for Publication in the Journal of Marine Structures.

45. Xu, T., and Bea, R. G. (1995g). *"Fatigue of Cracked Ship Critical Structural Details - Fracture Mechanics Model and Fracture Mechanics Based Fatigue Model,"* Submitted for Publication in the Journal of Engineering Fracture Mechanics.

46. Xu, T., and Bea, R. G. (1995f) *"Fatigue of Ship Critical Structural Details - Some Experience in S-N Analysis,"* Submitted for Publication in the Journal of Offshore Mechanics and Arctic Engineering, Society of Mechanical Engineers.

Table 1- SMP I sponsoring and participating (*) organizations

Sector	Organization
Government	U.S. Coast Guard Military Sealift Command Maritime Administration Naval Sea Systems Command National Defense Headquarters (Canada)
Classification	American Bureau of Shipping Bureau Veritas Lloyd's Registry of Shipping* Germanischer Lloyd*
Shipyard	Lisnave Estaeiros Navais De Lisboa S.A. Jurong Shipyard Ltd. Ishikawajima-Harima Heavy Industries Co. Ltd. Mitsubishi Heavy Industries Ltd. Newport News Shipbuilding & Dry Dock Daewoo Shipbuilding & Heavy Machinery Ltd West States Inc.*
Owners	Amoco Transport Co. Arco Marine Inc. B.P. Marine Inc. Exxon Company International Chevron Shipping Co. Mobil Shipping and Transport Co.

Table 2 - SMP I Studies and Researchers

Project Responsibility	Name, Organization
Study 1 - Fatigue	Prof. Robert Bea, UCB Prof. Stig Berge, U. of Trondheim, Norway Y-k Chen, ABS Rolf Schulte-Strathaus, Research Assistant Espen Cramer, Research Assistant Peter Friis-Hansen, Research Assistant
Study 2 - Corrosion	Prof. Robert Bea, UCB Y-k Chen, ABS Rob Pollard, Research Assistant Roger Mayoss, Research Assistant
Study 3 - Interaction of Details with Adjacent Structure	Prof. Randolph Paulling, UCB Jim Stear, Research Assistant Tao Xu, Research Assistant
Study 4 - Repairs	Prof. Robert Bea, UCB Robert Baker, Research Assistant Martin Cepauskas, Research Assistant Keith Gallion, Research Assistant
Study 5 - New Build Guidelines & Inspections	Prof. Robert Bea, UCB Prof. Laura Demzetz, UCB Kai-tung Ma, Research Assistant Lt. Rob Holtzman, Research Assistant
Study 6 - Software Development	Prof. William Webster, UCB Scott Morris, Programming Assistant John Reed, Programming Assistant
Consulting to All Studies	Prof. Alaa Mansour, UCB Y. K. Chen, ABS J. Conlon, PTC Chairman, ABS

STRUCTURAL MAINTENANCE
FOR
NEW AND EXISTING SHIPS

Study 1 - Fatigue Damage Evaluations
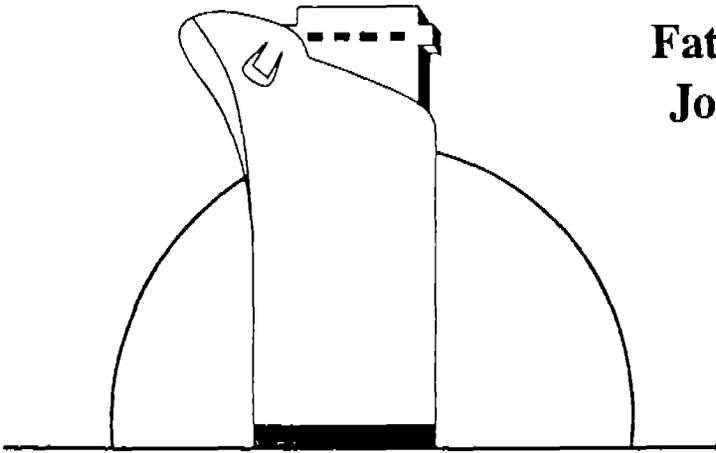
Fatigue Reliability of Welded Joints in Tanker Structures

by

Espen H. Cramer

and

Robert G. Bea

Report No. SMP-1-3
July 1992

Department of Naval Architecture & Offshore Engineering
University of California, Berkeley

PREFACE

The two year Joint Industry Research Project "**Structural Maintenance for New and Existing Ships**" was initiated in June 1990 by the Department of Naval Architecture and Offshore Engineering, University of California at Berkeley. The objective of this project was to develop practical tools and procedures for the analysis of proposed ship structural repairs and to prepare guidelines for the cost-effective design and construction of lower-maintenance ship structures.

This project was made possible by the following sponsoring organizations:

-American Bureau of Shipping   *-Lisnave - Estaleiros Navais De Lisboa S.A.*
-Amoco Transport Company   *-Maritime Administration*
-Arco Marine Incorporated   *-Military Sealift Command*
-BP Marine   *-Mitsubishi Heavy Industries Inc.*
-Bureau Veritas   *-Mobil Ship and Transport Company*
-Chevron Shipping Company   *-National Defense Headquarters (Canada)*
-Daewoo Shipbuilding & Heavy Machinery Ltd.   *-Naval Sea Systems Command*
-Exxon Company International   *-Newport News Shipbuilding & Dry Dock*
-Ishikawajima-Harima Heavy Industries Ltd.   *-United States Coast Guard*
-Jurong Shipyard Ltd.

In addition, the following organizations contributed to the project as observers:

-Germanischer Lloyd
-Lloyd's Register of Shipping
-West State Inc.

The project was organized into six studies:

Study 1 - Fatigue Damage Evaluations
Study 2 - Corrosion Damage Evaluations
Study 3 - Interaction of Details with Adjacent Structure
Study 4 - Fatigue and Corrosion Repair Assessments
Study 5 - Durability Guidelines for New Ships
Study 6 - Development of Software and Applications Examples

This report documents results from **Study 1 - Fatigue Damage Evaluations**. This report addresses the fatigue reliability of welded details in tanker structures having multiple fatigue crack initiation sites. The fatigue reliability model is extended to include the effect of inspection updating where not necessarilly the whole structure considered is inspected in each inspection.

31,32 X

ABSTRACT

The fatigue reliability of welded details in tanker structures having multiple crack initiation sites is investigated. The welds are considered as series systems, where failure of the welds are defined as fatigue failure of the largest of the crack sites along the welds. Two models are applied to describe the distribution of crack sites over the welds. The first model assumes the number and location of crack sites to be known. The second model assumes the number and location of crack sites to be unknown and described through a density distribution function. A homogeneous Poisson process is defined to model the distribution of crack sites in the latter case.

The fatigue reliability model is extended to include the effect of inspection updating where not necessarily all the welds are inspected in each inspection. The quality of the inspection procedures are modeled through stochastic detectable crack sizes, defined from probability of crack detection curves, where both common and independent detectable crack sizes are considered at the different inspection sites.

A probability based optimization procedure is further presented, defining optimal initial design, quality of welding procedure at fabrication, time of inspections, quality of inspections and length of weld to be examined at each inspection. The cost considered in the optimization is cost related to initial design, cost of fabrication, cost of inspection, expected repair cost and expected failure cost.

The developed probabilistic model is applied to investigate the fatigue reliability of continuous welds in a tanker structure containing hazardous material for which no leakage is permissible. A stochastic description of the wave induced stress range response is achieved applying a longterm frequency domain analysis, where uncertainties in the environmental model, the load model and the load response model are included. A stochastic description the fatigue capacity of the weld is used.

The study shows that the contribution to the fatigue damage from continuous welds on tanker structures is significant. A solid initial design against fatigue is crucial to secure a fatigue reliable structure over the whole service life. Given the present development of inspection techniques and methods, in-service inspections should not be relied upon to improve the fatigue reliability of ship structural components.

33,34 X

Acknowledgments

35,36X

Contents

37

39,40x

List of Figures

41

42

List of Tables

List of Symbols

$A,\ B$	Weibull parameters in calibrated long term distribution
$B_{th}(a)$	Threshold correction term
$B_{cor}(t)$	Corrosion correction term
$D(\ )$	Detection event
$D[\ ]$	Standard deviation
$E[\ ]$	Expected value
C	Fatigue material parameter
C_B	Block coefficient
C_D	Design Cost
C_F	Cost of failure
C_{Fa}	Fabrication cost
C_I	Inspection cost
C_R	Cost of repair
$F(\ )$	Cumulative distribution function
F_n	Froude number $= V/\sqrt{gL_s}$
$H(\ )$	Inspection event
H_s	Significant wave height
$H_{\sigma,M}$	Transfer function
$I_{yy,zz}$	Moment of inertia
K	S-N fatigue parameter
L	Loading condition
$L(\ )$	Likelihood function
L_s	Length of ship
N	Number of load cycles
$M(\ )$	Safety event
P_F	Failure probability
$P(D\mid a)$	Detection probability of crack of depth a
R	Stress ratio

47

S_η	Wave spectrum	
S_σ	Response spectrum	
$\bar{S}_{cor}(t)$	Stress correction term due to corrosion	
T_z	Mean zero crossing period	
V	Velocity	
U	Standard normally distributed variable	
$W_{y,z}$	Moment of resistance	
X	Basic stochastic variable	
Y	Inherent physical uncertainty	
$Y(\ )$	Geometry function	
a	Crack depth	
a_0	Initial crack depth	
a_N	Crack depth after N load cycles	
a_c	Critical crack depth	
a_d	Smallest detectable crack depth	
a_{min}	Lower crack depth for possible crack detection	
b	Plate width	
c	Crack length	
$f(\ )$	Probability density function	
f'	Prior distribution	
f''	Posterior distribution	
$g(\ )$	Limit state function	
g	Acceleration of gravity ($9.81\ m/s^2$)	
g	Shape parameter for Gamma distribution	
$h(\ )$	Backtracking function for initial crack size	
$k(\ )$	Measure of fraction of fatigue life experienced	
k	Wave number	
k	Shape parameter for Gamma distribution of a_0 and a_d	
k_c	Corrosion rate	
l	Weld length	
l_i	Inspection length	
m	Fatigue material parameter	
m_i	Number of detected defects in inspection i	
m_n	n'th spectral moment	
p_d	Probability of crack detection	
q	Inspection quality	
r_L	Fraction of time at sea	

$s_{b/t}$	Bending stress versios tension stress
s_z	Design factor
t	Time
t_0	Crack initiation term
t_D	S-N fatigue design life
t_{life}	Lifetime of the ship
w	Spreading function
z	Plate thickness
Δ_c	Critical fatigue damage
Δ_{N_L}	Fatigue damage after N_L load cycles
ΔK_{th}	Threshold level
ΔK	Stress intensity
$\Delta \sigma$	Stress range
$\Gamma( )$	Gamma function
$\Gamma(;)$	Incomplete Gamma function
$\Phi( )$	Standard normal distribution
$\Psi( )$	Fatigue damage measure function
$\tilde{\Psi}( )$	Psi function $\partial \ln \Gamma(\cdot)/\partial(\cdot)$
Θ	Model uncertainty
α_i	Unit vector in standard normal space
β	Reliability index
δ, γ, β	Weibull parameters describing scatter diagram
ϵ	Bandwidth parameter
$\gamma_{a/c}$	Aspect ratio
λ	Wave length
λ	Scale parameter for Gamma distribution of a_0
λ_m	Estimated crack length from measurment
λ_d	Smallest detectable crack length
μ	Intensity of defects
μ_i	Weighting factor of Marsden zones
ν	Scale parameter in Gamma distribution of μ
ν_0	Rate of zero crossings
ν_p	Rate of peaks
$\nu_x(a)$	Mean crossing rate of level a
ϕ	Direction of crack growth
$\phi( )$	Standard normal density function
ψ	Bias factor
ζ	Steepness of low frequency part in wave spectrum

49

σ	Stress level
σ_N	Extreme stress level out of N cycles
θ	Independent stochastic variable, $\Psi(a_d) - \Psi(a_0)$
θ	Wave heading direction relative to ship
$\bar{\theta}$	Wave direction relative to main wave direction
θ_0	Main wave heading direction relative to ship
ξ	Power of high frequency tail in wave spectrum
ξ	Shape parameter in Gamma distribution of μ
ψ	Bias factor
ρ	Correlation coefficient
ω	Angular frequency
ω_e	Encounter frequency
$\cap$	Intersection: (and)
$\cup$	Union: (or)

Chapter 1

Introduction

1.1 Overview and Background

Fatigue of tanker structures is a highly complex phenomena, being an area of great concern for the marine industry. Many of the factors related to the fatigue crack growth process are variable, indefinite, or unknown, leading to large uncertainties in the determination of the consequence of the fatigue process. Uncertainties in the evaluation of the fatigue damage are introduced both as inherent uncertainties in the load response process and in the fatigue capacity of the structure, and as model uncertainties due to the use of simplified models and approximate procedures.

As a result of the introduced uncertainties, less confidence is given to an estimated deterministic fatigue life, and a conservative computed deterministic fatigue life orders of magnitude larger than the intended service life of the tanker structure is commonly defined. A more realistic design is achieved by treating the uncertain quantities as random variables. The safety of the considered tanker against fatigue failure is then evaluated in a probabilistic sense.

Fatigue reliability procedures have been derived, and are at present applied for tubular joints in offshore jacket structures. Reliability methods are applied both in the design analysis to estimate the fatigue reliability level of single joints as well as in the evaluation of the inspection plan for the structure. As information from performed inspections becomes available, an updating of the inspection plan for the remaining service life of the structure may be derived.

It has long been recognized that the fatigue life of a single joint or weld does not yield a quantitative measure of safety of the tanker structure against fatigue failure. A tanker structure is defined through several thousands of meters of welds and joints in which possible fatigue crack growth might originate and propagate. Due to the size of today's tankers, a possible through thickness crack might lead to leakage with enormous environmental consequences. To properly account for this effect in the evaluation of the acceptable fatigue failure probabilities of the individual crack sites, the system effect must be considered, in which the fatigue failure probability of the system defines the acceptable

reliability level of the different sites.

Another issue is also apparent in the modeling of the system fatigue reliability of tanker structures; for non-welded structures, fatigue crack growth typically occurs at the location with the highest stress concentration. This will not always be the case for welded structures, where fatigue crack growth originates from small initial welding defects. These welding defects consist of both internal and surface defects, where surface defects especially contribute to the fatigue failure probability. This leads to some uncertainty with respect to both the specific location of potential crack initiation sites and the total number of crack initiation sites to consider over a defined area of the tanker structure. The distribution of crack initiation sites is typically influenced by the quality of the workmanship during fabrication.

Due to the lower stress concentration along continuous welds, the fatigue failure probability for a potential crack site along a continuous weld is generally lower than the fatigue failure probability of a crack site located at a 'hot-spot' or joint intersection. However, based on the large quantities of continuous welds typically present in tanker structures, resulting in a large expected number of crack initiation sites, the contribution to the system fatigue failure probability will be significant. Therefore, in the evaluation of the system fatigue failure probability of a section of a tanker structure, both the contribution to the fatigue failure probability from the joint intersections and the continuous welds should be included.

Due to the size of today's tankers, containing more than 1000 km of welds, it is an enormous task to inspect the whole structure in each inspection, and only certain parts of the structure are usually inspected due to, *e.g.*, access difficulties or economic aspects. However, the inspected parts are large enough that a number of potential crack initiation sites is contained. The reliability design and maintenance procedures applied currently in the offshore industry do not take the information gained from inspection of one joint into consideration in the reliability calculations for another joint. Inspection plans for the different joints thus develop rather independently. These methods need to be extended when the interest is in ship structures, containing a large number of joints and continuous welds under similar material and stress conditions. The information gained from the inspection is therefore also useful for the non-inspected parts, and procedures need to be developed to utilize the information gained from the inspected areas in the fatigue reliability updating of uninspected areas.

1.2   Objectives and Scope of Work

The objective of the present study is to derive an applicable probabilistic approach for evaluating the fatigue reliability of welded joints in tanker structures, where the effect of inspection updating from examinations of parts of, or all the considered joints, is included in the probabilistic formulation. Two models are considered; A model with a deterministic number of crack initiation sites, and a model where the crack initiation sites are not predictable in advance, but are defined through a

homogeneous density distribution function. The welds considered are assumed to have homogeneous material parameters and to be subjected to similar stress conditions.

The derived theoretical model is applied in the evaluation of the fatigue reliability of a welded section of a tanker structure. The effect of having multiple crack initiation positions along the weld is studied, where focus is on how the quality of the welding procedure affects the fatigue reliability.

The report is divided into 7 chapters. In Chapter 2, a description of the full distribution structural reliability method, which is being applied in the probabilistic fatigue analysis, is given.

Chapter 3 describes the fatigue model applied for evaluation of the fatigue reliability of welded joints. The chapter includes a formulation of the applied fracture mechanics fatigue model together with a description of the uncertainties involved in the evaluation of the fatigue capacity of tanker structures.

In Chapter 4, the fatigue reliability model for the weld having multiple crack initiation sites is derived, where the weld is modeled as a series system. The effect of inspection updating based on examination of parts of the weld is included in the derivation. Emphasis is on the formulation of the limit state function for the multi-site series system, having both a deterministic and a stochastic modeling of the number of crack sites.

Chapter 5 applies the derived probabilistic fatigue model in a probability based optimization procedure defining optimal design, fabrication and inspection strategy for a series system having multiple crack sites. Cost of design, fabrication, inspection, maintenance, and expected failure cost are included in the formulation.

Chapter 6 studies the fatigue reliability of a transverse continuous weld in a panel section of a tanker structure, utilizing the theoretical approach from Chapter 4. Emphasis is on the stochastic description of the longterm wave induced stress range response process and on the derivation of a realistic fatigue model for the tanker structure.

Chapter 7 summarizes the presented work and suggests areas for further research.

Chapter 2

Full Distribution Structural Reliability

2.1 Introduction

Sufficient safety against structural failure is the overall objective in structural design, where the safety of a structure is, in a probabilistic way, interpreted as the survival probability of the structure. The field of structural reliability is engaged with the derivation of this survival probability, taking into consideration the uncertainties related to the design concept investigated. Reliability methods, applying all the available information of the joint distribution of the uncertain parameters in the derivation of the survival probability, are defined as full distribution reliability methods.

The historical development of structural reliability theory from its early start in the 1920's until its rapid development in the last decade is summarized in Madsen *et al.* [50], where some main contributions to the field in the last decades are based on, among others, the work of Cornell [14, 15], Ditlevsen [21, 22], Hasofer and Lind [34], Lind [49], and Veneziano [92].

Structural reliability theory generally does not include the effect of gross human errors, which account for the vast portion of structural failures, Bea [6]. This will, however, not remove the validity of structural reliability theory in the design process, but rather defines it as a tool in the definition of acceptable design concepts and in the ranking of different structural designs. Structural reliability theory is also important in the evaluation and updating of inspection and maintenance procedures of structures subjected to time dependent failure modes, as *e.g.*, fatigue and corrosion.

In the evaluation of the survival probability of a structure, not only the inherent physical uncertainties influence the safety estimate. Uncertainties related to both the mathematical modeling of the capacity and the demand sides of the design concept, termed modeling uncertainty, and to the statistical modeling of these uncertainties, termed statistical uncertainties, also influence the

estimated reliability level of the structure. The estimated safety level of the structure is then not the true reliability level, but expresses rather the engineer's estimate of the survival probability of the structure based on the available information. More systematic definitions of inherent, model, and statistical uncertainties for the defined fatigue model are given later in Section 3.4.

In the full distribution reliability, the inherent, model and statistical uncertainties are expressed through random variables $\mathbf{X} = (X_1, X_2, \cdots X_n)$, where the probabilistic modeling of the uncertain variables and parameters are defined by a joint distribution density function $f_{\mathbf{X}}(\mathbf{x})$.

The failure criterion is modeled through a limit state function $g(\mathbf{X})$, for which both an analytical and a numerical description can be applied. The limit state function divides the state of the structure into two states, a failure domain and a safe domain,

$$g(\mathbf{X}) \begin{cases} < 0 : \text{in failure domain} \\ = 0 : \text{at failure surface} \\ > 0 : \text{in safe domain} \end{cases} \tag{2.1}$$

where $g(\mathbf{X}) = 0$ defines the limit state surface that separates the failure domain from the safe domain. The modeling of the limit state function depends on the failure criterion investigated, where failure criteria based on, *e.g.*, ultimate limit state, damage limit state or serviceability of the structure are possible definitions.

The estimated failure probability of the structure is then equal to the probability of the limit state function being in the failure domain,

$$P_F = P[g(\mathbf{X}) \le 0] = \int_{g(\mathbf{X}) \le 0} f_{\mathbf{X}}(\mathbf{x}) d\mathbf{x} \tag{2.2}$$

The reliability of the structure is the complement of P_F. It is important to remember that the estimated failure probability depends on the modeling of the limit state function and thereby on the definition of the failure criteria.

The multi-dimensional integral in Equation (2.2) is generally not possible to solve analytically, and standard numerical integration techniques for evaluation of the failure probability are generally not feasible for reliability problems involving more than 3-4 stochastic variables. Different approximate procedures have therefore been suggested. These procedures can essentially be divided into two types;

- Simulation procedures where the failure probability is estimated based on the relative occurrence of simulated outcome of the random variables within the failure domain.

- Transformation of the original problem into an n-dimensional independent standard normal space from which approximate solution methods are applied to estimate the failure probability.

Procedures based on a combination of these two methods have also been developed, where simulation methods are applied to update the evaluated failure probability.

In the following work, the failure probabilities are estimated based on the second solution strategy, applying first and second order reliability methods (FORM/SORM). A short overview covering the concept of these procedures is given in the following chapters, whereas a more thorough description of full distribution reliability methods is found in, *e.g.*, Bjerager [8], Ditlevsen [19], Madsen *et al.* [50], Melchers [59], and Thoft-Christensen and Baker [84].

The computational procedures for FORM/SORM have been extensively developed, and are today applicable for realistic engineering reliability formulations. Commercial software programs with FORM/SORM implemented are available, CALREL [45], PROBAN [64] and STRUREL [71].

2.2 First and Second Order Reliability

The use of FORM/SORM for evaluation of the multi-dimensional integral expressing the failure probability consists of three steps;

- A transformation of the vector of basic variables $\mathbf{X}$ into a set of independent standard normally distributed variables $\mathbf{U}$.

- An approximation of the failure surface at the most likely failure point in the standard normal space.

- A computation of the failure probability corresponding to the approximated failure surface.

The transformation to the standard normal space is performed to utilize the special properties of the standard normal distribution function, enabling simple standardized procedures to be applied in the computation of the failure probability. When the basic variables are mutually independent, the variables are transformed separately through,

$$u_i = \Phi^{-1} \left[F_{X_i}(x_i) \right] \tag{2.3}$$

where Φ is the cumulative standard normal distribution function. For dependent random variables, an equivalent procedure is applied, where the basic dependent variables are transformed into standard normal variables through successive conditioning, Hohenbichler and Rackwitz [36]. The transformation is usually referred to as the Rosenblatt transformation, Rosenblatt [74].

$$
\begin{aligned}
u_1 &= \Phi^{-1} \left[F_{X_1}(x_1) \right] \\
u_2 &= \Phi^{-1} \left[F_{X_2|X_1}(x_2|x_1) \right] \\
u_3 &= \Phi^{-1} \left[F_{X_3|X_1 X_2}(x_3|x_2 x_1) \right] \\
& \quad \ldots
\end{aligned}
\tag{2.4}
$$

Other types of transformations to the standard normal space for dependent stochastic variables exist. When the basic variables are described through marginal distributions and a correlation structure, the Nataf model suggested by Der Kiureghian and Liu [48] can be applied.

The failure surface is approximated in the transformed standard normal space. Depending on the type of approximation, a first or second order approximation, the method is characterized as FORM or SORM reliability method, respectively. In FORM, the failure surface is expressed through a tangent hyperplane through the most likely failure point, the design point. Applying SORM, different types of approximations to the failure surface are available, *e.g.* a second order Taylor expansion around the design point, or a curvature or point-fitted hyperparabolic surface, Fissler *et al.* [25], Breitung [10] and Der Kiureghian et al. [47]. Based on the rotational symmetry of the standard multi-normal density function, the design point is the point on the failure surface closest to the origin, found by applying an appropriate constrained optimization routine, *e.g.*, the NLPQL-algorithm, Schittkowski [78].

Due to the exponential decrease of the standard normal density function with the square of the distance from the origin, good estimates of the failure probability are computed from the approximated failure surfaces. Exact evaluation of the failure domain based on the approximated surface exists for the linear approximation, the second order Taylor approximation and the parabolic approximation, Breitung [10] and Tvedt [87, 88].

From the estimated failure probability, the reliability index β is defined,

$$\beta = -\Phi^{-1}(P_F) \qquad (2.5)$$

where a first order approximation of β is equal to the minimum distance of the failure surface from the origin in the standard normal space.

2.3 System Structural Reliability

In structural reliability theory, a system is defined by multiple limit state functions, whereas a component is defined by a single limit state function. In the following, parallel and series systems are discussed, but more general systems consisting of, *e.g.*, a parallel system of series systems, can be established.

2.3.1 Parallel System

An intersection of components is referred to as a parallel system, where failure of the parallel system is defined as failure of all the components in the system.

Expressing the different components in the parallel system by g_i, the failure probability of the system is given by,

$$P_{F_p} = P[\cap_{i=1}^n g_i(\mathbf{X}) \leq 0] = \int_{\cap_{i=1}^n g_i(\mathbf{X}) \leq 0} f_{\mathbf{X}}(\mathbf{x})dx \qquad (2.6)$$

A first order approximation of the failure probability of the parallel system is,

$$P_{F_p} \approx P_{FORM} = \Phi_n(-\beta, \mathbf{C}) \qquad (2.7)$$

where β is the vector of first order reliability indices for the different components in the system. $\mathbf{C}$ is the correlation coefficient matrix for the approximating first order safety margins,

$$C_{ij} = \alpha_i^T \alpha_j \tag{2.8}$$

where α_i is the outward unit normal vector in the standard normal space for component i.

A second order approximation, deriving a correction factor to the first order parallel failure probability, has been formulated by Hohenbichler [35].

In the following work, parallel systems are applied in the evaluation of conditional probabilities, where conditional probabilities are formulated to express the updated probability level of investigated systems from inspection results.

2.3.2 Series System

An union of components is referred to as a series system, where failure of the series system is defined as failure of one or more of the components in the system.

Expressing the different components in the series system by g_i, the failure probability of the system is given by,

$$P_{F_s} = P[\cup_{i=1}^n g_i(\mathbf{X}) \leq 0] = \int_{\cup_{i=1}^n g_i(\mathbf{X}) \leq 0} f_{\mathbf{X}}(\mathbf{x}) d\mathbf{x} \tag{2.9}$$

The series system can be evaluated in terms of the intersection of the complementary events. A first order probability estimate of the series system is then,

$$P_{F_s} \approx P_{FORM} = 1 - \Phi_n(\beta, \mathbf{C}) \tag{2.10}$$

A second order probability estimate is achieved by applying second order results for each of the separate components in the series system.

Alternative formulations, based on lower and upper bounds on the series system failure probability can be derived, Ditlevsen [23]. The bounds are based on FORM/SORM computed failure probabilities of the individual components as well as the coupled component intersections.

Series systems are applied in the following to evaluate the reliability level of a system consisting of multiple fatigue sensitive joints.

Chapter 3

Formulation of the Fatigue Problem

3.1 Introduction

Fatigue is the result of cumulative damage caused by repeated fluctuating loads. Each of the load cycles is generally not large enough to cause failure by itself, but failure occurs when the accumulated damage experienced by the structure reaches a critical level. To quantify the fatigue behavior of welded structures is a highly complicated task, and has been the area of considerable research in recent time. A number of textbooks have been written on the subject, where, among others, Fatigue Handbook [3], Gurney [32] and Rolfe and Barsom [73] give a good general overview.

The fatigue process can be divided into three stages, where each of the stages contributes to the fatigue life of the structure,

- crack initiation

- crack propagation

- final fracture

The first stage, the crack initiation stage, is related to the microscopic material behavior for which no rational theory seems to exist. However, the crack initiation stage is of less importance for welded structures, since weld defects will always exist in welded areas. These weld defects work as crack initiation sites from which fatigue cracks may originate and propagate. The weld defects consist of both internal and surface defects, where surface defects mainly influence the fatigue characteristic. The crack initiation stage will therefore only contribute to the fatigue life for post-weld improved welds, and the crack initiation stage is usually neglected in comparison to the crack propagation stage in the fatigue evaluation of welded structures.

The influence of weld defects on the fatigue behavior is implicitly included in the fatigue model through the modeling of equivalent initial crack sizes, which creates the basis for the crack propagation stage. The propagation stage is better understood than the initiation stage, and different fracture mechanics theories modeling the crack growth in this stage have been developed.

The overall dominating effect in the crack propagation stage is the stress range to which the detail is being exposed. The mean stress level is of less importance, and for welded details the mean stress level is generally neglected due to the existence of residual stresses in the heat affected zone around the weld. Both the geometry of the weld and the initial crack sizes due to welding defects have a large influence on the fatigue strength of the details. A general modeling of the crack propagation stage is given in the following sections.

Final fatigue fracture will eventually occur as the crack size reaches a critical size. Depending on a variety of variables as, *e.g.*, the toughness of the material, the temperature, and the loading rate, the fatigue failure may be due to brittle fracture, ductile fracture or plastic collapse. However, the fraction of the fatigue life in the final fracture stage is small compared to the crack propagation stage, and is usually disregarded. Instead, a critical crack size is commonly defined, modeling the crack size for which failure occurs. This critical crack size is usually defined as, *e.g.*, through-the-thickness crack or a crack size requiring costly repair procedures. Due to the rapid crack growth in the final stage of the crack propagation stage, the estimated fatigue life of the detail is not sensitive to the defined size of the critical crack.

The fatigue process affecting tanker structures is typically high-cycle fatigue, in contrast to low-cycle fatigue with fatigue life approximately less than $5 \cdot 10^3$ load cycles. High cycle fatigue is likely to occur in welded areas of the ship structure due to stress concentrations and geometric discontinuities, where crack growth will originate from surface defects as undercuts and ripples.

These surface defects are also present in continuous longitudinal and transverse welds, where they act as crack initiation sites along the weld. Due to the lower stress concentration for these continuous welds, the fatigue failure hazard for a potential weld defect located along a continuous weld is generally smaller than for an equivalent weld defect located in an area of geometric discontinuity, a so called 'hot-spot'. However, due to the large quantity of continuous welds present in tanker structures, resulting in a large expected number of crack initiation sites, the contribution to the fatigue failure hazard from continuous welds is of significance, and must be included in the fatigue design consideration.

In the evaluation of the fatigue failure probability of a tanker section, two models for the location of crack initiation sites are investigated;

- The location of the crack sites is known. This is the common assumption applying the 'hot-spot' approach. The crack site locations are typically chosen at structural intersections having large stress concentrations.

- The location of the crack initiation sites is unknown and described though a homogeneous

density distribution function. This model is applied to describe the location of crack sites along continuous transverse and longitudinal welds.

In the following, a general description of the fatigue crack propagation stage is given, for which a linear elastic fracture mechanics model is applied. This model is used to evaluate the accumulated fatigue damage in the present work. The fracture mechanics approach is preferred to the S-N approach, applying the Miner-Palmgren damage criteria, Miner [60] and Palmgren [66], since the developed fatigue model is intended to include the effect of inspection updating. The fracture mechanics model gives direct estimates of the propagated crack size with time, allowing updating of the estimated crack propagation from observed and measured crack sizes.

A fatigue reliability model incorporating the effect of inspection updating applying the S-N fatigue approach has been suggested by Cramer and Bea [17], and is presented in appendix A. The model applies experimental fatigue results to estimate the remaining fatigue life of inspected tubular joints on offshore jacket structures. Provided that equivalent experimental results existed for critical ship structural details, the simplicity of the S-N approach would make this a natural choice for the evaluation of the fatigue life in the present work. However, the fatigue reliability model presented in appendix A is directly applicable to the derived reliability procedures presented later in Chapter 4.

3.2 Fracture Mechanics Model

The fracture mechanics approach models the local crack growth behavior based on a global description model of loading, weld geometry, crack geometry and material properties. An excellent overview of the fracture mechanics approach is given by Engesvik in Ref. [3]. A linear elastic fracture mechanics model is applied here, where mode I fatigue is considered, Broek [13].

3.2.1 Derivation of Crack Growth Equation

In linear elastic fracture mechanics approach, the increment in crack size Δa, during a load cycle is related to the range of the stress intensity ΔK, for the load cycle. A simple relation, proposed by Paris and Erdogan [67] is sufficient for most purposes,

$$\Delta a = C(\Delta K)^m, \qquad \Delta K \geq 0 \tag{3.1}$$

where C and m are material parameters. A one-dimensional fatigue crack growth model is here assumed to adequately describe the crack growth behavior, but a two-dimensional fatigue crack growth model could also have been applied, Friis-Hansen and Madsen [30].

The crack increment in one cycle is small compared to the crack size, and the relation can

consequently be expressed as a differential equation,

$$\frac{da}{dN} = C(\Delta K)^m, \qquad \Delta K \geq 0 \qquad (3.2)$$

where N is the number of stress cycles.

The Paris equation is generally conservative, since experimental results have shown that the crack growth rate is lower than what the Paris equation suggests for smaller stress intensities and that there exists a lower threshold on the stress intensity, ΔK_{th}, under which no crack growth occurs. This is partly adjusted for by applying a lower bound on the stress intensity, $\Delta K \geq \Delta K_{th}$, in Equation (3.2).

The range of the stress intensity is a function of the far field stress range, and the size and geometry of the crack. It is defined as,

$$\Delta K = \Delta \sigma Y(a) \sqrt{\pi a} \qquad (3.3)$$

where $\Delta \sigma \sqrt{\pi a}$ is the theoretical result for the stress intensity of a crack in an infinite plate under uniform tension $\Delta \sigma$. The geometry function $Y(a)$ accounts for crack geometry, free surface effects, finite width effects and stress gradient effects. The form of the geometry function depends on the physical problem under evaluation.

By combining Equations (3.2) and (3.3), and separating the variables, the following differential equation is obtained,

$$\frac{da}{(Y(a)\sqrt{\pi a})^m} = C \Delta \sigma^m \, dN, \qquad a(N = 0) = a_0 \qquad (3.4)$$

where a_0 is the size of the initial crack.

The sequential order of the load cycles may have some influence on the crack growth rate due to retardation effects. However, Ritchie et al. [72] and Kam and Dover [43], found that the effect of crack closure was insignificant for longterm series of load responses typical for marine structures. Ignoring possible sequence effects, the differential equation is expressed as,

$$\int_{a_0}^{a_N} \frac{da}{(Y(a)\sqrt{\pi a})^m} = C \sum_{i=1}^{N} \Delta \sigma_i^m, \qquad \Delta \sigma \geq \Delta K_{th} / \left(Y(a) \sqrt{\pi a} \right) \qquad (3.5)$$

where a_N is the crack size after N stress cycles given the initial crack size a_0.

Numerical integration techniques must usually be applied to compute the crack size as a function of the number of load cycles a_N, unless a crack size independent geometry function is chosen. Numerical integration of the integral will greatly increase the computational time for the later probabilistic analysis, and it is therefore suggested that the semi-analytical integration technique proposed in Section 3.2.3 be applied in the evaluation of the damage function.

The stress range process is a random process, and each stress range cycle as well as the sum of the stress ranges are hence random variables. For high-cycle fatigue, being of concern for marine

structures, the randomness of the sum can be neglected due to the large number of stress cycles, and the process is adequately described by the expected value. The sum of the m'th order of the stress range history can then be expressed by the m'th moment of the longterm stress range process to which the investigated detail is exposed,

$$\sum_{i=1}^{N} \Delta\sigma_i^m = N \sum_{i=1}^{N} \frac{1}{N} \Delta\sigma_i^m \approx N E[\Delta\sigma^m] \tag{3.6}$$

The wave induced stress response on tanker structures from environmental loading is typically narrow-banded, letting the number of stress cycles to which a detail is exposed over service time t be defined by the rate of zero-crossings of the stress range process,

$$N = \nu_0 r t \tag{3.7}$$

where ν_0 the zero-crossing rate per time unit for the stress response process and r is the fraction of service time the tanker is at sea.

The wave induced longterm stress range response on tanker structures has been found to be well described through a Weibull distribution, see Chapter 6,

$$F_\Sigma(\sigma) = 1 - e^{-(\sigma/A)^B} \tag{3.8}$$

where A and B are the scale and shape distribution parameters in the Weibull stress range distribution function, respectively. The m'th moment of the stress range process is then equal to,

$$\begin{aligned} E[\sigma^m] &= \int_0^\infty \sigma^m f_\Sigma(\sigma) d\sigma \approx \int_0^\infty \sigma^m \frac{B\sigma^{B-1}}{A^B} e^{-(\sigma/A)^B} d\sigma \\ &= A^m \Gamma\left(1 + \frac{m}{B}\right) \end{aligned} \tag{3.9}$$

Due to the lower threshold on the stress intensity in the fatigue crack growth equation, the whole loading history does not contribute to the fatigue damage. The m'th moment of the stress range process contributing to the fatigue damage is for the Weibull distributed loading expressed through the incomplete Gamma function $\Gamma(;)$,

$$\begin{aligned} E_{dam}[\sigma^m] &= \int_{\Delta K_{th}/Y(a)\sqrt{\pi a}}^\infty \sigma^m f_\Sigma(\sigma) d\sigma \\ &= \int_{\Delta K_{th}/Y(a)\sqrt{\pi a}}^\infty \sigma^m \frac{B\sigma^{B-1}}{A^B} e^{-(\sigma/A)^B} d\sigma \\ &= A^m \Gamma\left(1 + \frac{m}{B}; \left(\frac{\Delta K_{th}}{A\,Y(a)\sqrt{\pi a}}\right)^B\right) \end{aligned} \tag{3.10}$$

The effect of the lower threshold is included in the fatigue crack growth equation through the term,

$$B_{th}(a) = \frac{E_{dam}[\Delta\sigma^m]}{E[\Delta\sigma^m]} = \frac{\Gamma\left(1 + \frac{m}{B}; \left(\frac{\Delta K_{th}}{A\,Y(a)\sqrt{\pi a}}\right)^B\right)}{\Gamma\left(1 + \frac{m}{B}\right)} \tag{3.11}$$

The lower threshold level for the stress intensity, ΔK_{th}, under which no crack growth occur, depends strongly on environmental conditions, but also on factors like the stress ratio R and the loading frequency, resulting in large uncertainties in the determination of the value of the lower threshold level. Also, due to the presence of initial cracks from weld defects, and the fact that the stress range level giving a stress intensity factor equal to the threshold level decreases with the crack size, the validity of using a lower threshold level for fatigue design of full scale welded structures is questionable. A neglect of the lower threshold level leads to a slightly conservative estimate of the fatigue life.

In addition to the influence of a corrosive environment on the material parameters C and m in the fatigue crack growth equation, a corrosive environment might lead to a general increase in the stress range level with time due to a reduction in the steel thickness. In the model, the relative increase in the stress level over time is expressed as,

$$\bar{S}_{cor}(t) = \frac{z}{z - k_{cor}t} = \frac{z}{z - k_{cor}N_t/(r\nu_0)} \quad , \qquad t < z/k_{cor} \tag{3.12}$$

where z is the steel thickness, k_{cor} is the corrosion rate and N_t is the number of load cycles at time t. The rate of corrosion will depend on the type of corrosive environment and on the use of cathodic protection in the area where the investigated detail is located. The influence of the thickness reduction on the longterm stress range level in Equation (3.6) is then,

$$
\begin{aligned}
\sum_{i=1}^{N_T} \left(\Delta\sigma_i \bar{S}_{cor}(t_i) \right)^m &= \sum_{i=1}^{N_T} \left(\Delta\sigma_i \frac{z}{z - k_{cor}(i-1)/(r\nu_0)} \right)^m \\
&\approx E[\Delta\sigma^m] \sum_{i=1}^{N_T} \left(\frac{z}{z - k_{cor}(i-1)/r\nu_0} \right)^m \\
&\approx E[\Delta\sigma^m] \int_0^{rt\nu_0} \left(\frac{z}{z - k_{cor}x/(r\nu_0)} \right)^m dx \\
&= E[\Delta\sigma^m] \frac{zr\nu_0}{k_{cor}(m-1)} \left(\left(\frac{z}{z - k_{cor}t} \right)^{m-1} - 1 \right)
\end{aligned}
\tag{3.13}
$$

The expression is rewritten as,

$$\sum_{i=1}^{N_T} \left(\Delta\sigma_i \bar{S}_{cor}(t) \right)^m = rt\nu_0 E[(\Delta\sigma)^m] \, B_{cor}(t) \tag{3.14}$$

where the term,

$$B_{cor}(t) = \frac{z}{k_{cor}t(m-1)} \left(\left(\frac{z}{z - k_{cor}t} \right)^{m-1} - 1 \right) \tag{3.15}$$

accounts for the effect of increased stress level over time due to corrosion. The above derivation is based on the assumption of a stationary stress range process over the lifetime.

The effect of increased stress level over time due to corrosion is assumed not to influence the derivation of the correction factor for the lower threshold, $B_{th}(a)$. This assumption is of minor

importance, since the reduction of plate thickness due to corrosion first shows some effect later in the design life, where a potential crack already will have propagated to a size where the effect of the threshold level is of less significance. However, the existence of a corrosive environment greatly affects the existence and the value of the crack propagation threshold, where a corrosive environment tends to increase the threshold value. This effect is accounted for directly in the modeling of the value of the threshold level ΔK_{th}.

The size of the propagated crack can then be expressed as a function of the service time for the tanker. By defining the function $\Psi(a)$ as,

$$\Psi(a) = \int_0^a \frac{1}{B_{th}(x)\left(Y(x)\sqrt{\pi x}\right)^m} \, dx \tag{3.16}$$

the crack size a at time t is,

$$a(t) = \Psi^{-1}\left(\Psi(a_0) + Cr\nu_0(t - t_0)E[\Delta\sigma^m]B_{cor}(t)\,\right) \tag{3.17}$$

where t_0 is the crack initiation time, the time to develop the initial crack size a_0. The crack initiation time is usually neglected for welded structures due to initial weld defects, and is therefore omitted in the further analysis. Equation (3.17) then expresses the fatigue crack size a at service time t, for an investigated detail, as a function of the initial crack size due to welding defects, the local longterm stress range response, the local weld geometry, the crack configuration, the material parameters, and the rate of corrosion.

3.2.2 Geometry Function

In order to predict the fatigue crack growth, it is necessary to include the effect of redistribution of stresses in the detail due to the presence of the crack. The redistribution of stresses is accounted for through the modeling of the geometry function $Y(a)$ in the expression for the stress intensity factor ΔK.

For simplicity, it is assumed that the fatigue crack initially has a semi-elliptical shape and that the shape of the crack remains semi-elliptical as the crack propagates. An empirical expression for the stress intensity factor for surface cracks in finite plates has been defined by Newman and Raju [61], and is in the following applied to express the form of the geometry function,

$$\Delta K = [\Delta\sigma_t + H\,(a/c, a/z)\,\Delta\sigma_b]\,F\,[\phi, a/c, c/b, a/z]\sqrt{\pi a} \tag{3.18}$$

The equation has been fitted from finite element analyses based on uniform tension and bending stresses, $\Delta\sigma_t$ and $\Delta\sigma_b$, over a plate of width b and thickness z. ϕ defines the direction of crack growth, a/c expresses the crack configuration, and c/b and a/z are the relative crack length and crack depth, respectively.

The present model is based on one-dimensional fatigue crack growth in the depth direction, giving crack growth direction $\phi = \pi/2$. Expressing the relationship between bending and tension stresses

as $s_{b/t}$ and the crack configuration as $\gamma_{a/c}$, where a crack size independent crack configuration is assumed, the geometry function is written as,

$$
\begin{aligned}
Y(a) &= [1 + s_{b/t}(1 + G_1(a/z) + G_2(a/z)^2)] \times \\
&\quad [M_1 + M_2(a/z)^2 + M_3(a/z)^4]Qf_w
\end{aligned}
\tag{3.19}
$$

where,

$$
\begin{aligned}
G_1 &= -1.22 - 0.12\gamma_{a/c} \\
G_2 &= 0.55 - 1.05\gamma_{a/c}^{0.75} + 0.47\gamma_{a/c}^{1.5} \\
M_1 &= 1.13 - 0.09\gamma_{a/c} \\
M_2 &= -0.54 + 0.89/(0.2 + \gamma_{a/c}) \\
M_3 &= 0.5 + 14.0(1 - \gamma_{a/c})^{24} - 1/(0.65 + \gamma_{a/c}) \\
Q &= (1 + 1.46\gamma_{a/c}^{1.65})^{-0.5} \\
f_w &= \left[\sec(\pi a/(2b\gamma_{a/c})) \sqrt{a/z} \right]^{1/2}
\end{aligned}
$$

A thorough discussion of the modeling and influence of the different terms in the geometry function is given in Newman and Raju [61].

In the above expression for the geometry function, the influence of the presence of the weld is not included. The weld leads to additional stiffness and thereby a higher stress concentration for transverse welds, whereas the effect of the weld on the general stress distribution for longitudinal welds is of minor importance. A magnification factor, accounting for the effect of the presence of the weld, is multiplied with the geometry function defined in Equation (3.19).

For transverse welds, the magnification factor suggested by Smith and Hurworth [81] is applied,

$$
Y_{t.weld} = 1.0 + 1.24e^{-22a/z} + 3.17e^{-357a/z}
\tag{3.20}
$$

The empirical expression is fitted to finite element results, and the validity of the last term can be questioned.

The effect of the weld is disregarded for longitudinal welds,

$$
Y_{l.weld} = 1.0
\tag{3.21}
$$

3.2.3 Semi-Analytical Integration Procedure

The integral in the expression for the fatigue crack size, Equation (3.16), is generally not possible to solve analytically for crack size dependent geometry functions, and numerical integration procedures such as Romberg integration must be applied. This will, however, involve considerable computational efforts in the probabilistic analysis, where the integral is solved multiple times due to the iterative procedure of finding the most likely failure point.
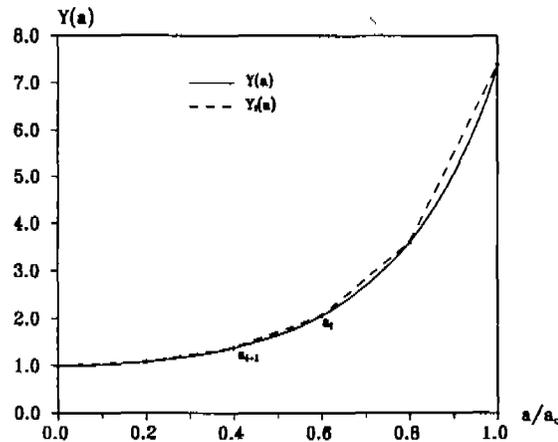
Figure 3.1: Linearized geometry function over the crack growth domain.

The shape and form of the geometry function is usually evaluated applying approximate procedures based on, *e.g.*, least squares fit of parametric expressions and engineering judgment for different crack configurations and weld geometries. The approximate way of modeling the geometry function puts into question the need for results from the integral evaluation that are accurate as a numerical integration will give. Another aspect is also that the geometry function is usually defined from finite elements analysis or experimental results, giving tabular values of the geometry function for different crack sizes.

In light of this, a semi-analytical integration routine for evaluation of the integral in the fatigue crack growth equation is suggested, requiring far less computational time than a numerical integration.

The semi-analytical approach is based on the following procedure;

- The geometry function $Y(a)$ is described through linear segments over the crack size domain of interest, see Figure 3.1.

- An analytical solution to the integral in the fatigue crack growth equation is derived over each of the linear segments, applying the material parameter $m = 3$.

- Solutions to the fatigue crack growth equation for general values of the material parameters m is estimated based on linearized values around the derived analytical solution for $m = 3$.

Depending of the desired level of accuracy, the degree of segment linearization is adjusted, but a modeling of $Y(a)$ into only 5 linear segments over the crack growth domain will give satisfactory results for most purposes.

The geometry function is approximated over segment i by,

$$Y(a) \approx Y_i(a) = \delta_i(1 + \beta_i a), \qquad a_{i-1} \leq a \leq a_i \tag{3.22}$$

where,

$$\beta_i = \frac{Y(a_i) - Y(a_{i-1})}{Y(a_{i-1})a_i - Y(a_i)a_{i-1}} \qquad \delta_i = \frac{Y(a_{i-1})a_i - Y(a_i)a_{i-1}}{a_i - a_{i-1}} \tag{3.23}$$

The linearization does not include the $\sqrt{\pi a}$ term in the expression for the stress intensity, due to the highly non-linear behavior of the inverse of this term for small crack sizes. The integral in the fatigue crack growth equation over the segment i is written as,

$$\int_{a_{i-1}}^{a_i} \frac{da}{(\sqrt{\pi a}Y(a))^m} \approx \int_{a_{i-1}}^{a_i} \frac{da}{(\sqrt{\pi a}\,(\delta_i(1 + \beta_i a)))^m}$$

$$= \frac{1}{(\sqrt{\pi}\delta_i)^m} \int_{a_{i-1}}^{a_i} \frac{da}{(\sqrt{a}(1 + \beta_i a))^m} \tag{3.24}$$

An analytical solution for the integral exists for integer values of the material parameter m, and a symbolic analytical solution for $m = 3$ is derived.

By the substitution,

$$u = \begin{cases} = \sqrt{\beta a} & \beta \geq 0 \\ = \sqrt{-\beta a} & \beta < 0 \end{cases} \tag{3.25}$$

the integral, Equation 3.24, is rewritten in the more manageable form, Gradshteyn and Ryzhik, [31],

$$\begin{aligned} \mathbf{I} &= \int \frac{da}{(\sqrt{a}(1 + \beta a))^m} = 2(\pm\beta)^{(m-2)/2} \int \frac{du}{u^{m-1}(1 \pm u^2)^m} \\ &= \frac{-2(\pm\beta)^{(m-2)/2}}{m-2} \left[\frac{1}{u^{m-2}(1 \pm u^2)^{m-1}} + (3m - 4) \int \frac{du}{(1 \pm u^2)^m} \right] \end{aligned} \tag{3.26}$$

where the product $u^{-(m-3)}$ has been disregarded from the last integral.

Through recursive integration, and assuming,

$$\int \frac{du}{(1 \pm u^2)^{m-2}} = \int \frac{du}{(1 \pm u^2)} \tag{3.27}$$

the integral is written as,

$\beta \geq 0$:

$$\begin{aligned} \mathbf{I} &= \frac{-1}{m-2} \left[\frac{1}{(1 + \beta a)^{m-1}} \left(\frac{2}{a^{(m-2)/2}} + \frac{(3m-4)\beta^{(m-1)/2}\sqrt{a}}{m-1} \right) \right. \\ &+ \frac{(3m-4)(2m-3)}{2(m-1)(m-2)} \times \\ &\left. \left(\frac{\beta^{(m-1)/2}\sqrt{a}}{(1 + \beta a)^{m-2}} + (2m - 5)\beta^{(m-2)/2} \tan^{-1}(\sqrt{\beta a}) \right) \right] \end{aligned} \tag{3.28}$$

$\beta < 0$:

$$\mathbf{I} = \frac{-1}{m-2} \left[\frac{1}{(1 + \beta a)^{m-1}} \left(\frac{2}{a^{(m-2)/2}} + \frac{(3m-4)(-\beta)^{(m-1)/2}\sqrt{a}}{m-1} \right) \right.$$

$$
\vdots \quad + \quad \frac{(3m-4)(2m-3)}{2(m-1)(m-2)} \times
$$
$$
\left(\frac{(-\beta)^{(m-1)/2}\sqrt{a}}{(1+\beta a)^{m-2}} - \frac{(2m-5)(-\beta)^{(m-2)/2}}{2} \ln\left(\frac{1+\sqrt{-\beta a}}{1-\sqrt{-\beta a}}\right) \right) \Bigg] \tag{3.29}
$$

where $m \neq 1, 2$. The analytical solution is strictly only valid for $m = 3$, but gives approximate good estimates for values of m close to 3.

The material parameter is later to be modeled as a stochastic parameter, with mean value in the area of 3 and a low coefficient of variation. It is, however, also seen from Equation 3.5, that the sensitivity to m in the fatigue crack growth equation is mainly contributed from the loading term $\sum \Delta\sigma_i^m$, justifying the above approximation so as to satisfy the required level of accuracy.

Substituting m with 3, gives

$$
\mathbf{I} = \begin{cases} \frac{-1}{(1+\beta a)^2}\left(\frac{2}{\sqrt{a}} + \frac{5}{2}\beta\sqrt{a}\right) - \frac{15}{4}\left(\frac{\beta\sqrt{a}}{1+\beta a} + \sqrt{\beta}\tan^{-1}\sqrt{\beta a}\right) & \beta \geq 0 \\[2mm] \frac{-1}{(1+\beta a)^2}\left(\frac{2}{\sqrt{a}} + \frac{5}{2}\beta\sqrt{a}\right) - \frac{15}{4}\left(\frac{\beta\sqrt{a}}{1+\beta a} - \frac{\sqrt{-\beta}}{2}\ln\frac{1+\sqrt{-\beta a}}{1-\sqrt{-\beta a}}\right) & \beta < 0 \end{cases} \tag{3.30}
$$

The use of the above procedure for evaluation of the integral in the fatigue crack growth equation does not involve any restrictions on the form or shape of the geometry function. The geometry function is still defined applying appropriate methods, but it is in the integration procedure approximated through a number of linear segments over the domain of integration.

An equivalent linearization of the m'th power of the geometry function could also be applied, having the approximation,

$$
Y^m(a) \approx \delta_i(1 + \beta_i a) \ , \qquad a_{i-1} \leq a \leq a_i \tag{3.31}
$$

where,

$$
\beta_i = \frac{Y^m(a_i) - Y^m(a_{i-1})}{Y^m(a_{i-1})a_i - Y^m(a_i)a_{i-1}} \qquad \delta_i = \frac{Y^m(a_{i-1})a_i - Y^m(a_i)a_{i-1}}{a_i - a_{i-1}} \tag{3.32}
$$

giving the result,

$$
\mathbf{I} = \begin{cases} -\frac{2}{(m-2)a^{(m-2)/2}} - 2\beta^{(m-2)/2}\tan^{-1}(\sqrt{\beta a}) & \beta \geq 0 \\[2mm] -\frac{2}{(m-2)a^{(m-2)/2}} + (-\beta)^{(m-2)/2}\ln\frac{1+\sqrt{-\beta a}}{1-\sqrt{-\beta a}} & \beta < 0 \end{cases} \tag{3.33}
$$

The above solution is simpler than the one presented earlier, but uses the generally more non-linear power m of the geometry function in the linearization.

When a lower threshold on the stress intensity factor is included in the formulation, the product $Y(a)B_{th}(a)^{1/m}$, or $Y(a)^m B_{th}(a)$) is linearized over each integration segment, and the same procedure is applied.

3.3   Defect Distribution Model

From a fracture mechanics point of view, a weld containing a number of crack initiation sites from weld defects may be modeled as a weakest link system with a random number of links, where the links represent the different crack initiation sites.

Ditlevsen [20] investigated this topic and suggested a simple homogeneous Poisson link model to describe the distribution of crack sites along the weld. This model assumes the location of crack initiation sites along the weld to be Poisson distributed, neglecting the effect of possible clustering. The assumption of Poisson distributed weld defects might not be satisfactory, since practical experience shows that weld defects tend to occur in clusters. However, in the evaluation of the failure probabilities of series systems, it is the expected number of components in the system that is of importance, and an exact modeling of the underlying location distribution has reduced importance.

Applying the homogeneous Poisson process to describe the distribution of defects along the weld, the number of crack sites n along the weld length l is given by,

$$P_N(n) = \frac{(\mu l)^n}{n!} e^{-\mu l} \tag{3.34}$$

where μ is the defect intensity, or the expected number of defects per unit length for the homogeneous defect distribution process.

A Poisson process has equal mean value and variance, and the relationship between the variance and the mean value of crack sites along the weld seam will then give a description of the degree of crack site clustering. An approach to describe the distribution of crack sites along the weld including the effect of clustering, is to apply a homogeneous Poisson process to model the distribution of cluster groups along the weld, where the number of crack sites within each cluster group is described by, e.g., another Poisson distribution. Applying μ to define the intensity of cluster groups k, and ν to define the expected number of crack sites m within each cluster group,

$$P_K(k) = \frac{(\mu l)^k}{k!} e^{-\mu l} \qquad P_M(m) = \frac{\nu^m}{m!} e^{-\nu} \tag{3.35}$$

the expected number and variance of crack sites along the weld is,

$$E[n] = E[km] = E[k]E[m] = \mu l \nu \tag{3.36}$$

$$Var[n] = E[n^2] - E[n]^2 = E[k^2 m^2] - E[km]^2 = \mu l \nu + (\mu l)^2 \nu + \mu l \nu^2 \tag{3.37}$$

This model defines a very simple procedure to include the effect of crack site clustering along a homogeneous weld. The clustering effect is modeled by fitting the mean number and variance of the double Poisson process to measured or experimental values.

More advanced defect distribution models can indeed be applied, e.g., the on-off Markov process suggested by Ditlevsen [20], but for the present application evaluating the fatigue failure probability of a continuous weld, the homogeneous Poisson link model is considered satisfactory.

3.4 Probabilistic Fracture Mechanics Model

Fatigue in marine structures is a highly complex phenomena affected by a considerable number of factors having large uncertainties. To properly account for these uncertainties, a probabilistic fatigue fracture mechanics model is applied. In the investigated fatigue analysis, a continuous weld having equivalent material parameters over the entire length is considered. The weld is defined as to have a number of crack initiation sites over the length due to welding defects, where all the crack sites are being exposed to the same stochastic loading process.

3.4.1 Uncertainty Modeling

The uncertainties related to the computation of the size of a fatigue crack over time can generally be grouped into inherent physical uncertainty, model uncertainty and statistical uncertainty.

- **Inherent Uncertainty**

  Inherent uncertainty is usually associated with physical randomness that, from a practical point of view, is not possible to predict.

  Inherent uncertainty exists in the description of the environment the ship is exposed to over the lifetime due to, *e.g.*, inherent randomness in the encountered sea states and wave heading angles. Inherent uncertainty is also connected with the distribution of weld defects along the continuous weld and in the evaluation of initial crack sizes from weld defects.

- **Model Uncertainty**

  Model uncertainty originates from simplifications and ignorance in the theoretical model being applied to describe a physical phenomena. These uncertainties can be of both a systematic (*e.g.*, systematic underestimation) or random nature.

  Model uncertainties in the applied formulation exist both in the computation of the load response on the ship structure and in the evaluation of the fatigue capacity for the different details. For the response model, model uncertainties are associated with, *e.g.*, use of linear theory in the evaluation of the short term response model and the accuracy of the finite element analysis being applied to determine the local stresses. For the fatigue capacity model, model uncertainties exist with respect to, *e.g.*, the validity of the applied linear elastic fracture mechanics model to evaluate the true fatigue damage and the modeling of the geometry function.

  The systematic model uncertainties are included through the use of bias factors, having a stochastic description to account for uncertainties in the modeling.

- **Statistical Uncertainty**

  Statistical uncertainty is defined as uncertainty in the parameter modeling due to lack of

statistical information. Statistical uncertainties can be associated with both deterministic parameters and distribution parameters in the stochastic modeling of inherent uncertainties.

Statistical uncertainties are applied in the modeling of the defect intensity of the homogeneous Poisson defect distribution model, and in the modeling of the distribution parameters in the initial crack size distribution.

These uncertainties are quantified and expressed through stochastic variables in the probabilistic analysis.

The mathematical formulation of the crack size as a function of time for a single crack site is given by Equation (3.17). The different types of uncertainties influence the estimate of the size of this crack and also the distribution of crack sites along the continuous weld.

Long Term Stress Range Distribution

The local longterm stress range distribution is defined as Weibull distributed with distribution parameters A and B. It is seen from Equation (3.6), that the contribution from physical uncertainties in the environmental description is of minor importance in the fatigue analysis, due to the large number of load cycles. However, modeling uncertainties in the computation of the local stress range response from the environmental description leads to uncertainties in the estimated value of the moments of the longterm stress range distribution. These uncertainties are included in the probabilistic fatigue model through a bi-variate stochastic description of the Weibull distribution parameters A and B, equal for all the investigated crack sites along the continuous weld.

The uncertainties in the Weibull distribution parameters are then a lumped representation of the uncertainties in the longterm characterization of the environmental conditions, the load model, the global response analysis and the calculation of the local reference stresses.

The procedure for incorporation of the load response modeling uncertainties in the stochastic description of the Weibull distribution parameters are described in detail in Chapter 6, where a longterm frequency response analysis is conducted. The systematic model uncertainties in the derivation of the load response are automatically included in the derivation of the bi-variate stochastic description of the Weibull distribution parameters.

Fatigue Crack Growth Model

Uncertainties in the ability of the linear elastic fracture mechanic model to give an adequate measure of the accumulated fatigue damage for the different weld defects, is modeled through a bi-variate stochastic description of the crack growth material parameters C and m. It is further assumed that the local area of the structure investigated is fabricated by the same material and weld-steel, giving a homogeneous stochastic description of the material parameters over the weld length.

74

To account for uncertainties in the local crack geometry and in the crack configuration, a stochastic description of the geometry function $Y(a)$ is included in the fatigue model.

The critical crack size leading to failure is defined in the analysis as the plate thickness, which for a ship containing liquid cargo leads to leakage with ensuing environmental consequences. Other definitions of the critical crack size could be applied, *e.g.*, a crack size corresponding to intensive repair or a crack size giving a critical fracture toughness for the detail. However, due to the rapid crack growth rate in the final stage of the fatigue life, the fatigue formulation is relatively insensitive to the definition of the size of the critical crack.

Systematic model uncertainties in the evaluation of the fatigue capacity are defined through the bias factor Y_0, having a stochastic description to account for the random model uncertainties.

Weld Defect

The distribution of crack sites due to welding defects is modeled as Poisson distributed along the continuous weld, having defect intensity μ. Statistical uncertainty is associated with the value of the defect intensity, since it will typically be a function of the welding procedure being applied. In the following, the defect intensity is modeled through a conjugate Gamma distribution.

The uncertainties in the equivalent initial crack sizes from welding defects are modeled by assuming independently identically distributed stochastic initial crack sizes at the different crack sites, where Gamma distributed initial crack sizes are applied. Statistical uncertainties in the modeling the initial crack size distribution are expressed through a stochastic modeling of the Gamma distribution parameters.

Statistical uncertainties are introduced in the modeling of the distribution of crack sites along the weld and in the modeling of the crack size distribution function, due to lack of concise information in the modeling of the influence of welding procedures on the outcome of surface weld defects and defects sizes.

3.4.2 Inspection Model

Marine structures are commonly inspected for crack sites during their service time to upgrade the estimated fatigue reliability level of the structure. These inspections can be performed at periodic or non-periodic time intervals and include the whole, or only parts of the structure at each inspection.

The quality of the inspections are modeled through the probability of detecting an existing crack, where the probability for crack detection depends on the size of the crack, the inspection method applied, and the experience of the inspection team. The inspection quality is commonly defined through the probability of crack detection (POD) curve, modeling the detection probability as a function of the size of the crack, $P(D \mid a)$. The shape and form of the POD curve is unique for each inspection method (and inspection team), and is defined from experience.

From the POD curve, a smallest detectable crack size, a_d, is defined, Madsen [53]. The probability of detecting a crack of size a is equal to the probability that the smallest detectable crack size is smaller than a. The cumulative distribution function of a_d is then derived from the POD curve,

$$F_{A_d}(a) = P(A_d \leq a) = P(D \mid a) \tag{3.38}$$

The above procedure for defining a smallest detectable crack size from the POD curve, is only valid for inspection methods having a monotonically increasing crack detection probability with the crack size, and will not be valid in cases where, e.g., the inspection method has interference in the detection of a certain crack size, leading to a local decrease in the detection probability.

Different cumulative distribution functions can be applied to describe the smallest detectable crack size, depending on the goodness of the fitting to the experimentally developed POD curve. In the following, a shifted Gamma distribution with inspection quality q is applied to model the smallest detectable crack size,

$$F_{Ad}(a) = \frac{\Gamma(k; q(a - a_{min}))}{\Gamma(k)} \tag{3.39}$$

having mean detectable crack size,

$$E_{Ad}[a] = \frac{k}{q} + a_{min} \tag{3.40}$$

where a_{min} is the lower level for possible crack detection for the applied inspection method, and k is the shape parameter. $k = 1$ gives the more commonly applied exponential form of the POD curve.

The defined smallest detectable crack sizes can be modeled as independent or correlated stochastic variables for the different crack initiation sites, depending on how the information provided by the POD curve is interpreted;

- The probability for a given inspector to detect a crack with a specified inspection method is defined by a step function at a_d, modeling, respectively, no-detection and detection of a crack size smaller and larger than the detectable crack size a_d, see Figure 3.2a. However, the value of a_d will change from inspector to inspector, and is therefore unknown. The information provided by the POD curve is based on experience, and gives the distribution function of the detectable crack size for different inspectors. Applying this philosophy, the POD curve stochastically models the value of the unknown detectable crack size a_d for the inspector performing the inspection, and the same detectable crack size is valid over the whole length examined at each inspection.

- The probability for a given inspector to detect a crack with a specified inspection method is defined through the POD curve, where the probability of the inspector detecting a crack of size a_1 is independent of whether or not he has detected a crack of size a_2, see Figure 3.2b. The POD curve then describes the probability for an inspector to detect a crack as a function of the crack size, and the defined smallest detectable crack size is independent from inspection site to inspection site.
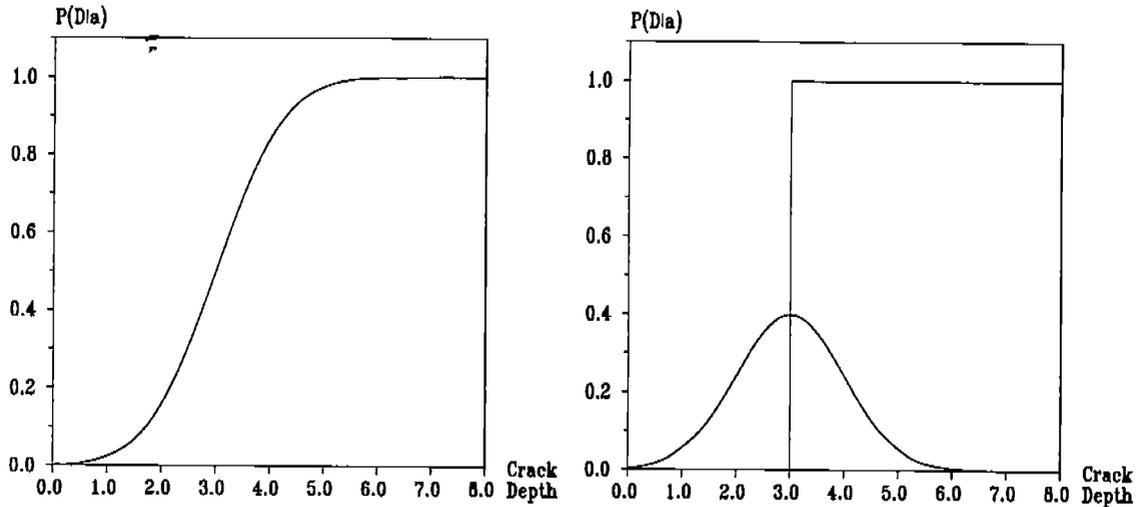
Figure 3.2: Interpretation of POD data for multiple inspected crack sites.

The different ways of applying the information provided by the POD curve do not influence the reliability formulation when only a single site is examined at each inspection, but for multiple examination sites at each inspection the various definitions will lead to different probabilistic inspection models. However, it would be reasonable to assume, that for an inspection along a continuous weld being performed by the same inspector, typically will result in a high correlation in the detectable crack size for the different inspection sites.

The probabilistic updating of the presented series system model includes both of the above formulations, having an equal detectable crack size and an independent detectable crack size for the different inspection sites over the inspection domain. Both models are assumed to have independent detectable crack sizes at different inspection times.

3.5 Bayesian Updating

The initial estimate of an unknown parameter can be updated through Bayesian updating as more information about the system is achieved. If a prior distribution $f'(\theta)$ is assumed for the unknown parameter θ, the updated posterior distribution of this parameter based on the information ϵ is,

$$f''(\theta) = f'(\theta \mid \epsilon) = \frac{P(\epsilon \mid \theta)f'(\theta)}{\int_{\Theta} P(\epsilon \mid \theta)f'(\theta)d\theta} \sim P(\epsilon \mid \theta)f'(\theta) \tag{3.41}$$

where $P(\epsilon \mid \theta)$ is the conditional probability, or likelihood, of observing the information ϵ, given the value of the parameter θ. The function is commonly referred to as the likelihood function of θ, denoted $L(\theta)$. The posterior distribution is then,

$$f''(\theta) = KL(\theta)f'(\theta) \sim L(\theta)f'(\theta) \tag{3.42}$$

where the parameter $K = [\int_{\Theta} L(\theta) f'(\theta) d\theta]^{-1}$ is the normalizing parameter.

In the following, Bayesian updating is applied to update the statistical uncertainties associated with the defect intensity in the Poisson distribution of weld defects, as information from inspections becomes available. A procedure is also presented for Bayesian updating of the statistical uncertainties of the scale parameter in the Gamma distribution of the independently identically distributed initial crack sizes. However, the scale and shape parameters in the Gamma crack size distribution are later indirectly updated together with the other model uncertainties through the formulation of inspection event margins.

3.5.1 Defect Occurrence along the Weld

A Poisson defect distribution model with defect intensity μ is assumed, modeling the location of crack sites along the weld. The value of the defect intensity is not known and is described through a prior distribution function, applying the conjugate Gamma distribution,

$$P_N(n) = \frac{(\mu l)^n}{n!} e^{-\mu l} \quad ; \quad f(\mu) = \frac{\nu(\nu\mu)^{\xi-1}}{\Gamma(\xi)} e^{-\nu\mu} \tag{3.43}$$

where ξ and ν are the shape and scale parameters in the Gamma distribution describing the defect intensity μ.

Inspection with Detection of all Cracks

Assuming a perfect inspection model where all crack sites over the examined part of the weld are detected, the likelihood function of the inspection outcome is,

$$L(\mu) = \prod_{i=1}^{n_{insp}} \frac{(\mu l_i)^{m_i}}{m_i!} e^{-\mu l_i} \tag{3.44}$$

where m_i is the number of (detected) defects over the inspected part of the weld l_i for inspection i, out of n_{insp} number of inspections at different areas of the weld. The updated posterior distribution of the defect intensity after inspection is,

$$f''(\mu) \sim L(\mu) f'(\mu) = \prod_{i=1}^{n_{insp}} \frac{(\mu l_i)^{m_i}}{m_i!} e^{-\mu l_i} \frac{\nu'(\nu'\mu)^{\xi'-1}}{\Gamma(\xi')} e^{-\nu'\mu} \tag{3.45}$$

giving,

$$f''(\mu) = \frac{\nu''(\nu''\mu)^{\xi''-1}}{\Gamma(\xi'')} e^{-\nu''\mu} \tag{3.46}$$

where,

$$\xi'' = \xi' + \sum_{i=1}^{n_{insp}} m_i \qquad \nu'' = \nu' + \sum_{i=1}^{n_{insp}} l_i$$

Inspection Including Probability of Crack Detection

All the crack sites over the inspected part of the weld are not necessarily found, unless a perfect inspection with an infinite inspection quality is performed. For non-perfect inspections, the updating of the defect intensity distribution must be modified to include the probability of detecting an inspected crack site.

The probability of detecting an inspected crack site at time t_i is

$$p_d = \int_0^\infty P(D \mid a) f_{A(t_i)}(a) \, da = P(A_d - A(t_i) \le 0) \tag{3.47}$$

where A_d is the smallest detectable crack size and $A(t_i)$ is the stochastic crack size at the time of inspection.

Assuming independent detection probabilities at the different inspection sites, the distribution of undetected defects along the examined area of the weld is described through a filtered homogeneous Poisson distribution with defect intensity $(1 - p_d)\mu$.

$$
\begin{aligned}
P_K(k) &= P_N(k + m \mid m) = \frac{P_B(m \mid k + m) P_N(k + m)}{\sum_{j=0}^\infty P_B(m \mid j + m) P_N(j + m)} \\
&= \frac{\frac{(k+m)!}{m!k!} p_d{}^m (1 - p_d)^k \frac{(\mu l)^{k+m}}{(k+m)!} e^{-\mu l}}{\sum_{j=0}^\infty \frac{(j+m)!}{m!j!} p_d{}^m (1 - p_d)^j \frac{(\mu l)^{j+m}}{(j+m)!} e^{-\mu l}} \\
&= \frac{((1 - p_d)\mu l)^k}{k!} e^{(1 - p_d)\mu l} \tag{3.48}
\end{aligned}
$$

where m is the number of detected defects. The result is seen directly, but is derived here to show the use of the Binomial distribution P_B, requiring independent detection probabilities at the different inspection sites. This requirement is, strictly speaking, not satisfied, since the different independent initial crack sizes are influenced by the same stochastic fatigue crack growth model, leading to an increasing correlation in the exceedance probabilities for the different sites with increasing threshold levels. However, for the threshold levels typically leading to crack detection, the correlation among the detection probabilities is relatively low, $(10\% \sim 30\%)$, and the above assumption is justified. The effect of correlation in the detection probabilities for multiple crack sites is investigated closer in the numerical study in Section 4.7.

Based on the assumption of independent detection probabilities, the distribution of detectable crack sites along the weld is Poisson distributed with defect intensity $p_d\mu$,

$$P_M(m) = \frac{(p_d \mu l)^m}{m!} e^{-p_d \mu l} \tag{3.49}$$

The posterior Gamma distribution of μ is then found by applying the distribution of detectable crack sites in the expression for the likelihood function,

$$f''(\mu) \sim L(\mu) f'(\mu) = \prod_{i=1}^{n_{insp}} \frac{(p_{di} \mu l_i)^{m_i}}{m_i!} e^{-p_{di} \mu l_i} \frac{\nu'(\nu'\mu)^{\xi'-1}}{\Gamma(\xi')} e^{-\nu'\mu} \tag{3.50}$$

which gives the posterior expression,

$$f''(\mu) = \frac{\nu''(\nu''\mu)^{\xi''-1}}{\Gamma(\xi'')} e^{-\nu'\mu} \qquad (3.51)$$

where,

$$\xi'' = \xi' + \sum_{i=1}^{n_{insp}} m_i \qquad \nu'' = \nu' + \sum_{i=1}^{n_{insp}} p_{di} l_i$$

For multiple inspections of the same areas of the weld, the Poisson distribution of the previously undetected crack sites creates the basis for the updating of the defect intensity μ. The probability of detecting a previously undetected crack site for inspection n is,

$$
\begin{aligned}
p_d &= \int_0^\infty P(D \mid a) f_{A(t)|\bar{D}_1...\bar{D}_{n-1}}(a)\, da \\
&= P\left(A_{dn} - A(t_n) \le 0 \mid A_{d1} - A(t_1) > 0 \cap \ldots \cap A_{dn} - A(t_n)\right)
\end{aligned}
\qquad (3.52)
$$

Due to the assumption of a homogeneous Poisson defect distribution model, the posterior distribution of the defect intensity μ is valid over the whole weld length.

3.5.2 Initial Crack Size Distribution

A Gamma distribution function with shape and scale parameters k and λ is applied to describe the distribution of the independent initial crack sizes from weld defects. The distribution parameters are modeled as unknown in the probabilistic analysis, and are indirectly updated from inspection results through the modeling of event margins.

A more traditional approach, where the distribution parameters are updated through Bayesian updating can, however, be formulated. Assuming known shape parameter k and unknown scale parameter λ, defined through the prior Gamma distribution $f(\lambda)$,

$$f_{A_0}(a_0) = \frac{\lambda^k a_0{}^{k-1} e^{-\lambda a_0}}{\Gamma(k)} \qquad f(\lambda) = \frac{\kappa^g \lambda^{g-1} e^{-\kappa\lambda}}{\Gamma(g)} \qquad (3.53)$$

where κ and g are scale and shape parameter in the prior distribution of λ, the following expressions are derived.

Inspection with Detection of all Cracks

The initial crack size distribution is updated based on measurements of the size of detected cracks at the time of inspection. The initial crack sizes a_{0i} are then not measured explicitly, but are estimates based on backtracking, applying the crack growth equation,

$$a_{0i} = h(a_i) = \Psi^{-1}\left(\Psi(a_i) - C\nu_0 r t_1 E[\Delta\sigma^m]\right) \qquad (3.54)$$

where a_i is the measured crack size at the time of inspection.

For a deterministic fatigue crack growth model, the likelihood function for an inspection outcome of m defect detections is,

$$
\begin{aligned}
L(\lambda) &= f_{\mathbf{A}(t)}(a_1, a_2 \ldots a_m) = \prod_{i=1}^{m} f_{A_0}(h(a_i)) \left| \frac{dh(a)}{da} \right|_{a=a_i} \\
&\sim \prod_{i=1}^{m} \frac{\lambda^k h(a_i)^{k-1} e^{-\lambda h(a_i)}}{\Gamma(k)} \sim \lambda^{mk} \exp\left(-\lambda \sum_{i=1}^{m} h(a_i)\right)
\end{aligned}
\tag{3.55}
$$

The corresponding posterior estimate of the distribution of the scale parameter λ is,

$$
f''(\lambda) \sim L(\lambda) f'(\lambda) \sim \lambda^{mk+g'-1} \exp\left(-\lambda \sum_{i=1}^{m} h(a_i) + \lambda \kappa'\right)
\tag{3.56}
$$

giving the Gamma posterior distribution,

$$
f''(\lambda) = \frac{\kappa''^{g''} \lambda^{g''-1} e^{-\kappa''\lambda}}{\Gamma(g'')}
\tag{3.57}
$$

with parameters,

$$
g'' = g' + mk \qquad \kappa'' = \kappa' + \sum_{i=1}^{m} h(a_i)
$$

For non-deterministic parameters in the fatigue crack growth equation, exact estimates of the corresponding initial crack sizes can not be predicted from the detected and measured crack sizes at the time of inspection. Expressing the stochastic variables in the crack growth equation by $\mathbf{X}$, the likelihood function of the inspection outcome is,

$$
\begin{aligned}
L(\lambda) &= \int_{\mathbf{X}} L(\lambda \mid \mathbf{x}) f_{\mathbf{X}}(\mathbf{x}) \, d\mathbf{x} \\
&\sim \int_{\mathbf{X}} \prod_{i=1}^{m} [f_{A_0}(h(a_i, \mathbf{x}))] f_{\mathbf{X}}(\mathbf{x}) \, d\mathbf{x}
\end{aligned}
\tag{3.58}
$$

The expression is difficult to solve analytically, and it is suggested that a numerical simulation procedure be applied. The likelihood function then has the form,

$$
L(\lambda) \sim \lambda^{mk} e^{-\alpha\lambda}
\tag{3.59}
$$

giving Gamma distribution parameters for the posterior distribution of λ,

$$
g'' = g' + mk \qquad \kappa'' = \kappa' + \alpha
$$

where α is defined from the simulation.

Inspection including Probability of Crack Detection

For non-perfect inspections, all the crack sites over the examined area of the weld are not necessarily found. Depending on the form of the POD curve, a higher probability exists for detecting larger

cracks. This higher probability introduces bias, leading to an underestimation of the posterior scale parameter in the initial crack size distribution.

However, by applying the crack size distribution function conditioned on detection in the estimation of the likelihood function, an unbiased estimate of the scale parameter is achieved. The conditional crack size distribution function is given as,

$$f_{A|D}(a) = \frac{P(D \mid a)f_A(a)}{p_d} \tag{3.60}$$

where p_d is the probability of detecting an inspected crack site and $f_A(a)$ is the crack size distribution at the time of inspection. The probability of crack detection depends on the scale parameter λ,

$$
\begin{aligned}
p_d(\lambda) &= \int_0^\infty P(D \mid a)f_A(a)\, da \\
&= \int_0^\infty P(D \mid a)f_{A_0}(h(a)) \left| \frac{dh(x)}{dx} \right|_{x=a} da \\
&\sim \int_0^\infty P(D \mid h^{-1}(a_0))f_{A_0}(a_0)\, da_0
\end{aligned}
\tag{3.61}
$$

where the initial crack size distribution function f_{A_0} is a function of λ.

For a deterministic fatigue crack growth model, the likelihood function of the scale parameter λ having m observations is,

$$
\begin{aligned}
L(\lambda) &= f_{\mathbf{A}(t)|D}(a_1, a_2 \ldots a_m) = \prod_{i=1}^m \frac{P(D \mid a)f_{A_0}(h(a_i)) \left| \frac{dh(a)}{da} \right|_{a=a_i}}{p_d(\lambda)} \\
&\sim \prod_{i=1}^m \frac{f_{A_0}(h(a_i))}{p_d(\lambda)} \sim \frac{\lambda^{mk} \exp\left(-\lambda \sum_{i=1}^m h(a_i)\right)}{p_d(\lambda)}
\end{aligned}
\tag{3.62}
$$

Including a stochastic description of the parameters in the fatigue crack growth equation, the likelihood function is,

$$
\begin{aligned}
L(\lambda) &= \int_{\mathbf{X}} L(\lambda \mid \mathbf{x})f_{\mathbf{X}}(\mathbf{x})\, d\mathbf{x} \\
&\sim \int_{\mathbf{X}} \prod_{i=1}^m \left[\frac{f_{A_0}(h(a_i, \mathbf{x}))}{p_d(\lambda, \mathbf{x})} \right] f_{\mathbf{X}}(\mathbf{x})\, d\mathbf{x}
\end{aligned}
\tag{3.63}
$$

It is again suggested that the expression be solved by using numerical simulation, resulting in an expression of the likelihood function of the form,

$$L(\lambda) \sim \lambda^{\beta_1 k} e^{-\beta_2 \lambda} \tag{3.64}$$

giving Gamma distribution parameters for the posterior distribution of λ,

$$g'' = g' + \beta_1 k \qquad \kappa'' = \kappa' + \beta_2$$

The above defined model for updating of the distribution parameters in the initial crack size distribution function is tedious due to the indirect way the initial crack sizes are estimated from measured crack sizes. However, if the statistical uncertainties of the initial crack size distribution function are modeled together with the inherent and model uncertainties in the stochastic modeling of the limit state function, an implicit updating of the prior estimate of the distribution parameters in the initial crack size distribution from inspection results is achieved. The formulation can easily include statistical uncertainties on both the shape and scale parameters, k and λ, in the initial crack size distribution function. This procedure is applied in Chapter 4.

84

Chapter 4

Reliability of Continuous System

4.1 Introduction

Fatigue reliability of welded structures has recently been an area of considerable research, having application to a wide range of marine structures, *e.g.*, jacket structure, semi-submersibles, TLPs and tankers. However, most of this work has been focused on the fatigue reliability of single fatigue sensitive joints, *e.g.*, Madsen *et al.* [53], Shetty and Baker [79] and Wirsching *et al.* [95], not including the effect of multiple crack initiation sites. For a realistic evaluation of the fatigue reliability of welded structures, the contribution to the fatigue failure probability from all the crack sites over the investigated area of the structure has to be considered.

In the following, a probabilistic procedure estimating the fatigue reliability of a welded structure consisting of multiple crack initiation sites over a continuous weld is derived. The formulation is presented for structures having both a known and a stochastic description of the location of crack sites.

The probabilistic fatigue model for the structure is defined as a series system, and the fatigue reliability of the structure is derived as the fatigue reliability of the crack site having the lowest fatigue resistance.

The probabilistic fatigue model is extended to include the effect of inspection updating, where parts of, or the whole structure is examined in each inspection.

In Section 4.2, the fatigue reliability model for a single crack site is presented, including the formulation of fatigue reliability updating from inspection results. In Section 4.3, the fatigue reliability of a continuous system having a deterministic number of crack sites is derived. Section 4.4 extends this formulation to include systems having a stochastic description of the number and location of crack sites over the structure. In Section 4.5, the incorporation of inspection results from examination of parts of the whole structure in the estimated updated fatigue reliability is formulated. Section 4.6 discusses briefly the concept of the estimated failure probability where both model and

statistical uncertainties are included in the reliability formulation in addition to the inherent physical uncertainties. A numerical study investigating the derived reliability model is presented in Section 4.7.

4.2   Single Crack Site

4.2.1   Fatigue Reliability Model

Defining the fatigue failure criteria as crack growth beyond a defined critical crack size a_c, the limit state function for a single crack site is formulated as, Madsen *et al.* [53],

$$g(\mathbf{x}) = a_c - a(t) \tag{4.1}$$

where $a(t)$ is the crack size at time t,

$$a(t) = \Psi^{-1}\left(\Psi(a_0) + Cr\nu_0 t E[\Delta\sigma^m] B_{cor}(t)\right) \tag{4.2}$$

and

$$\Psi(a) = \int_0^a \frac{1}{B_{th}(x)\left(Y(x)\sqrt{\pi x}\right)^m} \, dx \tag{4.3}$$

Based on the presented uncertainty model, the probability of having a crack size exceeding the critical crack size over the time period t is,

$$P_F = P(M(t) \le 0) \tag{4.4}$$

where the safety margin $M(t)$ is,

$$M(t) = a_c - a(t) \tag{4.5}$$

The model defines the fatigue failure probability of a single crack site due to fatigue crack growth.

4.2.2   Inspection Updating

The initially estimated fatigue failure probability of a single crack site is updated as information from inspections becomes available.

An inspection event margin $H(t)$ is defined,

$$H(t_i) = a_d - a(t_i) \tag{4.6}$$

where a_d is the smallest detectable crack size derived from the POD curve. The inspection event is positive if the crack size is smaller than the smallest detectable crack size at the time of inspection, resulting in no crack detection, and non-positive otherwise, resulting in crack detection;

No crack detection : $H > 0$
Crack detection   : $H \leq 0$

The updated fatigue failure probability of an inspected crack site having no crack detection is then written as, Madsen *et al.* [53],

$$P_F(t) = P(M(t) \leq 0 \mid H(t_i) > 0) = \frac{P(M(t) \leq 0 \cap H(t_i) > 0)}{P(H(t_i) > 0)} \qquad (4.7)$$

Having multiple inspections of the same crack site, the same formulation is applied. For a crack site being inspected n times, resulting in crack detection for, *e.g.*, inspection n only, the updated fatigue failure probability in the time period after inspection n is,

$$P_F(t) = P(M(t) \leq 0 \mid H(t_1) > 0 \cap \ldots \cap H(t_{n-1}) > 0 \cap H(t_n) \leq 0) \qquad (4.8)$$

The stochastic variable a_d, defining the smallest detectable crack size at each inspection, is modeled independent at the different times of inspection. The time period between consecutive inspections is typically in the order of 5-10 years.

If the detected cracks in addition are measured, more information from the inspection outcome is utilized by defining a detection event $D(t)$,

$$D(t_i) = a_m - a(t_i) \qquad (4.9)$$

where a_m is the detected and measured crack size. The detection event is equal to zero, since the size of the detected crack is equal to the measured crack size. If uncertainties are related to the measured crack size, a_m is modeled as a stochastic variable. The updated fatigue failure probability of a crack site being detected and measured at the second inspection is written as,

$$P_F(t) = P(M(t) \leq 0 \mid H(t_1) > 0 \cap D(t_2) = 0) \qquad (4.10)$$

For detected and repaired defects, the same approach is applied, where the modeling of the safety margin after repair, with respect to initial crack size and material parameters, depends on the type of repair, weld repair or grind repair. For weld repair new independent material parameters are to be applied, whereas for grind repair, if the crack initiation site is not removed completely, the same material parameters are applied.

4.3   Deterministic Number of Crack Sites

To model the effect of multiple crack sites over the continuous weld, the weld is modeled as a weakest link system. The links represent the crack initiation sites, and the weakest link corresponds to the crack site with the smallest safety margin. Based on the model with common uncertainties on the loading and material parameters over the continuous weld length, the weakest link is the crack site with the largest initial crack size a_0.

The fatigue failure criterion for the continuous weld is defined as crack growth beyond a critical crack size for one or more of the n crack sites along the weld. The fatigue failure probability of the weld is then equal to the failure probability of a series system having n components. The safety margin of the weld at time t is given by,

$$
\begin{aligned}
M_{\min n}(t) &= \min_{i=1,n}\left[a_c - a_i(t)\right] = a_c - \max_{i=1,n}\left[a_i(t)\right] \\
&= a_c - \max_{i=1,n}\left[\Psi^{-1}\left(\Psi(a_{0i}) + C\nu_0 rtE[\Delta\sigma^m]\right)\right] \\
&= a_c - \Psi^{-1}\left(\Psi\left(\max_{i=1,n} a_{0i}\right) + C\nu_0 rtE[\Delta\sigma^m]\right)
\end{aligned}
\tag{4.11}
$$

where $\max_{i=1,n} a_{0i}$ defines the largest initial crack size of the n crack initiation sites. The above derivation is conducted within the limit state function during each iteration of the full distribution reliability calculation, and is therefore conditioned on the outcome of the common stochastic variables. The derivation utilizes the monotonic increase of the function $\Psi(a)$ with a, see Equation (4.3).

The safety margin $M_{\min n}$ is negative if any of the n crack sizes along the weld are larger than the critical crack size a_c at time t. The failure probability of the weld is then equal to the failure probability of the crack site with the largest initial crack size,

$$
P_{Fsys}(t) = P(M_{\min n}(t) \leq 0)
\tag{4.12}
$$

Given the distribution of the largest initial crack size, it is possible to compute the failure probability for the weld seam through a simple component estimate, applying full distribution reliability methods.

The distribution of the largest initial crack size is equivalent to the maximum extreme value distribution of the initial crack size distributions. The initial crack size distributions are independent and identically distributed, and the extreme value distribution is therefore easily obtained applying order statistics,

$$
F_{\max A_0}(a) = P(\max_{i=1,n} A_{0i} \leq a) = P(A_0 \leq a)^n = F_{A_0}^n(a)
\tag{4.13}
$$

where n is the deterministic number of crack sites considered.

The argument of the extreme value distribution, modeling the largest initial crack size, is conveniently described in terms of an auxiliary standard normally distributed variable u as,

$$
F_{\max A_0}(a) = \Phi(u)
\tag{4.14}
$$

$$\Downarrow$$

$$a_{\max} \quad = \quad F_{A_0}^{-1}(\Phi(u)^{1/n}) \tag{4.15}$$

The cumulative distribution function of the initial crack size, F_{A0}, is easily inverted.

4.4 Stochastic Number of Crack Sites

To model the effect of multiple crack sites over the continuous weld having a stochastic number of crack sites, the weld is modeled as a weakest link system with a random number of links, where the links represent the crack initiation sites from weld defects. A homogeneous Poisson distribution is applied to model the stochastic description of crack sites along the weld seam.

Based again on the model with common uncertainties on the loading and material parameters over the continuous weld length, the weakest link is the crack site with the largest initial crack size a_0.

Applying the homogeneous Poisson crack site distribution model, the fatigue failure probability of the weld is defined as,

$$P_{Fweld}(t) = \sum_{n=0}^{\infty} P_{Fsys}(t \mid n)P_N(n) = \sum_{n=0}^{\infty} P_{Fsys}(t \mid n)\frac{(\mu l)^n}{n!}e^{-\mu l} \tag{4.16}$$

where μ is the intensity of crack sites over the weld length. An evaluation of the fatigue failure probability of the weld applying this approach, requires an (infinite) number of probabilistic evaluations of P_{Fsys} for different possible outcome of crack sites n over the weld length, requiring tedious computation. An estimate of the failure probability of the weld can also be achieved by applying the expected number of crack sites over the weld length, νl, in the evaluation of the failure probability of the series system, but this will only give an approximate value.

However, these problems are avoided and the computation is greatly simplified by including the stochastic description of the number of crack sites directly in the modeling of the safety margin of the weld $M_{\min n}(t)$. This is achieved by including the Poisson distribution of the number of crack sites n in the evaluation of the maximum extreme initial crack size distribution.

Special consideration must be taken regarding the possibility of not having any crack sites over the weld length. In the evaluation of the failure probability of the weld in accordance with Equation (4.16), this will not cause any problems, since the failure probability of the series system not having any crack sites is zero.

Two models are considered in the evaluation of the distribution function for the largest initial crack size, having a Poisson distributed number of crack sites;

- The intensity of crack sites μ is known.

- The intensity of crack sites μ is unknown, and described through the conjugate Gamma distribution $G(\xi, \nu)$.

$\mathscr{89}$

Having an unknown intensity of crack sites, the crack site intensity is updated applying Bayesian updating, as information from inspections becomes available.

4.4.1 Known Defect Intensity μ

For a known value of the crack site intensity μ in the Poisson distribution of crack initiation sites over the weld length, the extreme initial crack size distribution, conditioned on having one or more crack sites, is

$$
\begin{aligned}
F_{\max A0}(a) &= \sum_{n=1}^{\infty} F_{A0}^{n}(a) P_N(n) = \sum_{n=1}^{\infty} F_{A0}^{n}(a) \frac{(\mu l)^k}{k!} e^{-\mu l} \\
&= e^{-\mu l (1 - F_{A0}(a))} - e^{-\mu l}
\end{aligned}
\tag{4.17}
$$

The argument of the extreme value distribution is conveniently described through a normalized auxiliary cumulative standard normal distribution. It is necessary, however, to normalize the auxiliary distribution function in order to account for the non-zero probability of having no defects over the weld length.

The probability of having one or more defects over the weld length l is,

$$
P_N(n > 0) = 1 - e^{-\mu l}
\tag{4.18}
$$

leading to the expression for the largest initial crack size,

$$
F_{\max A0}(a) = (1 - e^{-\mu l}) \Phi(u)
\tag{4.19}
$$

$$
\Downarrow
$$

$$
a_{\max} = F_{A0}^{-1}\left(\frac{\ln\left((1 - e^{-\mu l})\Phi(u) + e^{-\mu l}\right)}{\mu l} + 1 \right)
\tag{4.20}
$$

The above expression is derived conditioned on the existence of crack sites over the weld seam. The fatigue failure probability of the weld is then written as,

$$
\begin{aligned}
P_{Fweld}(t) &= P(M_{\min n}(t) \le 0 \mid n > 0) \, P_N(n > 0) \\
&= P(M_{\min n}(t) \le 0 \mid n > 0)\,(1 - e^{-\mu l})
\end{aligned}
\tag{4.21}
$$

where the safety margin $M_{\min n}$ is defined by applying the formulation for the extreme initial crack size distribution given by Equation (4.20).

4.4.2 Unknown Defect Intensity μ

The statistical uncertainties on the defect intensity are expressed through a stochastic description of μ, for which the conjugate Gamma distribution is chosen, $f(\mu)$. The statistical uncertainties on μ influence the distribution of crack sites over the weld length and are included in the formulation

of the extreme initial crack size distribution of the Poisson distributed number of crack sites over the weld length.

Conditioning again on having crack sites over the weld length investigated, the maximum extreme initial crack size distribution is derived as,

$$
\begin{aligned}
F_{\max A_0}(a) &= \int_0^\infty \sum_{n=1}^\infty F_{A_0}^n(a) P_N(n) f(\mu) \; d\mu \\
&= \int_0^\infty \sum_{n=1}^\infty F_{A_0}^n(a) \frac{(\mu l)^n}{n!} e^{-\mu l} f(\mu) \; d\mu \\
&= \int_0^\infty \left(e^{-\mu l(1-F_{A0}(a))} - e^{-\mu l} \right) \frac{\nu(\nu\mu)^{\xi-1}}{\Gamma(\xi)} e^{-\nu\mu} \; d\mu \\
&= \frac{\nu^\xi}{(\nu + l(1 - F_{A_0}(a)))^\xi} - \frac{\nu^\xi}{(\nu + l)^\xi}
\end{aligned}
\tag{4.22}
$$

where ν and ξ are the scale and shape parameters of the Gamma distribution modeling the defect intensity μ.

The probability of having crack sites over the weld length is now equal to,

$$
\begin{aligned}
P_N(n > 0) &= \int_0^\infty (1 - e^{-\mu l}) f(\mu) \; d\mu = \int_0^\infty (1 - e^{-\mu l}) \frac{\nu(\nu\mu)^{\xi-1}}{\Gamma(\xi)} e^{-\nu\mu} \; d\mu \\
&= 1 - \frac{\nu^\xi}{(\nu + l)^\xi}
\end{aligned}
\tag{4.23}
$$

The argument of the maximum extreme initial crack size distribution is again derived applying the auxiliary standard normal distributed variable u, normalizing in order to account for the non-zero probability of having no defects over the weld,

$$
F_{\max A0}(a) = \left(1 - \frac{\nu^\xi}{(\nu + l)^\xi} \right) \Phi(u)
\tag{4.24}
$$

$$
\Downarrow
$$

$$
a_{\max} = F_{A_0}^{-1} \left(1 + \frac{\nu}{l} \left(1 - \frac{\nu + l}{(((\nu + l)^\xi - \nu^\xi)\Phi(u) + \nu^\xi)^{1/\xi}} \right) \right)
\tag{4.25}
$$

The above expression is derived conditioned on the existence of crack sites over the weld, giving the failure probability of the weld seam,

$$
\begin{aligned}
P_{Fweld} &= P(M_{\min n}(t) \le 0 \mid n > 0) P_N(n > 0) \\
&= P(M_{\min n}(t) \le 0 \mid n > 0) \left(1 - \frac{\nu^\xi}{(\nu + l)^\xi} \right)
\end{aligned}
\tag{4.26}
$$

where the safety margin $M_{\min n}$ is defined by applying the formulation for the extreme initial crack size distribution given by Equation (4.20).

4.5 Inspection Updating of System

4.5.1 Introduction

The initially estimated fatigue reliability estimate of the weld is updated over the service time of the structure as more information about the system is attained. The information gained from an inspection of the weld is applied in the updating of the uncertainties related to the system description. Since the same model uncertainties influence the whole weld length, inspection results from inspected areas of the weld will also influence the fatigue reliability estimate of the uninspected areas, in addition to the reliability estimate of the inspected areas.

The information achieved from an inspection results in;

- An updating of the statistical uncertainties in the intensity of crack sites along the weld, provided a stochastic prior distribution is assumed for the defect intensity. The statistical uncertainties on the distribution parameters for the initial crack size distribution are included in the probabilistic modeling of the system, and is implicitly updated from the inspection results.

- An updating of the estimated fatigue reliability of the crack sites over the inspected part of the weld.

- An updating of the estimated fatigue reliability of the potential crack sites over the uninspected part of the weld.

The quality of the inspections is described through the detectable crack size a_d, derived from the POD curve. The presented formulation is valid for both a deterministic and a stochastic description of the detectable crack size.

The derivation of the effect of inspection updating in the first two subsections is based on the assumption of having an equivalent detectable crack size over the whole inspection length for each inspection. Subsection 4.5.4 defines a similar approach, assuming independent detectable crack sizes at the different inspection sites.

4.5.2 Deterministic Number of Crack Sites

An inspection of n crack initiation sites at time t_j resulting in no crack detection, implies that the largest of the n inspected crack sizes is smaller than the smallest detectable crack size at the time of inspection.

The inspection event margin is then formulated as,

$$
\begin{aligned}
H_{\min n}(t_j) &= \min_{i=1,n} [a_d - a_i(t_j)] = a_d - \max_{i=1,n} [a_i(t_j)] \\
&= a_d - \max_{i=1,n} \left[\Psi^{-1} \left(\Psi(a_{0i}) + C\nu_0 r t_j E[\Delta\sigma^m] \right) \right]
\end{aligned}
$$

$$\vdots \qquad = \quad a_d - \Psi^{-1}\left(\Psi\left(\max_{i=1,n} a_{0i}\right) + C\nu_0 r t_j E[\Delta\sigma^m]\right) \qquad (4.27)$$

where both a stochastic or deterministic description of a_d is valid and $\Psi(a)$ is a monotonic increasing function of a. The event margin $H_{\min n}$ is positive if no cracks have been detected at the n inspection sites and negative if one or more cracks are observed.

The above derivation is based on the assumption of having an equivalent smallest detectable crack size at all the inspected sites.

The detection event is modeled in an equivalent manner, where the event is defined as being negative if all the sites crack included in the detection event formulation are detected, and positive otherwise. The detection event for k detected crack sites is then,

$$\begin{aligned}D_{\max k}(t_j) &= \max_{i=1,k}[a_d - a_i(t_j)] \\ &= a_d - \Psi^{-1}\left(\Psi\left(\min_{i=1,k} a_{0i}\right) + C\nu_0 r t_j E[\Delta\sigma^m]\right) \qquad (4.28)\end{aligned}$$

The minimum extreme initial crack size distribution is defined by applying order statistics,

$$\begin{aligned}F_{\min A_0}(a) &= P(\min_{i=1,k} A_{0i} \le a) = 1 - P(\min_{i=1,k} A_{0i} > a) \\ &= 1 - (1 - P(A_0 \le a))^k = 1 - (1 - F_{A_0}(a))^k \qquad (4.29)\end{aligned}$$

The argument of the minimum extreme initial crack size distribution is then again defined through the auxiliary standard normal variable u,

$$F_{\min A_0}(a) \quad = \quad \Phi(u) \qquad (4.30)$$

$$\Downarrow$$

$$a_{\min} \quad = \quad F_{A_0}^{-1}(1 - (1 - \Phi(u))^{1/k}) \qquad (4.31)$$

From the defined inspection and detection events, the estimated fatigue failure probability is updated from inspection results. The updated failure probability of a system consisting n crack sites being inspected at time t_j is considered, where k out of the n inspected crack sites resulted in the detection of a crack. Provided that no repair of the detected crack sites is conducted, the updated fatigue reliability of the system is,

$$\begin{aligned}P_{Fsys}(t) \quad = \quad & P(M_{\min n}(t) \le 0 \mid \\ & H_{\min(n-k)}(t_j) > 0 \cap D_{\max k}(t_j) \le 0) \\ = \quad & P(M_{\min(n-k)}(t) \le 0 \cup M_{\min k}(t) \le 0 \mid \\ & H_{\min(n-k)}(t_j) > 0 \cap D_{\max k}(t_j) \le 0) \qquad (4.32)\end{aligned}$$

In the above formulation, the safety margin $M_{\min n}$ is described through the union of the safety margins $M_{\min(n-k)}$ and $M_{\min k}$. The splitting of the total safety margin is conducted in order to

efficiently utilize the information provided from the inspection outcome. The same group of initial crack size distributions establishes the extreme value distributions for the safety and event margins. This means that the same extreme initial crack size distribution is applied in the modeling of both $M_{\min(n-k)}$ and $H_{\min(n-k)}$.

This will cause problems in the modeling of the events $M_{\min k}$ and $D_{\max k}$, derived based on the extreme maximum and minimum initial crack size distribution respectively. To utilize the information provided by the detection event in the evaluation of the safety margin, the bi-variate maximum and minimum extreme distribution has to be established in order to express the conditional cumulative maximum extreme distribution conditioned on the outcome of the minimum extreme distribution.

The minimum extreme distribution has been derived earlier, and the conditional maximum extreme value distribution for the initial crack size is given as,

$$F_{\max A0|\min A0}(a \mid a_{\min}) = \frac{F_{\max A0, \min A0}(a, a_{\min})}{F_{\min A0}(a_{\min})} \tag{4.33}$$

where $a_{\min}$ is defined from Equation (4.31). The corresponding argument of the conditional maximum crack size distribution to be applied in the limit state function is then found through an inversion of the marginal distribution,

$$F_{\max A0|\min A0}(a \mid a_{\min}) = \Phi(v) \tag{4.34}$$

where v is an auxiliary standard normal variable.

A simplified approach, not requiring the expression for the bi-variate distribution in utilizing the information from the detected crack sites is,

$$F_{\max}(a) = \left(\frac{F_{A0}(a) - F_{A0}(a_{\min})}{1 - F_{A0}(a_{\min})}\right)^{k} = \Phi(v) \qquad a \geq a_{\min} \tag{4.35}$$

$$\Downarrow$$

$$a_{\max} = F_{A0}^{-1}\left(F_{A0}(a_{\min}) + (1 - F_{A0}(a_{\min}))\Phi(v)^{1/k}\right) \tag{4.36}$$

where the cumulative initial crack size distribution has been normalized to account for the probability contents of having a crack size smaller than $a_{\min}$.

If the size of each detected crack is measured, the event of detection can be modeled more directly. One approach is to model each detected crack size separately through the detection event,

$$D_i(t_j) = a_i - \Psi^{-1}\left(\Psi(a_{0i}) + C\nu_0 r t_j E[\Delta\sigma^m]\right) \tag{4.37}$$

where a_i is the size of the measured crack i. Each of the events are modeled and included in the modeling of the inspection outcome. However, this will greatly complicate the reliability formulation for large number of crack detections.

Another suggested approach is to utilize the information of the largest of the detected and measured crack sizes, a_m. Applying this information, the detection event is written as,

$$
\begin{aligned}
D_{\min k}(t_j) &= \min_{i=1,k} [a_m - a_i(t_j)] \\
&= a_m - \Psi^{-1} \left(\Psi \left(\max_{i=1,k} a_{0i} \right) + C\nu_0 r t_j E[\Delta\sigma^m] \right)
\end{aligned}
\tag{4.38}
$$

The detection event is non-negative, since all the detected crack sizes are smaller or equal to a_m. This approach also eliminates the need for defining the bi-variate maximum-minimum extreme initial crack size distribution, since both the events $M_{\min k}$ and $D_{\min k}$ are based on the same maximum extreme initial crack size distribution. The above formulation of the detection event, $D_{\min}$, is applied in the further analysis.

Detected and repaired crack sites are included in the reliability formulation having new independent initial crack size distributions, where the initial crack size distributions for repaired cracks do not need to be identical to the original initial crack size distributions. The fatigue material parameters C and m, to be applied in the evaluation of the fatigue crack growth of repaired cracks, are modeled as independent or equal to the original material parameters, depending on the repair method, weld repair or grind repair, respectively.

The derived approach defines a simple model for updating of the fatigue reliability of a continuous weld with multiple fatigue sensitive crack sites. Having, *e.g.*, a weld consisting of a total of m crack sites, the updated fatigue failure probability of the weld after an inspection of n crack sites at time t_j, resulting in k crack detections is model as,

$$
\begin{aligned}
P_{Fsys}(t) &= P(M_{\min(m-n)}(t) \leq 0 \cup M_{\min(n-k)}(t) \leq 0 \cup M_{\min k}(t) \leq 0 \mid \\
&\quad H_{\min(n-k)}(t_j) > 0 \cap D_{\min k}(t_j) > 0)
\end{aligned}
\tag{4.39}
$$

In the above formulation, the safety margin $M_{\min n}$ is divided into three sub safety margins, allowing the information from the inspection outcome to be applied directly in the modeling of the safety margin of the weld after inspection.

However, when the number of potential crack sites over the weld is unknown and described through a density function, the uncertainties in the existence of crack sites over an examined area of the weld must be included in the derivation of the updated fatigue reliability after inspection. This topic is investigated further in the following section.

4.5.3 Stochastic Number of Crack Sites

Known Defect Intensity

Having the distribution of crack sites along the weld described by a homogeneous Poisson distribution with known crack site intensity, the fatigue failure probability of the weld can be updated from

inspection results by applying the same probabilistic procedures derived in the previous section. However, the probability of occurrence of crack sites over an examined area must be included in the reliability formulation, since, *e.g.*, the inspection result of not detecting any crack sites might be due to either no crack site occurrence over the investigated area of the weld, or the fact that the occurring crack sites had crack sizes smaller than the smallest detectable crack size for the inspection method applied.

The distribution of undetected crack sites for a weld having Poisson distributed crack sites with intensity μ is shown in Chapter 3 to be adequately described by a filtered Poisson distribution having crack site intensity $(1 - p_d(t_j))\mu$,

$$P_M(m) = \frac{((1 - p_d)\mu l_i)^m}{m!} e^{-(1-p_d)\mu l_i} \tag{4.40}$$

where p_d is the probability of detecting a potential crack site at the time of inspection. The probability of having crack sites over an uninspected and inspected area of the weld, $(l - l_i)$ and l_i, is then,

$$P_N(n > 0) = 1 - e^{-\mu(l-l_i)} \tag{4.41}$$

$$P_M(m > 0) = 1 - e^{-(1-p_d)\mu l_i} \tag{4.42}$$

The inspection event margin for m undetected defects is defined as earlier by

$$H_{\min m}(t_j) = a_d - \Psi^{-1}\left(\Psi\left(\max_{i=1,m} a_{0i}\right) + C\nu_0 r t_j E[\Delta\sigma^m]\right) \tag{4.43}$$

where the number of undetected crack sites m is given by Equation (4.40). From the filtered Poisson distribution, the maximum extreme initial crack size distribution is then given by,

$$a_{\max} = F_{A0}^{-1}\left(\frac{\ln\left((1 - e^{-(1-p_d)\mu l_i})\Phi(u) + e^{-(1-p_d)\mu l_i}\right)}{(1 - p_d)\mu l_i} + 1\right) \tag{4.44}$$

where u is an auxiliary standard normal variable.

The inspection event for detected crack sites is equivalent to the formulation presented in the previous section, where a deterministic number of crack sites is detected during each inspection.

The updated fatigue failure probability of an examined weld length after an inspection resulting in k crack detections at time t_j is then written as,

$$\begin{aligned}
P_{Fweld}(t) = \quad & P(M_{\min m}(t) \leq 0 \cup M_{\min k}(t) \leq 0 \mid \\
& H_{\min m}(t_j) > 0 \cap D_{\min k}(t_j) > 0)P_M(m > 0) \\
+ \quad & P(M_{\min k}(t) \leq 0 \mid D_{\min k}(t_j) > 0)P_M(m = 0)
\end{aligned} \tag{4.45}$$

where m is the Poisson distributed number of undetected crack sites. Both possibilities for the inspection outcome of undetected crack sites are included in the formulation; $m > 0$, implies that

existing cracks were not detected, and $m = 0$, that no other cracks existed over the inspected area of the weld.

The procedure is also applicable for updating of the fatigue reliability of a continuous weld having Poisson distributed number of crack sites when only a fraction of the weld is examined in each inspection. The updated failure probability of the weld seam after inspection of l_i of the length l at time t_j, is formulated as,

$$
\begin{aligned}
P_{Fweld}(t) = \ & P(M_{\min n}(t) \leq 0 \cup M_{\min m}(t) \leq 0 \cup M_{\min k}(t) \leq 0 \mid \\
& H_{\min m}(t_j) > 0 \cap D_{\min k}(t_j) > 0)P_N(n > 0)P_M(m > 0) \\
+ \ & P(M_{\min m}(t) \leq 0 \cup M_{\min k}(t) \leq 0 \mid \\
& H_{\min m}(t_j) > 0 \cap D_{\min k}(t_j) > 0)P_N(n = 0)P_M(m > 0) \\
+ \ & P(M_{\min n}(t) \leq 0 \cup M_{\min k}(t) \leq 0 \mid \\
& D_{\min k}(t_j) > 0)P_N(n > 0)P_M(m = 0) \\
+ \ & P(M_{\min k}(t) \leq 0 \mid D_{\min k}(t_j) > 0)P_N(n = 0)P_M(m = 0)
\end{aligned}
\tag{4.46}
$$

where n is the original Poisson distributed number of crack sizes over the uninspected length, m is the filtered Poisson distributed number of undetected crack sites over the inspected area of the weld, and k is the deterministic number of detected crack sites.

The formulation accounts for all possible combinations of occurrence / no-occurrence of crack sites over the examined and unexamined areas of the weld. The first term models the failure probability, given undetected crack sites over the inspected area and crack sites over the uninspected area, the second and third terms are conditioned on not having crack sites over one of these areas, and the last term is conditioned on not having any crack sites over the system, expect for the k detected cracks.

Unknown Defect Intensity

If the value of the intensity of crack sites over the weld length is not known, but described through a prior Gamma distribution function, the information from the inspection outcome is also applied to update the statistical uncertainties in the description of the crack site intensity.

The inspection outcome is then applied to update both the intensity of crack sites and the estimated rate of fatigue crack growth.

- From the number of crack sites detected over an examined area of the weld, a posterior estimate of the crack intensity is derived in accordance with Equation (3.51).

- From the size of the detected cracks, or undetected cracks being smaller than the smallest detectable crack size for the inspection method applied, the rate of crack growth is updated based on the initial crack size a_0 and the material and loading conditions.

The updating procedure, having a stochastic description of the intensity of crack sites over the weld length, is equivalent to the procedure being applied for a deterministic crack site intensity, except that the posterior estimate of the crack site intensity is applied in the evaluation of the fatigue reliability level of the weld after inspection. The updated posterior distribution is valid over the whole weld length being described by the homogeneous Poisson process.

The expressions for the maximum extreme initial crack size distribution function for the undetected crack sites over the examined area of the weld is given by,

$$a_{\max} = F_{A_0}^{-1}\left(1 + \frac{\nu}{(1-p_d)l_i}\left(1 - \frac{\nu + (1-p_d)l_i}{(((\nu + (1-p_d)l_i)^\xi - \nu^\xi)\Phi(u) + \nu^\xi)^{1/\xi}}\right)\right) \qquad (4.47)$$

where the maximum extreme initial crack size distribution function for non-examined area of the weld is given by Equation (4.25). Posterior estimates are applied on the Gamma distribution parameters ξ and ν describing the crack site intensity μ.

4.5.4 Independent Detectable Crack Sizes   -

The derived procedures for updating of the fatigue reliability of the weld have so far been based on the assumption of equivalent detectable crack sizes for all the inspected crack sites during an inspection, however, allowing independent detectable crack sizes at different inspection times.

For an inspection procedure, having independent detectable crack sizes at the different inspection sites, the event margin modeling the inspection outcome for no crack detection needs to be modified.

The no-detection inspection event for multiple crack sites has previously been expressed through a maximum extreme initial crack size being smaller than the smallest detectable crack size. Having independent detectable crack sizes at the different sites, the no-detection inspection event for n inspected crack sites is formulated as,

$$
\begin{aligned}
H_{\min n}(t_j) &= \min_{i=1,n}\left[\Psi(a_{di}) - \Psi(a_{0i}) + C\nu_0 rt_j E[\Delta\sigma^m]\,\right] \\
&= \min_{i=1,n}\left[\Psi(a_{di}) - \Psi(a_{0i})\right] + C\nu_0 rt_j E[\Delta\sigma^m] \\
&= \min_{i=1,n}[\theta_i] + C\nu_0 rt_j E[\Delta\sigma^m] \qquad\qquad (4.48)
\end{aligned}
$$

where $\theta_i = \Psi(a_{di}) - \Psi(a_{0i})$. θ is a new independent stochastic variable, given as a function of the stochastic initial crack size and smallest detectable crack size at the different sites.

The distribution function of θ has to be defined in order to estimate the above event margin of the series system through the use of order statistics. The cumulative distribution of θ is derived directly from the distribution functions of the initial crack size a_0 and the smallest detectable crack size a_d,

$$
\begin{aligned}
F_\Theta(\theta) &= P(\Theta \leq \theta) = P(\Psi(A_d) - \Psi(A_0) \leq \theta) \\
&= \int_A P(\Psi(A_d) \leq \theta + \Psi(a) \mid a)f_{A0}(a)\,da
\end{aligned}
$$

$$
\begin{aligned}
&= \int_A P(A_d \leq \Psi^{-1}(\theta + \Psi(a)) \mid a) f_{A0}(a) \, da \\
&= \int_A F_{Ad}(\Psi^{-1}(\theta + \Psi(a))) f_{A0}(a) \, da
\end{aligned}
\tag{4.49}
$$

where the last step is based on independence between A_d and A_0. The cumulative distribution function of the new independent stochastic variable Θ is then given directly as a function of the density and cumulative distribution functions of A_0 and A_d.

The above derivation is conducted within the limit state function during each iteration of the full distribution reliability calculation, and is therefore conditioned on the outcome of the common stochastic variables.

The formulation can easily be extended to include multiple independent stochastic variables at the different crack sites. In addition to having independent initial crack sizes and detectable crack sizes at the different sites, *e.g.*, the aspect ratio a/c and the geometry function $Y(a)$ can be modeled as independent for the different sites. The modeling of recursive systems having correlated components is derived in Friis-Hansen and Cramer [28].

The cumulative minimum extreme distribution function of Θ is further defined, applying order statistics,

$$
F_{\min \Theta}(\theta) = 1 - (1 - F_{\Theta}(\theta))^n
\tag{4.50}
$$

where the expression must be expanded to account for a possible Poisson distribution of crack sites n along the weld, eventually having a stochastic description of the site intensity.

The argument of the cumulative minimum extreme distribution of Θ is further expressed applying an auxiliary standard normal variable u as described earlier, where the non-zero probability of not having any crack sites over the weld seam for the Poisson distributed number of crack sites is included in the formulation. The procedure is based on an inversion of F_{Θ}, for which a numerical inversion is applied.

4.5.5 Multiple Inspections

Having multiple inspections over the same area of the weld, an extended approach of the earlier described procedure is applied.

The weld is divided into areas having equal inspection history, *i.e.*, number and time of inspections, in order to establish equivalent extreme initial crack size distributions for the different safety and inspection event margins. The use of equivalent extreme initial crack size distributions for the event margins greatly simplifies the evaluation of the updated fatigue reliability after inspection.

The failure probability of the weld is then estimated as the union of the failure probabilities of the different areas of the weld having equal inspection history, conditioned on the inspection result from all the performed inspections.

A weld length, which for simplicity is defined to have a deterministic number of crack sites with known crack locations, is partly examined at times t_1 and t_2. The expression for the updated total fatigue failure probability of the weld length after the second inspection can then be formulated. The following notation is applied;

k : crack sites inspected at time t_1

l : crack sites detected at time t_1

m : crack sites inspected at time t_2

n : crack sites detected at time t_2

p : crack sites inspected both at time t_1 and t_2 (no detection)

q : crack sites not inspected at time t_1 or t_2

The updated fatigue failure probability of the weld is then written as,

$$
\begin{aligned}
P_{Fsys}(t) \;=\; & P(M_{k-l}(t) \leq 0 \cup M_l(t) \leq 0 \cup M_{m-n}(t) \leq 0 \cup \\
& M_n(t) \leq 0 \cup M_p(t) \leq 0 \cup M_q(t) \leq 0 \mid \\
& H_{k-l}(t_1) > 0 \cap D_l(t_1) > 0 \cap H_{m-n}(t_2) > 0 \cap \\
& D_n(t_2) > 0 \cap H_p(t_1) > 0 \cap H_p(t_2) > 0)
\end{aligned}
\tag{4.51}
$$

The subscript min is omitted in all the terms in the above equation to simplify the notation.

For a stochastic description of the number of crack sites, where the crack site distribution function is, *e.g.*, Poisson distributed, the probability of having crack sites over the different areas of the weld must be included in the above formulation.

4.6   Incorporation of Modeling and Statistical Uncertainty

In the presented probabilistic formulation, there has been no distinction made between the different types of uncertainties in the modeling of the stochastic vector **X**, and it has been assumed that **X** incorporates inherent physical uncertainties, model uncertainties and statistical uncertainties.

However, the combination of all the different types of uncertainties into a common stochastic variable leads to confusion regarding the interpretation of the estimated reliability level. In work by Der Kierughian [44], a separation of the different types of uncertainties has been conducted in the reliability analysis.

A vector of uncertain parameters Θ, representing the model and statistical uncertainties, and a vector of random variables **Y**, solely representing the inherent physical uncertainties, are introduced. The uncertainties are represented in the limit state function as, $g(\mathbf{Y}, \Theta)$, where both **Y** and Θ are defined using a full distribution description of the stochastic variables and parameters. The modeling and influence of model uncertainties on the estimated reliability level is investigated in Der Kierughian [46].

The philosophy behind a separation between inherent physical uncertainties, and model and statistical uncertainties is obvious. A reliability estimate of the structure based on the total uncertainty vector $\mathbf{X}$ is influenced by the modeling and formulation of the stochastic reliability problem. Consequently, the reliability estimate does not represent the true reliability level of the system, but rather the designer's estimate of the reliability level based on the at time available information.

The "true" failure probability of the system can only be estimated as a conditional probability, conditioned on the modeling and statistical uncertainties,

$$P_F(\Theta = \theta) = \int_{g(\mathbf{Y},\theta)\leq 0} f_{\mathbf{Y},\Theta=\theta}(\mathbf{y},\theta)\ d\mathbf{y} \qquad (4.52)$$

where a bi-variate distribution function of $\mathbf{Y}$ and Θ is applied to account for the influence of statistical uncertainties on the $\mathbf{Y}$ distribution parameters and the possible dependence on the inherent uncertainties in the probabilistic modeling of Θ.

The estimated true failure probability is stochastic due to the stochastic description of Θ. In Der Kierughian [44], two approaches are applied to account for these uncertainties.

- A predictive failure probability is computed, $\tilde{P}_F$, where the different natures of the uncertainties are disregarded.

- The distribution of the failure probability, or another applied measure of safety, is computed.

In the present work, the first approach is applied, where the physical, model and statistical uncertainties are treated equally in the probabilistic analysis, and the predictive fatigue failure probability is referred to the estimated fatigue failure probability.

$$
\begin{aligned}
P_F &= E[P_F(\Theta)] = \int_{g(\mathbf{Y},\Theta)\leq 0} f_{\mathbf{Y},\Theta}(\mathbf{y},\theta)\ d\mathbf{y}d\theta \\
&= \int_{g(\mathbf{X})\leq 0} f_{\mathbf{X}}(\mathbf{x})\ d\mathbf{x}
\end{aligned}
\qquad (4.53)
$$

The computed fatigue failure probability of the system then does not represent the true failure probability, but the estimated failure probability based on the available information.

From the estimated predictive failure probability, the reliability index is defined as,

$$\beta = \Phi^{-1}(1 - P_F) \qquad (4.54)$$

which is a predictive measure of safety.

4.7   Numerical Study

The presented probabilistic fatigue reliability model is investigated through some numerical examples. The focus is on studying the effect of multiple crack sites on the estimated fatigue reliability of the weld and the effect of different inspection strategies on the updated fatigue reliability after inspection. A realistic stochastic description of the uncertain variables in the fatigue capacity and loading demand model is attempted, but the applied stochastic variables in the numerical study do not necessarily describe a real life situation.

The following areas are investigated:

Deterministic Number of Crack Sites:

- The fatigue reliability of a system depending on the number of crack sites in the system.

- The effect of inspection updating of a single crack site

- The effect of inspection updating of a single uninspected crack site, depending on the inspection outcome of other inspected sites.

- The updated fatigue reliability of a group of crack sites depending on the number of inspected sites.

Stochastic Number of Crack Sites:

- The fatigue reliability of a continuous weld depending on the length of the weld.

- The effect of inspection updating of a continuous weld with Poisson distributed crack sites.

- The effect of inspection updating of an uninspected area of a continuous weld with Poisson distributed crack sites depending on the inspection outcome of inspected areas.

- The updated fatigue reliability of a specified weld length depending on the length of the weld being examined.

The numerical study is conducted based on the variables given in Table 4.1. The independent initial crack size distribution in the presented stochastic model is defined to be Gamma distributed with unknown scale parameter λ and known shape parameter k. The statistical uncertainties on the scale parameter λ represent uncertainties with respect to the influence of welding surface defects on the fatigue capacity. The statistical uncertainties of the scale parameter are naturally modeled as common for all the investigated crack sites. A model, where both Gamma distribution parameters are modeled with statistical uncertainty could also have been applied.

The intensity of crack sites in the Poisson distribution of crack sites along the weld length in the probabilistic model is defined to be unknown, and a Gamma distributed crack site intensity is applied to model the statistical uncertainties.

102

The systematic and random model uncertainties in the evaluation of the load response are indirectly accounted for in the modeling of the longterm Weibull stress range distribution parameters A and B. The model uncertainties in the evaluation of the fatigue capacity are modeled through the geometry function parameter Y_0.

In Chapter 6, a more thorough study concerning the fatigue reliability of a panel section of a tanker structure is presented, where focus is on a realistic probabilistic modeling of the longterm load effect and the fatigue capacity.

4.7.1 Deterministic Number of Crack Sites

Based on the described input model, the fatigue reliability of multiple crack sites over the lifetime is estimated. In Figure 4.1 the fatigue reliability is computed for a series system consisting of 1, 2, 5, and 10 crack sites. It is seen from the figure that the fatigue reliability of the system is already relatively low in the beginning of the service life. This is mainly due to the statistical uncertainties of the scale parameter in the initial crack size distribution, leading to a non-negligible fatigue failure probability of the crack sites in the time period after fabrication. The scale parameter in the initial crack size distribution is defined as Gamma distributed with mean value 2.0 and coefficient of variation 0.5. The correlation in the fatigue failure probabilities among the crack sites after 20 years of service is 51%.

Figure 4.2 shows the effect of inspection updating of a single crack site after 10 years of service for different inspection qualities. The smallest detectable crack size is modeled as Exponentially distributed, with inspection qualities $q_1 = .238$, $q_2 = .429$ and $q_3 = .715$, leading to 80% probability of detecting a crack of length 90, 50 and 30 mm, respectively. The results show that the effect of inspection updating is highly dependent on the quality of the performed inspection. One should here also notice that visual and MPI inspections are dependent on the crack length, whereas the crack depth is the critical measure in the fatigue reliability calculations, leading to a high influence of the aspect ratio in the effect of the inspection updating. A crack configuration $a/c = 0.15$ has here been assumed.

Figures 4.3, 4.4 and 4.5 show the result of inspection updating of an uninspected crack site as a function of the number of other inspected crack sites not leading to any crack detection. The results are given for different inspection qualities, where an equal detectable crack size has been assumed for the different inspection sites. It is seen that due to the common uncertainties in the fatigue and load response model, the fatigue reliability uninspected crack sites can be updated from the inspection result of other examined crack sites. It is here interesting to notice the influence of the number of crack sites inspected and the quality of these inspections on the updated fatigue reliability

In Figure 4.6, the effect of assuming independent or equal detectable crack sizes for the different inspection sites is investigated. The estimated updated fatigue reliability after 20 years of service for an uninspected site is shown for different numbers of other inspected crack sites. An inspection

quality having 80% probability of detecting a crack of length 50 mm after 10 years of service is applied. It is seen that the effect of assuming independent detectable crack sizes for the different inspection sites increases the effect of the inspection updating. This can also be verified directly from Equation (4.48), applying order statistics. It can therefore be concluded, that with respect to inspection updating of uninspected areas of the structure, the assumption of having a common detectable crack size over the inspected area is conservative.

In Figure 4.7, the fatigue reliability of a system consisting of 10 crack sites is investigated as a function of the number of the sites examined during an inspection after 10 years of service. The results are shown for an inspection quality $q_2 = .429$. It is seen that from inspection of 1, 2 and 5 of the crack sites, resulting in no crack detection, the total fatigue reliability of the system is extended with around 2, 4 and 7 years, respectively. Based on inspection of only a fraction of the crack sites in the system, it is therefore possible to have a considerable increase in estimated fatigue reliability of the system.

4.7.2   Stochastic Number of Crack Sites

The fatigue reliability of a continuous weld with Poisson distributed number of crack sites with unknown crack intensity μ is considered. The crack site intensity μ is modeled as being Gamma distributed with mean value 1.0, where the effect of the uncertainty on μ is investigated.

In Figure 4.8, the fatigue reliability of the continuous weld over the service time is shown for different weld lengths. Figure 4.9 shows the fatigue reliability of the weld after 10 and 20 years, depending on the weld length. Both figures are based on a COV of μ equal to zero, giving a deterministic estimate of μ equal to one. It is seen how the fatigue failure probability of the weld increases with the weld length.

In the derivation of the filtered Poisson distribution describing the distribution of undetected crack sites over the examined area of the weld, independence in the detection probabilities of the different crack sites has been assumed. The different crack sites, having independent initial crack sizes, have correlated exceedence probabilities due to the influence of a common stochastic fatigue crack growth model. The detection probability is defined as the probability of a crack size exceeding a defined detectable crack size level, and the exceedence probability is, in that sense, comparable to the detection probability.

However, the correlation decreases with decreasing threshold levels, and for detectable crack lengths of 66, 40 and 13 mm will be 24%, 12% and 2%, respectively. In Table 4.2, the normalized log-probability of exceeding these threshold levels for multiple crack sites is given. These exceedence probabilities are equivalent to the probability of detecting n out of n inspected crack sites. Having independent detection probabilities, $\rho = 0$, the logarithm of the detection probability of multiple crack sites decreases linearly with the number of inspected sites. It is concluded from the table that for the evaluated detectable crack lengths, the influence of the correlation in the detection

probabilities is of less importance, and the assumption of Poisson distributed undetected crack sites is justified.

Assuming no crack detection, the updated fatigue reliability of one meter of uninspected weld length, based on the length examined of other areas of the continuous weld, is derived. The results are computed for different inspection qualities, and are shown in Figures 4.10, 4.11 and 4.12, having a crack site intensity with mean value 1.0 and COV of .0, .5 and 1.0, respectively. It is seen that the statistical uncertainty of the crack site intensity μ influences the effect of the inspection updating on the predictor fatigue failure probability. For prior large statistical uncertainty on μ, the estimated updated (predictor) reliability is more sensitive to the inspection outcome.

Figure 4.13 shows the effect of inspection updating of one meter of the weld length for different inspection qualities. Both one meter of the inspected and uninspected area of the weld are considered. The updated fatigue reliability of the weld is computed based on an examination of 10 meters of the weld length, not resulting in any crack detection. A COV of .5 is applied to model the crack site intensity. The figure shows the combined influence of inspection quality and inspection quantity on the updated fatigue reliability of examined and unexamined areas of the weld.

Figure 4.14 investigates the total fatigue reliability of a 10 meter long weld. The updated total fatigue reliability of the weld length is given for different inspection lengths, resulting in no crack detection. The computation is based on an inspection quality corresponding to 80% probability of detecting a crack of length 50 mm, having a COV of .5 on the modeled crack site intensity. Already after inspection of only 10-20 % of the total weld length, an increase in the total estimated fatigue reliability of the weld is experienced.

In Table 4.3, the sensitivity of the updated fatigue reliability of the 10 meter long weld after 20 years of service is investigated. The sensitivity of the predictor reliability index is estimated for the inspection quality q, the mean and standard deviation of the defect intensity μ, and the mean and standard deviation of the Gamma distributed scale parameter in the initial crack size distribution. A high dependence on these parameters on the estimated fatigue reliability is seen.

Variable	Distrib.	Mean	Standard Deviation
Init. crk. a_0	Gamma	$E[a_0] = k/\lambda$	$D[a_0] = \sqrt{k}/\lambda$
Shape par. k	Fixed		parameter study
Scale par. λ	Gamma	g/κ	$\sqrt{g}/\kappa$
Dist. of sites	Poisson	μ	μ
Site intensity μ	Gamma	ξ/ν	$\sqrt{\xi}/\nu$
Str. range $\Delta\sigma$	Weibull	$A\Gamma(1 + 1/B)$	$A\sqrt{\Gamma(1 + 2/B) - \Gamma(1 + 1/B)^2}$
Wbl. par. A	Normal	$E[\ln A] = 2.0$	$D[\ln A] = 0.15$
Wbl. par. B	Normal	$E[1/B] = 1.3$	$D[1/B] = 0.1$
Det. crk. a_d	Expon.	$1/q$	$1/q$
Insp. quality q	Fixed		parameter study
Crit. crk. a_c	Fixed	25.0 mm	
Aspect ratio a/c	Fixed	0.15	
Life time t_{life}	Fixed	20 years	
Insp. time t_{insp}	Fixed	10 years	
Cycle rate ν_0	Fixed	$5 \cdot 10^6$ year^{-1}	
Exposure rate r	Fixed	1.0	
Mat. par. C	Lognorm.	$E[\ln C] = -29.8$	$D[\ln C] = 0.5$
Mat. par. m	Normal	$E[m] = 3.0$	$D[m] = 0.1$
Geom. fun. Y_0	Normal	$E[Y_0] = 1.0$	$D[Y_0] = 0.1$
Threshold ΔK_{th}	Fixed	0.0	
Corr. rate k_c	Fixed	0.0	
Correlation	$\rho[\ln A, 1/B]$	-0.79	
Correlation	$\rho[\ln C, m]$	-0.89	

Table 4.1: Modeling of input variables. Units in N and mm if otherwise not specified.

4.1 Summary and Conclusion

A fatigue reliability model for evaluation of the fatigue reliability systems having multiple fatigue crack sites is derived, where the location and number of crack sites in the system is not necesarily known. The model is extended to include the effect of updating of the fatigue reliability of the system from inspection results.

Due to common uncertainties in the load response model and in the fatigue capacity for the different crack sites in the system, the fatigue reliability of uninspected crack sites can be updated based on inspection results of examined sites.

The effect of the inspection updating is dependent on the correlation in the fatigue failure probability for the different crack sites. Continuous welds being exposed to similar stress conditions are having common model uncertainties for the different weld defects. This leads to a high correlation in estimated fatigue failure probability of the different crack sites, and thereby a large effect of the inspection results from examination of only fraction of the weld length on the total failure probability of the weld.

Threshold	Corr.	$\log(P_1)$	$\log(P_2)$	$\log(P_3)$	$\log(P_4)$	$\log(P_5)$
$A_d = 1.0$	$\rho = 2\%$	-0.6580	-1.3003	-1.9241	-2.5261	-3.1022
	$\rho = 0\%$	-0.6580	-1.3160	-1.9741	-2.6321	-3.2901
$A_d = 3.0$	$\rho = 12\%$	-1.5840	-3.1680	-4.7519	-6.3359	-7.9200
	$\rho = 0\%$	-1.5840	-2.8732	-3.8701	-4.6500	-5.2829
$A_d = 5.0$	$\rho = 24\%$	-2.1598	-4.3196	-6.4793	-8.6391	-10.7989
	$\rho = 0\%$	-2.1598	-3.5677	-4.5378	-5.2721	-5.8639

Table 4.2: The effect of correlation in the detection probability of multiple crack sites.

Insp. length:	0 m	1 m	2 m	5 m	10 m
$d\beta/dq$		0.042	0.077	0.180	0.770
$d\beta/dE[\mu]$	−0.380	−0.330	−0.310	−0.270	−0.410
$d\beta/dD[\mu]$	0.059	0.082	0.095	0.120	0.260
$d\beta/dE[\lambda]$	1.700	1.500	1.400	1.200	0.530
$d\beta/dD[\lambda]$	−0.660	−0.560	−0.490	−0.350	−0.043

Table 4.3: Sensitivity of fatigue reliability after 20 years of service
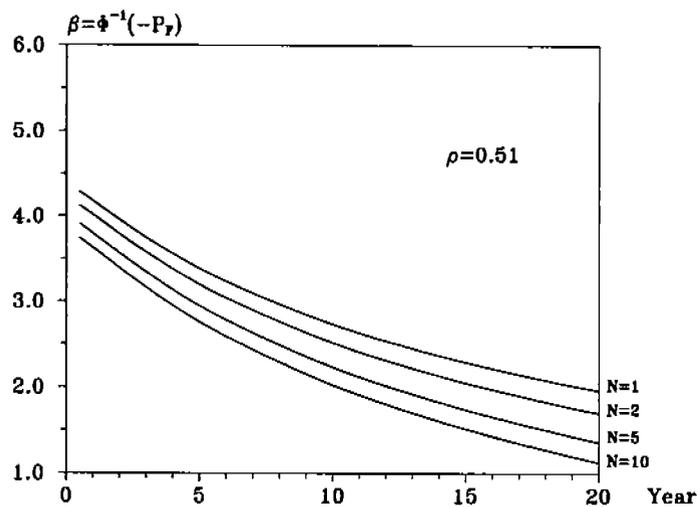
Figure 4.1: Fatigue reliability of a series system depending on the number of crack sites in the system.
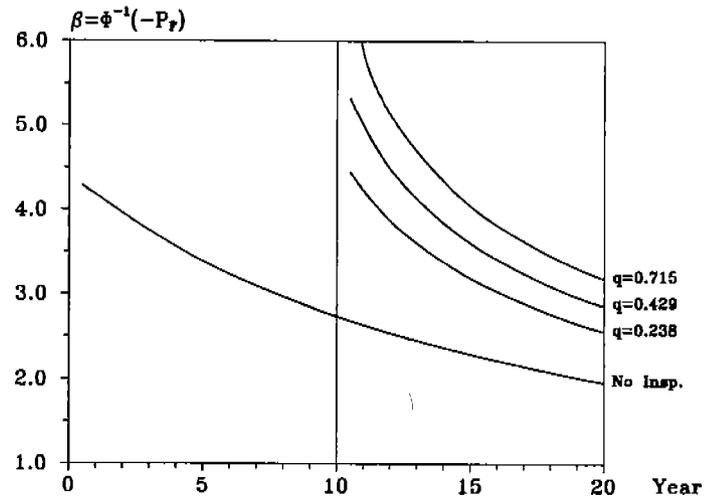
Figure 4.2: Inspection updating of an inspected crack site for different inspection qualities.
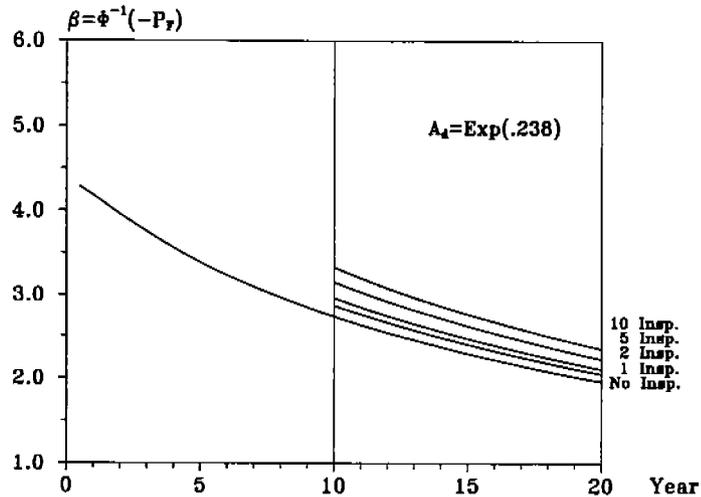
Figure 4.3: Inspection updating of a single uninspected crack site having an inspection with 80% probability of detecting a 90 mm crack.
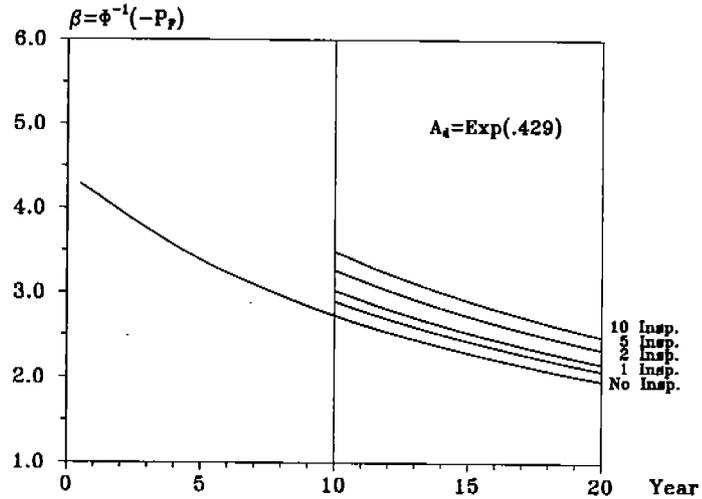
Figure 4.4: Inspection updating of a single uninspected crack site having an inspection with 80% probability of detecting a 50 mm crack.
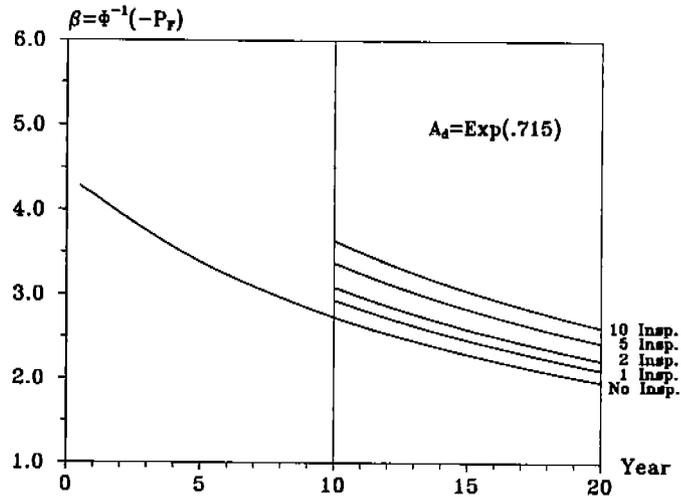
Figure 4.5: Inspection updating of a single uninspected crack site having an inspection with 80% probability of detecting a 30 mm crack.

109
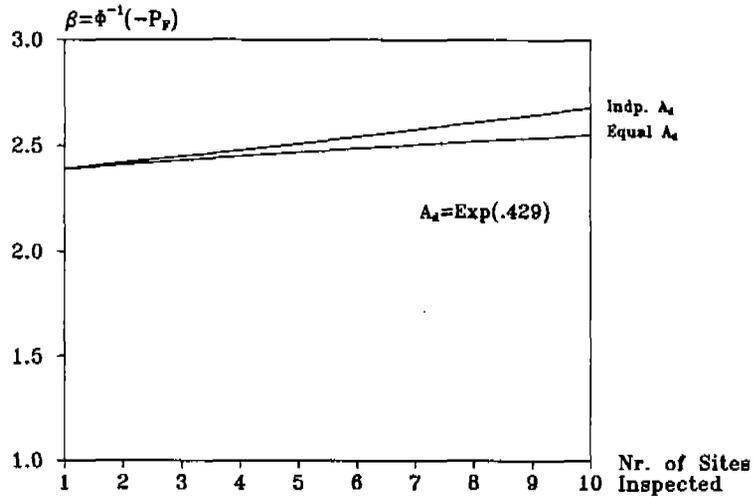
Figure 4.6: Effect of assuming independent or common detectable crack sizes for the different inspection sites during an inspection. Fatigue reliability for a single uninspected crack site after 20 years of service.
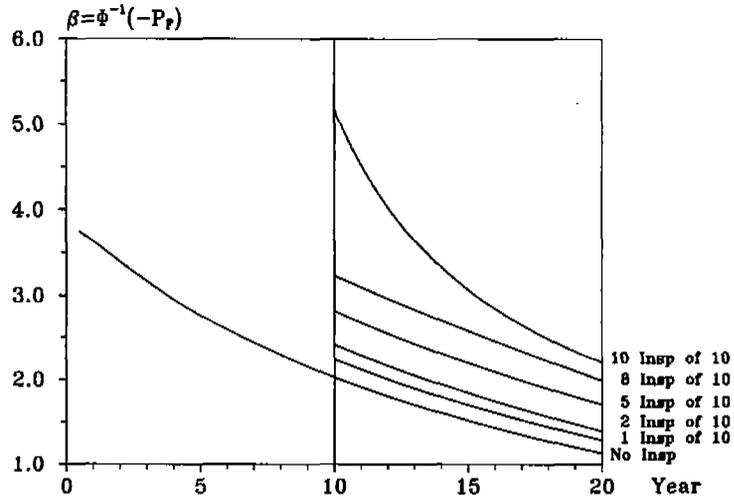
Figure 4.7: Updated total fatigue reliability of a system consisting of 10 crack sites, having different number of crack sites inspected after 10 years of service. The inspection has a 80% probability of detecting a crack of length 50 mm.
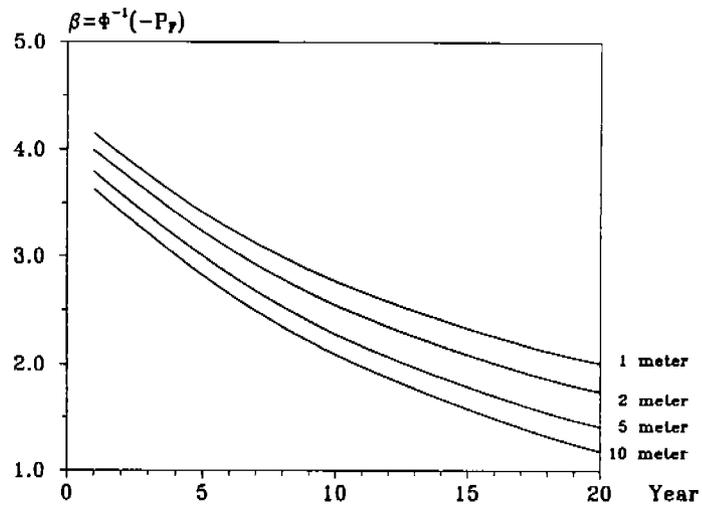
Figure 4.1: Fatigue reliability of the continuous weld over the service life for different weld lengths.
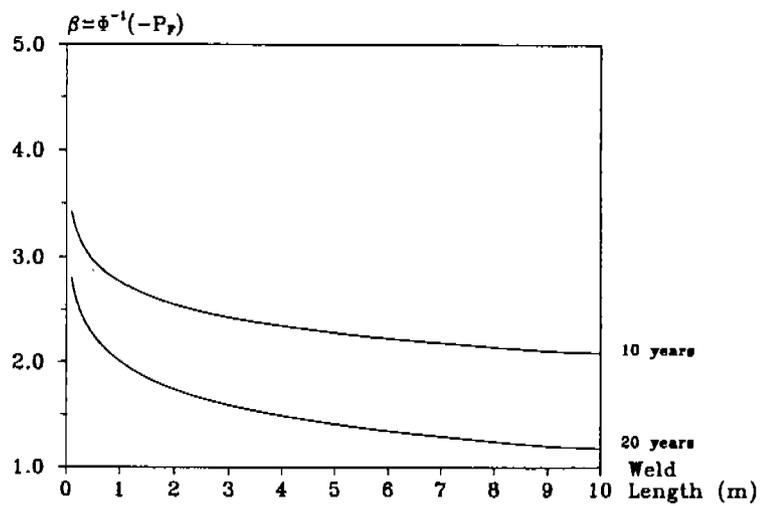
Figure 4.2: Fatigue reliability of the continuous weld after 10 and 20 years of service for different weld lengths.
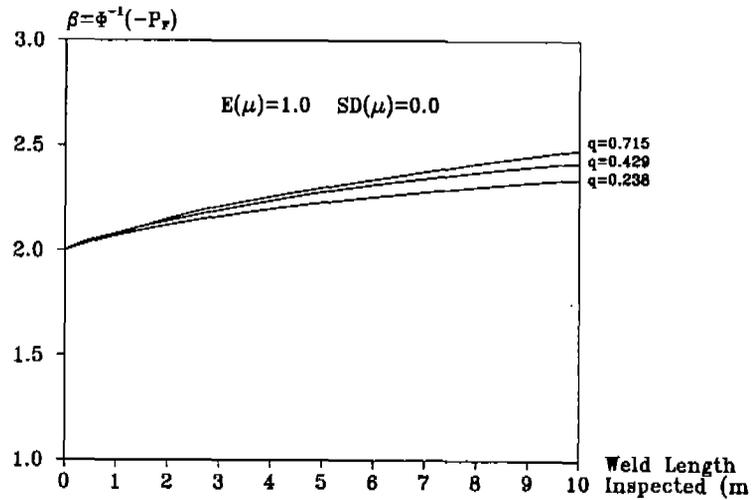
Figure 4.3: Updated fatigue reliability of one meter of the uninspected weld length, having known crack site intensity.
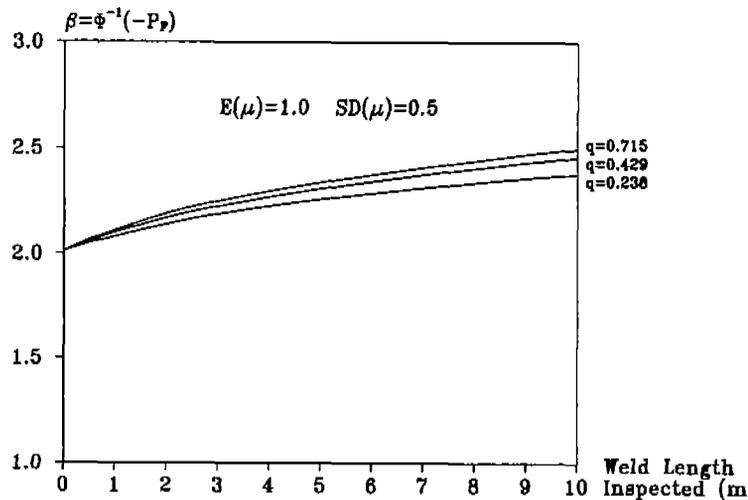
Figure 4.4: Updated fatigue reliability of one meter of the uninspected weld length having crack site intensity with COV=0.5.
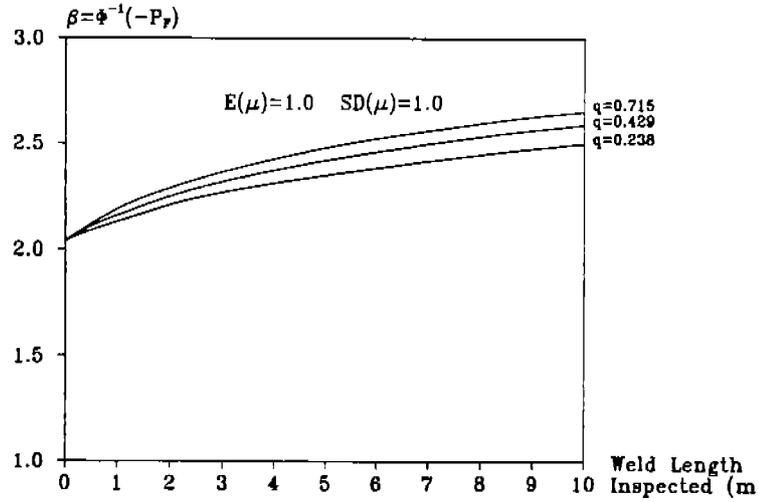
Figure 4.5: Updated fatigue reliability of one meter of the uninspected weld length having crack site intensity with COV=1.0.
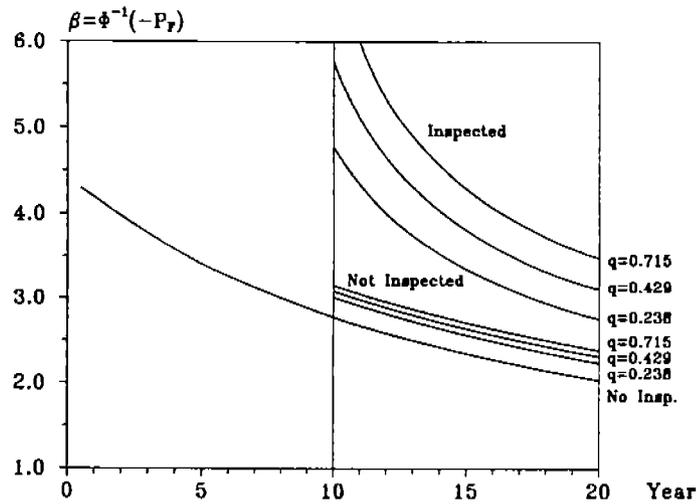
Figure 4.6: Updated fatigue reliability of one meter of both the uninspected and inspected area of the weld after inspection of 10 meters of the weld resulting in no crack detection.

113
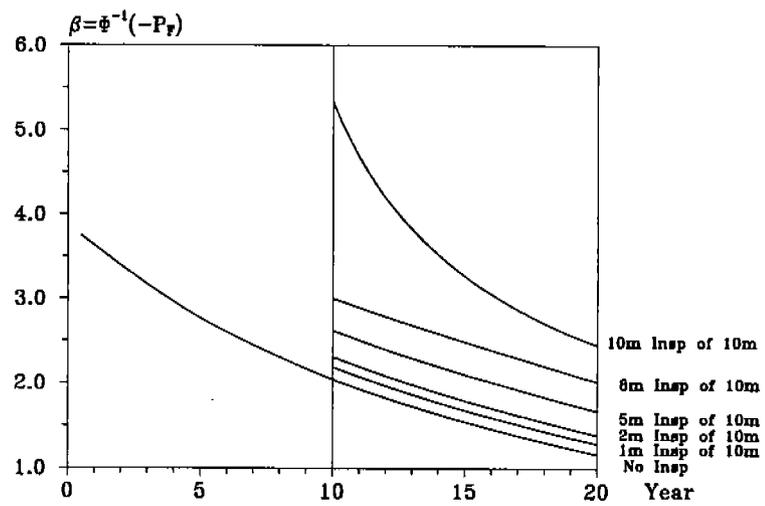
Figure 4.7: Updated total fatigue reliability of a weld length of 10 meter for different inspection lengths after 10 years of service.

Chapter 5

Cost Optimal Design and Maintenance

5.1 Introduction

Sufficient safety of welded structures against fatigue damage is achieved through the use of several safety procedures, design of the structure, quality control of the welding procedure during fabrication, and inspection for fatigue cracks with subsequent repair of detected cracks. Each safety procedure has a certain cost, and it is important to minimize the total expected cost over the lifetime of the structure.

The present chapter presents a probability based optimization procedure defining optimal initial design, quality of welding procedure at fabrication, time of inspections, quality of inspections and length of weld to be inspected at each inspection. The cost considered in the optimization is cost related to initial design, cost of fabrication, cost of inspection, expected repair cost and expected failure cost.

The probabilistic optimization problem is formulated for a homogeneous continuous weld located in a tanker structure containing hazardous material for which no leakage is permissible. The weld seam considered has multiple potential crack initiation sites from weld defects.

Probability based cost benefit analyses for fatigue sensitive structures have been presented, see, e.g., Ref. [52, 54, 55, 85]. These procedures establish an excellent approach for solving the probabilistic optimization problem for a single fatigue sensitive detail, and are applied as the theoretical basis for the presented model. However, these procedures fall short of transferring information from the inspection outcome of one detail of the structure to the reliability calculation of another detail. Further, they also assume that the crack initiation positions are predictable in advance.

For continuous welded structures containing long welding under similar stress conditions, a multiple number of crack initiation positions exist, and the crack initiation positions are not necessarily predictable in advance. In the following these issues are addressed, and a probabilistic procedure for determination of optimal design, fabrication and inspection strategy with respect to inspection time, inspection length and inspection quality is presented.

Uncertainties in the longterm stochastic load process, the fatigue strength and the crack size of the different initial defects are considered in the procedure.

5.2   Model Formulation

5.2.1   Fatigue Model

A homogeneous continuous weld of specified length, containing a number of initial crack sites from weld defects is investigated. Fatigue failure of the weld is defined as fatigue crack growth beyond a critical crack size for one or more of the crack sites along the weld seam.

The same fatigue model as presented earlier is applied, with independent identically distributed initial crack sizes over the homogeneous weld with stochastic material parameters, where the whole weld seam is exposed to the same stochastic loading process.

5.2.2   Optimization Variables

Design Variable

A structural design parameter z is introduced to model the influence of different designs on the crack growth formulation, Madsen [52]. For a stiffener weld seam, the structural design parameter typically represents the plate thickness, or an unspecified design option leading to continuous change of the general stress range level. The base value of z for which the Weibull distribution parameters are computed is z_0. The effect of different designs is included in the model by multiplying each stress range cycle by the design factor s_z,

$$s_z = c_z \frac{z_0}{z} + (1 - c_z)\left(\frac{z_0}{z}\right)^2, \quad z^{min} \le z \le z^{max}, \quad 0 \le c_z \le 1 \qquad (5.1)$$

where c_z models the influence of design change on the stress range level.

Fabrication Variable

To model the effect of the welding quality at fabrication, the defect intensity in the homogeneous Poisson distribution describing the density of defects over the weld seam is defined as an optimization variable.

The defect intensity models the degree of initial quality control of the welding procedures and the weld-seam during fabrication, before the structure is put into service. The defect intensity can

have values within,

$$\mu_{min} \leq \mu \leq \mu_{max} \qquad (5.2)$$

where μ_{min} represents an extensive quality control and μ_{max} no quality control at fabrication.

Inspection Time

The time intervals between inspections are defined as optimization variables.

Inspection Length

The length of the weld seam to be examined in each inspection is defined as an optimization variable.

Inspection Quality

The ability of the inspection method to detect an inspected crack is defined through the detectable crack size a_d. The detectable crack size depends on the inspection method applied and the experience of the inspector, and is in the cost analysis defined as an exponentially distributed stochastic variable with inspection quality q,

$$F_{Ad}(a) = 1 - e^{-qa} \qquad (5.3)$$

The inspection quality is assumed equal for all the examined crack sites during an inspection.

The variable q is a measure of the quality of the inspection and is introduced in the optimization as a continuous optimization variable, describing different possible inspection methods.

In reality, however, only a discrete number of inspection qualities are available, suggesting the use of integer optimization. To avoid the problems related to integer optimization, the optimization problem is formulated in two steps, where fixed inspection qualities are selected in the second optimization, based on the results of the first optimization having continuous inspection qualities.

5.2.3 Safety and Event Margins of Weld Seam

Failure of the weld seam is defined as crack growth beyond a critical crack size a_c for one or more of the crack sites along the weld seam. The critical crack size is selected equal to the plate thickness, leading to a leakage failure criterion.

The limit state function g for failure before a time t for the weld seam is,

$$g = a_c - a(t) \qquad (5.4)$$

where $a(t)$ is the depth of the largest crack at time t

Equivalently, an inspected defect is detected if the crack size at the time of inspection is larger than the detectable crack size, giving the limit state function for detection of one or more defects at time t_j,

$$g = a_d - a(t_j) \qquad (5.5)$$

117

The safety margin of the weld seam with n crack sites is then,

$$M_{\min n}(t) = a_c - \Psi^{-1}\left(\Psi(\max_{i=1,n} a_{0i}) + C\nu_0 r(t - t_0)s_z E[\Delta\sigma^m]\right) \qquad (5.6)$$

The safety margin M_n is negative if any of the n crack sizes are larger than a_c at time t.

In an equivalent manner, the inspection event margin for k inspected crack sites is,

$$H_{\min k}(t_j) = a_d - \Psi^{-1}\left(\Psi(\max_{i=1,k} a_{0i}) + C\nu_0 r(t_j - t_0)s_z E[\Delta\sigma^m]\right) \qquad (5.7)$$

The event margin is positive if all of the k crack sizes are smaller than the detectable crack size a_d, resulting in no crack detection.

The safety and event margins are expressed through the extreme initial crack size distributions, defined through an auxiliary standard normal distribution function as shown in Chapter 4.

5.3   Failure and Event Probabilities

5.3.1   Probability of Defect Detection

The probability of detecting a crack for an inspection at time t_j is,

$$p_d = P(M_{\min 1}(t_j) > 0 \cap H_{\min 1}(t_j) \leq 0) \qquad (5.8)$$

For multiple inspections of the same area of the weld, the probability of detecting a crack at the s'th inspection that has not been detected at the $s - 1$ previous inspections, is

$$\begin{aligned} p_d = \ & P(H_{\min 1}(t_1) > 0 \cap \ldots \cap H_{\min 1}(t_{s-1}) > 0 \cap \\ & M_{\min 1}(t_s) > 0 \cap H_{\min 1}(t_s) \leq 0) \end{aligned} \qquad (5.9)$$

The estimated probability for crack detection is applied in the formulation of the Poisson distribution of undetected defects.

5.3.2   Failure and Event Probabilities of the Weld

Deterministic Number of Sites

The estimated failure probability of the weld seam is equivalent to the failure probability of a series system of n-components, where n is the number of crack initiation sites along the weld,

$$P_F(t) = P(M_{\min n}(t) \leq 0) \qquad (5.10)$$

At time t_1, $n - m$ of the total number of sites are inspected. In the time period after inspection, the failure probability of the weld is,

$$P_F(t) = P_F(t_1) + \Delta P_F(t_1, t) \qquad (5.11)$$

118

where

$$\Delta P_F(t_1, t) =$$
$$P\left((M_{\min k}(t_1) > 0 \cap H_{\min k}(t_1) > 0 \cap M_{\min k}(t) \le 0) \cup \right.$$
$$\left. (M_{\min m}(t_1) > 0) \cap M_{\min m}(t) \le 0)\right) \tag{5.12}$$

and k is the number of undetected crack sites among the inspected sites. k is binomially distributed, but is for simplicity defined by the expected value,

$$E[k] = (1 - p_d)(n - m) \tag{5.13}$$

In the above formulation, it is assumed that all detected cracks are repaired and do not contribute further to the failure probability of the weld.

Stochastic Number of Sites

For a Poisson distributed number of crack initiation sites, the failure probability of the weld length l is

$$P_F(t) = P(M_{\min n}(t) \le 0)P_N(n > 0) \tag{5.14}$$

where,

$$P_N(n > 0) = 1 - e^{-\mu l} \tag{5.15}$$

At time t_1, l_1 of the total weld length l is inspected. In the time period after inspection, the failure probability of the weld is,

$$P_F(t) = P_F(t_1) + \Delta P_F(t_1, t) \tag{5.16}$$

where

$$\Delta P_F(t_1, t) = \tag{5.17}$$
$$P\left((M_{\min k}(t_1) > 0 \cap H_{\min k}(t_1) > 0 \cap M_{\min k}(t) \le 0) \cup \right.$$
$$\left. (M_{\min m}(t_1) > 0) \cap M_{\min m}(t) \le 0)\right) P_K(k > 0)P_M(m > 0)$$
$$+ \quad P\left(M_{\min k}(t_1) > 0 \cap H_{\min k}(t_1) > 0 \cap M_{\min k}(t) \le 0\right) \times$$
$$P_K(k > 0)P_M(m = 0)$$
$$+ \quad P\left(M_{\min m}(t_1) > 0\right) \cap M_{\min m}(t) \le 0) \, P_K(k = 0)P_M(m > 0)$$

where P_K and P_M are the Poisson distribution of undetected cracks over the inspected area of the weld l_1 with defect intensity $(1 - p_d)\mu$, and the Poisson distribution of cracks over the uninspected area of the weld $l - l_1$ with defect intensity μ, respectively.

For a low failure intersection probability for the different areas of the weld, Equation (5.17) is simplified to,

$$\Delta P_F(t_1, t) =$$

$$P\left(M_{\min k}(t_1) > 0 \cap H_{\min k}(t_1) > 0 \cap M_{\min k}(t) \leq 0\right) P_K(k > 0)$$

$$+ \quad P\left(M_{\min m}(t_1) > 0\right) \cap M_{\min m}(t) \leq 0) P_M(m > 0) \tag{5.18}$$

The detected defects are not included in the above formulation of the failure probability of the weld seam, and it is assumed that all detected defects are repaired and do not contribute further to the failure probability of the weld. However, detected and repaired defects can easily be included in the further reliability analysis, having equal, or independent material parameters, dependent on the repair method, grind repair or weld repair, Madsen *et al.* [53].

Multiple Inspections

An extended, though similar, procedure is applied for multiple inspections, where it is assumed that consecutive inspection initiation points occur where the previous inspections ended, leading to a continuous loop in the inspection history when the total inspection length for multiple inspections exceeds the weld length.

At time t_2, the remaining of the m uninspected crack sites from the first inspection are examined, together with p earlier inspected undetected crack sites. In the time period after inspection, the failure probability of the weld is,

$$P_F(t) = P_F(t_2) + \Delta P_F(t_2, t) \tag{5.19}$$

where

$$\Delta P_F(t_2, t) =$$

$$P\left[(M_{\min q}(t_2) > 0 \cap H_{\min q}(t_1) > 0 \cap H_{\min q}(t_2) > 0 \cap M_{\min q}(t) \leq 0)\right.$$

$$\cup (M_{\min k-p}(t_2) > 0 \cap H_{\min k-p}(t_1) > 0 \cap M_{\min k-p}(t) \leq 0)$$

$$\left. \cup (M_{\min r}(t_2) > 0) \cap H_{\min r}(t_2) > 0 \cap M_{\min r}(t) \leq 0)\right] \tag{5.20}$$

and k is the number of earlier inspected undetected crack sites, q is the number of undetected crack sites being inspected twice and r is the number of undetected crack sites among the m sites being examined at the second inspection only.

For a Poisson distributed number of sites, all possible combinations of having / not-having crack sites over the different areas of the weld seam are included in the formulation.

5.3.3   Expected Number of Repairs

The expected number of repairs and the probability of having repair are of interest in the evaluation of the cost function, since each repair and the act of performing repair on the structure are related

to a certain cost level.

It is assumed that all detected cracks are repaired, giving the expected number of repairs for an inspection of n sites,

$$E[n_{rep}] = E[n_d] \simeq p_d n \tag{5.21}$$

and the probability of having repair,

$$P_{rep} = 1 - (1 - p_d)^n \tag{5.22}$$

For the Poisson distributed number of crack sites, the expected number of repairs after an inspection of weld length l_i is,

$$E[n_{rep}] = E[n_d] = p_d \mu l_i \tag{5.23}$$

and the probability of having repair is,

$$P_{rep} = 1 - e^{-p_d \mu l_i} \tag{5.24}$$

where p_d is the probability of detecting a crack at an inspected site at time t_i.

For multiple inspections of the same are of the weld, the same formulation is applied, where p_d is defined from Equation (5.9).

5.4 Cost Modeling

The total expected cost of the structure over the lifetime includes the cost of design, fabrication, inspection and maintenance, and the expected failure cost. This corresponds to the following cost items,

Design cost	C_D	$=$	$C_D(z)$
Fabrication cost	C_{Fa}	$=$	$C_{Fa}(\mu)$
Inspection cost	C_I	$=$	$C_I(q, l \text{ or } n)$
Cost of repair	C_R	$=$	$C_R(n_{rep})$
Cost of failure	C_F	$=$	$C_F(t)$

The design cost depends on the design parameter z, typically representing the plate or weld thickness. The influence of a change of design on the design cost is expressed through a second order Taylor expansion around the base design parameter $z = z_0$,

$$C_D(z) = C_{D0} + C_{D1}(z - z_0) + C_{D2}(z - z_0)^2 \tag{5.25}$$

For the model defining the Poisson distribution of weld defects along the weld seam, a fabrication cost is introduced. The fabrication cost relates the cost of fabrication to the intensity μ of crack

initiation sites along the weld seam. A higher fabrication cost, implying better welding procedures and initial quality assurance during fabrication, results in a lower intensity of surface weld defects. The fabrication cost is expressed as a second order function of the inverse defect intensity,

$$C_{Fa}(\mu) = C_{Fa0} + C_{Fa1}\frac{1}{\mu} + C_{Fa2}\frac{1}{\mu^2} \tag{5.26}$$

The cost of inspection is defined as a constant term modeling the cost of having an inspection, and a linear and quadratic term of the inspection quality q, proportional to the number of crack sites, or length of weld, being inspected. The inspection cost then models the cost of the inspection quality and inspection quantity for each inspection.

Deterministic number of crack initiation sites:

$$C_I(q, n) = C_{I0} + \left(C_{I1}q + C_{I2}q^2\right)n \tag{5.27}$$

Poisson distributed number of crack initiation sites:

$$C_I(q, l) = C_{I0} + \left(C_{I1}q + C_{I2}q^2\right)l \tag{5.28}$$

The repair cost is defined as a constant term modeling the cost of performing a repair at all, and a term proportional to the expected number of repairs at each inspection.

$$C_R(n_{rep}) = C_{R0}P(n_{rep} > 0) + C_{R1}E[n_{rep}] \tag{5.29}$$

Deterministic number of crack initiation sites:

$$C_R(n_{rep}) = C_{R0}\left(1 - (1 - p_d)^n\right) + C_{R1}p_d n \tag{5.30}$$

Poisson distributed number of crack initiation sites:

$$C_R(n_{rep}) = C_{R0}\left(1 - e^{-p_d\mu l}\right) + C_{R1}p_d\mu l \tag{5.31}$$

This repair cost is based on the philosophy that all detected cracks over the inspected area of the structure are repaired.

The cost of failure is assumed independent of time, modeling all the costs related to a possible failure, e.g., loss of structure, environmental cost and human casualties.

$$C_F(t) = C_F \tag{5.32}$$

The mean values of all cost items are assumed to decrease with the rate of inflation. The difference between the corporate rate of return for the project and the rate of inflation, r, is assumed constant over the lifetime of the structure.

5.5 Optimization Problem

5.5.1 Optimization Model

From the presented structural model, the reliability model and the cost model, an optimization procedure is defined for estimating the optimal initial design, fabrication quality, number of inspections, and inspection lengths and inspection qualities for each inspection.

The number of inspections over the lifetime of the structure is selected beforehand to avoid an optimization with a mixture of integer and real value optimization variables. The number of inspections is included in the optimization procedure by repeated analysis for different number of inspections, comparing the different resulting optimal expected costs.

The optimization problem for p inspections has the following optimization variables,

Structural design parameter	: z	
Fabrication defect intensity	: μ	
Time of inspections	: t_i	$i = 1, p$
Quality of inspections	: q_i	$i = 1, p$
Inspection sites, length	: n_i or l_i	$i = 1, p$

The optimization is now formulated as:

$$
\begin{aligned}
\min_{i=1,p} \quad & C(z, \mu, t_i, q_i, n_i \text{ or } l_i) = \\
\min_{i=1,p} \quad & C_D(z) + C_{Fa}(\mu) + \\
& \sum_{i=1}^{p} \left(C_I(q_i, n_i \text{ or } l_i) + C_R(n_{rep})\right)(1 - P_F(t_i))\frac{1}{(1+r)^{t_i}} \\
& + C_F(t_0)P_F(t_0) + \int_{t_0}^{t_{life}} C_F(t)\frac{\partial P_F(t)}{\partial t}\frac{1}{(1+r)^t}\, dt
\end{aligned} \tag{5.33}
$$

where the last term is approximated by,

$$
\sum_{i=1}^{p+1} C_F(t_i)(P_F(t_i) - P_F(t_{i-1}))\frac{1}{(1+r)^{t_i}} \tag{5.34}
$$

and $P_F(t_0) = 0$ and $t_{p+1} = t_{life}$.

5.5.2 Optimization Method

The optimization problem is solved by modeling the formulated optimization problem, Equation (5.33), within a modified, Friis-Hansen [27], development version of PROBAN [64], containing an option for reliability based structural optimization. The actual optimization is solved as a nested optimization, where the structural reliability analysis is done within the structural optimization. For the outer optimization, both the algorithm proposed by Han and Powell [56] and by Schittkowski

[78] have been applied. For the numerical examples presented, no significant difference between the performance of the two algorithms has been observed. Both algorithms solved the problem fairly easily (12-20 function calls, depending on the starting point).

It is of interest to notice that to be able to formulate the optimization problem, the gradient and the value of the detection probability p_d must be known. This is solved by applying the information from the component computation of the detection probability directly in the component modeling of the failure probabilities.

5.6   Example Application

To present the proposed probabilistic optimization procedure for the continuous weld containing multiple crack sites, an example is given.

A welded structure containing hazardous material for which no leakage is permissible is considered. The structure consists of 20 meters of fatigue sensitive weld being exposed to cyclic loading. The weld is investigated with respect to possible fatigue crack growth leading to through-thickness cracks.

An optimal design, fabrication quality of the weld, time of inspection and inspection quality are sought for the case of having one inspection of 25%, 50% or 75% of the weld seam over the lifetime of the structure.

Two models are considered:

- The number and locations of the weld defects are known, and 20 crack initiation sites are defined along the weld seam.

- The number and locations of weld defects along the weld seam are described by a Poisson distribution with a cost dependent defect intensity μ.

The weld defects are assumed to have Gamma distributed independent initial crack sizes a_0. The weld seam has uncertain fatigue strength due to uncertainties in the material parameters C and m. Uncertainties in the loading effect are modeled through uncertainties in the Weibull distribution parameters describing the stress range process to which the weld is exposed. The uncertainties in the material parameters and in the Weibull distribution parameters are modeled through two-dimensional distribution functions of C, m and $\ln A, 1/B$, respectively. The geometry function Y in the fatigue crack growth equation is defined as a crack size independent stochastic variable.

The value for the detectable crack sizes is equal for all the inspection sites during an inspection, but is modeled independently for the different inspection times.

The input data to the numerical analysis is given in Table 5.1, with units in N and mm unless otherwise specified. The relative relationships among the cost parameters applied to the numerical

Variable	Distrib.	Mean	St. Dev.
Init. crk. a_0	Gamma	$E[a_0] = 0.15$	$D[a_0] = 0.21$
Crit. crk. a_c	Fixed	25.0	
Det. crk. a_d	Exponential	q^{-1}	q^{-1}
Mat. par. C	Lognormal	$E[\ln C] = -29.8$	$D[\ln C] = 0.5$
Mat. par. m	Normal	$E[m] = 3.0$	$D[m] = 0.1$
Geom. fun. Y	Normal	$E[Y] = 1.0$	$D[Y] = 0.1$
Wbl. par. A	Normal	$E[\ln A] = 2.2$	$D[\ln A] = 0.15$
Wbl. par. B	Normal	$E[B^{-1}] = 1.3$	$D[B^{-1}] = 0.1$
Cyc./year ν_0	Fixed	$5 \cdot 10^6$	
Life time t_{life}	Fixed	20 years	
Weld length l	Fixed	20 meters	
Correlation	$\rho[\ln A, B^{-1}]$	-0.79	
Correlation	$\rho[\ln C, m]$	-0.89	

Table 5.1: Basic variables applied in the analysis. Units in N and mm if otherwise not specified.

analysis are subjectively assessed, and shown in Table 5.2. The units are not specified, but is to be compared with the estimated total cost.

For the model with known weld defect locations, the results from the optimization and the total expected cost are given in Table 5.3 for the three different inspection quantities of 5, 10 and 15 crack sites.

For the model with Poisson distributed defect locations, the results from the optimization with the total expected cost are given in Table 5.4 for an inspection length of 5, 10 and 15 meters.

In both of the examples given, it is seen that an increase in the inspected part of the structure results in a decrease in the design variable z.

It is also seen that an increase in the inspected part leads to a lower total expected cost, with an optimum for the entire structure inspected. This is a consequence of the linear inspection cost model applied, having no restrictions.

Further, by comparing the two examples, it is seen that the total expected cost is lower for the case having Poisson distributed crack initiation sites, a consequence of the lower expected number of crack initiation sites in this case.

5.7 Summary and Conclusion

A procedure for probabilistic optimal design, fabrication and inspection strategy for a continuous welded structure has been presented.

Fatigue crack growth has been described by the Paris and Erdogan equation and failure has been

Type of Cost	Parameter	Value
Design Cost $C_D(z)$	C_{D0}	0.0
	C_{D1}	10.0
	C_{D2}	0.1
Fabrication Cost $C_{Fa}(\mu)$	C_{Fa0}	0.0
	C_{Fa1}	0.01
	C_{Fa2}	0.04
Inspection Cost $C_I(q, n/l)$	C_{I0}	0.0
	C_{I1}	0.005
	C_{I2}	0.0
Repair Cost $C_R(n_{rep})$	C_{R0}	0.0
	C_{R1}	0.2
Failure Cost $C_F(t)$	C_F	1000.0

Table 5.2: Relative relationship among cost parameters applied in the analysis. No units specified.

Nr.Inspected.	5	10	15
Total cost $E[C]$	4.61	4.37	4.20
Design variable z	1.37	1.36	1.32
Inspect. time t_1	12.7	12.7	12.0
Insp. quality q	0.35	0.35	0.56
$P_d(t_1)$ single site	$0.70 \cdot 10^{-1}$	$0.60 \cdot 10^{-1}$	$0.91 \cdot 10^{-1}$
$P_F(t_1)$ whole weld	$0.71 \cdot 10^{-4}$	$0.96 \cdot 10^{-4}$	$0.12 \cdot 10^{-3}$
$P_F(t_{life})$ insp. part	$0.50 \cdot 10^{-4}$	$0.11 \cdot 10^{-3}$	$0.13 \cdot 10^{-3}$
$P_F(t_{life})$ uninsp. part	$0.99 \cdot 10^{-3}$	$0.90 \cdot 10^{-3}$	$0.83 \cdot 10^{-3}$

Table 5.3: Optimal solution for the case of 20 crack initiation sites.

Length Inspected	5	10	15
Total cost $E[C]$	4.22	4.03	3.67
Design variable z	1.30	1.28	1.23
Defect intensity μ	0.34	0.33	0.32
Inspect. time t_1	10.4	10.4	10.4
Insp. quality q	0.77	0.78	1.00
$P_d(t_1)$ single site	0.12	0.12	0.15
$P_F(t_1)$ whole weld	$0.22 \cdot 10^{-4}$	$0.33 \cdot 10^{-4}$	$0.75 \cdot 10^{-4}$
$P_F(t_{life})$ insp. part	$0.31 \cdot 10^{-4}$	$0.66 \cdot 10^{-4}$	$0.96 \cdot 10^{-4}$
$P_F(t_{life})$ uninsp. part	$0.11 \cdot 10^{-2}$	$0.11 \cdot 10^{-2}$	$0.12 \cdot 10^{-2}$

Table 5.4: Optimal solution for the case of Poisson distributed crack initiation sites.

defined as through-thickness crack of one or more of the weld defects along the weld seam. Reliability and associated sensitivity calculations have been performed by use of full distribution reliability methods. A structural design variable, a fabrication variable modeling the intensity of defects along the weld, the inspection times and the inspection qualities at each inspection have been applied as optimization variables.

Chapter 6

Fatigue Reliability of Tanker Panel

6.1 Introduction

In the following, the derived probabilistic model for evaluation of the fatigue reliability of multi-site homogeneous welded structures is applied to evaluate the fatigue reliability of continuous welds on a tanker structure. A realistic modeling of the environmental load response and the fatigue capacity is used.

The fatigue problem of tanker structures compared to, *e.g.*, jacket structures, is special in the sense that;

- A large number of potential crack sites exist over local areas of the structure, *e.g.*, along stiffener welds.

- The crack sites over a local area of the structure can be assumed to be exposed to an identical load response.

- Critical fatigue failure mode for structural details is usually through-thickness crack with leakage following, and not ultimate collapse of the structure due to overloading.

These considerations make the derived probabilistic model very suitable for evaluation of the fatigue reliability of local areas of a tanker structure as, *e.g.*, a plate panel, satisfying the limitations of the probabilistic model as to have identical load distribution for all the different crack sites considered.

Shinozuka [80], has presented a model for non-periodic inspection of marine structures. The model applies the Bayesian method to update the failure probability of a series system of multiple crack sites from inspection findings, and is based on material presented earlier by Itagaki *et al.*

[38, 39, 40] involving reliability updating of ship structures. The model gives an elegant solution to a difficult problem involving inspections and reliability updating of a multi-component series system subjected to fatigue crack growth and exposed to an external extreme stochastic loading process.

However, the model assumes independent exceeding probabilities of the extreme external loading process for the different joints investigated. This might be a questionable assumption in the evaluation of the fatigue reliability of a tanker structure, consisting of closely spaced critical structural details being exposed to nearly the same stochastic load response. The implications of the dependence in the exceeding probabilities of the extreme load process should be considered if the model is to be applied in the updating of the fatigue reliability of a multi component section of a tanker structure.

The assumption of independence in the loading for the different crack sites is conservative in the estimation of the failure probability of the series system prior to inspection, but can be greatly un-conservative in the evaluation of the failure probability after inspection, where the estimated likelihood of the inspection outcome is applied in the updating of the fatigue reliability model. A further discussion and comparison of the model presented in Ref. [80] and the model presented in Chapter 4 for evaluation of the fatigue reliability of tanker structures is given in Cramer [16]

In the following, the fatigue reliability of continuous welds in tanker structures is considered. The evaluation of the fatigue reliability of ship structural details requires an adequate description of the longterm stress range response to which the fatigue sensitive details are exposed, and a realistic model defining the fatigue capacity.

A procedure for evaluating the long-term stress range response on tanker structures based on a global environmental description, the sailing profile over the lifetime and the philosophy of maneuvering in higher sea states is first presented, Cramer and Friis-Hansen [18]. The fatigue capacity of the continuous weld is derived applying a linear elastic fracture mechanics model for crack initiation sites assumed to originated from surface weld defects along the weld. The fatigue reliability of a transverse weld on the tanker hull is then studied, where the effect of corrosion and inspection updating are considered.

6.2   Environmental Modeling

6.2.1   Sea Condition

The sea surface of the earth is divided into squares, known as Marsden zones [11]. Each of these zones covers a geographic area over which the wave conditions are fairly uniform, and describes the relative occurrence of different sea states, significant wave height H_s and zero crossing period T_z, combinations. The wave data for each Marsden zone is obtained through observations and measurements, under the assumption of ergodicity.

From the worldwide mission profile of the ship, the relative time period within each Marsden

zone is estimated, and the frequency of occurrence of different sea conditions is found as the weighted average of the available wave statistics in the different zones:

$$(H_s, T_z)_{lifetime} = \sum_{i=1}^{N} \mu_i (H_s, T_z)_i \tag{6.1}$$

where $(H_s, T_z)_i$ is the scatter diagram for the i'th Marsden zone, μ_i the fraction of the lifetime within which the ship is in Marsden zone i, and N the total number of zones passed by the ship over the lifetime.

It is of interest to find a continuous analytical expression of the joint distribution of the obtained weighted global discrete scatter diagram. In earlier work, the joint distribution has been expressed through a marginal two-parameter Weibull distribution in the significant wave height H_s, and a conditional 2-parameter Log-normal distribution or Weibull distribution (see Schall *et al.* [77]) in the mean zero crossing period T_z. In these approaches, the lower limit of the mean zero crossing period T_z has been taken as constant, which is a questionable assumption based on available wave statistics.

A 3-parameter marginal Weibull distribution of H_s and a 3-parameter Weibull distribution of T_z conditioned on H_s, where all the three Weibull parameters are determined through non-linear least-squares fitting is applied here, Cramer and Friis-Hansen [18]. This implies that the lower limit of the conditional distribution of the wave period T_z is estimated as a function of H_s,

$$F_{Hs}(h_s) = 1 - \exp(-\delta_h(h_s - \gamma_h)^{\beta_h}) \tag{6.2}$$

$$F_{Tz}(t_z \mid h_s) = 1 - \exp(-\delta_{t|h}(t_z - \gamma_{t|h})^{\beta_{t|h}}) \tag{6.3}$$

6.2.2 Wave Spectrum

Assuming stationarity over a short period of time (1~3 hours), the sea elevation can be described as a stationary, relatively narrow-banded, Gaussian random process, where the distribution of wave energy over different frequencies ω is expressed by a wave spectrum. For a specified H_s and T_z combination, the wave spectrum is adequately assumed to be described by the one-sided Gamma spectrum,

$$S_\eta(\omega \mid h_s, t_z) = A\omega^{-\xi} \exp(-B\omega^{-\zeta}), \quad \omega > 0 \tag{6.4}$$

The parameter ξ gives the power of the high frequency tail, and the parameter ζ describes the steepness of the low frequency part. A and B are uniquely related to H_s and T_z, leading to a simple description of the wave spectrum for different sea states,

$$A = \frac{1}{16}h_s^2\zeta\left(\frac{2\pi}{t_z}\right)^{\xi-1}\frac{\Gamma\left(\frac{\xi-1}{\zeta}\right)^{\frac{\xi-3}{2}}}{\Gamma\left(\frac{\xi-3}{\zeta}\right)^{\frac{\xi-1}{2}}} \tag{6.5}$$

$$B = \left(\frac{2\pi}{t_z}\right)^{\zeta} \frac{\Gamma\left(\frac{\xi-1}{\zeta}\right)^{\frac{\zeta}{2}}}{\Gamma\left(\frac{\xi-3}{\zeta}\right)^{\frac{\zeta}{2}}} \tag{6.6}$$

For $\zeta = 4$ and $\xi = 5$, the Gamma spectrum is equivalent to the Pierson-Moskowitz spectrum. In the analysis, both ξ and ζ are modeled as stochastic parameters.

6.2.3 Wave Energy Spreading Function

The wave energy spreading function is introduced to account for the energy spreading in different directions for a short crested sea. Short crested sea waves are described by a two-dimensional directional spectrum, where the distribution of wave energy from the main wave direction is included in the wave spectrum description. The directional spectrum is, however, difficult to obtain, and it is commonly assumed that the directional spectrum is approximated by two independent functions,

$$S_\eta(\omega, \overline{\theta}) = S_\eta(\omega) w(\overline{\theta}) \tag{6.7}$$

where $w(\cdot)$ is the spreading function, and $\overline{\theta} = \theta - \theta_0$ the spreading angle measured from the main wave component direction. To account for the short-crestedness of the waves, the following spreading function is applied:

$$w(\overline{\theta}) = \begin{cases} k\cos^n(\overline{\theta}) & ; \quad |\overline{\theta}| \leq \frac{\pi}{2} \\ 0 & ; \quad |\overline{\theta}| > \frac{\pi}{2} \end{cases} \quad ; \quad k = \frac{1}{\sqrt{\pi}} \frac{\Gamma\left(\frac{N}{2}+1\right)}{\Gamma\left(\frac{N}{2}+\frac{1}{2}\right)} \tag{6.8}$$

where n is the spreading parameter, typically modeled as a function of sea state.

It is not possible to obtain a closed form solution to the cumulative distribution function of w for non-integer values of n. The cumulative distribution function is requested in the evaluation of the long term wave response distribution, and is derived by applying numerical integration.

6.3 Wave Response

Assuming that the ship response to wave excitation is linear, the total response in a seaway is described by a superposition of the response to all regular wave components that constitute the irregular sea, leading to a frequency domain analysis. Given the linearity, the response is described by a stationary, ergodic, but not necessarily narrow-banded Gaussian process.

The linear model assumption is generally adequate, but in very severe seas the response for certain ship structures may not be linear and a non-linear analysis should be conducted.

6.3.1 Transfer Function

The transfer function $H_\sigma(\omega)$, modeling the response due to a sinusoidal wave with a unit amplitude for different frequencies, is usually obtained either from towing tank experiments or from calculations

based on the theory of ship motions in potential flow with linearized free surface conditions. The estimated transfer function is, however, only valid for a specified ship velocity V, wave heading angle Θ, and loading condition. The loading conditions are typically represented by two discrete cases, full load and ballast load, while a more continuous variation of the parameters V and Θ is requested in the analysis. In the following, a continuous description of the transfer function in the $V - \Theta$ plane is achieved by applying a two dimensional bicubic, semi-cyclic spline in the modulus squared of the transfer function, cyclic in the Θ direction. A natural spline is used in the frequency plane. The use of the bi-cubic spline function enables a continuous description of the modulus squared of the transfer function in the $V - \Theta$ plane to be obtained, having only a discrete computed representation in this plane.

The transfer function for any linear combination of the sectional forces is easily obtained by combining the complex transfer functions. For example, the transfer function for the axial stress due to combined vertical and horizontal bending is obtained at any location in the cross section using Navier's formula,

$$H_\sigma(\omega) = \frac{H_{Myy}(\omega)}{I_{yy}} z - \frac{H_{Mzz}(\omega)}{I_{zz}} y \tag{6.9}$$

where H_{Myy} and H_{Mzz} are the complex transfer functions for horizontal and vertical bending, respectively.

6.3.2 Response Spectrum

The response spectrum of the ship based on the linear model is directly given by the wave spectrum,

$$S_\sigma(\omega_e \mid h_s, t_z, v, \theta, l) = \mid H_\sigma(\omega_e \mid v, \theta; l) \mid^2 S_\eta(\omega_e \mid h_s, t_z, v, \theta) \tag{6.10}$$

where ω_e is the encountered wave frequency and $\mid H_\sigma(\omega_e) \mid$ is the modulus of the transfer function. The wave spectrum experienced by the ship, $S_\eta(\omega_e)$, is different from the wave spectrum estimated from the specified sea state, $S_\eta(\omega)$, since the latter wave spectrum is described with respect to a non-moving coordinate system.

The modification of the wave spectrum due to encounter frequency ω_e is based on frequency mapping (see, *e.g.*, Price and Bishop [70]). The relative velocity between the wave and the ship is given by

$$V_{rel} = V_{wave} - V_{ship} \cos \theta \tag{6.11}$$

The encountered wave frequency is therefore

$$\omega_e = \mid V_{wave} - V_{ship} \cos \theta \mid k = \mid \omega - k V_{ship} \cos \theta \mid \tag{6.12}$$

where the wave velocity is expressed as ω/k, $k = 2\pi/\lambda$ is the wave number and λ is the wave length. For deep water gravity waves $\omega^2 = kg$ and therefore, the encounter frequency is

$$\omega_e = \mid \omega - \frac{\omega^2}{g} V_{ship} \cos \theta \mid \tag{6.13}$$

Based on energy conservation, the response spectrum expressed in wave frequency is,

$$S_\sigma(\omega) = S_\sigma(\omega_e)\frac{\partial \omega_e}{\partial \omega} \tag{6.14}$$

The n'th spectral moment of the response spectrum experienced by the ship is,

$$\begin{aligned}
m_n &= \int_0^\infty \omega_e{}^n S_\sigma(\omega_e \mid h_s, t_z, v, \theta, l)d\omega_e \tag{6.15} \\
&= \int_0^\infty \mid \omega - \frac{\omega^2}{g}V_{ship}\cos\theta \mid^n S_\sigma(\omega \mid h_s, t_z, v, \theta, l)d\omega
\end{aligned}$$

where the response spectrum is given by,

$$S_\sigma(\omega \mid h_s, t_z, v, \theta, l) = \mid H_\sigma(\omega \mid v, \theta, l) \mid^2 S_\eta(\omega \mid h_s, t_z) \tag{6.16}$$

and $H_\sigma(\omega)$ is the transfer function in the wave frequency domain.

An efficient procedure for calculating the spectral moments is to use integration by parts, and thereby perform an analytical integration with respect to the wave spectrum. This procedure is possible since the modulus squared of the transfer function is given in terms of a spline. The integral in Equation (6.15) is then rewritten as a sum of the spline coefficients multiplied by an incomplete Gamma function expression.

Note that calculating the n'th order spectral moment of the response spectrum in the encounter wave frequency domain requires evaluation of the 2n'th order spectral moment in the absolute wave frequency domain. Therefore caution must be taken when calculating the higher order spectral moments due to the possibility of a diverging integral.

6.3.3 Operational Philosophy

In severe sea states, it is a common practice to change the speed and course of the ship in order to reduce the wave induced responses such as slamming and large rolling motions. The long term response distribution is sensitive to the higher sea states, and the effect of maneuvering should therefore be included in the response analysis.

The combined effect of course change (relative to the main wave heading direction) and speed reduction as a function of the significant wave height is modeled as, Cramer and Friis-Hansen [18],

$$f_{V\Theta|H_s}(v, \theta_0 \mid l, h_s, t_z) = f_{V|\Theta H_s}(v \mid \theta_0, l, h_s, t_z)f_{\Theta|H_s}(\theta_0 \mid l, h_s, t_z) \tag{6.17}$$

where $f_{\Theta|H_s}$ defines the density function for course selection as a function of significant wave height, and $f_{V|\Theta H_s}$ the conditional density of speed.

Heading Angle - $f_{\Theta|H_s}$

Under normal wave conditions the ship generally travels independently of the main wave heading angle θ_0. For larger wave heights the captain tries to reduce the wave induced response on the

Figure 6.1: Heading angle as a function of sea state H_s.

ship by changing the heading direction. Soares [82] has shown data describing how the change of course in higher sea states is conducted in practice, which indicates a reduction in the relative rate of occurrence of beam sea.

The proposed procedure for modeling the distribution of ship heading angles relative to the main wave direction in different sea states is the application of a directional distribution function within specified feasible domains of the heading angle. The feasible domains are given as a function of H_s, where the feasible domain for the ship heading angle is $[0, 2\pi]$ in lower sea states. For severe seas, the feasible interval is continuously decreased as a function of the significant wave height, in the sense that the possibility for beam waves is reduced. In extreme sea states, it is assumed that all the waves are encountered as head waves. The possible areas for main wave heading direction as a function of the significant wave height is shown in Figure 6.1, where the density function for possible main wave directions is assumed uniform within each area. This implies that a possible long term effect of directionality in the wave heading direction relative to the ship sailing course is ignored.

The heading directions described in Figure 6.1 are the main wave heading directions. For a short crested sea, the waves have a spread around this main wave direction given by

$$\theta = \theta_0 + \bar{\theta} \tag{6.18}$$

where the distribution function of the spreading $\bar{\theta}$ is as given in Equation (6.8).

Ship Speed - $f_{V|\Theta,H_s}$

The ship is assumed to travel at a specified cruising speed V_C under normal sea conditions. At a certain significant wave height H_1, depending on the wave heading angle, the captain decreases the speed (or changes the heading direction) in order to reduce the wave response. At another higher significant wave height H_2, it is assumed that the wave induced response is so drastic that the

Figure 6.2: Ship speed change as a function of wave angle θ and sea state H_s.

captain is forced to reduce the speed to steering speed V_S. In the intermediate phase between H_1 and H_2, a linear reduction of the ship speed with H_s is assumed. The significant wave heights H_1 and H_2 are functions of the main wave heading angle. Figure 6.2 shows the above description to model the mean ship speed as a function of θ and H_s.

Loading Condition - f_L

The ship is assumed to operate solely under two different loading conditions, fully loaded and ballast. The fraction of the lifetime under full loading condition depends on the type of ship and the sailing route. The loading condition influences the operational philosophy, since the captain makes different decisions with respect to maneuvering, depending on the loading condition (reduction of the ship speed and change of heading angle as a function of the significant wave height).

6.4 Response Statistics

6.4.1 Short Term Response

From the estimated response spectrum, the peak distribution of the response in each stationary short term period is determined using the response spectral moments.

Peak Distribution

Under the assumption of a stationary, zero mean Gaussian wave elevation process within each short term period, the response process for the linear system is also a stationary zero mean Gaussian process. For a narrow banded response process, the peaks are Rayleigh distributed,

$$F_p(a) = 1 - \exp\left(-\frac{a^2}{2m_0}\right) \tag{6.19}$$

where m_0 is the spectral moment of order zero, equal to the mean square of the response process. Depending on the response transfer function, the narrow band assumption for the response process might not be adequate. It is shown by Rice, see, *e.g.*, Ref. [50], that the peak distribution of a general zero mean stationary Gaussian process has the form,

$$F_p(a) = \Phi\left(\frac{a}{\epsilon\sqrt{m_0}}\right) - \sqrt{1-\epsilon^2}\exp\left(-\frac{a^2}{2m_0}\right)\Phi\left(\frac{\sqrt{1-\epsilon^2}}{\epsilon}\frac{a}{\sqrt{m_0}}\right) \tag{6.20}$$

where ϵ^2 is the bandwidth parameter, defined as

$$\epsilon^2 = 1 - \frac{m_2{}^2}{m_0 m_4} \tag{6.21}$$

and m_n is the spectral moment of order n. The distribution in Equation (6.20) is usually referred to as the Rice distribution. Both these distributions, Equations (6.19) and (6.20), are given directly as functions of the spectral moments of the response spectrum. It should be emphasized that the above distributions are conditional on H_s, T_z, v, θ and L. The effect of the narrow band assumption on the estimated extreme wave load distribution on a ship structure within a short term period has been investigated by Mansour [58].

The number of peaks within each time period is estimated from the rate of peaks ν_p.

$$\nu_p \approx \frac{1}{2\pi}\sqrt{\frac{m_4}{m_2}} \tag{6.22}$$

For a narrow banded process, the rate of peaks is approximated by the rate of zero crossings ν_0,

$$\nu_p \approx \nu_0 = \frac{1}{2\pi}\sqrt{\frac{m_2}{m_0}} \tag{6.23}$$

Stress Range Distribution

In the fatigue analysis, the stress range distribution is of interest. For a zero mean narrow banded process, the stress range is twice the amplitude, leading to the following stress range distribution for a narrow banded process,

$$F_{\Delta\sigma}(s) = 1 - \exp\left(-\frac{s^2}{8m_0}\right) \tag{6.24}$$

For increasing bandwidth, the process starts to include both negative and positive maxima. A fatigue analysis based on the narrow-band model ignores the effect of an increasing number of

small amplitude, high frequency oscillations. In an average sense, this leads to actual smaller peak and stress range values than the narrow band model predicts, and consequently, the narrow-band assumption will generally lead to conservative results.

Different procedures for adjusting the obtained fatigue damage applying a narrow band approach for a wide-band response process have been suggested. Veers *et al.* [91] have computed the fatigue damage of a wide-band process based on an empirical modification of the estimated Rayleigh distributed stress range and the rate of peaks. The modification is based on racetrack filtering of simulated time-series from different power spectra, leading to nearly equivalent fatigue damage as the original data. Wirsching and Light [96] have derived a wide-band correction factor for the narrow band number of peaks. Estimates of the correction factor were obtained by computing the fatigue damage from a rainflow analysis by digital simulation. For tanker structures, the correction due to wide-bandness is small and the correction factor on the narrow band number of peaks is typically in the area of 0.95~1.0.

6.4.2 Long Term Response

The long term peak distribution of the response effect over the lifetime is obtained by unconditioning the short term distribution,

$$
\begin{aligned}
F_{Long \ \Delta\sigma}(s) \ = \ & \int_{H_s}\int_{T_z}\int_L\int_\Theta\int_V \overline{\nu}_{hs,tz,l,\theta,v} F_{\Delta\sigma}(s \mid h_s,t_z,v,\theta,l) \times \\
& f_{V\Theta}(v,\theta \mid l,h_s,t_z) f_{H_sT_z}(h_s,t_z) f_L(l) \ dv \ d\theta \ dl \ dt_z \ dh_s \qquad (6.25)
\end{aligned}
$$

$\overline{\nu}_{hs,tz,l,\theta,v}$ is a weighting factor, which expresses the relative rate of response peaks within each sea state. $f_{V\Theta}(v,\theta \mid l,h_s,t_z)$ accounts for the effect of maneuvering in heavy weather with respect to sailing speed and relative heading angle, $f_L(l)$ is the discrete distribution of loading conditions and $f_{H_sT_z}$ is the two-dimensional description of the sea-state experienced by the ship over the lifetime.

It is not possible to obtain a closed form solution of Equation (6.25). Therefore the value of the integral is obtained by Monte Carlo simulation (MCs). The MCs is generally preferable for multi-dimensional integral evaluations compared to other numerical integration techniques, as there are less strict requirements on the analytical properties of the function to be integrated, and functions of a non-structured, "black-box" type can be used. The basic concepts of the MCs method are described in numerous papers and text books, *e.g.*, Rubinstein [75], and only the basic philosophy will be reviewed here.

Let's consider an integral

$$
p = \int_{\mathbf{x}\in\mathcal{R}^n} \frac{f_{\mathbf{X}}(\mathbf{x})}{h_{\mathbf{X}}(\mathbf{x})} h_{\mathbf{X}}(\mathbf{x}) \ d\mathbf{x} \qquad (6.26)
$$

where $h_{\mathbf{X}}(\mathbf{x})$ is the non-negative sampling density. By performing N simulations of the vector $\mathbf{x}$

with respect to $h_{\mathbf{X}}(\mathbf{x})$, p is estimated as the average of the sampling values

$$p \approx \frac{1}{N}\sum_{i=1}^{N} p_i = \frac{1}{N}\sum_{i=1}^{N}\frac{f_{\mathbf{X}}(\mathbf{x}_i)}{h_{\mathbf{X}}(\mathbf{x}_i)} \qquad (6.27)$$

For evaluating the integral in Equation (6.25), $h_{\mathbf{X}}(\mathbf{x})$ is conveniently taken as

$$h_{\mathbf{X}}(\mathbf{x}) = f_{V\Theta}(v,\theta \mid l,h_s,t_z)f_{H_sT_z}(h_s,t_z)f_L(l) \qquad (6.28)$$

thereby approximating Equation (6.25) as

$$F_{Long\ \Delta\sigma}(s) \approx \frac{1}{N}\sum_{i=1}^{N}\overline{\nu}_{h_s,t_z,l,\theta,v,i}\ F_{\Delta\sigma}(s \mid h_{si},t_{zi},v_i,\theta_i,l_i) \qquad (6.29)$$

Even with the use of MCs technique, the integral in Equation (6.25) is too complex to be applicable directly in a structural reliability analysis. The expression is therefore fitted to an equivalent long term peak distribution, which is calibrated to the simulated outcome of the MC simulation.

For the fatigue analysis, a Weibull distribution is found to give a good representation of the long term stress range distribution on ship structures, Mansour [57].

$$F_{Wbl}(s) = 1 - \exp(-(s/A)^B) \qquad (6.30)$$

If, e.g., a structural analysis requiring an estimate of the longterm extreme value distribution is conducted, a similar approach is applied, see Cramer and Friis-Hansen [18], where a longterm Gumbel extreme value distributions is fitted to the computed distribution.

The fittings of the Weibull parameters are based on the fractile values which approximately divide the contribution to the fatigue damage into three areas of equal magnitude,

$$\int_0^{s_1} s^m f_S(s)\ ds = \int_{s_1}^{s_2} s^m f_S(s)\ ds = \int_{s_2}^{\infty} s^m f_S(s)\ ds = \frac{1}{3}E[s^m] \qquad (6.31)$$

The fractile s_1 and s_2 are dependent on the fatigue material parameter m and the Weibull shape parameter B. In Figure 6.3 the lower and higher fractile values are given as a function of the shape parameter for different m values. For typical values, $B=1$ and $m=3$, the two fractile values are 0.95 and 0.99. The Weibull distribution parameters are then given as,

$$\ln A = \frac{k\ln s_{0.95} - \ln s_{0.99}}{k-1} \qquad ; \qquad B = \frac{\ln(-\ln 0.99)}{\ln s_{0.95} - \ln A} \qquad (6.32)$$

where

$$k = \frac{\ln(-\ln 0.95)}{\ln(-\ln 0.99)}$$

A fitting of the Weibull distribution parameters based on least square of the logarithm could also have been conducted.

Lower fractile value   Higher fractile value
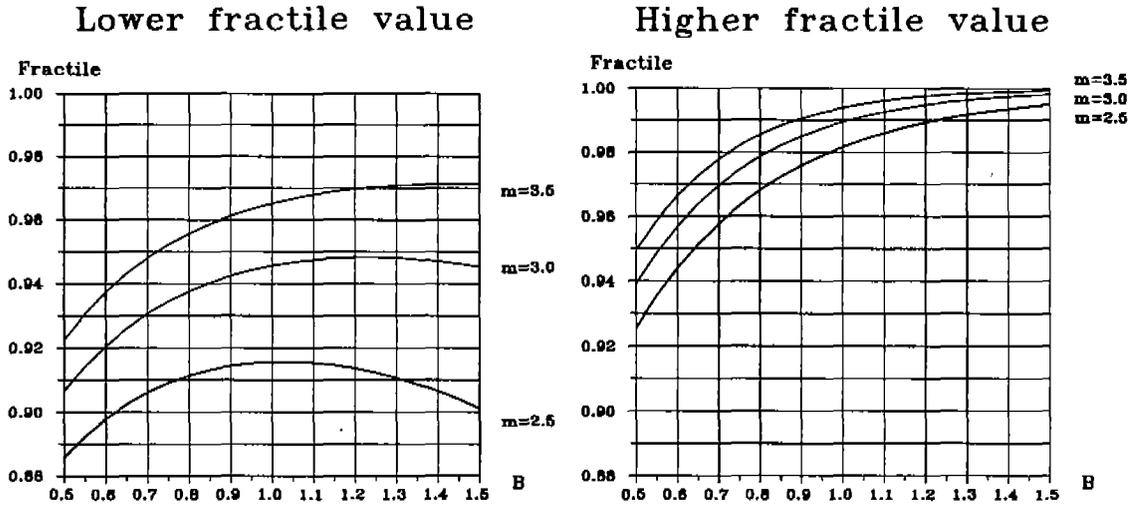
Figure 6.3: Fractile values dividing the contribution to the fatigue damage into 3 areas of equal magnitude.

The average rate of stress cycles over the lifetime is found in the simulation procedure for the evaluation of the long term response distribution,

$$\nu_0 = \frac{1}{N} \sum_{i=1}^{N} \nu_{hs,tz,l,\theta,v,i} \tag{6.33}$$

where $\nu_{hs,tz,l,\theta,v,i}$ is the rate of stress cycles for the specified short term condition i and N is the number of simulations used in evaluating the integral. The number of stress cycles the ship is exposed to in its lifetime t_L is then given by,

$$N_{peak} = \nu_0 r_L t_L \tag{6.34}$$

where r_L models the fraction of the lifetime the ship is expected to be at sea.

6.4.3 Uncertainty Modeling

In evaluation of the fatigue damage on a ship structure, it is the cumulative damage from multiple wave induced load cycles that is of concern. Due to the generally high number of load cycles necessary to cause fatigue damage, the physical uncertainties in the environmental description are of less importance in the evaluation of the fatigue damage. The focus of the uncertainty modeling of the stress response analysis will therefore be on the model uncertainties in the environmental description and in the load response evaluation, where both the systematic and random model uncertainties are considered.

The systematic model uncertainties are accounted for through the use of bias factors in the theoretical model for evaluation of the stress response. The systematic uncertainties are then indirectly

included in the response model through the estimated longterm stress distribution parameters. The random model uncertainties are equivalently included in the analysis applying stochastic variables in the model deriving the longterm stress response. The physical, model and statistical uncertainties are then represented through a bi-variate stochastic description of the distribution parameters in the estimated longterm stress distribution.

Uncertainty in Sea State Description

From the available wave scatter diagram, estimates of the Weibull distribution parameters δ_h, β_h, γ_h and $\delta_t(h)$, $\beta_t(h)$, $\gamma_t(h)$ are obtained. In order to include the uncertainties in the wave scatter diagram, these estimates are modeled as stochastic variables having a correlation matrix equal to the one obtained from the non-linear least squares fit. The coefficient of variation of the variables should be chosen according to the quality of the data. The quality of the data is classified according to the quality of the observation method, *i.e.* visual observation, instrumental measurements or hind-cast simulation. The available wave heights and wave periods are often obtained from measurements of short duration, which may not adequately account for seasonal and climatological variations.

Uncertainty in Wave Spectrum

The parameter ξ might be set equal to 5 (see Phillips [68]), and the bandwidth parameter ζ is taken as a random variable in order to account for uncertainties in the wave spectrum and the band width variation. The standard deviation of the ζ parameter σ_ζ is selected in accordance with the confidence in the spectrum.

Uncertainty in Wave Energy Spreading Function

In order to include the uncertainty in the wave energy spreading function in Equation (6.8), the H_s dependent parameter N in Equation (6.8) is multiplied by a Lognormally distributed random variable with mean value equal to 1 and a specified coefficient of variation depending on the sailing route.

Uncertainty in Operational Philosophy

The operational philosophy has an important influence on the long term peak distribution. It is therefore of importance to include uncertainties in the modeling of the wave heights for which heading direction and sailing speed are changed, see Figures 6.1 and 6.2. The operational philosophy is subjectively judged by the captain/ship owners, and may vary from ship to ship. Consequently, it is recommended to assign a rather high standard deviation to the significant wave heights for which changes are conducted.

Uncertainty in Ship Speed

It is assumed that the ship operates under fairly constant speed in a particular sea state according to the operational philosophy. Consequently, the uncertainty in the estimated ship speed is small.

Uncertainty in Transfer Function

The uncertainty related to the modeling of the transfer function is the dominant uncertainty in the prediction of the longterm stress range distribution for the fatigue analysis. The uncertainty in the transfer function describes the uncertainty in the ability to determine the nominal stress response to a unit sinusoidal wave.

The uncertainty in the prediction of the nominal stress response is due to,

- Uncertainty with respect to the assumption of linear response.

- Uncertainty in the computation of inertia forces from wave excitation.

- Uncertainty in the geometry from manufacturing imperfections.

- Uncertainty in the prediction of global and local stress response from inertia forces applying beam theory or finite element analysis.

Soares [82] has conducted an extensive study over the various bias terms affecting the transfer function calculation. Including the bias factors, the transfer function may be rewritten as

$$\hat{H}(\omega) = \psi_L \psi_{SH} H_L(\omega) \tag{6.35}$$

where ψ_L is a bias factor representing the difference between experiments and the mathematically estimated transfer functions and ψ_{SH} is a non-linear bias factor. When the calculation of the transfer functions is based on the theory of Salvesen, Tuck and Faltinsen [76], the bias factor ψ_L is given as in Ref. [82],

$$\psi_L = \begin{cases} -0.005\theta + 0.42F_n + 0.70C_B + 1.25 & ; \quad 90 < \theta \le 180 \\ 0.0063\theta + 1.22F_n + 0.66C_B + 0.06 & ; \quad 0 \le \theta < 90 \end{cases} \tag{6.36}$$

where F_n is the Froude number and C_B is the block coefficient.

In Bach-Gansmo *et al.* [5], it is reported that traditional two-dimensional strip theory will overestimate the vertical midships bending moment due to the neglect of three dimensional effects. For a ship with block coefficient of 0.8, the overestimation is reported to be 15 ~ 25 % for wave lengths equal to the ship length.

The non-linearity bias factor ψ_{SH} accounts for the difference in sagging and hogging moments, and depends on the accuracy of the assumption that the ship sides are vertical,

$$\psi_S = 1.74 - 0.93C_B \qquad \text{(sagging)} \tag{6.37}$$

/42

$$\psi_H = 0.26 + 0.93C_B \qquad \text{(hogging)} \qquad (6.38)$$

Note that when applying these non-linearity factors for fatigue analysis, one should apply $(\psi_S + \psi_H)/2 = 1$, implying that the non-linear sagging/hogging effect on the estimated fatigue damage has no influence.

Studies, *e.g.*, Winterstein [94] and Jensen [41], show that the non-linearities in the longitudinal stress component can lead to an increase in the fatigue damage on container ships on the order of 50~100 %, depending on the forward speed. For tanker structures, however, the non-linearities are found to have minor influence with respect to the estimated fatigue damage, Jensen and Pedersen [42].

A general description of uncertainties involved in the stress analysis on ship structures is given in Nikolaidis and Kaplan [62]. An uncertainty in the wave load prediction resulting in a COV of 10% is suggested here. In addition, uncertainties related to the derivation of the nominal stress level must be included.

6.4.4 Boot Strapping

To include the above mentioned uncertainties in the calibration of the long term Weibull distribution, the boot-strapping technique is applied. For consecutive outcomes of the uncertain parameters, values of $\ln A$ and B in Equation (6.30) are calculated. The mean values, the standard deviations and the correlation of the parameters are then obtained. The simplified estimated long term Weibull response distribution with correlated stochastic distribution parameters may then be directly applied in the following structural fatigue reliability analysis.

Stable results for the stochastic parameter estimation after approximately 200 simulations of the uncertain parameters have been found.

To take full advantage of the presented procedure for calculation of the long term wave induced response on ship structures, a qualitative description of the maneuvering philosophy in higher sea states and realistic estimates of the uncertainties involved in the evaluation of the local response must be provided.

Based on the boot-strapping approach, all the uncertainties related to the prediction of the nominal stress response are represented through the bi-variate stochastic description of the longterm Weibull distribution parameters A and B.

6.5 Fatigue Model

Experience with ship structures shows that fatigue represents a durability problem rather than a hull girder strength problem, Bach-Gansmo *et al.* [5]. For this reason, through thickness crack is considered critical in the fatigue analysis, having a critical crack depth equal to the plate thickness. A general discussion of the fatigue problem on ship structures is given in Thayamballi *et al.* [83].

6.5.1   Distribution of Weld Defects

Ship structures consist of a large amount of continuous transverse and longitudinal welds, represented through both butt and fillet welds. The continuous welds are exposed to stress distributions that are fairly uniform over large areas of the structure, as, *e.g.*, at deck, bottom or side shell panels. Fatigue cracking of welded structures will typically originate from the weld region. The fatigue crack initiation positions are therefore unpredictable and might occur at many locations along the welds.

For continuous transverse welds, the points of crack initiation are typically the notches at the edges of the weld reinforcement, being parallel to the direction of the applied stress.

For continuous longitudinal welds, the notches at the edge of the weld reinforcement are parallel to the applied stress and are therefore innocuous, Gurney [32]. However, weld rippling (pronounced change in the longitudinal profile) is important since the ripples form notches transverse to the direction of applied stress. More ripples will generally exist for manual welds than automatic welds, which have a smoother surface. The typical mode of failure of a continuous longitudinal weld involves cracking from the most severe ripple, which for manual welds tends to be at start-stop positions in the welding procedure.

Weld defects are a product of low quality fabrication processes. The defects can generally be grouped into internal defects and surface defects. Surface defects, *e.g.*, undercuts, are usually of more concern for fatigue crack growth analysis than internal defects because they are located normal to applied stress at point of stress concentration. However, if the weld is ground smooth in order to improve its fatigue performance, internal defects become crucial. A general overview of different types of weld defects and their importance is given by Wastberg and Karlsen in Ref. [3].

The distribution of weld defects along continuous welds depends highly on the choice of welding procedure and quality of workmanship, and no concise information exists with respect to the rate of occurrence of weld defects as a result of applying different welding techniques and welding procedures.

For internal defects, Wong and Rogerson [97] have reported an average internal defect rate of 0.7 /meter after ultrasonic examination of a total length of manual weld of 1000 meters on an offshore structure. An equivalent examination by Bokalrud and Karlsen [9] of 3,200 meters of machine butt welds randomly selected from a ship hull sample of 40,000 meters, resulted in an internal defect rate of 0.1 /meter.

For surface defects, Bokalrud and Karlsen reported, in the same study, a rate of undercuts of 16 /meter. This occurrence rate was based on 827 replicas from silicon rubber covering a total of 20 meters of various manual welds in a ship hull. Førli and Pettersen [26], have investigated the rate of occurrence of different types of weld defects by examining 66 meters of butt welded plates and pipes. They reported a rate of incomplete penetration, rate of lack of fusion and rate of crack equal to 0.5 /meter, 1.8 /meter and 0.7 /meter, respectively.

The scarcity in available data and the inconsistency in the reported results, especially for surface defects, result in large uncertainties with respect to the modeling of the rate of occurrence of crack

initiation sites along continuous welds. For a ship structure entering service, the distribution of crack sites in the structure will depend on the acceptable defect size in accordance with classification societies and rate of defects not being detected during fabrication.

6.5.2 Initial Crack Size

Crack growth usually originates from initial weld defects at fabrication, where experience has shown that almost all fatigue cracks have started to grow from initial surface defects. Surface defects, like undercuts and lack of penetration, are similar in nature to fatigue cracks, having sharp edges from which crack growth will occur. The number of cycles to initiate a fatigue crack from surface defects is therefore small, and usually negligible. The size of the initial crack to be applied in fatigue fracture mechanics analysis consequently corresponds to the size of the surface weld defect.

The size of the initial surface defect at the beginning of service life depends on the welding material, the quality of the welding procedure, and the extent of initial inspection routines during fabrication. Inherent uncertainties are therefore associated with the estimation of the initial crack size from surface defects.

In Bokalrud and Karlsen [9], the size of 325 surface defects found over 20 meters of examined ship hull weld were reported to be exponentially distributed, having a mean value of 0.11 mm. Eide and Berge [24] conducted fatigue tests of large scale transverse stiffeners and found that fatigue cracks initiated from weld defects at the weld toe, having initial defect sizes in the range of $0.05 \sim 0.40$ mm, with mean value of 0.15 mm. A general overview of different experimental results confirming the above values is given in Ref. [3].

For transverse welds, the multiple fatigue cracks initiated at different locations along the weld will influence each other during the crack growth stage, and crack coalescence of two or more cracks might typically occur. The coalescence of fatigue cracks reduces the aspect ratio of the crack and will therefore influence (increase) the crack growth rate in the depth direction. However, from the experimental study of Eide and Berge [24], it was found that crack coalescence first occurred at crack depths of around 5 mm, independent of the plate thickness. A main part of the fatigue life had therefore already been experienced before crack coalescence occurred, reducing the effect of crack coalescence on the estimated fatigue life of a crack.

Friis-Hansen *et al.* [29] studied the influence of crack coalescence applying a stochastic two-dimensional fatigue crack growth model, and concluded that the fatigue reliability of the weld seam is less influenced by crack coalescence than the fatigue reliability of each single crack site. This is due to the fact that crack coalescence leads to a smaller number of fatigue cracks over the specified weld length, which reduces the series system effect. The effect of crack coalescence is therefore not included in the following probabilistic analysis of a continuous weld.

Environment	m	$E[\ln C]$	$D[\ln C]$
Non-Corrosive (B&K)	3.1	-28.84	0.55
Non-Corrosive (DnV)	3.1	-29.84	0.55
Corrosive (B&K)	3.3	-28.89	0.79
Corrosive (DnV)	3.5	-31.01	0.77

Table 6.1: Modeling of fatigue material parameters.

6.5.3 Fatigue Parameters

The fatigue crack growth material parameters C and m determine the rate of fatigue crack growth for a specified stress intensity range. However, experimental results by Virkler *et al.* [93] have shown a large degree of scatter in the crack growth rate, suggesting a stochastic description of the fatigue material parameters.

The scatter in the crack growth rate is apparent not only for the different specimens, but irregularity is also shown within each specimen for increasing crack sizes. The irregularity within each specimen is due to in homogeneous material properties, which can be included in the stochastic model by describing C as a stochastic process of the crack size, Ortiz [65]. The in homogeneous material properties for each specimen, however, do not generally influence the fatigue capacity of the weld, and it is assumed that the same material properties exist over the welded area. The uncertainty related to the scatter in the fatigue crack growth rate is modeled through a stochastic description of the material parameters.

In the study by Bokalrud and Karlsen [9], 2,900 different crack growth measurements in structural steel from various investigations were analyzed, whereas 700 of these measurements were reported from a corrosive environment. Applying a model where m is fixed and C is Lognormally distributed, the values presented in Table 6.1 were suggested by the authors for a corrosive and non-corrosive environment. Also presented in the table are values suggested by DnV [1], recommended to be applied when no other information exists.

It is seen from the table that a corrosive environment influences the fatigue crack growth material parameters. However, as is shown in Chapter 3, a corrosive environment can also lead to a general increase in the stress range level over time due to reduced steel thickness.

In Ohyagi [63], a study on the effect of corrosion on ship structural members has been conducted. For corrosion in upper deck, side shell, bottom shell and bulkhead of oil tankers, a Lognormally distributed corrosion rate with mean value 0.1 and COV of 0.8 per year is reported. Akita [2], suggests an Exponentially distributed corrosion rate, with a Gamma distributed mean corrosion rate. The stochastic modeling of the mean rate of corrosion accounts for the statistical variation in the degree of corrosion for different ships. It is also expected that the rate of corrosion depends on the type of tank investigated. In Pollard and Bea [69], a thorough study of the effect of corrosion

damage in cargo and ballast tanks of crude and product carriers has been performed. It is here shown that the rate of corrosion is highly dependent on tank type and location within tank. A mean corrosion rate as high as 0.15~0.19 mm/year for some locations was reported.

A large fraction of the environmental load response on ship structures are in the domain of low crack growth rate. The modeling of the lower threshold level, ΔK_{th} under which stress intensity no crack growth is assumed to occur, therefore influences the evaluation of the accumulated fatigue damage. The threshold level is influenced by numerous factors such as, e.g., the mean stress level, residual stresses, sequence effects and environmental conditions. British Standards Institution, [12] recommends the following form of the threshold level,

$$\Delta K_{th} = 190 - 144R \quad [Nmm^{-3/2}] \tag{6.39}$$

where R is the stress ratio.

Large uncertainties are associated with the modeling of the mean still water stress level and the residual stresses in ship structures, and large uncertainties are therefore associated with the derivation of the lower threshold level ΔK_{th}.

6.5.4 Stress Intensity Factor

The modeling of the stress intensity factor is of crucial importance in the evaluation of the fatigue life of structural members in the ship hull. In the following, the empirical expression fitted by Newman and Raju [61] from finite element analyses is applied. A correction for the presence of the weld according to Smith and Hurworth [81] is included. Both expressions are defined in Chapter 3.

Due to model uncertainties, a stochastic bias factor Y_0 is defined to account for systematic and random uncertainties in the fatigue capacity model.

The modeling of the stress intensity factor is influenced by the aspect ratio of the assumed semi-elliptical crack, which again is influenced by the bending/tension stress ratio. In a theoretical study by Friis-Hansen and Madsen [30], applying a stochastic two-dimensional fatigue crack growth model, it was found that the aspect ratio a/c converged quite rapidly to 0.1 and 0.8 under pure bending and tension stresses, respectively. For combined bending and tension stress configuration, an aspect ratio within these boundaries is to be expected.

In the fatigue test by Eide and Berge [24], an aspect ratio of 0.5 was reported for fatigue cracks developing along the weld toe for transverse stiffener welds. The fatigue test confirms the theoretical results, since the presence of the transverse weld leads to a non-uniform stress distribution over the parent material, leading to a lower aspect ratio than pure tension stresses would give.

6.5.5 Inspection Quality

Common practice for inspection of internal structural members on ship structures are periodic inspections every fourth or fifth year. However, the reliability of visual inspections for detection
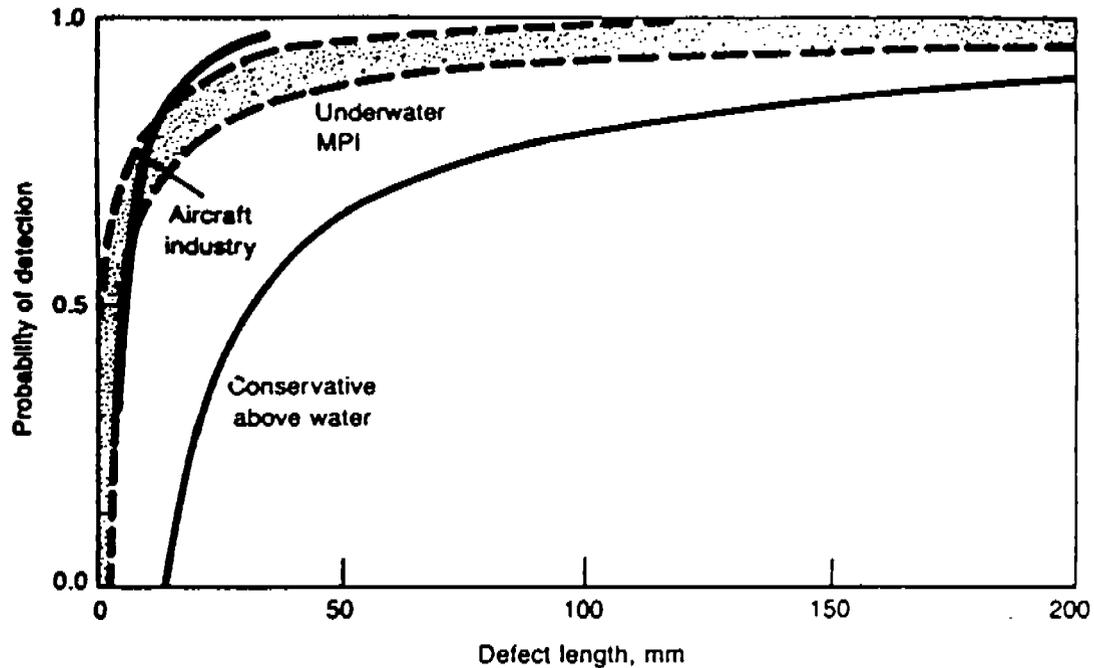
Figure 6.4: Probability of crack detection curves for different inspection procedures.

of surface cracks is questionable, unless the cracks are associated with significant openings or are delineated by corrosion products.

The probability of detecting (POD) a fatigue crack through visual inspection is associated with large uncertainties, and no concise information describing the detection probability as a function of the surface crack length seems to exist for visual inspections. In Figure 6.4, Ref. [90], established POD curves for underwater MPI inspections and the aircraft industry are shown. The figure also includes a conservative above water curve, defining a possible POD curve for visual inspection. However, in the probabilistic modeling, it is important to apply realistic rather than conservative estimates for the uncertain variables. All three curves show a typical exponential form, suggesting an exponentially distributed smallest detectable crack size in the modeling of the detection probability.

The figure indicates a conservative 50% probability of detecting a crack of length 30 mm for above water inspection. Assuming the aspect ratio of $a/c = 0.5$, this corresponds to an inspection quality $q = 0.1$, having an exponentially distributed smallest detectable crack size. Comparatively, an underwater MPI inspection leads to a 85%~ 95% detection probability of a 30 mm long crack, having an inspection quality of $q = 0.3 \sim 0.4$. The inspection quality for an above water MPI inspection can be expected to be even higher. However, an MPI inspection is costly and time consuming, and it is unrealistic to believe that an MPI inspection on a large scale can be applied for general inspections of ship structural members.

/48

The main fraction of the crack growth life of a fatigue crack is usually experienced while the crack size is small, say less than 5~10 mm deep, corresponding to a crack of length 20~40 mm. The probability of detecting a crack of this size by visual inspection is less than 50%, and the inspection result of no crack detection of an inspected crack site for visual inspection will therefore not contribute significantly to the updated estimated fatigue life of a potential crack site after inspection.

In Holzman [37], a summary of practical problems related to tank inspection is given. It is reported here, based on a survey of U.S. Coast Guard inspectors, that as the size of the vessels increases, the percentage of internal structural members being inspected during a periodic inspection decreases. For a tanker structure of 200 KDWT, only 20%~25% of a tank is generally inspected (bottom walking only). This will drastically reduce the detection probability in the upper areas of the tank. In the study by Holzman, a general discussion of fatigue cracks not being detected (missed cracks) during realistic visual inspections on ship structures is given.

The dimensions of today's VLCC (Very Large Crude Carriers) and ULCC (Ultra Large Crude Carriers) are enormous, having typically 50~60 km of longitudinal stiffeners and more than 1,000 km of welds, whereas ca. 30% is hand welding. These dimensions will generally lead to a tradeoff between a complete general inspection of the whole tanker structure and a partial inspection of critical structural areas of the tanker, applying a higher inspection quality. The critical structural areas can, *e.g.*, be defined as areas having high stress response or a history of problems. The information gained from the inspection of these areas can then be applied to update the general reliability level of uninspected areas.

The reliability of a visual or an MPI inspection is a function of the crack length, whereas the failure criteria is usually based on a critical crack depth. Estimates of the crack aspect ratio must therefore exist if the inspection results are to be applied in the updating of the fatigue life. As described earlier, this aspect ratio is a function of the type of loading condition, the relationship between bending and tension stresses.

Due to the influence of the inspector's experience, the type of tank and the access ability on the quality of a visual inspection, large uncertainties are associated with the modeling of a POD curve for visual tank inspection. However, theoretical procedures have been developed for inclusion of inspection results in the probabilistic fatigue analysis, Madsen [51], and it is stressed that effort should be made by the industry to establish reliable POD curves for tanker inspection.

6.6 Numerical Study

In the following, the fatigue reliability of a continuous transverse fillet weld on the bottom midships section of a tanker structure is considered, Figure 6.5. This location, along with the middle third section of the side shell, was found by Bea *et al.*, Structural Maintenance for New and Existing Ships

Structural parameter	Dimension
Length overall	274.170 m
Length between perpendiculars	262.130 m
Length at 17.450 m water line	269.600 m
Scantling length	261.520 m
Breadth molded	52.410 m
Depth molded	22.810 m
Scantling draft	17.450 m
Displacement molded (17.450 m WL)	196500 T
Block coefficient C_B	0.809
Midship moment of inertia I_{yy}	544.781 m^4
Midship moment of inertia I_{zz}	1688.300 m^4
Distance N-A to bottom y_0	11.158 m
Distance C-L to side shell z_0	26.205 m
Deck/Bottom plate thickness z	18.5 mm

Table 6.2: Principal dimensions of tanker structure.

[7], to be of major concern for the fatigue life of tanker structures.

The 164,000 DWT segregated ballast tanker structure investigated is shown in Figure 6.6, where the principal dimensions are given in Table 6.2. The tanker structure is assumed to sail in a transatlantic route over the service life, having an equal relative occupation time in Marsden zones 15, 16, 24 and 25. In Figure 6.7 the two-dimensional distribution of significant wave height (H_s) and zero crossing period (T_z) experienced by the tanker is shown. The bi-variate distribution is expressed through a 3-parameter marginal Weibull distribution of H_s, and a 3-parameter Weibull distribution of T_z conditioned on H_s. The marginal distribution parameters of H_s were,

$$\delta = 0.22, \quad \beta = 1.54, \quad \gamma = 0.09 \qquad (6.40)$$

The conditional distribution parameters of T_z as a function of H_s are given in Figure 6.8.

The uncertainties related to the modeling of the long term stress response are described in Table 6.3. A realistic environmental description is attempted, where uncertainties related to the maneuvering philosophy in higher sea states is included. In the table, the modeled significant wave heights H_s leading to speed reduction and forced cruising speed in higher sea states is given for head, beam and following sea.

The systematic model uncertainties in the theoretical estimate of the transfer function is included in the response model through the use of the bias factor suggested by Soares [82], Equation (6.36), being modeled with a 10% COV. Non-linear effects are assumed not to be of influence in the derivation of the longterm stress range distribution. A bias factor is also included in the modeling of the wave scatter diagram

From the stochastic modeling of the environment, the loading and the load effect, the stochastic

_ /50

Variable	Distribution	Mean	COV
Bias on wave scatter diagram	Normal	1.00	0.01
Wave spectrum param. ξ	Fixed	5.00	-
Wave spectrum param. ζ	Normal	4.00	0.20
Spreading parameter n	Fixed	2.00	-
Transfer function	Lognormal	1.00	0.25
Linear bias factor	Normal	1.00	0.10
Non-linear bias factor	Fixed	1.00	-
Operational wave height	Lognormal	1.00	0.05
Cruising speed	Normal	7.21	0.05
Steering speed	Normal	2.06	0.05
H_s Speed reduction in head sea	Normal	8.00	0.10
H_s Speed reduction in beam sea	Normal	5.00	0.10
H_s Speed reduction in fol. sea	Normal	6.00	0.10
H_s Cruising speed in head sea	Normal	10.00	0.10
H_s Cruising speed in beam sea	Normal	7.00	0.10
H_s Cruising speed in fol. sea	Normal	8.00	0.10

Table 6.3: Uncertainties in the stress response modeling. SI units.

$E[\ln A]$	$D[\ln A]$	$E[B]$	$D[B]$	ρ	ν_0
2.08	0.24	0.88	0.01	0.01	$3.25 \cdot 10^6$

Table 6.4: Mean and standard deviation for Weibull parameters.

description of the wave induced nominal longterm stress range distribution is derived and expressed through a longterm Weibull stress range distribution having stochastic distribution parameters. The longterm stress range Weibull distribution represents the distribution of the nominal longitudinal wave induced stresses in the tank bottom at midships, due to the combined effect of vertical and horizontal bending of the ship hull.

In Table 6.4 the joint bi-variate distribution of the Weibull distribution parameters are given. The uncertainties reflected in the joint distribution of $\ln A$ and B represent the uncertainties in the stress response modeling, Table 6.3. It is seen from the table that a relatively high COV of 0.11 has been derived for the scale parameter $\ln A$, whereas a nearly deterministic estimate is defined for the shape parameter B. However, it is important to remember that $\ln A$ and B have been evaluated together and must be considered as a pair in the analysis. Due to the low uncertainty assigned to the distribution of B, the correlation between $\ln A$ and B is also small, close to zero. The table also shows a computed number of wave induced load cycles per year of $3.25 \cdot 10^6$.

Figure 6.9 shows the natural logarithm of the computed longterm Weibull stress range distribution for mean values of the distribution parameters. The curve has a slight curvature due to the

value of the shape parameter less than one. Equivalent results are also shown for $E[\ln A] \pm D[\ln A]$. It is seen that large uncertainties are expressed on the longterm nominal stress range distribution due to the uncertainties in the environmental model and in the computation of the load effect.

The longterm Weibull stress range distribution is computed here applying a longterm frequency domain analysis. This is a very computationally costly approach, requiring unconditioning with respect to sea state conditions, ship speeds, wave heading angle and loading condition. Another simplified approach commonly applied to evaluate the longterm stress range distribution is to compute the extreme stress response for a specified extreme environmental condition over a certain time period. The computed extreme stress response is then applied together with a chosen value for the shape parameter B to evaluate the longterm stress range response.

Defining σ_N as the maximum wave induced stress response out of N wave cycles, the Weibull scale parameter A is written as,

$$P(\sigma \leq \sigma_N) = 1 - \exp(-(\sigma_N/A)^B) = 1 - 1/N \tag{6.41}$$

$$\Rightarrow \quad A = \sigma_N(\ln N)^{-1/B} \tag{6.42}$$

The expression for the m'th moment of the stress range process modeling the fatigue damage is then further,

$$E[\sigma^m] = A^m \Gamma(1 + \frac{m}{B}) = \sigma_N^m (\ln N)^{-m/B} \Gamma(1 + \frac{m}{B}) \tag{6.43}$$

This approach requires good estimates for the computed extreme stress response and for the chosen Weibull shape parameter B to be made to ensure realistic estimates of the wave induced fatigue damage. It is seen that the m'th moment of the response process is sensitive to the value of the shape parameter B, especially if a low exceedence probability (high N value) has been applied in the evaluation of the extreme stress response.

Values of N in the area of $N^4 \sim 10^8$ are commonly applied by the marine industry. However, these high value of N leads to a high sensitivity and dependence on the chosen value of B on the estimated wave induced fatigue damage. Assuming the material parameter $m = 3$ and the number of load cycles defining the extreme loading condition $N = 10^4$, a variation of $B = 1.0 \pm 10\%$, from $0.9 \sim 1.1$, leads to a relative change in the accumulated fatigue damage of around $\pm 30\%$, $0.74 \sim 1.31$. If the extreme loading condition is based on $N = 10^8$, the change in the accumulated damage would be even more extreme, $(0.58 \sim 1.59)$. Applying the simplified approach in the evaluation of the longterm stress range distribution, large uncertainties are therefore introduced in the estimation of the accumulated fatigue damage from uncertainties in the modeling of B.

However, it is seen from Equation (6.43) that $\Gamma(\cdot)$ decreases and the term $(\ln N)^{-m/B}$ increases with increasing B values. It is therefore possible to define an optimal extreme loading condition N that minimizes the uncertainties in the fatigue damage from uncertainties in the choice of shape parameter,

$$\frac{\partial E[\sigma^m]}{\partial B} = \frac{\partial \sigma_N^m (\ln N)^{-m/B} \Gamma(1 + \frac{m}{B})}{\partial B} = 0 \tag{6.44}$$

/52

Variable	Distrib.	Mean	Standard Deviation
Dist. of sites	Poisson	μ	μ
Site intensity μ	Fixed		parameter study
Det. crk. a_d	Expon.	$1/q$	$1/q$
Insp. quality q	Fixed		parameter study
Corr. rate k	Fixed		parameter study
Init. crk. a_0	Gamma	$E[a_0] = 0.15$ mm	$D[a_0] = 0.15$
Crit. crk. a_c	Fixed	18.5 mm	
Aspect ratio a/c	Lognormal	$E[a/c] = 0.5$	$D[a/c]=0.05$
Stress rel. S_b/S_t	Fixed	0.05	
Life time t_{life}	Fixed	20 years	
Insp. time t_{insp}	Fixed	10 years	
Weld length l	Fixed	20 m	
Cycle rate ν_0	Fixed	$3.25 \cdot 10^6$ year^{-1}	
Exposure rate r	Fixed	0.8	
Mat. par. C	Lognorm.	$E[\ln C] = -29.84$	$D[\ln C] = 0.55$
Mat. par. m	Fixed	3.1	
Bias geom. fn. Y_0	Normal	$E[Y_0] = 1.0$	$D[Y_0] = 0.1$
Threshold ΔK_{th}	Fixed	0.0	

Table 6.5: Modeling of input variables for fatigue model. Units is N and mm if otherwise not specified.

$$\Rightarrow \quad N = \exp(\exp(\tilde{\Psi}(1 + \frac{m}{B}))) \tag{6.45}$$

where $\tilde{\Psi}(\cdot)$ is the Psi function, $\partial \ln \Gamma(\cdot)/\partial(\cdot)$. In Figure 6.10 the N value minimizing the influence of uncertainty of the chosen shape parameter B is given. For $m = 3.1$ and $B = 0.88$, this procedure suggests that the extreme stress condition σ_N should be estimated from $N = 60$ load cycles in order to minimize the influence of uncertainties of B on the estimated fatigue damage.

In Figure 6.11 the relative influence of the chosen shape parameter B on the estimated fatigue damage is shown depending on the number of cycles being applied to define the extreme loading condition. It is seen that for high values of N, the estimated fatigue damage is sensitive to uncertainties of B. It is therefore suggested that an estimate of the longterm stress range distribution applying the longterm frequency domain analysis be applied in the evaluation the fatigue damage on marine structures, unless good estimates of the shape parameter exist for the investigated structure under the specified environmental conditions.

The continuous transverse fillet weld in the tanker structure studied is shown in Figure 6.12, having multiple crack initiation sites along the weld. Based on the discussed fatigue reliability model on ship structures, the stochastic fatigue model shown in Table 6.5 is applied in the probabilistic analysis.

The fatigue reliability of the weld over the lifetime of 20 years is studied, where it is assumed

that the tanker has a sailing rate of 80%.

Due to the lack of concise data enabling a realistic modeling of the rate of occurrence of weld defects along continuous welds, a reasonable definition of the defect intensity μ is difficult to obtain. No specific value of the rate of crack sites along the weld is therefore applied, and a parameter study of the influence of μ on the estimated fatigue reliability is conducted instead.

From the estimated longterm load response and the stochastic fatigue capacity model, the fatigue damage is estimated. Defining accumulated fatigue damage leading to failure as 1.0, the cumulative distribution of the fatigue damage over a lifetime of 20 years for a single fatigue crack site is shown in Figure 6.13, having mean value and COV,

$$E[\Delta_{20}] = 6.9 \cdot 10^{-2} \qquad COV[\Delta_{20}] = 150\% \tag{6.46}$$

It is seen that the uncertainties on the estimated fatigue damage is relatively high.

In Figure 6.14 the fatigue reliability of the weld is computed for different numbers of crack sites over the weld length. For a single crack site, the fatigue reliability after 20 years is $\beta = 3.0$. Due to the common model uncertainties, a correlation in the fatigue failure probabilities for the different crack sites as high as 80% is derived. It is seen that considering a system of 100 crack sites, the fatigue reliability against fatigue failure of any of the crack sites is still relatively high, $\beta = 2.0$. The system effect is therefore reduced due to the high correlation in the fatigue failure probability for the different crack sites along the weld.

In Figure 6.15 the influence of the mean initial crack size on the estimated fatigue reliability of a single crack site is investigated. Changing the mean value by ± 0.05 mm leads to a change of the reliability index of ∓ 0.4. The estimated fatigue reliability of the weld is therefore sensitive to the modeling of the initial crack size distribution.

The estimated fatigue reliability is highly dependent on the environmental corrosive conditions. A corrosive environment influences not only the fatigue material parameters C and m, but also reduces the steel thickness and thereby increases the relative stress level over time. In Figure 6.16 the fatigue reliability is computed for a corrosion rate of 0.1 and 0.2 mm/year, applying both non-corrosive and corrosive material parameters as shown in Table 6.1 (DnV). It is seen that a corrosive environment applying corrosive material parameters greatly reduces the fatigue reliability level. As expected, it is seen that effect of the corrosion rate on the fatigue reliability increases with the fatigue lifetime considered. After 20 years, a corrosion rate of $k_{cor} = 0.1$ reduces the reliability index by 0.2.

In Figure 6.17 the fatigue reliability of the weld having a homogeneous Poisson distributed number of crack sites over the weld length is considered. The expected number of crack sites over the weld is μl, where l is the length of the weld. Considering the weld length of 20 meters, it is seen that the fatigue reliability changes, from having an occurrence rate of crack sites from $\mu = 0$ to $\mu = 5$ per meter. Due to the high correlation in the fatigue failure probability of the crack sites, the fatigue failure probability of the weld stabilizes and reduces only slightly for increasing expected

number of crack sites when more than 30 ∼ 40 crack sites are considered. However, the results show that the continuous weld investigated is having a fairly high failure probability already with an occurrence rate of weld defects in the area of $\mu = 1$, indicating the importance of including the contribution from continuous welds in the evaluation of the total fatigue failure probability of the tanker.

The inspection procedure on tanker structures commonly consist of visual inspection, having only a low probability of detecting a surface crack. For a visual-inspection having a 50% probability of detecting a 30 mm long crack, an Exponentially distributed smallest detectable crack size with inspection quality of $q = 0.1$ is defined. The effect of the visual inspection on the estimated fatigue reliability is shown in Figure 6.18 for an inspection after 10 years of service not leading to any crack detection. It is seen that the visual inspection only leads to an increase in the estimated fatigue life of 2 years for the examined crack site. The result of no crack detection for visual inspection therefore contributes little to the updated estimated fatigue reliability level.

Applying an MPI inspection with a 90% probability of detecting a 30 mm long crack, modeled with inspection quality $q = 0.3$, not leading to any crack detection, an updating of the estimated fatigue life of 4∼5 years is experienced. The increase in the estimated reliability level is still not enormous, but is more than twice the contribution from the visual inspection.

Figure 6.18 also shows the effect of inspection updating of an unexamined crack site based on the inspection result of no crack detection of another examined crack site. It is seen that the effect of inspection updating of uninspected crack sites is of less importance, but that a definite increases in the estimated reliability level is experienced.

Both visual and MPI inspections depend on the crack lengths, whereas the crack depth is of importance in the evaluation of the fatigue reliability. Due to the low local level of bending stress compared to the tension stress in the evaluation of the midships bending moment induced stress level, a high crack aspect ratio is experienced, $E[a/c] = 0.5$. This reduces the effect of the inspection procedures in the updating of the fatigue reliability level of tanker structures. It is therefore important to have a solid initial design against fatigue to secure a fatigue reliable structure over the whole service life.

6.1 Summary and Conclusion

The developed fatigue reliability model for evaluation of the fatigue reliability of continuous welds having multiple fatigue crack sites is applied to evaluate the fatigue reliability of a transverse weld in a tanker structure containing hazardous material for which no leakage is permissible.

Uncertainties in the modeling of the load response and the fatigue capacity are accounted for by applying stochastic bias factors, modeling both random and systematic model uncertainties.

A stochastic description of the wave induced stress range response is derived applying a longterm frequency domain analysis, where uncertainties in the environmental model, the load model and the load response model are included. Large uncertainties are related to the derived longterm response distribution due to uncertainties in the estimated transfer function and the maneuvering philosophy in higher sea states.

A relatively high uncertainty in the estimated fatigue damage are experienced for the different potential crack sites along the weld with a $COV[\Delta] = 150\%$. Due to the common uncertainties in the modeling of the fatigue capacity and in the load response, the a correlation in the estimated fatigue failure probability of the different crack sites along the weld of 80% is found, reducing the system effect in the evaluation of the total fatigue reliability of the weld. The effect of a corrosive environment is found to greatly reduce the fatigue capacity of the weld, not only due to an influence on the estimated material parameters governing the fatigue crack growth behavior, but also due to an increase in the general stress level over time from reduced plate thickness caused by corrosion.

In the study it is found that the inspection outcome of no crack detection is not contributing significantly to the updated estimated fatigue reliability of a potential crack site for visual inspections, due to the low probability of detecting a potential surface crack. However, it is found that there is little definitive information available to define reasonable POD curves for different types of visual in-service inspection methods and procedures commonly applied on tankers, and it is concluded that this is an important area for additional research.

Based on a parameter study investigating the influence of the rate of occurrence of weld defects along continuous welds, it is found the the occurrence rate greatly influence the fatigue reliability of the weld. It is further found that continuous welds significantly contribute to the total fatigue failure hazard of the structure, and that the fatigue failure probability of continuous welds must be included in the evaluation of the total fatigue failure probability of the structure. Again, however, no concise information exist with respect to the distribution of weld defects along continuous welds and the influence of different welding procedures on occurrence rate. To fully be able to model the fatigue reliability of continuous welds, further research is needed in this area.
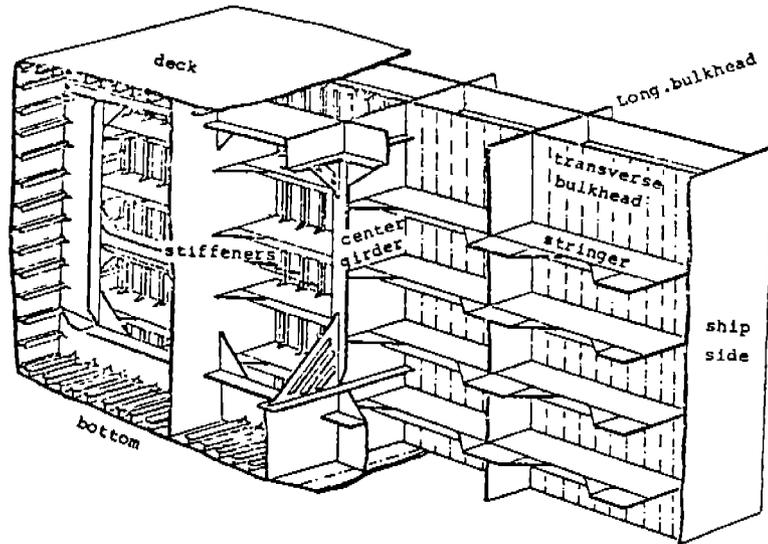
Figure 6.5: Midships tanker section.

Profile

Upper Deck
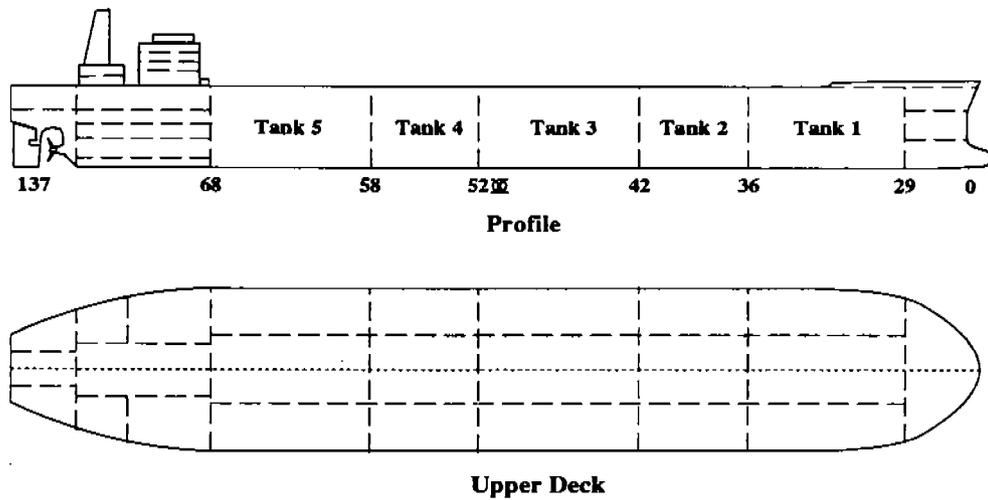
Figure 6.6: Tanker structure.
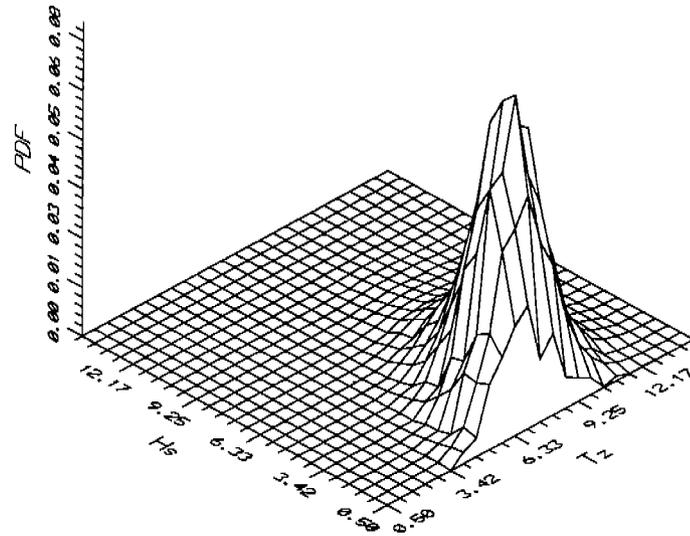
Figure 6.3: Weighted global scatter diagram for the Marsden zones 15, 16, 24 and 25.
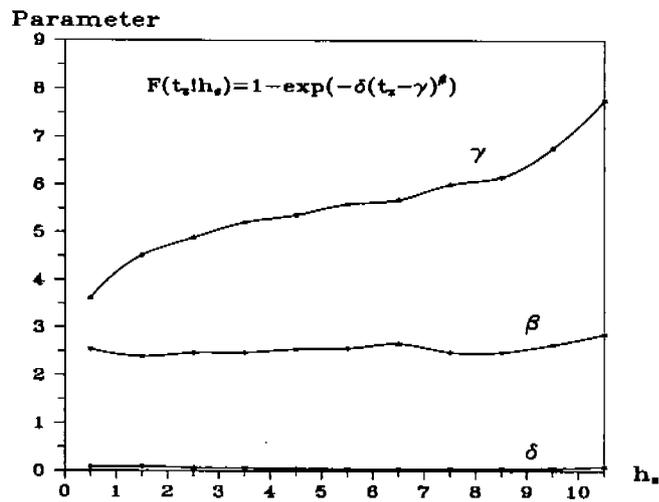
Figure 6.4: Conditional Weibull distribution parameters of T_z given H_s.

Long Term Stress Range

$-\ln(1-F(\sigma))$

Solid : E(lnA) and E(B)
Dashed: +/−D(lnA)

$\Delta\sigma$ (MPa)
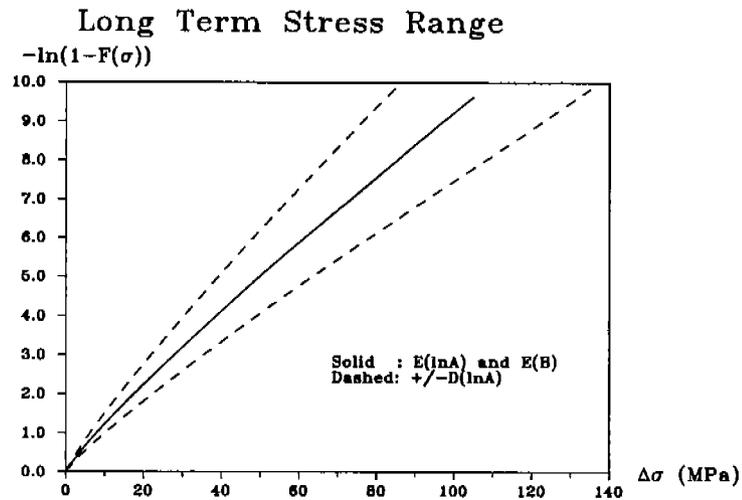
Figure 6.5: Stress range distribution

N   Value of N, giving minimal influence of B

m=3.5

m=3.0

m=2.5

B
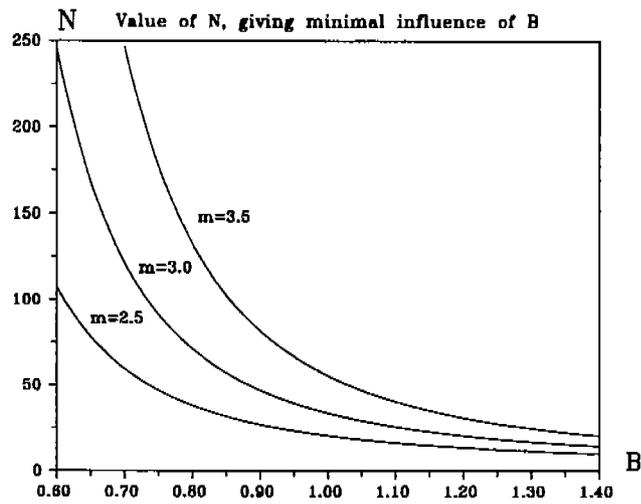
Figure 6.6: Extreme number of cycles N minimizing the influence of uncertainty on B on the estimated induced fatigue damage.
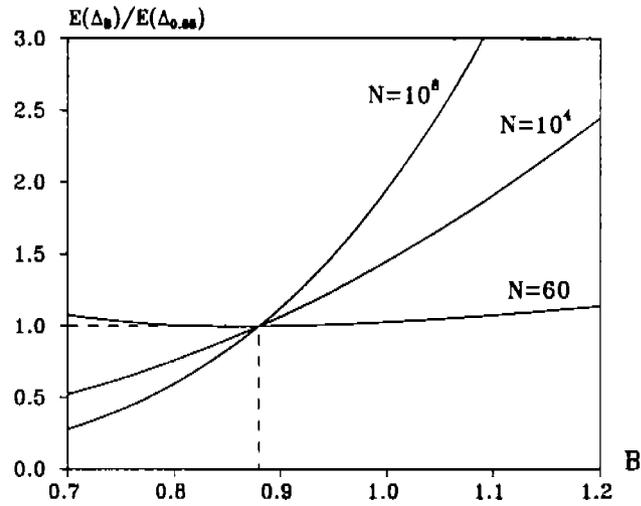
Figure 6.11: Relative influence of the chosen shape parameter B on the estimated fatigue damage, depending on the number of cycles being applied to define the extreme loading condition.
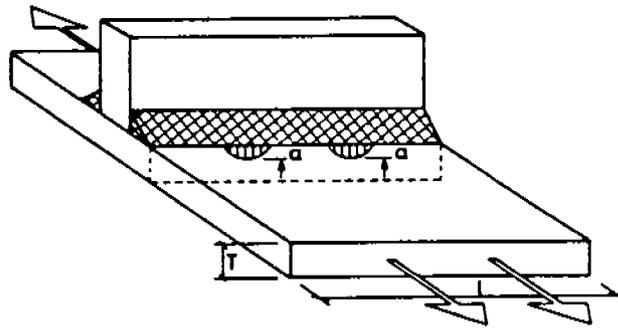
Figure 6.12: Investigated continuous transverse fillet weld.
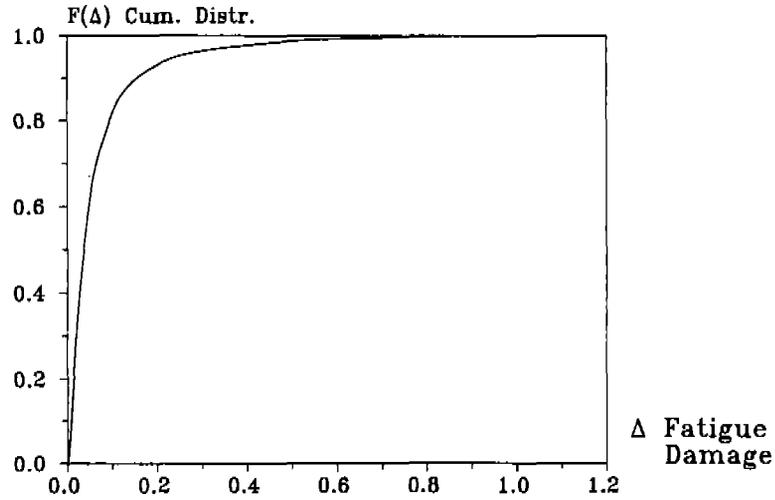
Figure 6.9: Cumulative distribution of accumulated fatigue damage for a single crack site over a lifetime of 20 years.
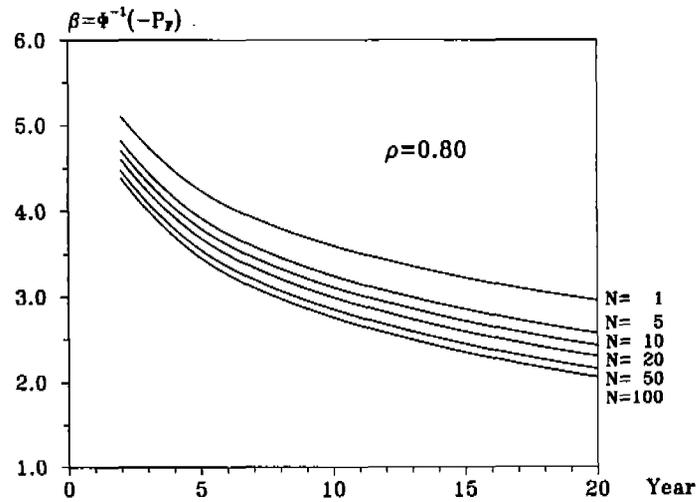
Figure 6.10: Fatigue reliability of the weld over service life for different number of crack sites over the weld length considered.
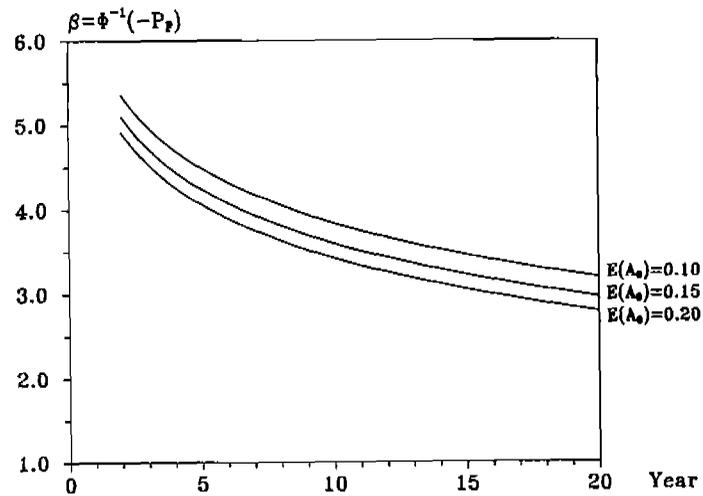
Figure 6.11: Fatigue reliability of a single crack site depending on the modeling of the mean initial crack size.
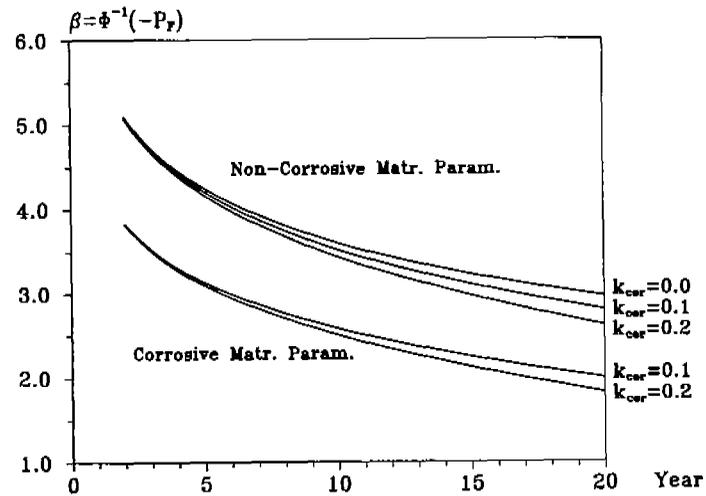
Figure 6.12: Fatigue reliability of a single crack in a corrosive and non-corrosive environment, including the effect of different corrosion rates.
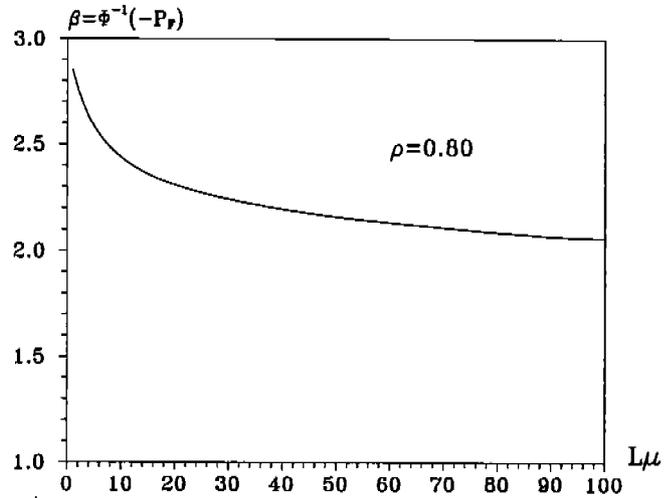
Figure 6.13: Fatigue reliability of a continuous weld for increasing expected number of crack sites over the weld length.
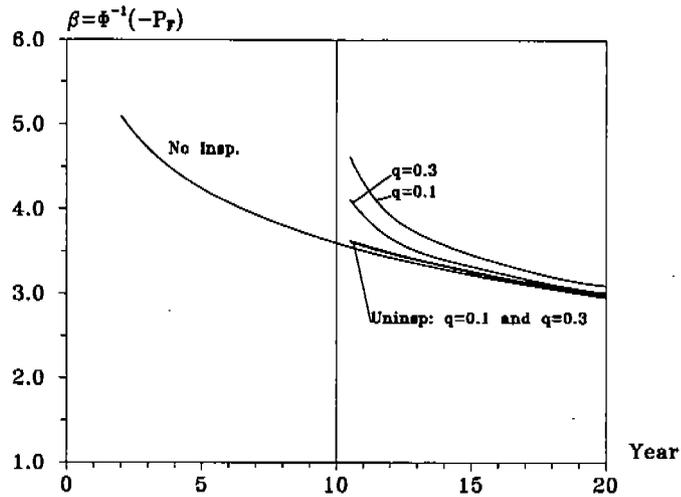
Figure 6.14: Updated fatigue reliability of inspected and un-inspected crack site after inspection of a single crack site not leading to crack detection. Both visual (q=0.1) and MPI (q=0.3) inspections are considered.

Chapter 7

Conclusion and Recommendations

7.1 Conclusion

It has long been recognized that the fatigue reliability of a weld seam is not adequately described through the fatigue reliability of a single randomly selected defect along the weld, and that the contribution to the fatigue failure probability from all the occurring weld defects along the weld must be considered.

In the present work, an analytic procedure has been developed for evaluation of the fatigue reliability of welds having multiple crack initiation sites. The model is extended to include unknown locations of the different defects along the weld. For the case where the crack site locations are not known, the distribution of crack sites is defined through a Poisson distribution process. The fatigue crack growth process is described by the Paris and Erdogan equation and failure is defined as through-thickness crack of one or more of the weld defects along the weld seam.

The fatigue reliability model for the weld is extended to include the effect of inspection updating. Based on inspections of the weld, where the whole weld length or only fractions of the weld might be examined at each inspection, an updated estimate of the fatigue reliability of the weld is computed.

Extending the derived fatigue reliability model, a procedure for probabilistic optimal design, fabrication and inspection strategy for the weld having multiple crack initiation sites is developed. A structural design variable, a fabrication variable modeling the intensity of defects along the weld, the inspection times and the inspection qualities at each inspection are applied as optimization variables.

Reliability and associate sensitivity calculations have been performed by use of full distribution reliability methods. In the uncertainty modeling, inherent physical uncertainties, modeling uncertainties and statistical uncertainties are considered.

The developed fatigue reliability model is applied to evaluate the fatigue reliability of a transverse weld in a tanker structure, where a stochastic description of the wave induced response is derived

applying a longterm frequency domain analysis including the effect of maneuvering in higher sea states.

The numerical study indicates the importance of having an adequate description of realistic POD curves. With the inspection techniques today commonly applied on tanker structures, appropriate initial design and quality of fabrication is of crucial importance to ensure sufficient safety against fatigue failure of the ship structure over the lifetime. However, based on suggested POD curves from the offshore industry, the inspection result of no crack detection applying visual inspections does not greatly influence the estimated fatigue failure probability, due to the low probability of detecting a surface crack for this inspection method.

The study also shows that the rate of occurrence of weld defects along the weld greatly influence the fatigue reliability of the weld and that the weld is having a fairly high failure probability already for low occurrence rates of weld defects. Considering the large quantity of welds existing in tanker structures (1000 km), the contribution to the fatigue failure probability from continuous welds is significant in the evaluation of fatigue failure probability of the total structure. Due to the size of today's tanker structure, a possible through thickness crack with following leakage might lead to significant environmental consequences, and continuous weld must be considered in the design against fatigue failure.

7.2   Recommendations for Further Research

The presented work defines a model for evaluation of the fatigue reliability of a homogeneous weld having multiple crack initiation sites being exposed to similar stress conditions. Areas for extension of this work includes;

- The derivation of a simplified formulation of the fatigue reliability of the weld, where the local stress response at each crack site is not necessarily identical.

- To be able to utilize the theoretical reliability models today available in the evaluation of the fatigue reliability of ship structures, a realistic stochastic descriptions of the physical variables applied in the fatigue model must exist. Unfortunately, this is not always the case. Specially, models defining the effect of welding quality on the occurrence rate of weld defects and the corresponding equivalent initial crack sizes must be provided both for manual and machine welds. Also, crack detection probabilities for commonly applied inspection procedures on ship structures is an area where hardly any information is available. To fully be able to utilize the information from inspections in the fatigue reliability updating, models defining the crack detection probability as a function of the crack size is necessary.

Appendix A

Reliability Updating of S-N Analysis

Abstract

The use of predicted fatigue crack growth behavior in the updating of the estimated fatigue design life is investigated. From experience and experimental fatigue crack growth tests, the relationship between developed crack size and remaining fatigue life can be established for groups of geometries. The probabilistic estimated fatigue design life is then updated from inspection results, independent of type of fatigue model applied.

The updating procedure is demonstrated by use of a probabilistic S-N fatigue analysis model where the effects of inspection quality and repair philosophy on the fatigue failure probability is investigated.

A.1 Introduction

The fatigue failure probability of welded structures is usually estimated applying probabilistic linear elastic fracture mechanics or S-N fatigue life calculations. The initial estimates for the fatigue behavior can be updated during the lifetime of the structure through inspections. With the additional information available from inspections, some of the uncertainties present at design stage are removed and improved estimates of the fatigue failure probability are made.

It is demonstrated in Madsen *et al.* [53], that the probabilistic fracture mechanics analysis is easily combined with results from inspections. However, if the fatigue failure probability is estimated applying the S-N approach, the inspection results can not explicitly be applied in the reliability analysis, since the crack size is not included as a parameter in the fatigue model. An updating of the fatigue analysis from inspection results can then only be achieved if a relationship exists

between the developed crack length and the corresponding fraction of the total design life for the detail investigated. Updated estimates of the design life are then established from the inspection results and the time of inspection.

This section shows how results from inspections are used to update the S-N fatigue failure probability by use of full distribution reliability methods and Bayesian updating technique.

A.2   Miner-Palmgren Fatigue Damage Model

In S-N fatigue approach, the fatigue strength is expressed in terms of a $\Delta S - N$ relation, giving the number of stress cycles N of constant stress range ΔS leading to failure,

$$N \, \Delta S^m = K \tag{A.1}$$

where K and m are fatigue material parameters, ASCE [4]. The model is often used with a positive lower threshold on ΔS, below which no damage is assumed to occur. Usually, the amplitude of the stress range is not constant over the lifetime of the structure. The fatigue damage under varying loading are calculated by the Miner-Palmgren model, Miner [60] and Palmgren [66]. It is here assumed that the damage on the structure per load cycle is constant at a given stress level ΔS_i. The total damage the structure is experiencing is then expressed as the accumulated damage from each load cycle at different stress range levels, independent of the sequence in which the stress cycles occur,

$$\Delta_{N_L} = \sum_{i=1}^{N_L} \frac{1}{n(\Delta S_i)} \tag{A.2}$$

where Δ_{N_L} is the accumulated damage over the time period with N_L load cycles and $n(\Delta S_i)$ is the number of load cycles of range ΔS_i causing failure. Combining these equations, the following expression for the accumulated damage is achieved,

$$\Delta_{N_L} = \frac{1}{K} \sum_{i=1}^{N_L} \Delta S_i^m \tag{A.3}$$

If the number of load cycles are sufficiently large, the expression can be simplified to the sum of the expected value of the stress range process,

$$\Delta_{N_L} = \frac{1}{K} \sum_{i=1}^{N_L} \Delta S_i^m = \frac{1}{K} N_L \sum_{i=1}^{N_L} \frac{1}{N_L} \Delta S_i^m \approx \frac{1}{K} N_L E[\Delta S_i^m] \tag{A.4}$$

The failure criterion is taken as the accumulated damage exceeding the critical Miner-Palmgren damage index Δ_c, defining, *e.g.*, through the thickness crack. Conventionally this damage index is taken as one. The design life of the structure is then defined as,

$$t_D = \frac{\Delta_c K}{\nu_0 E[\Delta S^m]} \tag{A.5}$$

168

where ν_0 is the zero crossing frequency of the loading process in unit $[year^{-1}]$.

The safety margin M against fatigue failure within the lifetime t_L of the structure is then given by,

$$M = t_D - t_L = \frac{\Delta_c K}{\nu_0 E[\Delta S^m]} - t_L \tag{A.6}$$

and the fatigue failure probability against through the thickness crack is,

$$P_F = P(M \leq 0) \tag{A.7}$$

In the modeling of the fatigue failure probability, it is important that best estimates, rather than conservative estimates, are used for the material parameters K and m.

A.3 Model Updating from Inspection

In service inspections are performed in order to assure that the existing cracks in the structure, which may be present at design stage or arise at a later stage during the service time, do not grow to a critical size.

The result from an inspection is either no detection or detection of a crack. In the case of no crack detection in an inspection, the crack size is smaller than a defined smallest detectable crack size,

$$2c(N_i) \leq \lambda_d \tag{A.8}$$

where $2c(N_i)$ is the crack length after N_i load cycles and λ_d is the smallest detectable crack size, dependent on inspection method and procedures applied, e.g., visual or MPI. λ_d is generally stochastic, since a crack, dependent on the size of the crack, is only detected with a certain probability. The cumulative distribution function of λ_d is modeled based on the probability of detection (POD) curve for the inspection method applied.

In the case of crack detection, the size of the detected crack λ_m is measured,

$$2c(N_j) = \lambda_m \tag{A.9}$$

where λ_m is the observed crack length after N_j load cycles. λ_m is also usually random, since accurate estimates of the length of the detected crack might be difficult due to possible measurement errors and errors in the interpretations of measurement signals.

To apply the inspection results in the updating of the estimated fatigue design life of the structure, it is necessary to define a model describing the relationship between the crack growth over the exposed time period and the remaining time to fatigue failure. This relationship can be established from backtracking and comparative calculations of the fatigue life, applying a fracture mechanics approach, or through experimental results where the crack size as a function of number of cycles is measured until fatigue failure.

Tweed and Freedman [89] have established a model defining the relationship between developed crack size and remaining fatigue life for tubular joints based on experimental results. Equivalent relationships could be established for other groups of geometries, *e.g.*, common geometries applied in ship structural design. The model defines the fraction of design life, or the time to through the thickness crack, already being experienced by the detail, as a probabilistic function of the normalized developed crack length. From inspection results, the relative remaining fatigue life of the component can then be estimated. This estimated remaining fatigue life is further applied to update the original design life estimate. The model is extended to include the effect of crack initiation time and initial crack size.

From the experimental data, the relationship endurance/endurance to through the thickness cracking, (t/t_c), is described as a function of the normalized surface crack length/member thickness $(2c/z)$,

$$t/t_c = k(2c/t) \tag{A.10}$$

where $k(\cdot)$ is the probabilistic function describing this relationship. By defining design life as the time to through the thickness crack, an estimate of the design life from the developed crack length $2c_i$ over the time period t_i can be computed,

$$t_D = \frac{t_i}{k(2c_i/z)} \tag{A.11}$$

The inspection estimated design life, t_D, is stochastic due to the probabilistic form of $k(\cdot)$.

The additional information available from inspections is through the definition of event margins, applied to update the earlier estimated design life. The event margin H is defined as,

$$H = t_D - \frac{t}{k(2c/z)} \tag{A.12}$$

For the inspection result of no crack detection at an inspection at time t_i, the event margin is positive since the crack size is smaller than the smallest detectable crack size λ_d,

$$H_i = t_D - \frac{t_i}{k(\lambda_d/z)} \geq 0 \tag{A.13}$$

In the case of crack detection of a crack of size λ_m, the event margin is zero,

$$H_i = t_D - \frac{t_i}{k(\lambda_m/z)} = 0 \tag{A.14}$$

The updated fatigue failure probability based on, *e.g.*, s inspections with crack detection for inspection s only, is expressed as,

$$
\begin{aligned}
P_F &= P(M \leq 0 \mid H_1 \geq 0 \cap \cdots \cap H_{s-1} \geq 0 \cap H_s = 0) \\[2mm]
&\simeq \frac{P(M \leq 0 \cap H_1 \geq 0 \cap \cdots H_{s-1} \geq 0 \cap H_s = 0)}{P(H_1 \geq 0 \cap .. \cap H_{s-1} \geq 0 \cap H_s = 0)} \tag{A.15}
\end{aligned}
$$

The effect of crack initiation is included in the model by the definition of an initial crack size λ_0 and a crack initiation time t_0. The event margin is then

$$H = t_D - \frac{t - t_0}{k(2c/z) - k(\lambda_0/z)}(1 - k(\lambda_0/z)) - t_0 \qquad (A.16)$$

The uncertainties involved in the estimation of the initial crack size and the crack initiation time are included in the probabilistic fatigue analysis by a stochastic modeling of these parameters.

In the case of repair of a detected crack λ_r at time t_{rep}, the safety and event margins for the repaired crack are modeled as,

Safety Margin:

$$M = (t_{rep} + t_{Drep}) - t_L = t_{rep} + \frac{\Delta_c K_{rep}}{\nu_0 E[(\Delta S)^{m_{rep}}]} - t_L \qquad (A.17)$$

where K_{rep} and m_{rep} are the material parameters after repair and t_{Drep} is the estimated design life after repair.

Event Margin H at time of repair:

$$H = t_D - \frac{t_{rep}}{k(\lambda_{rep}/z)} = 0 \qquad (A.18)$$

Event Margin H for inspections at time after repair:

- No new crack detection:

$$H_{rep} = t_{Drep} - \frac{t_i - t_{rep}}{k(\lambda_{di}/z)} \geq 0 \qquad (A.19)$$

- New crack detection:

$$H_{rep} = t_{Drep} - \frac{t_j - t_{rep}}{k(\lambda_{mj}/z)} = 0 \qquad (A.20)$$

The dependence in the estimated design life before and after repair, t_D and t_{Drep}, is included in the analysis by defining a correlation between these time estimates directly or by introducing a correlation matrix describing the relationship among the material parameters K, K_{rep}, m, m_{rep} and between the loading processes before and after repair. If the geometry of the detail is not changed as a consequence of the repair, the same modeling uncertainties on the loading material parameters will typically exist before and after repair.

The combined effect of crack initiation at design stage and also crack initiation after repair is modeled by combining the event margin defined in Equation (A.16) with the event margins described above.

Event Margin H at time of repair:

$$H = t_D - \frac{t_{rep} - t_0}{k(\lambda_{rep}/z) - k(\lambda_0/z)}(1 - k(\lambda_{0rep}/z)) - t_{0rep} = 0 \qquad (A.21)$$

Event Margin H for inspections at time after repair:

- No new crack detection:

$$H_{rep} = t_{Drep} - \frac{t_i - t_{rep} - t_{0rep}}{k(\lambda_{di}/z) - k(\lambda_{0rep}/z)}(1 - k(\lambda_{0rep}/z)) - t_{0rep} \geq 0 \qquad (A.22)$$

- New crack detection:

$$H_{rep} = t_{Drep} - \frac{t_j - t_{rep} - t_{0rep}}{k(\lambda_{mj}/z) - k(\lambda_{0rep}/z)}(1 - k(\lambda_{0rep}/z)) - t_{0rep} = 0 \qquad (A.23)$$

where t_{rep} is the time of repair and t_0 and t_{0rep} is the crack initiation time at design stage and after repair. λ_{rep} is the length of the repaired crack, λ_0 and λ_{0rep} are the initial crack sizes at design stage and after repair and λ_{di} and λ_{mj} are the smallest detectable crack size and the detected crack size at inspections after repair has been performed.

The effect of crack repair by grinding compared to welding is modeled by assuming a longer crack initiation period after repair t_{0rep} using the grinding method and by applying equivalent material parameters before and after repair.

A more general situation including inspections of several locations with potential crack growth can be considered applying the same updating procedure. Dependence among basic variables referring to different locations, as loading process and material parameters must then, however, be included in the model formulation.

A.4   Reliability Method

The reliability method applied for evaluating the failure probability is the first order reliability method (FORM). This method is reviewed thoroughly in Madsen *et al.* [50] and only a short description is given here.

In full distribution reliability methods, the basic stochastic variables $\mathbf{X}$ defining the safety and event margins are transformed into a set of independent and standardized normal variables $\mathbf{U} = T(\mathbf{X})$. The limit state surface divides the space into a safe set and a failure set, and the failure probability is the probability contents of the failure set $M(\mathbf{X}) \leq 0$.

In the first order reliability method the limit state surface is approximated by a tangent hyperplane through the point on the limit state surface closest to the origin, defined as design point. The parallel-system defined in Equation (A.15), is approximately computed by an linearization of the limit state surface through the joint design point of the safety and event margins.

The failure probability of the parallel-system is then estimated applying the multi-normal distribution,

$$P_F \approx \Phi(-\beta; \rho) \qquad (A.24)$$

where β is the vector of the first order reliability indexes for the safety and event margins of the parallel-system, ρ is the correlation matrix for these margins and Φ is the standardized multi-normal

distribution. A detailed description of this approximation and the modeling of the event margins with equality constraints is given in Madsen [51].

The evaluation of the fatigue failure probabilities in the numerical examples are carried out applying the computer program PROBAN, [64, 86].

A.5 Numerical Example

A probabilistic fatigue analysis of a tubular joint is performed. The distribution of the parameters involved in the analysis are chosen to exemplify the method and do not necessarily represent a real life situation.

The surface crack development data presented in Tweed and Freedman [89] are applied in the probabilistic analysis. These data describe the probabilistic endurance/endurance to through the thickness cracking as a function of the normalized surface crack length/member thickness, see Figure A.1. From a regression analysis of these data, Hanna and Karsan [33] estimated the mean and standard deviation of the relative remaining joint fatigue life to be:

$$E[k(2c/z)] = 0.383(2c/z)^{1/3.0} \quad SD[k(2c/z)] = 0.143(2c/z)^{1/10.6} \tag{A.25}$$

The probabilistic distribution describing the relative remaining joint life will necessarily be bounded by 0 and 1. A Beta distribution with these bounds and the expressions for the mean and standard deviation given above is applied to describe the distribution of the relative remaining joint fatigue life as a function of the crack length,

$$f_{2c/z}(x) = \frac{(x-a)^{r-1}(b-x)^{s-r-1}}{(b-a)^{(s-1)}\int_0^1 u^{r-1}(1-u)^{s-r-1}du} \tag{A.26}$$

where a and b are the lower and upper bounds and the parameters r and s are derived from the given mean and standard deviation.

$$E[x] = a + (b-a)\frac{r}{s} \quad D[x] = (b-a)\frac{r}{s}\frac{\sqrt{(s-r)}}{\sqrt{r(s+1)}} \tag{A.27}$$

The updating of the fatigue analysis from inspection results can be performed with the stress range distribution resulting from a detailed uncertainty modeling of the environmental conditions, load model, global response and stress calculation. It is, however, convenient to calibrate a long term stress range distribution to the results from the longterm analysis, and apply the calibrated longterm distribution in the fatigue reliability calculations. In the following, a Weibull longterm stress range distribution is chosen,

$$F_{\Delta S}(s) = 1 - e^{-(s/A)^B} \tag{A.28}$$

where the Weibull distribution parameters A and B are stochastic, representing the uncertainties associated with the evaluation of the longterm response. A bi-variate normal distribution for

$(\ln A, 1/B)$ is defined to represent these uncertainties, typically modeling the loading condition for a North Sea jacket structure,

$$E[\ln A] = 1.60 \quad SD[\ln A] = 0.22$$

$$E[1/B] = 1.31 \quad SD[1/B] = 0.14 \quad \rho[\ln A, 1/B] = -0.79$$

The m'th moment of the stress range process is also random due to the random distribution parameters.

$$E[\Delta S^m] = A^m \Gamma(1 + \frac{m}{B}) \tag{A.29}$$

The qualities of the inspections are modeled through the detectable crack length λ_d, defined from the POD curve. The probability of detection curve POD is assumed to be of exponential form, giving the cumulative distribution of the detectable crack length,

$$P_{detect} = F_{\lambda d}(\lambda) = 1 - e^{-q\lambda} \tag{A.30}$$

where q defines the quality of the inspection method, giving a mean value for the detectable crack length equal to q^{-1}. The numerical example is based on an $q^{-1} = 6.21$, $q^{-1} = 18.63$ and $q^{-1} = 55.89$, modeling an MPI inspection with 80% probability of detecting a crack of length 10 , 30 and 90 mm. To include confidence bounds on the POD curve, the inspection quality q can be modeled as a random variable.

The S-N curves are founded on statistical analysis of appropriate experimental data. They consist of linear relationships between $\log_{10} \Delta S$ and $\log_{10} N$. The design curve is defined as the mean minus two standard deviations of $\log_{10} N$. Best estimate values rather than conservative values must be applied in a probabilistic analysis, and the randomized mean values are here applied. Department of Energy suggests the following mathematical form of the design S-N curve for tubular joints in seawater with cathodic protection,

$$\begin{aligned} \log_{10} N &= \log_{10} K - m \log_{10}(\Delta S) \\ &= 12.16 - 3.0 \log_{10}(\Delta S) - \frac{m}{4} \log_{10}(z/32) \end{aligned} \tag{A.31}$$

where the last term is the thickness correction factor and z is the thickness in mm through which the potential crack will grow. The $\log_{10} K$ is modeled as $N(12.66, 0.24)$.

The damage measure Δ_c, is modeled with a coefficient of variation of 0.20, to include the uncertainties involved in determining the Miner sum at through the thickness crack.

The probability of fatigue failure as a function of years in service based on a S-N fatigue analysis is shown in Figure A.2. No initial crack size or crack initiation period were assumed. The results are expressed in terms of the reliability index β, uniquely related to the failure probability as

$$\beta = -\Phi^{-1}(P_F) \tag{A.32}$$

174

From inspections, more information about the fatigue behavior of the detail is gained, and some of the uncertainties present at the initial design stage are reduced. Figure A.3, A.4 and A.5 show how the reliability index changes based on MPI inspections with $q^{-1} = 6.21$, $q^{-1} = 18.63$ and $q^{-1} = 55.89$ and no crack detection at any of the inspections. The time of inspections are chosen based on a maximum permissible failure probability of $1 \cdot 10^{-4}$ over the lifetime of the structure. The figures show that a higher inspection quality gives more confidence in the inspection results, higher estimated reliability of the structure and then longer inspection intervals.

Figure A.6 shows the change in the reliability index based on inspection with detection of a crack of size 16 mm and 50 mm after 18 years of service. For both observations, we are seeing a drastic reduction of the estimated reliability index, indicating a high probability for a through the thickness crack within the lifetime of the structure, unless a repair is performed.

Figure A.7 and A.8 show the effect of weld and grind repair of a detected 50 mm long crack, with no crack detection at the first inspection after repair. Weld repair is modeled by assuming independent, identically distributed material parameters before and after repair, with no crack initiation period. Grind repair is modeled by assuming identical material parameters before and after repair and a Lognormal distributed crack initiation period with mean value 10 years and a coefficient of variation equal to 0.5. The crack initiation period is in addition modeled as a function of the stress range by applying a negative correlation between stress range process and the crack initiation time.

The results for grind repair are here highly dependent on the choice of crack initiation period. The reliability level of grind repair will after some time fall below the reliability level of weld repair, due to the assumption of identical material parameters before and after repair.

A.6 Conclusion

An analytical procedure has been developed to incorporate results from inspections and repair operations into S-N curve based evaluations of fatigue reliability. The procedure is founded on an experimentally based relationship between surface crack length and the cyclic strains required to cause complete separation of the weld.

Numerical analyses of an example tubular joint in a North Sea platform indicate the critical importance of the inspection method and procedure in providing a basis for determining inspection intervals. Inspection intervals are reduced by a factor of two when the 80 percent POD a crack of length 10 mm is changed to 90 mm. There is little definitive information available to define reasonable POD curves for in-service structures using various practical inspection methods and procedures. This is an important area for additional research.

Similarly, the numerical results indicate the importance of assumptions regarding the effectiveness

of repairs on inspection intervals and fatigue reliability. Again, definitive information for characterizing the effectiveness of various types of repairs (particularity those made underwater) does not exist. This is also an important area for additional research.

/176
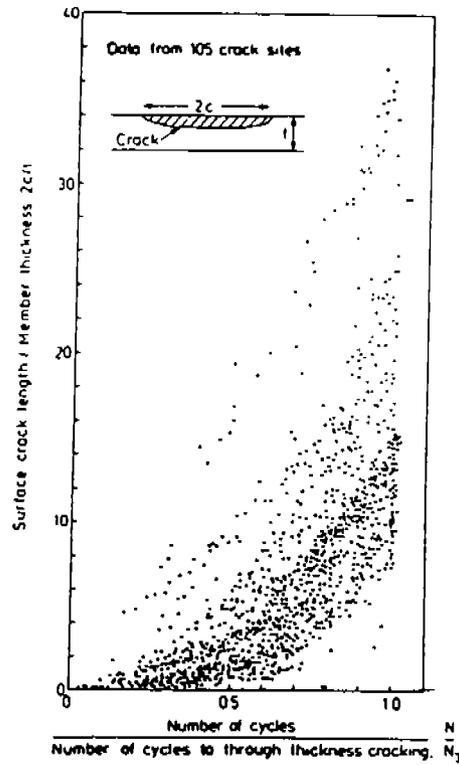
Figure A.1: Database for surface crack development in tubular joint fatigue test.
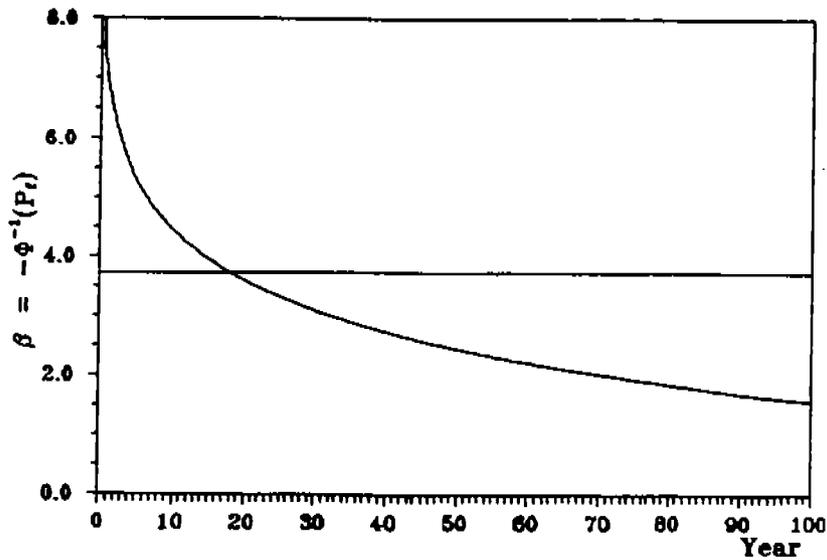
Figure A.2: Estimated fatigue reliability having no inspection.
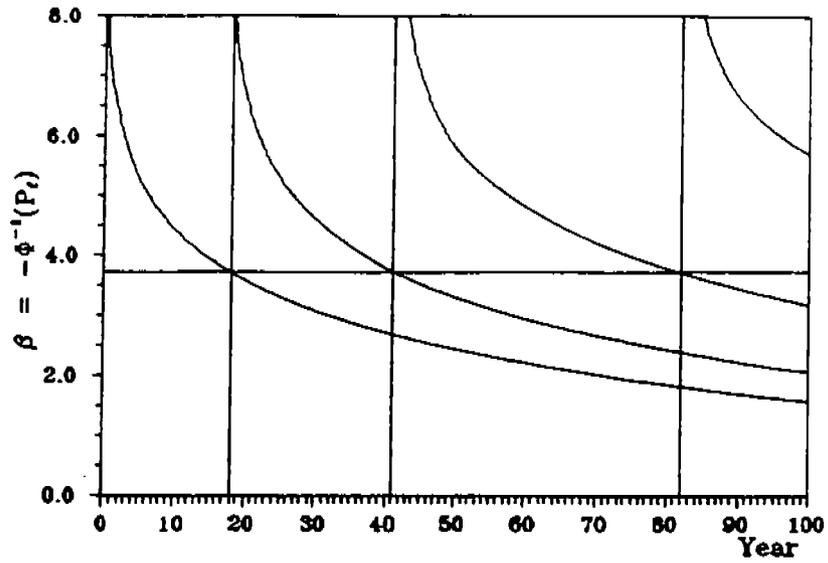
Figure A.3: Estimated fatigue reliability having no crack detection for inspection with 80% probability of detecting a crack of length 10 mm.
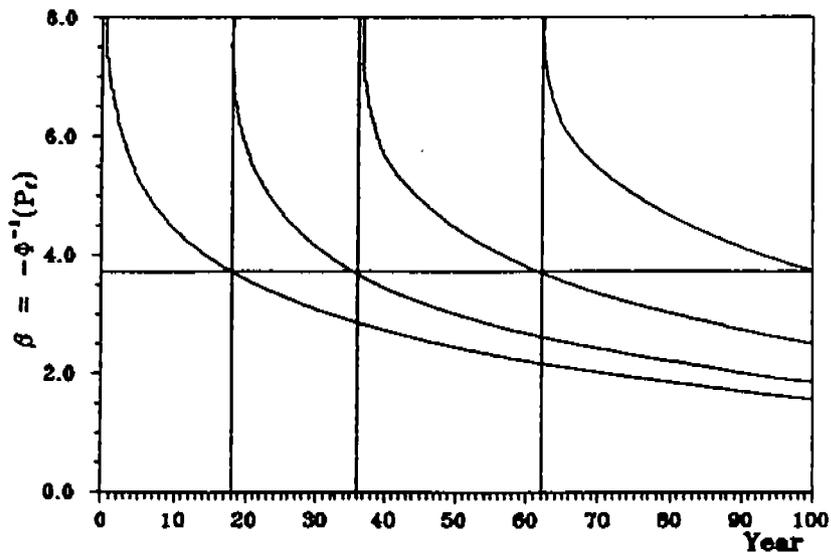
Figure A.4: Estimated fatigue reliability having no crack detection for inspection with 80% probability of detecting a crack of length 30 mm.

178
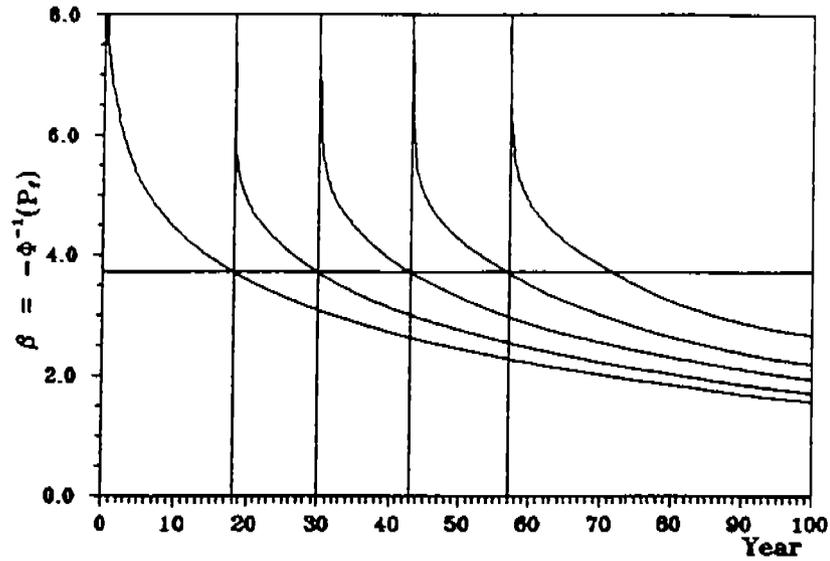
Figure A.5: Estimated fatigue reliability having no crack detection for inspection with 80% probability of detecting a crack of length 90 mm.
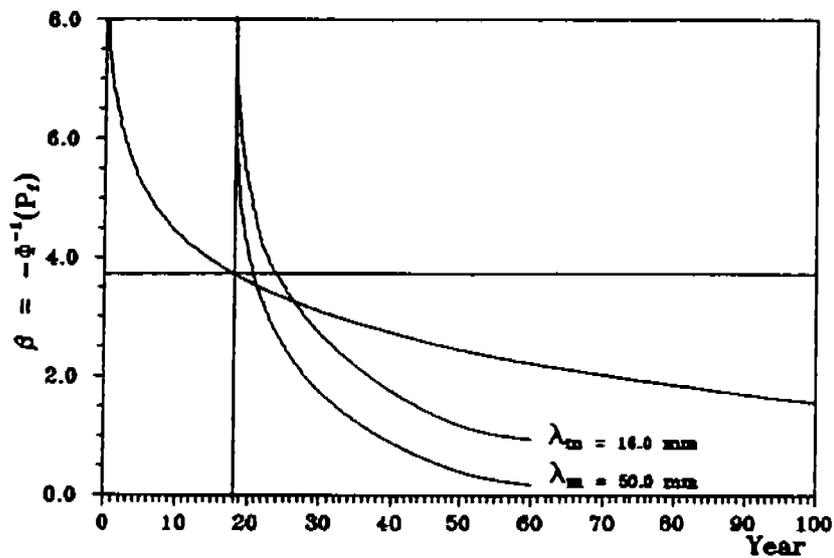
Figure A.6: Estimated fatigue reliability having detection of crack of length 16 mm and 50 mm after 18 years of service.

179
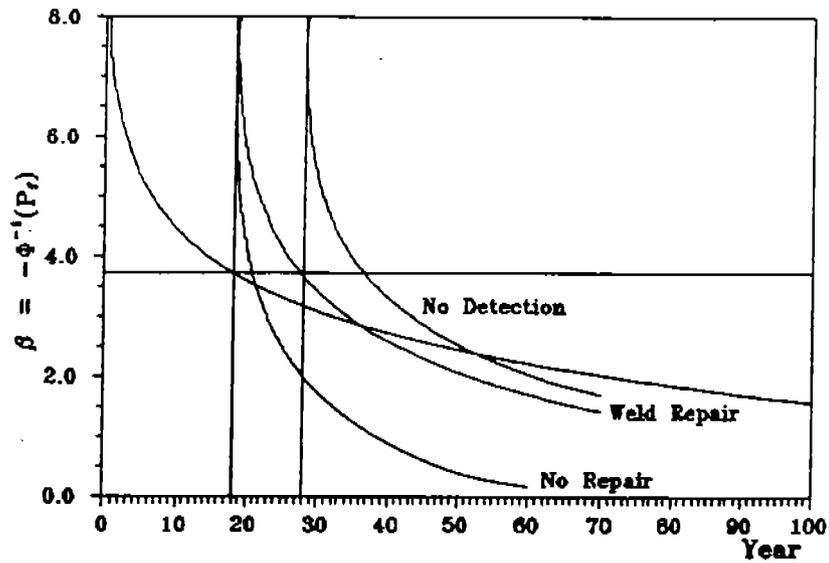
Figure A.7: Estimated fatigue reliability of weld repaired detected crack of 50 mm after 18 years of service, with no new crack detection for inspection with 80% probability of detecting a crack of length 10 mm.
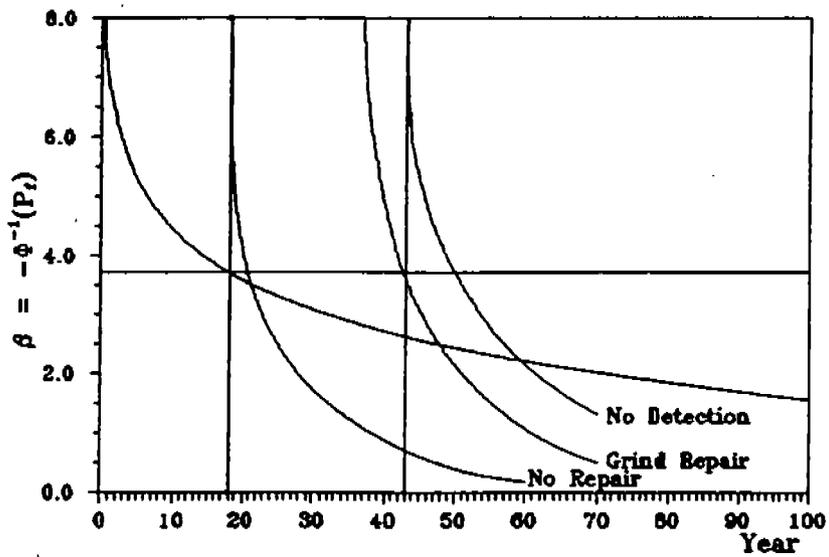
Figure A.8: Estimated fatigue reliability of weld repaired detected crack of 50 mm after 18 years of service, with no new crack detection for inspection with 80% probability of detecting a crack of length 10 mm.

Bibliography

[1] Fatigue strength analysis for mobile offshore units. 1984.

[2] Yoshio Akita. Reliability and damage of ship structures. *Marine Structures*, 1988.

[3] A. Almar-Næss. *Fatigue Handbook, Offshore Steel Structures*. Tapir, 1985.

[4] ASCE Committee on Fatigue and Fracture Reliability. Fatigue reliability (a series of papers). *Journal of Structural Division*, 108(ST1), 1982.

[5] O. Bach-Gansmo, C.A. Carlsen, and T. Moan. Fatigue assessment of hull girder for ship type floating production vessels. 1987.

[6] R.G. Bea. *Marine Structural Integrity Programs*. Technical Report, Ship Structure Committee, Oct. 1991. Report SSC-365.

[7] R.G. Bea, R. Polaard, R. Schulte-Strathaus, and R. Baker. Structural mainenance for new and existing ships: overview, fatigue cracking and repair. In *Marine Structural Inspection, Maintenance, and Monitoring Symposium*, March 1991.

[8] P. Bjerager. Probabilistic computation methods in structural and mechanical reliability. In W. K. Lin and T. Belytschko, editors, *Mechanics of Probabilistic and Reliability Analysis*, Elme Press International, Switzerland, Feb. 1989.

[9] T. Bokalrud and A. Karlsen. Probabilistic fracture mechanics evaluation of fatigue from welds defects in butt welded joints. In *Fitness for Purpose Validation of Welded Constructions*, November 17-19 1981.

[10] K. Breitung. Asymptotic approximation for multinormal integrals. *Journal of Engineering Mechanics*, 110(3):357–366, 1984.

[11] British Maritime Technology Ltd. *Global Wave Statistic*. Unwin Brothers, 1986.

[12] British Standard. *Guidance on some methods for the derivation of acceptable levels of defects in fusion welded joints*. BS PD 6493:1980, British Standard Institution, London, England, 1980.

[13] D. Broek. *Elementary engineering fracture mechanics*. Martinus Nijhoff Publishers, Dordrecht, 1986.

[14] C. A. Cornell. A probability-based structural code. *Journal of the American Concrete Institute*, 66(12):974–985, 1969.

[15] C. A. Cornell. Some thoughts on maximum probable loads and structural safety insurance. In *Memorandum*, Department of Civil Engineering, Massachusetts Institute of Technology, to Members of ASCE Structural Safety Committee, March 1967.

[16] E.H. Cramer. Comparison of pocedures for evaluation of updated fatigue reliability of ship structure. 1992. Internal Report, Dept. of Naval Architecture and Offshore Engineering, U.C. Berkeley.

[17] E.H. Cramer and R.G. Bea. Fatigue reliability model for inspection, updating and repair of welded geometries. In *Marine Structural Inspection, Maintenance and Monitoring Symposium*, SNAME, 1991.

[18] E.H. Cramer and P. Friis-Hansen. Stochastic modeling of the longterm wave induced response of ship structures. April 1992. Submitted to Marine Structures.

[19] O. Ditlevsen. *Baerende Konstrukstioners Sikkerhed*. SBI-Rapport 221, Statens Byggeforskningsinstitut, Hoersholm, Denmark, 1990.

[20] O. Ditlevsen. Fracture mechanical reliability theory of butt welds in plates. *Dialog, Danish Engineering Academy*, 1-78, 1978.

[21] O. Ditlevsen. Generalized second-moment reliability index. *Journal of Structural Mechanics*, 7:435–451, 1979.

[22] O. Ditlevsen. *Structural Reliability and the Invariance Problem*. Research Report 22, Solid Mechanics Division, University of Waterloo, Waterloo, Canada, 1973.

[23] O. Ditlevsen. *Uncertainty Modeling*. McGraw Hill, 1981.

[24] O.I. Eide and S. Berge. Fracture mechanics analysis of welded girders in fatigue. In *Inernational Conference on Fatigue of Welded Constructions*, April 7-9 1987.

[25] B. Fissler, H.J. Neumann, and R. Rackwitch. Quadratic limit states in structural reliability. *Journal of Engineering Mechanics*, 105:661–676, 1979.

[26] O. Førli and B. Pettersen. The performance of conventional ultrasonic and radiographic weld examination. *British Journal of NDT*, 364–366, November 1985.

182

[27] P. Friis-Hansen. Numerical modification for evaluation of general cost function in PROBAN. 1992. Internal Report.

[28] P. Friis-Hansen and E.H. Cramer. On system analysis of correlated identical events. 1992. To be submitted to Journal of Probabilistic Mechanics.

[29] P. Friis-Hansen, E.H. Cramer, and H.O. Madsen. Two-dimensional fatigue crack growth including the effect of crack coalescence. In *Computational Stochastic Mechanics*, September 17-19 1991.

[30] P. Friis-Hansen and H.O. Madsen. *Two-Dimensional Fatigue Crack Growth*. Internal Report, The Danish Engineering Academy, 1990.

[31] I. S. Gradshteyn and I. M. Ryzhik. *Table of Integrals, Series, and Products*. Academic Press, 1965.

[32] T.R. Gurney. *Fatigue of welded structures*. Cambridge University Press, Cambridge London New York Melbourne, 1979.

[33] S.Y. Hanna and D.I. Karsan. Fatigue data for reliability based offshore platform inspection and repair. 1990.

[34] A. M. Hasofer and N. C. Lind. Exact and invariant second moment code format. *Journal of Engineering Mechanics Division, ASCE*, 100:111–121, 1974.

[35] M. Hohenbichler. An asymptotic formula for the probability of intersection. In *Berichte zur Zuverlassigretstheorie der Bauwekere*, pages 21–48, Technical University of Munich, 1984.

[36] M. Hohenbichler and R. Rackwitz. Non-normal dependent vectors in structural reliability. *Journal of Engineering Mechanics*, 107(3):1127–1238, June 1981.

[37] R.S. Holzman. Probability of detecting cracks during internal structural surveys of tankers. 1992. NA 290C Term Paper, Dept. of NAOE, U.C.,Berkeley.

[38] H. Itagaki, Y. Akita, and A. Nitta. Application of subjective reliability analysis to the evaluation of inspection procedures on ship structures. In *International Symposium on the Role of Design, Inspection and Redundancy in Marine Structural Reliability*, National Academy Press, Nov. 1983.

[39] H. Itagaki, S. Itoh, and N. Yamamoto. Bayesian reliability analysis for evaluating in-service inspection. In *Current Japanese Material Research*, Elsevier Applied Science, 1989.

[40] H. Itagaki and N. Yamamoto. Bayesian analysis of inspection on ship structural members. In *ICOSSAR 85*, 1985.

183

[41] J.J. Jensen. *Fatigue Analysis of Ship Hulls Under Non-Gaussian Wave Loads*. DCAMM report no. 389, The technical University of Denmark, April 1989.

[42] J.J Jensen and P.T. Pedersen. Bending moments and shear foces in ships sailing in irregular waves. *Journal of Ship Research*, 25:243–251, 1981.

[43] J.C.P. Kam and W.D. Dover. Structural integrity of welded tubular joints in random load fatigue combined with size effects. In *International Conference on Marine and Offshore Safety*, 1987.

[44] A. Der Kiureghian. Bayesian analysis of model uncertainty in structural reliability. In P. Toft-Christensen, editor, *3rd IFIP Working Conference on Reliability and Optimization on Structural Systems*, Springer-Verlag, Germany, March 1990.

[45] A. Der Kiureghian. *CALREL*. University of California, Berkeley.

[46] A. Der Kiureghian. Measures of structural safety under imperfect states of knowledge. *Journal of Structural Engineering*, 1989.

[47] A. Der Kiureghian, H.-Z. Lin, and S. J. Hwang. Second-order reliability approximations. *Journal of Engineering Mechanics*, 113(8):1208–1225, Aug. 1987.

[48] A. Der Kiureghian and P.-L. Liu. Structural reliability under incomplete probability information. *Journal of Engineering Mechanics*, 112(1):85–204, Jan. 1986.

[49] N. C. Lind. The design of structural design norms. *Journal of Structural Mechanics*, 1:357–370, 1973.

[50] H. O. Madsen, S. Krenk, and N. C. Lind. *Methods of Structural Safety*. Prentice Hall, 1986.

[51] H.O. Madsen. Model updating in first-order reliability theory with application to fatigue crack growth. In *Second International Workshop on Stochastic Methods in Structural Mechanics*, 1985.

[52] H.O. Madsen. *PRODIM: Probability Based Design, Inspection and Maintenance, Theoretical manual*. No. 88-2019, Veritas Research, Høvik, Norway, 1988.

[53] H.O. Madsen, R. Skjong, A.G. Tallin, and F. Kirkemo. Probabilistic fatigue crack growth analysis of offshore structures, with reliability updating through inspection. In *SNAME*, October 5-6 1987.

[54] H.O. Madsen, J.D. Sørensen, and R. Olesen. Optimal inspection planning for fatigue damage of offshore structures. In *ICOSSAR89*, 1989.

[55] H.O. Madsen, R. Torhaug, and E.H. Cramer. Probability based cost benefit analysis of fatigue design, inspection and maintenance. In *SNAME 91*, March 1991.

[56] K. Madsen and O. Tingleff. *Robust Subroutines for Non-Lienar Optimization*. Technical Report, Numerical Institute, The Technical University of Denmark, 1990.

[57] A. Mansour. Probabilistic concepts in ship structural safety and reliability. *Trans. SNAME*, 1972.

[58] A.E. Mansour. A note on the extreme wave load and the associated probability of failure. *Journal of Ship Research*, 30(2), June 1986.

[59] R. E. Melchers. *Structural Reliability: Analysis and Prediction. Ellis Horwood Series in Civil Engineering*, Halsted Press, 1984.

[60] M.A. Miner. Cumulative damage in fatigue. *Journal of Applied Mechanics-ASME*, 12, 1945.

[61] J. Newman and I. Raju. An empirical stress-intensity factor for the surface crack. *Engineering Fracture Mechanics*, 22(6):185–192, 1981.

[62] E. Nikolaidis and P. Kaplan. *Uncertainties in Stress Analysis on Marine Structures*. Technical Report, Ship Structure Committee, April 1991. Report SSC-363.

[63] Masahiro Ohyagi. Statistical survey on wear of ship's structural members. *NK Technical Bulletin*, 1987.

[64] R. Olesen. *PROBAN-2 User-Manual*. Technical Report, Veritas Research, Høvik, Norway, 1989.

[65] Ortiz. *On the Stochastic Modeling of the fatigue crack growth*. PhD thesis, Department of Civil Engineering, Stanford University, Stanford, California, 1985.

[66] A. Palmgren. Die Lebensdauer von Kugellagern. *Zeitschrift der Vereines Deutches Ingenieure*, 68(4):339–341, 1924.

[67] P. Paris and F. Erdogan. A critical analysis of crack propagation laws. *Journal of Basic Engineering*, Dec:528–534, 1963.

[68] O.M. Phillips. The equilibrium range in the spectrum of wind-generated waves. *Journal of Fluid Mechanics*, 4(4), 1958.

[69] R.R. Pollard and R.G. Bea. *Evaluation of Corrosion Damage in Crude and Product Carriers*. SMP-2-1, Dept. of Naval Arch. and Offshore Eng., U.C. Berkeley, Berkeley, California, 1991.

[70] W.G. Price and R.E.D. Bishop. *Probabilistic Theory of Ship Dynamics*. Chapmann and Hall Ltd., 1974.

[71] R. Rackwitz. *STRUREL*. RCP GmbH, Munchen, Germany.

[72] D. Ritchie, P.A.J. van der Veer, and K. Smith. Fatigue crack growth under broad band stationary and non-stationary random loading. In *Steel in Marine Structures*, June 1987.

[73] S.T. Rolfe and J.M. Barsom. *Fracture and Fatigue Control in Structures*. Prentice Hall, 1977.

[74] M. Rosenblatt. Remarks on a multivariate transformation. *The Annals of Mathematical Statistics*, 23:470–472, 1952.

[75] R.Y. Rubinstein. *Simulation and The Monte Carlo Method*. John Wiley & Sons, 1981.

[76] N. Salvesen, E.O. Tuck, and O. Faltinsen. Ship motions and sea loads. In *Vol. 78*, pages 250–287, SNAME Transactions, 1970.

[77] G. Schall, M. Scharrer, C. Ostergaard, and R. Rackwitz. Fatigue reliability investigation for marine structures using a response surface method. In *Volume 2, Safety and Reliability*, pages 247–254, OMAE 91, 1991.

[78] K. Schittkowski. NLPQL: A fortran subroutine solving constrained nonlinear programming problems. *Annal of Operations Research*, 5:485–500, 1986.

[79] N.K. Shetty and M.J. Baker. *Fatigue Reliability of Tubular Joints in Offshore Structures: Crack Propagation Model*. Technical Report, Dept. of Civil Engineering Imperial College of Science Technology and Medicine, London, 1985.

[80] M. Shinozuka. *Relation of Inspection Findings to Fatigue Reliability*. Technical Report, Ship Structure Committee, November 1989. Report SSC-355.

[81] I.J. Smith and S.J. Hurworth. Probabilistic fracture mechanics evaluation of fatigue from welds defects in butt welded joints. In *Fitness for Purpose Validation of Welded Constructions*, November 17-19 1981.

[82] C. Guedes Soares. *Probabilistic models for load effects in ship structures*. Technical Report, Marinteknisk Avdeling, Norges Tekniske Høgskole, 1984. Report no UR-84-38.

[83] A. Thayamballi, Y-K Chen, and D. Liu. Fracture mechanics based assessment of fatigue reliability in ship structures. In *SNAME*, October 15-16 1984.

[84] P. Thoft-Christensen and M. J. Baker. *Structural Reliability Theory and its Application*. Springer-Verlag, Germany, 1982.

[85] P. Thoft-Christensen and J.D. Sørensen. Optimal strategy for inspection of structural systems. *Civil Engineering System*, 4, 1988.

[86] L. Tvedt. *PROBAN-2 Theory-Manual.* Technical Report, Veritas Research, Høvik, Norway, 1989.

[87] L. Tvedt. Quadratic forms in the normal space - an application to structural reliability. *Journal of Engineering Mechanics*, 116(6), June 1990.

[88] L. Tvedt. Second-order reliability by an exact integral. In P. Toft-Christensen, editor, *2nd IFIP Working Conference on Reliability and Optimization on Structural Systems*, Springer-Verlag, Germany, Sept. 1988.

[89] J.H. Tweed and J.H. Freeman. *Remainig Fatigue Life of Defective Tubular Joints - An Assessment Based on Data for Surface Crack Growth in Tubular Joint Fatigue Tests.* Technical Report OTH 87 259, HMSO, 1987. Offshore Technology Report.

[90] Underwater Engineering Group. 1991.

[91] P.S. Veers, S.R. Winterstein, D.V. Nelson, and C.A. Cornell. Variable amplitude load model for fatigue damage and crack growth. In *Symposium on Development of Fatigue Loading Spectra*, ASTM, Cincinnati, Ohio, April 29 1987.

[92] D. Veneziano. *Contributions to Second-Moment Reliability Theory.* Research Report R74-33, Department of Civil Engineering, Massachusetts Institute of Technology, Cambridge, Massachusetts, April 1974.

[93] D.A. Virkler, B.M. Hillberry, and P.K. Goel. The statistical nature of fatigue crack propagation. *J. Eng. Materials and Tech. Trans. ASME*, 101:148–153, 1979.

[94] S.R. Winterstein. Normal responses and fatigue damage. *Journal of Engineering Mechanics, ASCE*, 111(10):1291–1295, 1985.

[95] P.H. Wirsching. Fracture mechanics fatigue model in a reliability format. In *Offshore Mechanics and Arctic Engineering*, Houston, Texas, 1987.

[96] P.H. Wirsching and M.C. Light. Fatigue under wide band random stresses. *Journal of Structural Division, ASCE*, 106(ST7), July 1980.

[97] W.K. Wong and J.H. Rogerson. Weld defect in offshore structures and their influence on structural reliability. In *OTC*, May 3-6 1982.

STRUCTURAL MAINTENANCE
FOR
NEW AND EXISTING SHIPS

Study 1 - Fatigue Damage Evaluations
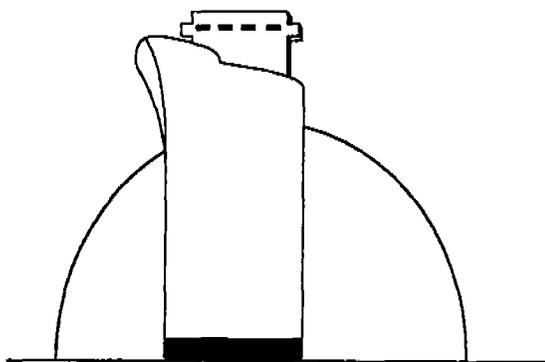
**Fatigue Damage
Evaluation Software:**
Theory Documentation

by
Espen H. Cramer
Rolf Schulte-Strathaus
and
Robert G. Bea

Report No. SMP-1-5
September 1992

189,190x

PREFACE

The two year Joint Industry Research Project "**Structural Maintenance for New and Existing Ships**" was initiated in 1990 by the University of California at Berkeley Department of Naval Architecture and Offshore Engineering to both develop practical tools and procedures for the analysis of proposed ship structural repairs and to prepare guidelines for the cost-effective design and construction of lower-maintenance ship structures.

This project was made possible by the following sponsoring organizations:

- **American Bureau of Shipping**
- **Amoco Transport Company**
- **BP Marine**
- **Bureau Veritas**
- **Chevron Shipping Company**
- **Daewoo Shipbuilding & Heavy Machinery Ltd.**
- **Exxon Company International**
- **Ishikawajima-Harima Heavy Industries Co. Ltd.**

- **Jurong Shipyard Ltd.**
- **Lisnave Estaleiros Navais de Lisboa,S.A.**
- **Military Sealift Command**
- **Mitsubishi Heavy Industries Inc.**
- **Mobil Ship and Transport Company**
- **National Defense Headquarters (Canada)**
- **Naval Sea Systems Command**
- **Newport News Shipbuilding & Dry Dock Co.**
- **United States Coast Guard**

In addition, the following organizations contributed to the project as observers:

- *Germanischer Lloyd*
- *West State Inc.*
- *Lloyd's Register of Shipping*

This project was organized into six studies:

> **Study 1 – Fatigue Damage Evaluations**
> **Study 2 – Corrosion Damage Evaluations**
> **Study 3 – Interaction of Details with Adjacent Structure**
> **Study 4 – Fatigue and Corrosion Repair Assessments**
> **Study 5 – Durability Considerations for New & Existing Ships**
> **Study 6 – Development of Software and Applications Examples**

This report documents results from Study 1 – **Fatigue Damage Evaluations** whose objective is to develop and verify engineering guidelines for the evaluation of fatigue damage to critical structural components of existing ships.

In particular, the *theory* behind the Fatigue Damage Evaluation Software is contained in this report. This a summary of the general fatigue life evaluation and fracture mechanics procedures, a description of the long-term loading, a description of the uncertainties, and a description of the probabilistic and deterministic calculation procedures.

Contents

2

193

List of Figures

194

List of Tables

Chapter 1

Introduction

In the following, the theoretical foundation for the Structural Maintenance for New and Existing Ships Project (SMP) computer program FATIGUE is presented.

The SMP project is a two-year international joint industry project, which was initiated by the Department of Naval Architecture & Offshore Engineering at the University of California at Berkeley in June 1990. The project has two technical goals:

- To develop practical tools and procedures for analysis of proposed ship structural repairs in order to minimize time and materials within the constraints of regulatory and class requirements and prudent engineering practices.

- To prepare guidelines for the cost-effective design and construction of lower-maintenance ship structures which also facilitate future inspections and repairs.

The objective of the fatigue study of this project is to derive and verify engineering approaches to assess fatigue effects on the performance characteristics of critical structural details in tanker hulls, including the effects of inspection, maintenance and repair.

The FATIGUE computer program has been developed as a part of this study. This program performs the following tasks:

- Provide a tool for fatigue design of existing CSD and development of improved CSD;

- Provide a tool for residual life calculation for cracked details;

- Provide information on uncertainties for different design and repair alternatives;

1

197

The report is divided into 6 chapters; In **Chapter 2** the theoretical background for the S-N fatigue and fracture mechanics analysis is documented. Only the basic concepts that are of importance for the development of the integrated *Fatigue Life Evaluation* software are included.

Chapter 3 explains in detail the *S-N Classification of Critical Structural Details, (CSD)*. This includes the selection of the appropriate S-N curves for uncracked CSD and the fracture mechanics approach used to calculate the fatigue life for cracked CSD.

Chapter 4 defines different approaches for modelling of the longterm stress range process to be applied in the fatigue analysis of ship structures. This chapter contains a summary of the theory used for the development of the *Long-Term Loading* software. The complete documentation of this theory is found in [6].

Chapter 5 defines the stochastic uncertainty model being applied for the fatigue analysis. This includes descriptions of all uncertainties that are included in the model.

In this report a short review of the methods used for fatigue life calculations is given. Then the development of the hybrid method and the unified scheme to combine this method with the traditional design S-N curves is described.

Also the possible effects on the fatigue life of critical structural details due to the use of high tensile steel (HTS) is examined. The analysis of existing test data has indicated that HTS has comparable fatigue properties as normal steel.

For the fracture mechanics calculations the computer program LIFE [7] will be used. The theory behind this program especially for the calculation of the stress intensity factors is explained in detail.

The other issue in this report is the documentation of the results of the literature study on evaluations and management of fatigue reliability. In this background study, first a review of the existing major literature on fatigue reliability has been performed followed by a more detailed description of two well established methods, which demonstrate the application for fatigue life calculations respectively fracture mechanics calculations. Finally a short outline of a possible combination of the two methods, which accounts for the special characteristics of the hybrid S-N /FM approach is presented.

2

198

Chapter 2

Fatigue Calculation

2.1 Cumulative Damage

The fatigue life of a structural detail can be calculated using the theory of cumulative damage. Cumulative damage is in general the fatigue damage under stochastic or random loading. The most well-known theory to calculate the cumulative damage is the *Miner summation*.

The basic assumption in the Miner summation method is that the damage D for one load cycle is

$$D = \frac{1}{N} \qquad (2.1)$$

For a stress spectrum consisting of i blocks of stress ranges $S_{r,i}$ each with a number of cycles n_i the complete damage is

$$D = \sum_i \frac{n_i}{N_i} \qquad (2.2)$$

Failure occurs for D = 1. Fig. 2.1 shows qualitatively the procedure. It will be shown that the Miner summation conforms with the integration of the Paris equation. This fact is of major importance for the development of the Hybrid S-N / FM approach, which will be used to calculate the residual life of critical structural details.

2.2 Establishing of Design SN Curves

Design SN curves are based on test data. The SN curves are supposed to be linear on log-log scale. A mean line is fitted by regression analysis and confidence intervals for individual results were calculated. The confidence interval defines the probability that similar SN test results will be within the given limits. Design curves for a given class of welds are defined by the mean line and the standard deviation for different safety levels, fig. 2.2 shows schematically the mean fatigue life, mean minus one standard deviation (b)

3

/99

and minus two standard deviations (c). Most design curves use curve (c) to account for a confidence level of 94.5 %.

2.3 Overview of Building Codes for Fatigue Design (S-N Curves)

For the fatigue design of structural details several building codes have been established, primarily for tubular joints in the offshore industry and for welded structures like bridges etc.. The fatigue strength is here normally characterized by a set of empirical S-N curves for different welded details. The building codes of the DoE, AWS, DnV and NPD use the S-N curves established by the DoE. These curves have been derived on the basis of statistical analyses of S-N data for each design class. This procedure has resulted in differences in the slope of the curves, the fatigue limit and the categorization of weld details between the curves for the design classes. Fig. 2.3 shows these S-N curves.

In the recommendations of the IIW and the ECCS the inverse procedure has been used. Here conveniently spaced S-N curves have been defined a priori, see fig. 2.4, and the various weld details have been allocated to these curves by judgement based on statistical analysis of S-N data. For the purpose of fatigue design this set of S-N curves is more convenient to use.

2.4 Linear Elastic Fracture Mechanics (LEFM) used for Fatigue Analysis

2.4.1 Analytical Basis of LEFM

The material describing the general background of LEFM is mainly taken from the following publications [4], [22],[9].

The basis of LEFM is an analysis of the elastic stress field at the tip of a crack. In general there are three different opening modes for cracks, see Fig. (2.5). Their superposition describes the general case of cracking. For the purposes described here only mode I is considered.

The stresses and displacements at any point near the crack tip can be derived, using theory of elasticity and complex stress functions. The resulting equations show that the elastic stresses near the crack tip only depend on r, Θ, and K. Fig. 2.10 shows the definition of the polar coordinates r and Θ. K or more precise K_I is the mode I stress intensity factor.

The magnitude of the stresses at a given position (r, Θ) depends only on K. This fact is very important, since it states that the whole stress field at the crack tip is known, if K is known. All global parameters, like loading and geometry are incorporated in K.

4

This property of K allows it to incorporate all external factors into a single parameter. One value of K is thus valid for a great variety of loading and geometry configurations other than those from which they where originally obtained.

2.4.2 Evaluation of Stress Intensity Factors

The development of stress intensity factor solutions for the more complex critical structural details in ships is of crucial importance for the calculation of the residual life of cracked details. Therefore the methods to derive these stress intensity factors are described in detail.

The general form of the stress-intensity factor is given by

$$K = \sigma \cdot \sqrt{a} \cdot f(g) \tag{2.3}$$

The function f(g) depends on the specimen and crack geometry. For many configurations, crack sizes, orientations and shapes and loading conditions this functions have been published in various papers and handbooks. Their derivation is presented for the most common ones in [22]. Fig. 2.7 shows some examples of geometries, for which solutions are available.

For unusual crack geometries, the superposition of configurations with known stress intensity factors is the most common and simplest method. See [4] and [22] for details.

Another way to account for complex stress/geometry combinations of actual cracked structures is the use of *influence coefficients* or *influence functions*. This method leads to the introduction of a hybrid method for calculating K, combining the influence function method and the superposition method. Deriving the stress intensity factor for a complex structural detail using this method has the advantage that only one FEM calculation of the stress distribution in the uncracked detail is necessary.

Since this procedure is used in the computer program LIFE and will therefore be described in detail in the following section:

2.4.3 The Hybrid Method for the Calculation of the Stress Intensity Factors

The hybrid method is actually an influence function - and a superposition method. It is described in [4], [27] and most comprehensive in [8]. The hybrid method has been incorporated in the computer program LIFE. This is described in detail in [7]. It has been modified using parametric expressions developed by Newman and Raju [20] for part through thickness cracks. This is described in

As described in 2.4.1 the stress intensity factor K contains all information regarding the geometry and stress distribution of the considered detail. For

5

simple details solutions for K are published in the literature. Most of these solutions are of the general form:

$$K = \sigma\sqrt{\pi a} \cdot F \qquad (2.4)$$

with F being a correction factor for the specific configuration.

The correction factor F in equation (2.4) takes into account for instance the effects of

- a free surface close to the crack tip

- finite sheet thickness

- finite sheet width

- crack shape

- curvature of a cylindrical shell

- non-uniform stresses

- crack tip plasticity

Consequently the equation for F has the following form:

$$F = F_S \cdot F_T \cdot F_W \cdot F_E \cdot F_C \cdot F_G \cdot F_P \qquad (2.5)$$

with

F_S = free surface correction factor
F_T = finite thickness correction factor
F_W = finite width correction factor
F_E = crack shape correction factor
F_C = curvature correction factor
F_G = non-uniform stress correction factor
F_P = plasticity correction factor

The factor F_C can be set to 1 for the applications considered here. In [27] also the factor F_P, which accounts for the plasticity at the crack tip is set to 1 since for the majority of fatigue situations (at least for high cycle fatigue) the extension of a plastic zone will tend to be small compared with the crack length.

Part-through Crack Case

In [27] a set of parametric formulae is used to account for the factors F_S, F_T, F_W, F_E for the case of a part-through thickness crack.

6

The derivation of these formulae by Newman and Raju is described in detail in [20] and is outlined in the following.

Newman and Raju found a method to calculate crack growth by means of an empirical stress intensity factor equation that considers both tension and bending stresses through the thickness of the plate.

$$K = (\sigma_t + H \cdot \sigma_b) \cdot \sqrt{\frac{\pi a}{Q}} \cdot F(\frac{a}{t}, \frac{a}{c}, \frac{c}{b}, \phi) \qquad (2.6)$$

with

σ_t = remote uniform-tension stress
σ_b = remote uniform-bending stress
H = function, dependent on $\phi, \frac{a}{c}, \frac{a}{t}$
a = depth of surface crack
Q = shape factor for elliptical crack
F = stress intensity boundary-correction factor
t = plate thickness
c = half-length of surface crack
b = half-width of cracked plate
ϕ = parametric angle of the ellipse

See also Fig. (2.8).

The factor Q takes into account the effect of crack front curvature, i.e. crack shape. A useful approximation for Q has been developed by Rawe [14]:

$$Q = 1 + 1.464(\frac{a}{c})^{1.65} \qquad (\frac{a}{c} \le 1) \qquad (2.7)$$

The functions F and H are defined so that the boundary correction factor for tension is equal to F and the correction factor for bending is equal to the product of F and H.

The function F was obtained from a systematic curve-fitting procedure by using double-series polynomials in terms of a/c, a/t, and angular functions of ϕ. The function F was taken to be

$$F = [M_1 + M_2(\frac{a}{t})^2 + M_3(\frac{a}{t})^4]f_\phi \; g \; f_w \qquad (2.8)$$

where

$$M_1 = 1.13 - 0.09(\frac{a}{c}) \qquad (2.9)$$

$$M_2 = -0.54 + \frac{0.89}{0.2 + (a/c)} \qquad (2.10)$$

7

203

$$M_3 = 0.5 - \frac{1.0}{0.65 + (a/c)} + 14(1.0 - \frac{a}{c})^{24} \qquad (2.11)$$

$$g = 1 + [0.1 + 0.35(\frac{a}{t})^2](1 - \sin\phi)^2 \qquad (= 1 \ for \ \phi = \pi/2) \qquad (2.12)$$

The function f_ϕ an angular function from the embedded elliptical-crack solution is

$$f_\phi = [(\frac{a}{c})^2 \cos^2\phi + \sin^2\phi]^{1/4} \qquad (= 1 \ for \ \phi = \pi/2) \qquad (2.13)$$

The function f_w, a finite width correction from [16] is

$$f_w = [\sec(\frac{\pi c}{2b}\sqrt{\frac{a}{t}})]^{1/2} \qquad (2.14)$$

The function H is of the form

$$H = H_1 + (H_2 - H_1) \cdot \sin^p\phi \qquad (= H_2 \ for \ \phi = \pi/2) \qquad (2.15)$$

where

$$p = 0.2 + \frac{a}{c} + 0.6\frac{a}{t} \qquad (2.16)$$

$$H_1 = 1 - 0.34\frac{a}{t} - 0.11\frac{a}{c}(\frac{a}{t}) \qquad (2.17)$$

$$H_2 = 1 + G_1(\frac{a}{t}) + G_2(\frac{a}{t})^2 \qquad (2.18)$$

In this equation for H_2

$$G_1 = -1.22 - 0.12\frac{a}{c} \qquad (2.19)$$

$$G_2 = 0.55 - 1.05(\frac{a}{c})^{0.75} + 0.47(\frac{a}{c})^{1.5} \qquad (2.20)$$

The remote bending stress σ_b and tension stress σ_t in equation (2.6) refer to the pure bending or tension stress. Therefore a correction of Newman-Raju's equation with regard to the actual stress gradients has to be made.

This stress gradient correction factor F_G (also called " geometry correction factor") can be derived from known solutions for K. This solution of a crack stress field problem can be visualized as a two step process, fig. 2.9

204

1. The stress distribution problem is solved in a manner satisfying the boundary conditions (displacements, stresses) but with the crack considered absent.

2. To this stress field is superposed another stress field which cancels any stresses acting directly across the crack along the line of the crack.

Step 1 is a non-singular elasticity problem and can be solved by e.g. a FEM analysis. As the addition of a non-singular stress field ($\sigma(x)$, Step 1) does not affect the value of K (caused by $-\sigma(x)$, Step 2) the resulting K will be identical with that obtained from Step 2.

To evaluate K from Step 2, an influence (Green's) function method is employed. An influence function can be defined as (see fig. 2.10)

$$G_I(b,a) = \frac{1}{P}K_{IP}(b,a) \tag{2.21}$$

where K_{IP} = due to a load P at x = b

P   = load per unit sheet thickness / width

Hence, $G_I(b,a)$ is the K_I value arising from a unit force (per unit thickness/width) applied at abscissa x=b. $G_I(b,a)$ is independent of loading and depends merely on all the geometric parameters of the cracked body. I.e. if a solution for the stress intensity factor is known for any particular load system, then this information is sufficient to determine the stress intensity factor for any other load system.

A pressure p(x) applied on an infinitesimal surface t (or W) $\cdot$ dx results in an infinitesimal stress intensity factor.

$$dK_I(x,a) = G_I(x,a) \cdot p(x)dx \tag{2.22}$$

Thus, the K_I resulting from the total crack surface loading is

$$K_I(a) = \int_0^a G_I(x,a) \cdot p(x)dx \tag{2.23}$$

In a part-through crack case the computation of the stress gradient correction factor F_G might be based on the following solution of the problem shown in fig. 2.10.

$$K_I = \frac{2P}{\sqrt{\pi a}} \cdot \frac{1}{\sqrt{1-(b/a)^2}} \cdot F(b/a) \tag{2.24}$$

Therefore the influence function in this case is

$$G_I = \frac{2}{\sqrt{\pi a}} \cdot \frac{1}{\sqrt{1-(b/a)^2}} \cdot F(b/a) \tag{2.25}$$

9

Equation (2.23) with G_I from Equ. (2.25) and $p(x) = \sigma(x)$, yields

$$K_I = \sqrt{\pi a} \cdot \frac{2}{\pi} \cdot \int_0^a \cdot F(x/a) dx \qquad (2.26)$$

where $\sigma(x)$ can be obtained from a FEM analysis.

The stress distribution could be represented by a polynomial expression and equ. (2.26) could be integrated analytically. However it is more convenient to use a discretized stress distribution as shown in fig. 2.11. Equ. (2.26) may then be reformulated as

$$K \simeq \sqrt{\pi a} \frac{2}{\pi} \sum_{i=1}^n \sigma_{b_i} \cdot F(\overline{b}/a) \int_{b_i}^{b_{i+1}} \frac{dx}{\sqrt{a^2 - b^2}} \qquad (2.27)$$

where σ_{b_i} = stress in block no. "i"
$\overline{b_i}$ = $1/2(b_i + b_{i+1})$

The integration is carried out over the block width, and the summation over the number of blocks. After factoring out the nominal stress, σ, applied remotely from the crack, integration of equ. 2.27 leads to

$$K \simeq \sigma\sqrt{\pi a}\left\{\frac{2}{\pi} \sum_{i=1}^n \cdot \frac{\sigma_{b_i}}{\sigma} \cdot F(\overline{b_i}/a) \cdot [\arcsin \frac{x}{a}]_{b_i}^{b_{i+1}}\right\} \qquad (2.28)$$

$$= \sigma\sqrt{\pi a}\left\{\frac{2}{\pi} \sum_{i=1}^n \cdot \frac{\sigma_{b_i}}{\sigma} \cdot w_{b_i}\right\} \qquad (2.29)$$

$$= \sigma\sqrt{\pi a} \cdot F \qquad (2.30)$$

where w_{b_i} = weight of block no. "i".

For the case of an edge crack described here the effect of the stress gradient on the free surface correction factor F_S can be included in F_G in the following way [27], [7].

$$F_G = \frac{F}{1.122} \qquad (2.31)$$

The resulting expression used in computing F_G in the case of an edge crack might then be written as

$$F_G = \frac{2}{1.122 \cdot \pi} \cdot \sum_{i=1}^n \left\{\frac{\sigma_{b_i}}{\sigma} \cdot F(\overline{b_i}/a) \cdot [\arcsin \frac{b_{i+1}}{a} - \arcsin \frac{b_i}{a}]\right\} \qquad (2.32)$$

In order to apply Newman-Raju's empirical stress intensity factor equation in the case of an arbitrary stress field the following transformations have to be made.

10

For tension stresses F is replaced by $F \cdot F_{G,at}$
For bending stresses F is replaced by $F \cdot F_{G,ab}$
H is replaced by $H/F_{G,nb}$

$F_{G,at}$ and $F_{G,ab}$ are correction factors, which account for the difference between a uniform and a non-uniform tension or bending stress distribution in the crack growth plane. These factors are calculated using equ. (2.32) with the actual through thickness stress distributions (tension for $F_{G,at}$ and bending for $F_{G,ab}$). A calculation for a *linear* bending stress distribution (pure bending) provided the extraction ot the effect of this distribution and gave $F_{G,nb}$.

Through Crack Case

The problem of estimating the stress intensity factor K for the case of a through thickness crack can be solved by using the hybrid method only. Here it is only necessary to take the finite width correction factor F_W and the stress gradient correction factor F_G into account . It is therefore not necessary to apply the Newman / Raju method.

$$K = \sigma\sqrt{\pi a} \cdot F \qquad (2.33)$$

Here F is a function of the stress gradient correction factor F_G and the finite width correction factor F_W only.

$$K = \sigma\sqrt{\pi a} \cdot F_G \cdot F_W \qquad (2.34)$$

The computation of F_G in the case ot a through crack might be based on a solution of the problem shown in fig. 2.12

As described for the part-through crack the stress gradient correction factor can be determined by using a superposition method combined with an influence (Green's) function method.

The following exact solution for the stress intensity factor for a crack in an infinite sheet subjected to a pair of spitting forces, which do not have to be at the center of the crack is used.

$$K_{I_{\pm a}} = \frac{P}{\sqrt{\pi a}} \cdot \sqrt{\frac{a \pm b}{a \mp b}} \qquad (2.35)$$

This case yields the following expression for F_G :

$$(F_G)_{\pm a} = \frac{1}{\pi}\sum_{i=1}^{n}\left\{ \frac{\sigma_{b_i}}{\sigma}\left[\arcsin\frac{b_{i+1}}{a} - \arcsin\frac{b_i}{a} \mp \sqrt{1 - \left(\frac{b_{i+1}}{a}\right)^2} \mp \sqrt{1 - \left(\frac{b_i}{a}\right)^2}\right]\right\}$$

$$(2.36)$$

11

where $\qquad b \in (-a, +a)$

The finite width correction factor F_W can be calculated using one of the methods described in [7]

It is one of the objectives of the fatigue study of the SMP to calculate the residual life of critical structural details. Since part through-thickness cracks are hardly ever detected in ship inspections, they are not considered in this study. For this reason only the methods to calculate the stress intensity factors for through-thickness cracks will be used.

2.4.4 Fracture Mechanics applied to Fatigue Problems

For the purpose of calculating the fatigue life of a structural component it is necessary to estimate the crack growth rate da/dN.

Fig. (2.13) shows a schematic crack growth rate curve with the three relevant regions threshold, intermediate and failure region. Here ΔK is the alternating stress intensity, ΔK_{th} is the threshold stress intensity and K_c is the stress intensity at final failure.

The simplest and probably most well-known equation is the *Paris equation* [19].

$$\frac{da}{dN} = C(\Delta K)^m \tag{2.37}$$

This equation provides an adequate description only for region B in Fig. (2.13). The regions A and C are replaced by vertical lines in order to allow the integration of equation (2.37). Since normally most of the fatigue life of a structural component is spent in regions A and B, the *Paris equation* will in general yield *conservative* results.

In the last years offshore structures have been the subject of intensive research on the field of fracture mechanics. In addition to the general references mentioned above [21] gives a good overview of the use of fracture mechanics in the offshore industry.

2.4.5 Estimation of fatigue life

In general the fatigue life (N_f) can be subdivided in a crack initiation period (N_i) and a crack growth period (N_p), ending with failure.

$$N_f = N_i + N_p \tag{2.38}$$

For welded joints and welded structural components the crack initiation usually occupies only a small part of the fatigue life and is therefore often neglected causing only small errors in the conservative direction.

The crack propagation part of the fatigue life can be calculated for constant amplitude loading using the following formula:

$$N_p = \int_{a_i}^{a_p} \frac{da}{(da/dN)} \tag{2.39}$$

12

where: a_i = Initial crack length (depth)

a_p = final (critical) crack length (depth)

For *constant amplitude loading* the following estimate for the crack propagation life can be obtained:

$$N_p = \frac{1}{C \cdot \Delta\sigma^m \cdot \pi^{m/2}} \int_{a_i}^{a_f} \frac{da}{a^{m/2} \cdot F^m} \qquad (2.40)$$

In general F will be a function of a, which complicates the solution significantly. In many cases it is therefore useful and possible to assume F = const.

For welded components, it will be difficult to apply equation (2.40) in calculations of fatigue life, due to large uncertainties in assessing crack growth rates in region A (see Fig. (2.13), and in estimating the length of the initial crack., a_i. For problems involving large initial cracks, e.g. residual life assessments, equation (2.40) may give very accurate predictions. The results obtained are always useful in a qualitative sense

2.5 Recommended Practice for Residual Life Assessment

For residual life assessments of welded details with flaws no rules are issued by classification societies or regulatory bodies. Instead some organizations have specified recommended practices for residual life assessment. The general procedure for fracture mechanics calculations is outlined in the following:

For the assessment of the residual life of a cracked structural detail a fracture mechanics approach has to be used. For practical purposes it is usually conservative and sufficient to use the *Paris equation* to calculate the crack growth da/dN.

$$\frac{da}{dN} = C(\Delta K)^m \qquad (2.41)$$

Here C and m are constants, which depend on the material and the applied conditions, and ΔK is the range of the stress intensity factor.
For $\Delta K < \Delta K_0$, da/dN is assumed to be zero.

The stress intensity factor range, ΔK, is a function of structural geometry, stress range and crack length:

$$\Delta K = Y(\Delta\sigma)\sqrt{\pi a} \qquad (2.42)$$

By substituting equation (2.42) in equation (2.41) and integrating, the overall life can be predicted:

$$N_{res} = \int_a^{a_f} \frac{da}{da/dN} = \frac{1}{Const.(\Delta\sigma)^m} \int_a^{a_f} \frac{da}{(\frac{\Delta K}{\Delta\sigma})^m} \qquad (2.43)$$

13

with:

$$(\frac{\Delta K}{\Delta \sigma})^m = (\sqrt{\pi a}Y(a))^m$$

depending only on the initial crack length a.

Equation (2.43) can be expressed in the usual form of S-N curves.

$$N_{res}(\Delta \sigma)^m = Const \qquad (2.44)$$

The above constant depends on the initial crack length a. It is therefore possible to obtain a set of S-N curves, where each curve represents a specific initial crack length. Fig. (2.14) shows this qualitatively.

In the IIW RP (recommended practice) [2] this procedure has been used to establish S-N curves for simple details with initial imperfections under uniaxial stress, see Fig. (2.15).

2.6 IIW Recommended Practice for the Assessment of Known Flaws

In the RP published by the IIW a simplified procedure for the assessment of planar flaws subjected to either axial or bending loading is presented.

A grid of S-N curves is used, each curve representing a particular quality category. A flaw is acceptable if its actual quality category is the same or higher than the required quality category.

The required quality category must be determined for the service conditions to be experienced by the flawed weld. This can be done either on the basis of the stress ranges and the total number of cycles of fatigue loading anticipated in the life of the weldment or by referring to an adjacent standard design detail and stating that the quality category of the flawed weld need not to be higher than the category of the standard design detail.

In the IIW recommendations the quality categories are defined by 15 S-N curves, labelled Q100 to Q20, shown in Fig. (2.15). These curves are parallel and have a slope of -1/3 in the $\log \Delta \sigma$ v $\log N$ plot.

For compatibility with the IIW design recommendations these curves are characterized in terms of the stress range corresponding to a fatigue life of 2×10^6 cycles. For steels, it is this value to which the number in the quality category refers.

This procedure facilitates the comparison of the fatigue lives of flaws with those of standard weld details since the quality categories for steel Q100 - Q45 are identical to the design S-N curves, corresponding to 97.7% survival limits,for classes 100 - 45 in the IIW fatigue design recommendations, [18].

2.7 Method for Calculating the Remaining Fatigue Life of Cracked Structures

At the OMAE conference in 1988 T.M. Hsu has presented a paper titled: "A Simplified Method for Calculating the Remaining Fatigue Life of Cracked Structures", [11]. This method uses an equivalent S-N approach, which is very similar to the one outlined above. Hsu also gives a comparison of his simplified method with the results of a rigorous fracture mechanics approach. Therefore this method is reviewed in detail to serve as a reference.

Linear Elastic Fracture Mechanics is used to derive the following equation for the total number of cycles, N, required to grow the crack from an initial length of a_i to the final length a_f.

$$ N = \frac{1}{c\pi^{m/2}} \int_{a_i}^{a_f} \frac{a^{-m/2}\beta^{-m}}{(\Delta S)^m} da \qquad (2.45) $$

In most cases this equation has to be integrated numerically since the load on the structure is normally not constant and the stress intensity factor K is almost always a function of the crack length.

A series of equivalent S-N curves can be constructed by repeating these calculations for different initial crack lengths. These equivalent S-N curves can be combined into a single conventional S-N equation by representing the intercept of the S-N curve as a function of the crack length. With this relationship the method can easily be used by engineers who have little or no knowledge of fracture mechanics, but have some knowledge of conventional S-N fatigue, to predict the remaining fatigue life of a structure with any initial crack length subjected to any anticipated spectrum of loads.

The above method is then used to illustrate the procedures of developing equivalent S-N curves and their use in predicting the remaining fatigue life of such cracked structures. A comparison with a rigorous fracture mechanics approach showed very good agreements of the results. Fig. (2.16) shows this for the combined load case. In this figure, the curves are predictions using the simplified method and the symbols are results calculated using the conventional fracture mechanics method. As can be seen from this figure, the simplified method gives good predictions when compared with the conventional fracture mechanics calculations.

2.8 Conclusions for Tanker Critical Details under Consideration in the SMP

The IIW recommendations have been established for simple details and uniaxial or bending loading. For the critical details under consideration in the SMP the situation is different.

- The complex geometry of these details results in stress distributions, which are normally not uniaxial.

- The high degree of redundancy in ship structures results in load shedding effects which change the crack growth behaviour significantly, Fig. (2.17).

For these reasons the IIW recommendations are *very* conservative for ships.

For the purposes of this project a different set of S-N curves has to be established in order to account for the complex geometry of the details. The scheme provided by the IIW can serve as a good starting point and it will also result in a very consistent approach for both the fatigue design and the residual life assessment.

Within the scope of this project it will not be possible to account for the load shedding effects within the structure. The verification cases will serve as a means to calibrate the fatigue models.

2.9 Proceedings

2.9.1 S-N Curves for Fatigue Design

For the critical details mentioned above S-N curves have to be found. The S-N data needed will be provided by ABS or will be found in the literature, e.g. Munse's collection of S-N data [15].

For details, where no data can be obtained, the fracture mechanics approach described in section 2.5 can be used to obtain S-N curves. The main difficulty here will be to define an initial crack length.

For offshore platforms and even more for airplanes, it is assumed that there are cracks present in the structure with a length equal to the minimum length, which can be detected by non-destructive inspection methods. This is a very realistic assumption since welds will always have initial imperfections.

For this reason a similar argumentation should be used in order to establish design S-N curves. The main problem with this approach is the fact that with the inspection methods used in ships only comparatively large cracks can be detected. The use of these crack lengths would result in very conservative S-N curves. Therefore this point has to be discussed very thoroughly.

2.9.2 S-N curves for details with cracks

In order to obtain S-N curves for the critical details using the procedure described in 2.5 the stress intensity factors for these details have to be found. For this it is inevitable to know the stress distribution in the particular detail,

16

which has to be calulated with the help of detailed Finite Element models. This calculations will be performed within the *Global - Local Interactions Study* of the Structural Maintenance Project.

2.10 Fatigue Properties of High Tensile Steel (HTS)

The use of HTS allows development of higher design stresses; thus, decreasing member thicknesses and helping reduce building costs. For this reason the use of HTS has rapidly increased in the last years. This fact has led to increased research activity especially with regard to the fatigue properties of HTS in order to determine the influences of the use of HTS on the overall strength of ships and on the fatigue behaviour of ship structural details built of HTS.

A study conducted by British Steel [12] has tried to summarize the results of research regarding the fatigue behaviour of HTS . The tests were performed on 50 mm thick parent plate and welded T-joints of 25, 50 and 80 mm. The joints were both in air and in seawater. Fig. (2.18) shows the geometry of the T-joint. The variables for the tests were plate thickness, stress ratio and PWHT (Post Weld Heat Treatment).

The results of this test programs imply that the fatigue endurance of HTS in air and seawater is similar to that of a lower strength steel for a similar thickness of joint. It can therefore be concluded that the design rules for lower strength steel are applicable to HTS. This means that the same S-N curves can be used for both the lower strength steels and HTS. For this reason it can be benefical to use HTS especially in areas not sensitive to fatigue loading.

In a different publication [13] it is stated that the use of HTS has brought about better designing of structural details to avoid high stress concentration and better production quality control. The 'penalties of using HTS, which include lower relative fatigue strength and buckling by corrosion can be minimized by further research and technical development. Although this paper is therefore very optimistic about the use of HTS, it does not imply that HTS has to be treated differently for fatigue life calculations.

On the basis of this information, it has been concluded that the same S-N curves can be used for both mild steels and HTS.

17

Table 2.1: DoE: Details of Basic S-N curves - Air

	$N \leq 10^7$				$N > 10^7$	
Class	$\log a$	$\log s$	$\log \bar{a}$	m	$\log \bar{a}$	m
B	15.3697	0.1821	15.01	4.0	17.01	5.0
C	14.0342	0.2041	13.63	3.5	16.47	5.0
D	12.6007	0.2095	12.18	3.0	15.63	5.0
E	12.5169	0.2509	12.02	3.0	15.37	5.0
F	12.2370	0.2183	11.80	3.0	15.00	5.0
F2	12.0900	0.2279	11.63	3.0	14.72	5.0
G	11.7525	0.1793	11.39	3.0	14.32	5.0
W	11.5662	0.1846	11.20	3.0	14.00	5.0
T	12.6606	0.2484	12.16	3.0	15.62	5.0

The S-N curve is written as

$$\log(N) = \log a - 2\log s - m\log\Delta\sigma$$
$$= \log\bar{a} - m\log\Delta\sigma$$

where:

N predicted number of cycles to failure for stress range $\Delta\sigma$

$\log a$ cut of the the $\log N$-axis by the mean S-N curve

$\log s$ standard deviation of $logN$

m negative inverse slope of the S-N curve

$\log\bar{a}$ $\log a - 2\log s$
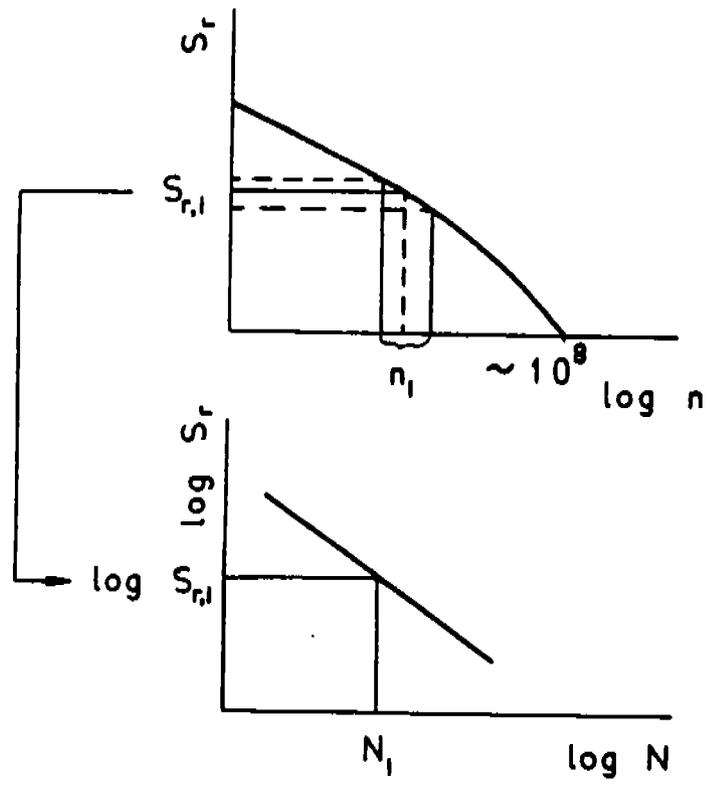
Figure 2.1: The Miner summation procedure for one stress block
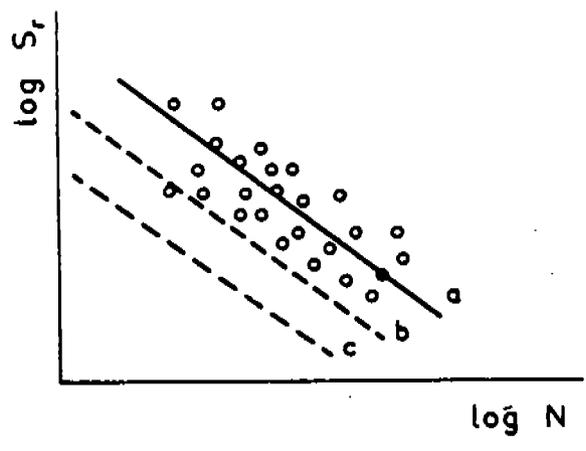
Figure 2.2: Schematic regression lines for fatigue life at different safety factors

19
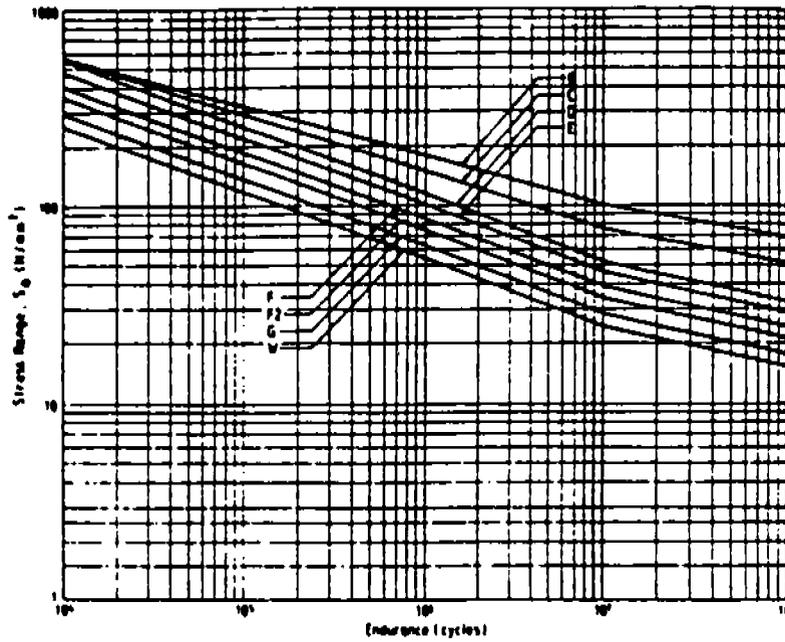
Figure 2.3: Fatigue design S-N curve for planar welded joints, DoE, NPD, DnV
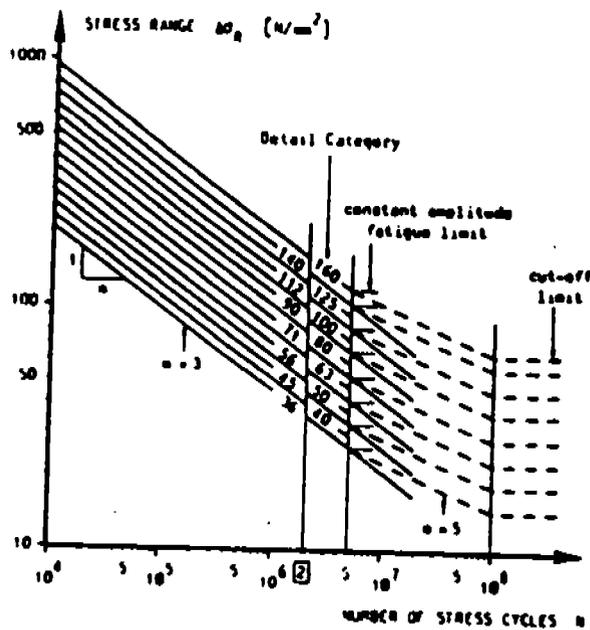
Figure 2.4: Fatigue design S-N curve for planar welded joints, IIW/ECCS

20
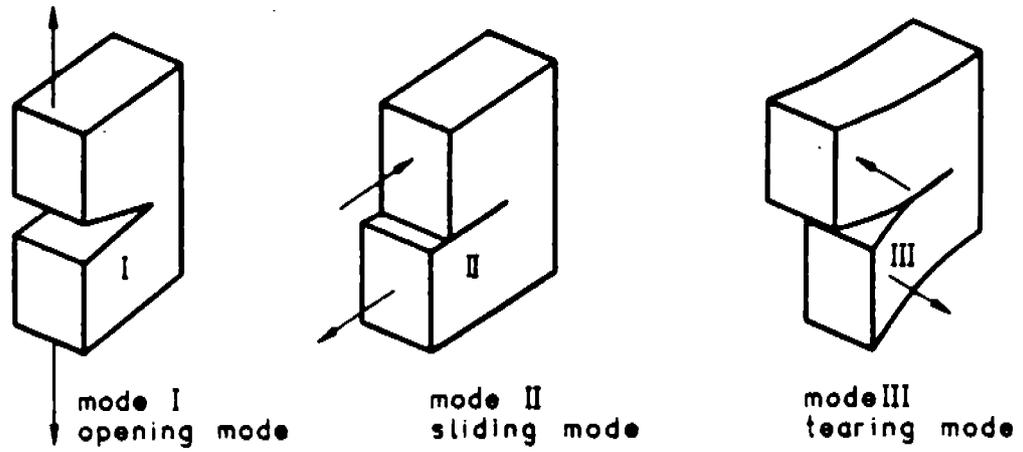
Figure 2.5: The three modes of cracking
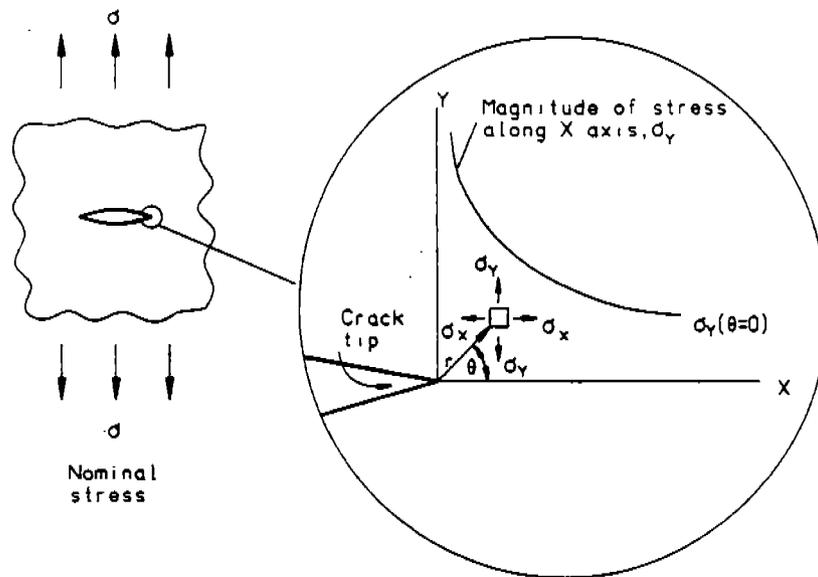
Figure 2.6: Elastic stress field distribution near the tip of a crack (mode I)

21

$$K = Y(\alpha)\, \sigma\sqrt{\pi a}$$

$$\alpha = a/b$$
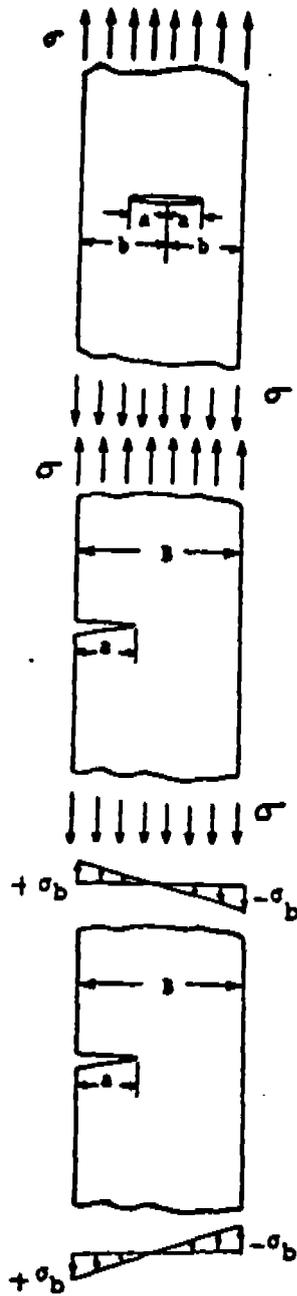
$$Y(\alpha) = \left[1 - 0.025\,\alpha^2 + 0.06\alpha^4\right]$$
$$\cdot \sqrt{\sec\frac{\pi\alpha}{2}}$$

Through Crack in a Finite Width Plate

$$K = Y(\alpha)\, \sigma\sqrt{\pi a}$$

$$\alpha = a/B$$

$$Y(\alpha) = \sqrt{\frac{2}{\pi\alpha}\tan\frac{\pi\alpha}{2}} \cdot$$

$$\frac{0.752 + 2.20\alpha + 0.37\left(1-\sin\frac{\pi\alpha}{2}\right)^3}{\cos\frac{\pi\alpha}{2}}$$

Edge Crack Under Axial Load

$$K = Y(\alpha)\, \sigma\sqrt{\pi a}$$

$$\alpha = a/B$$

$$Y(\alpha) = \sqrt{\frac{2}{\pi\alpha}\tan\frac{\pi\alpha}{2}} \cdot$$

$$\frac{0.923 + 0.199\left(1 - \sin\frac{\pi\alpha}{2}\right)^4}{\cos\frac{\pi\alpha}{2}}$$

Figure 2.7: Examples of Geometries for Stress Intensity Factor Solutions

22

218
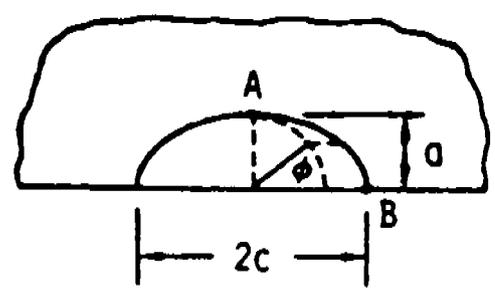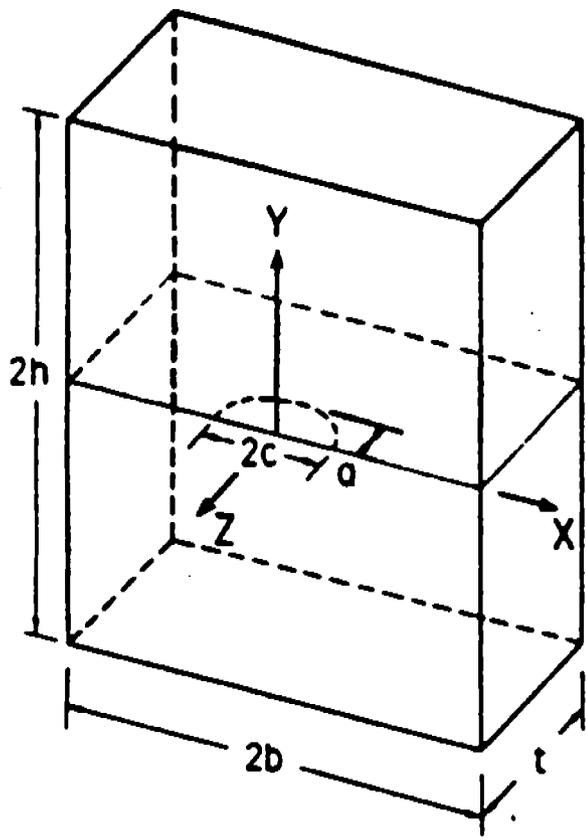
Figure 2.8: Surface Crack in a Finite Plate)
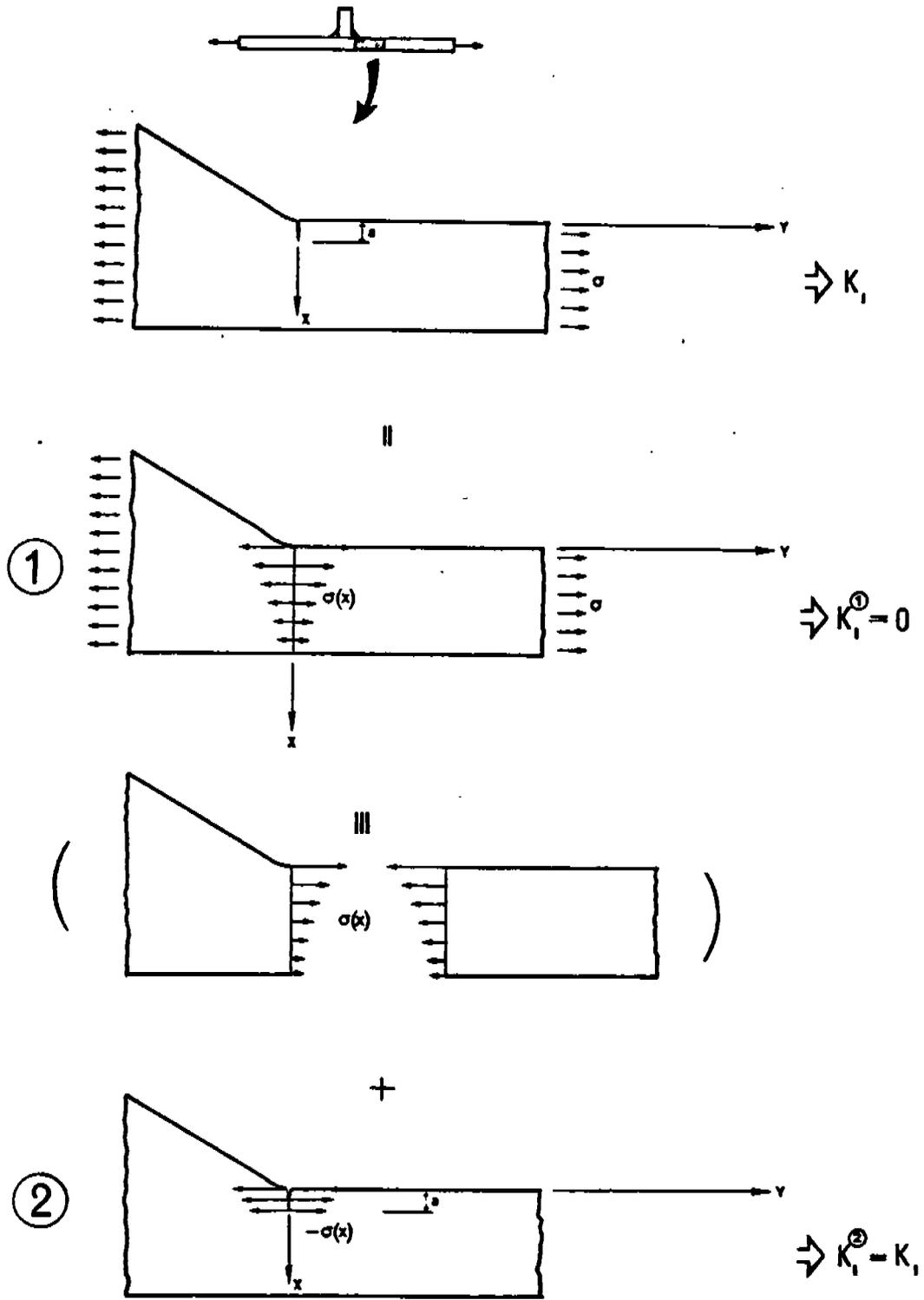
Figure 2.9: Superposition of Stresses in a Welded Joint

24
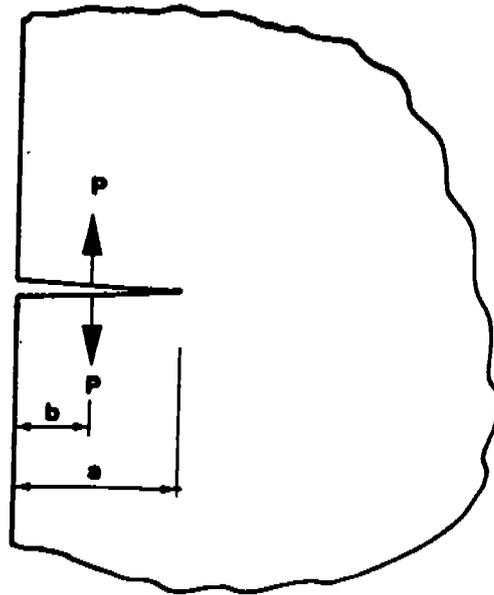
$$K_I = \frac{2P}{\sqrt{\pi a}} \cdot \frac{a}{\sqrt{a^2 - b^2}} \cdot F\left(\frac{b}{a}\right)$$
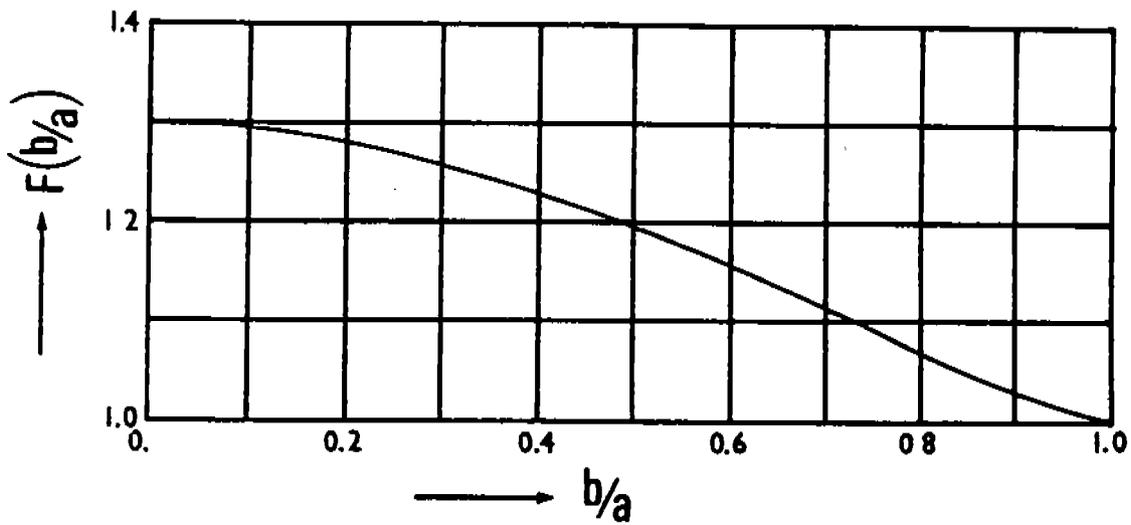
Figure 2.10: Calculation of K-Value by a Pair of Splitting Forces applied to the Crack Surface
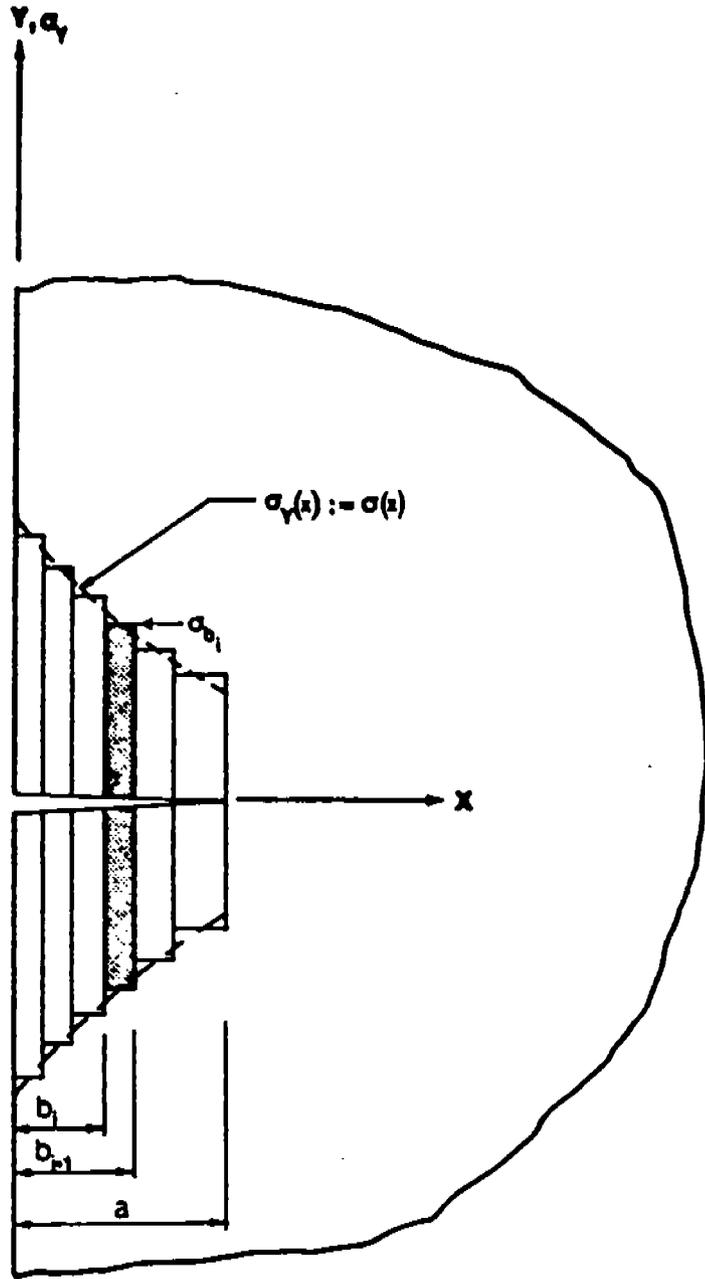
Figure 2.11: Discretized Stress Distribution

223
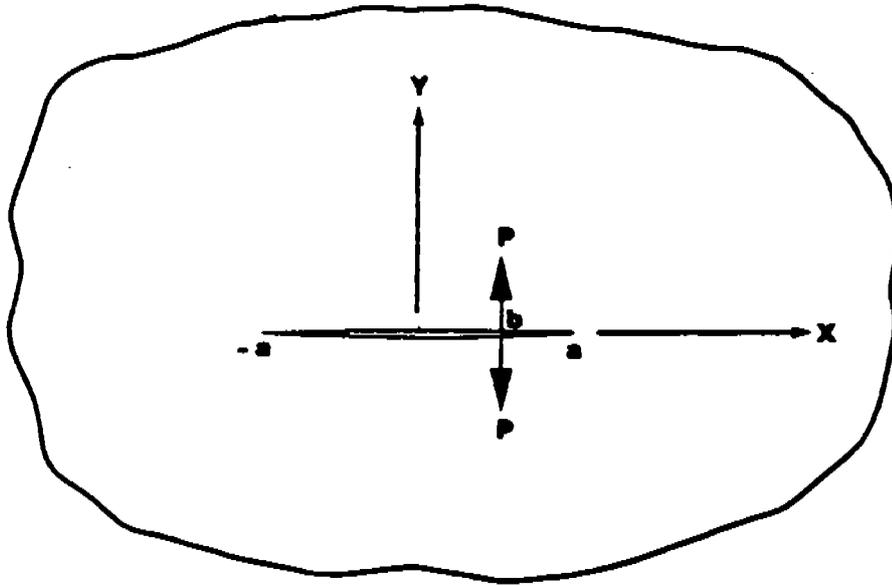
$$\{K_1\}_{\pm_a} = \frac{P}{\sqrt{\pi a}} \cdot \sqrt{\frac{a \pm b}{a \mp b}}$$

Figure 2.12: One Pair of Splitting Forces on a Through Crack in an Infinite Sheet
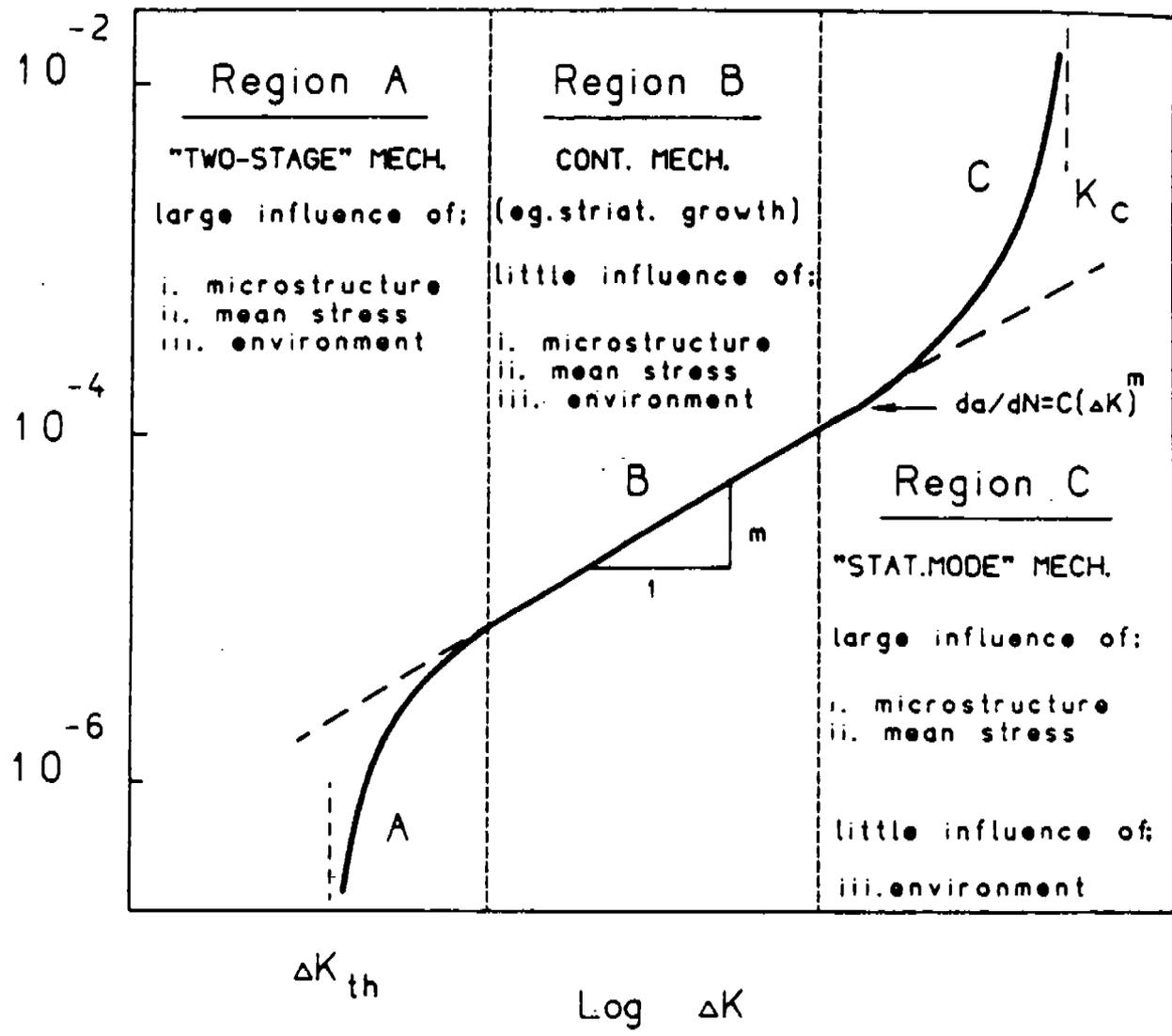
Figure 2.13: Schematic Crack Growth Rate Curve

224
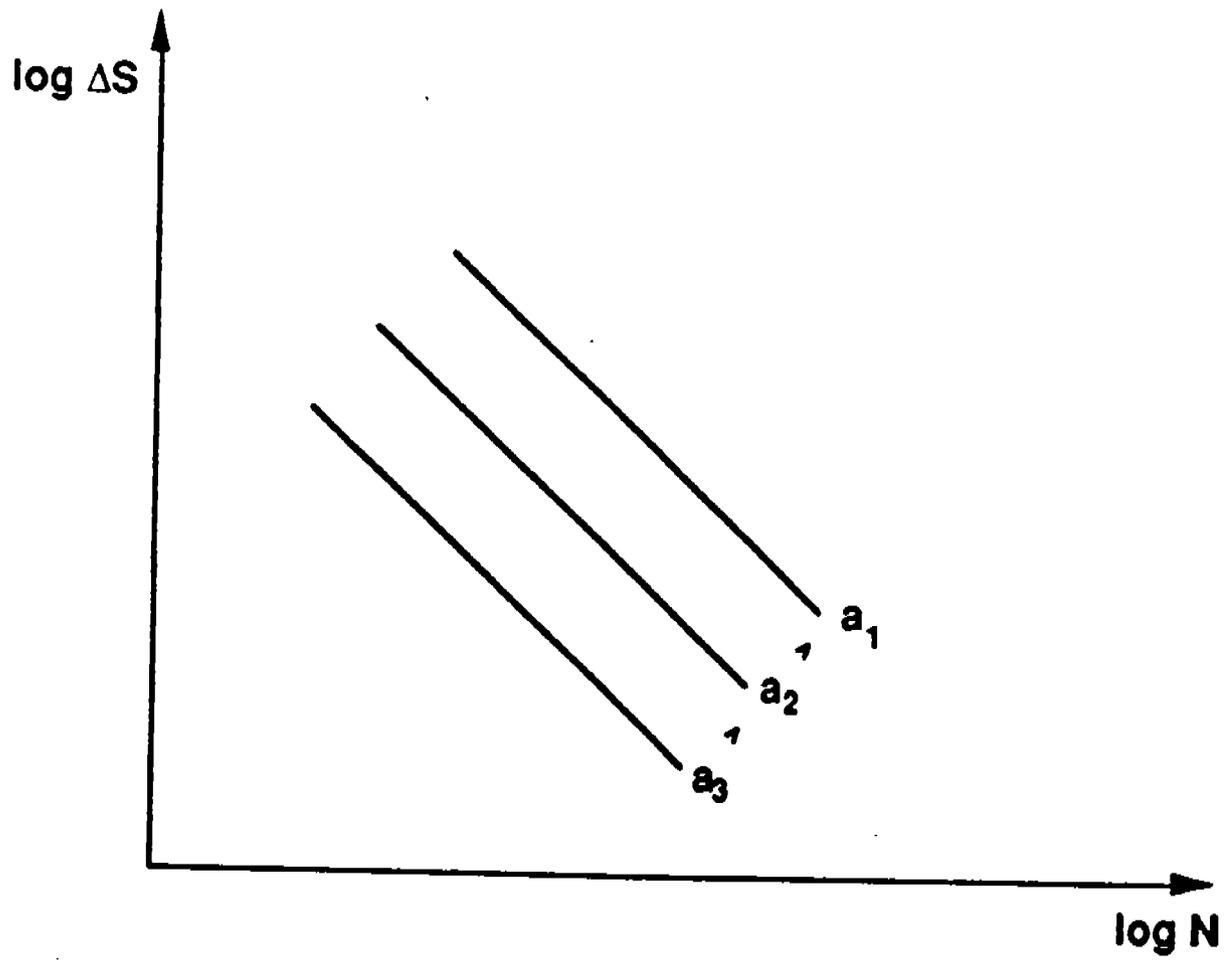
Figure 2.14: S-N Curves for Structural Details with Initial Cracks (qualitative)

29
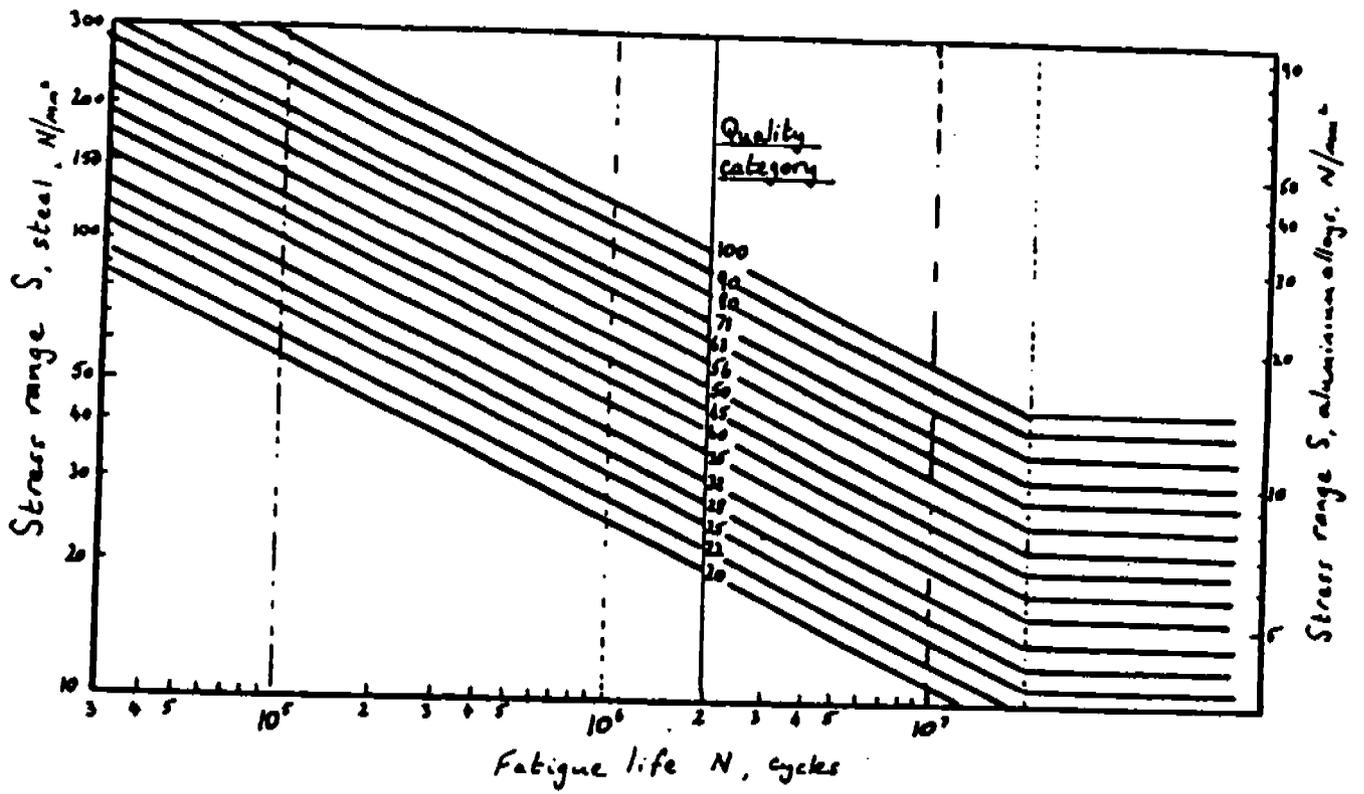
Figure 2.15: IIW Quality Categories for Planar Flaws

30
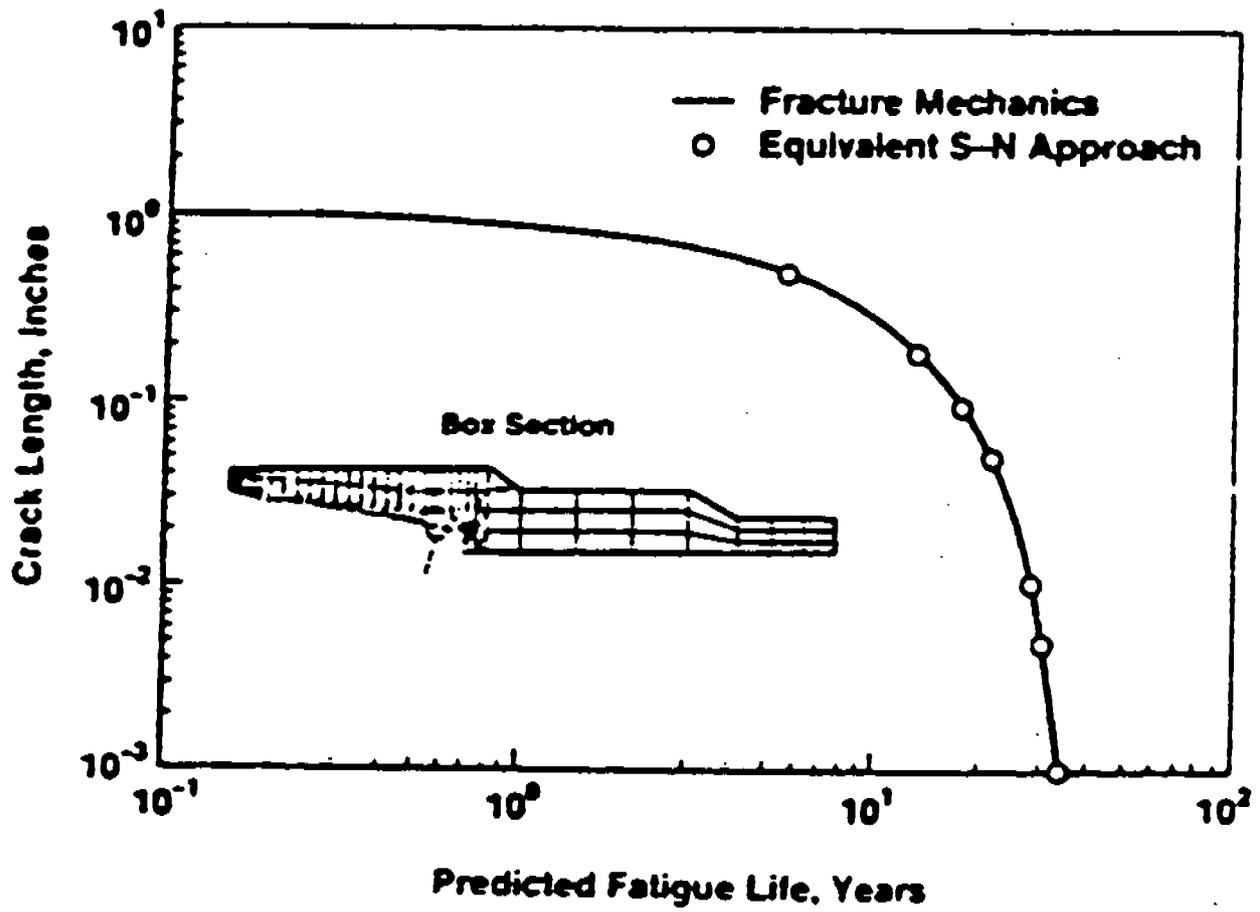
Figure 2.16: Predicted Fatigue Life (Comparison of Results)
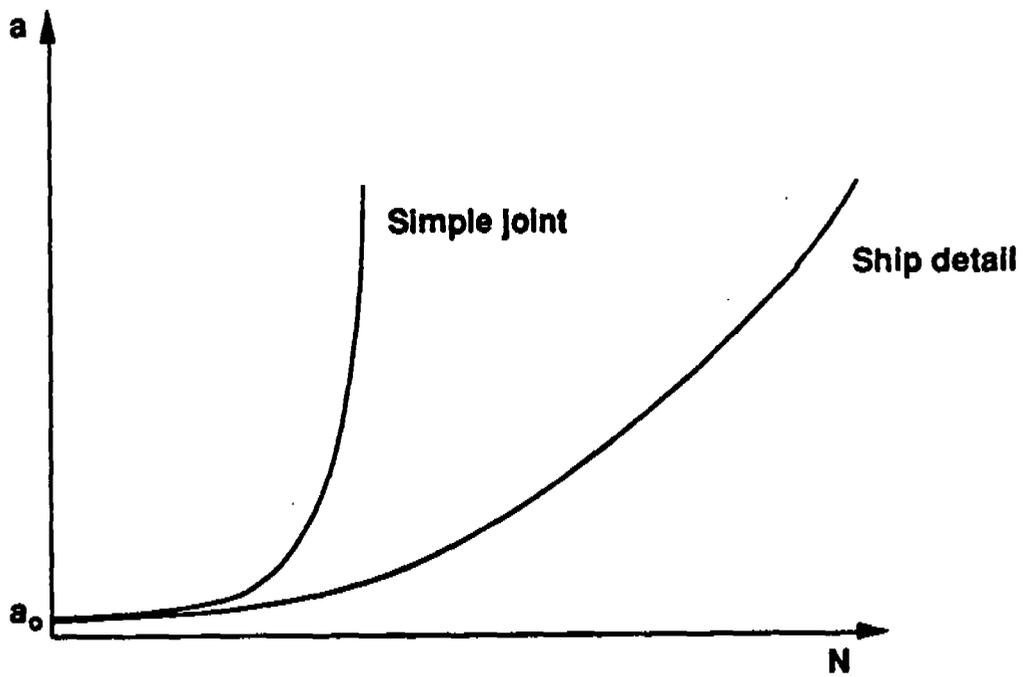
Figure 2.17: Crack Growth Behaviour for Simple and for Complex Details
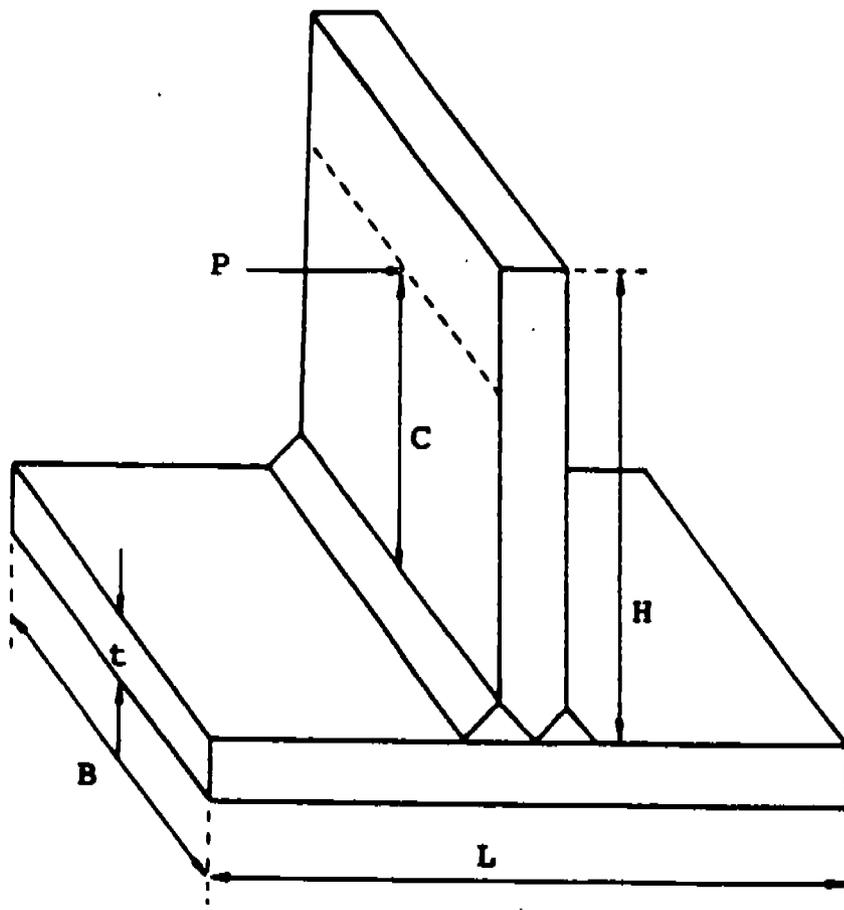
Figure 2.18: Geometry for HTS T-joint

Chapter 3

S-N Classification

3.1 Introduction

The accuracy of the estimated fatigue life of a structural detail depends strongly on the representation of the *load* and the *capacity*. The method used to obtain an estimate of the long-term cyclic load is described in chapter 4. The estimation of these long-term loads contains the largest uncertainties and requires, especially for the seaway loads of ships, further research.

The *capacity* to resist metal fatigue can be expressed by the S-N curve used for the location that is investigated. Standard procedures have been developed for the selection of S-N curves for standard details. For details as complex as ship critical structural details these procedures are rather difficult to use for the following reasons:

- Due to complex loading and geometry the resulting stress distribution is often multi-axial and can in general not be obtained easily.

- Most standard S-N curves are developed for small welded specimen. Considerable judgement is necessary to determine the most suitable curve for complex details.

- The standard S-N curves are developed for the use of a *nominal* stress far away from the weld. The use of these curves in combination with the results of a FE analysis requires further research.

- A strucural detail has in general more than one possible crack location. A crack will in general start at a hot-spot, a location with a high stress concentration.

These issues are addressed in this chapter. For one type of critical structural detail (CSD) S-N curves have been selected for a set of chosen hot-spots. The considerations that led to this selection are described and can be used for the future development of different types of CSD.

34

3.2 General Considerations

In general the estimation of the fatigue life of a structural detail requires knowledge about the long-term distribution of the stress ranges the detail is subjected to and the fatigue strength of the detail. The method used to determine the *load* will influence the decision about the representation of the fatigue *strength*.

3.3 Finite Element Analysis and S-N Curves

The finite element analysis is widely used to determine stresses for complex structural details. With this method it is possible to determine very exactly the stresses in each location of interest. In general the analysis is performed under the assumption of a linear, elastic material. Reducing the mesh size will in general converge to the exact solution. It is only for sudden changes of geometry (singularity) that the solution does not converge.

The determination of the nominal stress requires the exact definition of the location and the assumed direction of the stress. It is nearly impossible to pre-define this location without visually inspecting the stress distribution in the detail. The use of the nominal stress also neglects valuable information about local effects that influence the stress response near the hot-spot.

The effect of these local effects has to be accounted for through the choice of the S-N curve. This again will involve substantial engineering judgement.

As an alternative it is possible to use the hot-spot stresses directly. The main problem in doing so is that S-N curves have to be used that are calibrated for this purpose. This calibration is especially important for hot-spots at singularities. Further research is required to establish a set of S-N curves that is calibrated for the use with hot-spot stresses.

For this project it has been decided to use the hot-spot stresses despite the lack of well researched and calibrated S-N curves. For the one type of Critical Structural Detail (CSD) the hot-spots and the S-N curves to be used have been selected based on engineering judgement.

3.4 S-N Curves for Un-cracked CSD

3.4.1 CSD Type selected for Implementation

It is the intent of the Structural Maintenance Project (SMP) do develop an integrated software system that can be used to perform fatigue life analyses of Critical Structural Details in oil tankers. The system has to perform the following tasks:

- Generate Finite Element mesh of CSD based on user-supplied dimensions.

35

- Generate unit-loads necessary to obtain stress concentration factors.

- Perform finite element analysis and produce table of stress concentration factors for hot-spots.

- Estimate long-term load distribution based on user-supplied travel route, maneouvring philosophy and ship transfer functions.

- Perform fatigue life analysis based on estimated long-term loading and user-supplied uncertainty information

The developed software will be verified by comparing the results with crack data obtained from database analysis. This verification is documented in [25].

In order to achieve this functionality it is necessary to define classes of CSD. Within a class it is then possible to develop the procedures necessary to create the FE mesh, to apply the loads, to estimate the long-term load distribution and to perform the fatigue life analysis.

As a first class the *Connection of a sideshell longitudinal to a transverse webframe* has been chosen. This type of detail is of main concern since the majority of fatigue failures occurs in this type of detail, see [24]. Only for this detail enough information is available for all parts of the SMP project.

The *Connection of a sideshell longitudinal to a transverse webframe* consists of the following components:

- Sideshell plating

- Transverse webframe

- Longitudinal

- Cutout of webframe

- Forward bracket (optional)

- Aft bracket (optional)

Fig. (3.1) shows an overview of the chosen CSD.

3.4.2 Definition of Hot-Spots

In order to to calculate the fatigue life of a CSD it is necessary to obtain the stress concentration factor for a unit load at the location that is analysed. For the same location the S-N curve has to be specified.

In a conventional analysis all the above steps are performed interactively. The choice of the location and the selection of the S-N curve is based on the judgement and experience of the user.

For the anticipated automated system a discrete number of hot-spots has been defined. For each hot-spot the direction of the crack has been chosen. This makes it possible to automatically determine the stress concentration factor from the results of the finite element analysis.

The choice of the hot-spots and the crack directions is based on the experience gained through the database analysis and the advice of owner/operators and classification societies. The report [5] has been the source of valuable information.

Hot-spots have been defined for the cutout of the webframe. Fig. (3.2) shows the possible hot-spots for a generic cutout. Fig. (3.3) shows the same information for a generic bracket.

For each hot-spot the direction of a crack originating at this location has to be defined. This is necessary since the stresses perpendicular to the crack have to be obtained from the finite element analysis. Fig. (3.4 shows the crack directions for each hot-spot for both the webframe cutout and the bracket.

3.4.3 Selection of S-N curves

For the selected hot-spots in both the cutout and the bracket S-N curves have to be selected. As stated in chapter 3.3 the choice of a S-N curve depends strongly on the type of stress used in the analysis. It has been decided to use the hot-spot stresses instead of the *nominal stresses*. This requires the definition of the stress recovery procedures especially for hot-spots at a location with a sudden change of geometry (singularity).

Figs. (3.5,3.6) show the chosen stress recovery procedures for the hot-spots in the cutout and the bracket, respectively. Three different procedures are used:

- **Stress interpolation**: For hot-spots at singularities (e.g. toe of bracket) where a large stress gradient can be expected the shown extrapolation method is used. The stresses perpendicular to the crack at the center of the last two elements are linearly extrapolated to the weld toe. Fig. (3.7) shows the procedure.

- **Stress in element next to hot-spot**: In cases where the geometry does not permit a clear development of a stress gradient can not be assumed, the stress in the element next to the hot-spot is used.

- **Stress in truss element**: At hot-spots that are not at a singularity (e.g. radius of cutout) the stress at the hot-spot can be used directly. It is obtained by using a truss element with zero stiffness that is located at the edge of the cutout.

Based on the defined stress recovery procedures S-N curves have been

37

defined for each hot-spot using the work on *Fatigue Classification of Ship Structural Details* that has been presented in [5] as a starting point.

In order to be compatible with this report and general industry practice the S-N curves recommended by the Department of Energy [3] will be used to describe the fatigue strength at the hot-spots of the CSD. Fig. (3.8) shows these S-N curves and Table (2.1) contains a summary of the curve parameters.

The curves are used without consideration of the change in slope for $N > 10^7$. This is a rather conservative assumption that makes the S-N curves compatible with the curves developed for *cracked* CSD.

The chosen S-N curves for the hot-spots in the cutout of the webframe and in the bracket are shown in Fig. (3.9). For some hot-spots at the connection of two components the chosen S-N curve depends on the type of connection, *lap weld* or *butt weld.* For hot-spots were both types of connections are possible, two curves are specified depending on the type of welded connection.

It has to be stated again that the further research is required to obtain S-N curves that are properly calibrated for the use with the hot-spot stresses obtained from finite element analyses.

3.5   S-N Curves for CSD with Initial Defects (Cracks)

It has been the objective of the SMP project to develop procedures that also allow it to estimate the residual fatigue life of Critical Structural Details with initial defects (cracks).

Using the approach outlined in chapter 2.7 it is possible to develop S-N curves for *cracked CSD* that depend on the initial and the final (critical) cracklength. These S-N curves can then easily be incorporated into the *Fatigue Life Evaluation Software.*

3.5.1   Approach

It has originally been anticipated to use the fracture mechanics program LIFE, which is described in detail in [7] to calculate the a-N relationship (a - Cracklength, N - Number of cycles). This program uses the *hybrid method* to determine the stress intensity factor, see chapter 2.4.3.

Although the use of the *hybrid method* will result in more accurate solution for the a-N relationship, it has not been used for the development of S-N curves for cracked CSD. This decision is based on the following reasons:

- The hybrid method requires knowledge of the stress distribution along the crack front, which has to be determined by using the finite element method. For each possible configuration of the CSD a finite element model has to be created and analysed.

38

- The program LIFE is proprietary and can not be distributed. The fracture mechanics calculations for each possible configuration have to be performed prior to the release of the program. This limits the usefullness of the program severely. It also requires that all finite element analyses have to be performed prior to the release of the program. This was not possible due to the lack of time and manpower.

For these reasons the current version of the *Fatigue Evaluation Software* uses a simplified closed form solution that does not require a finite element analysis. It requires only the knowledge of the initial and the final cracklength, an estimate of the stress intensity factor that is assumed to be independent of the cracklength and the fracture toughness parameter C.

The following closed form expression for the number of cycles can be derived, see [4]:

$$N = \frac{1}{C \Delta \sigma \pi^{m/2} F^m} \frac{a_f^{1-m/2} - a_i^{1-m/2}}{1 - m/2} \quad , \quad m \neq 2 \qquad (3.1)$$

where:

- a_i initial cracklength
- a_f final cracklength
- C crack growth parameter
- m crack growth parameter
- F influence function
- $\Delta \sigma$ stress range

Comparing this equation to the standard equation for the S-N curve

$$N = K(\Delta \sigma)^{-m} \qquad (3.2)$$

it can be seen that the S-N curve parameter K can be calculated using the above closed form fracture mechanics equation

$$K = \frac{1}{C \pi^{m/2} F^m} \frac{a_f^{1-m/2} - a_i^{1-m/2}}{1 - m/2} \quad , \quad m \neq 2 \qquad (3.3)$$

The crack growth parameter m is in general assumed to be ≈ 3.0. Based on crack propagation results an empirical relation has been established for the crack growth parameter C, see [9]:

$$C = \frac{1.3151 0^7}{28.31^m} \qquad \frac{da}{dN} \ (m/cycle) \quad \Delta K \ (MPa\sqrt{m}) \qquad (3.4)$$

It has to be mentioned that this approach does not take into account the complex stress distribution that is in general present in a CSD. It has however the advantage that no finite element analysis is necessary and the S-N curve for a given initial cracklength can be easily obtained. It is anticipated that the more complex approach using the hybrid method to determine the stress intensity factor will be implemented in a future effort and the results of the two approaches compared.

Overall Geometry
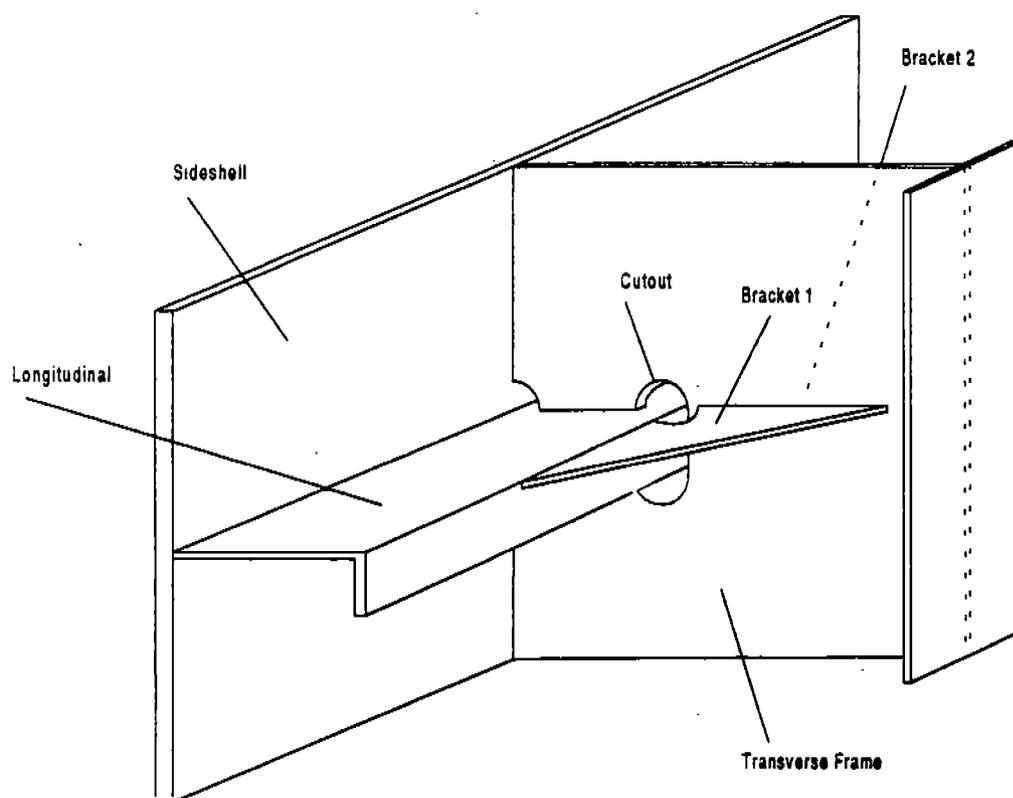
Figure 3.1: Critical Structural Detail for SMP Software

Definition of Codenames
for Hot-Spots
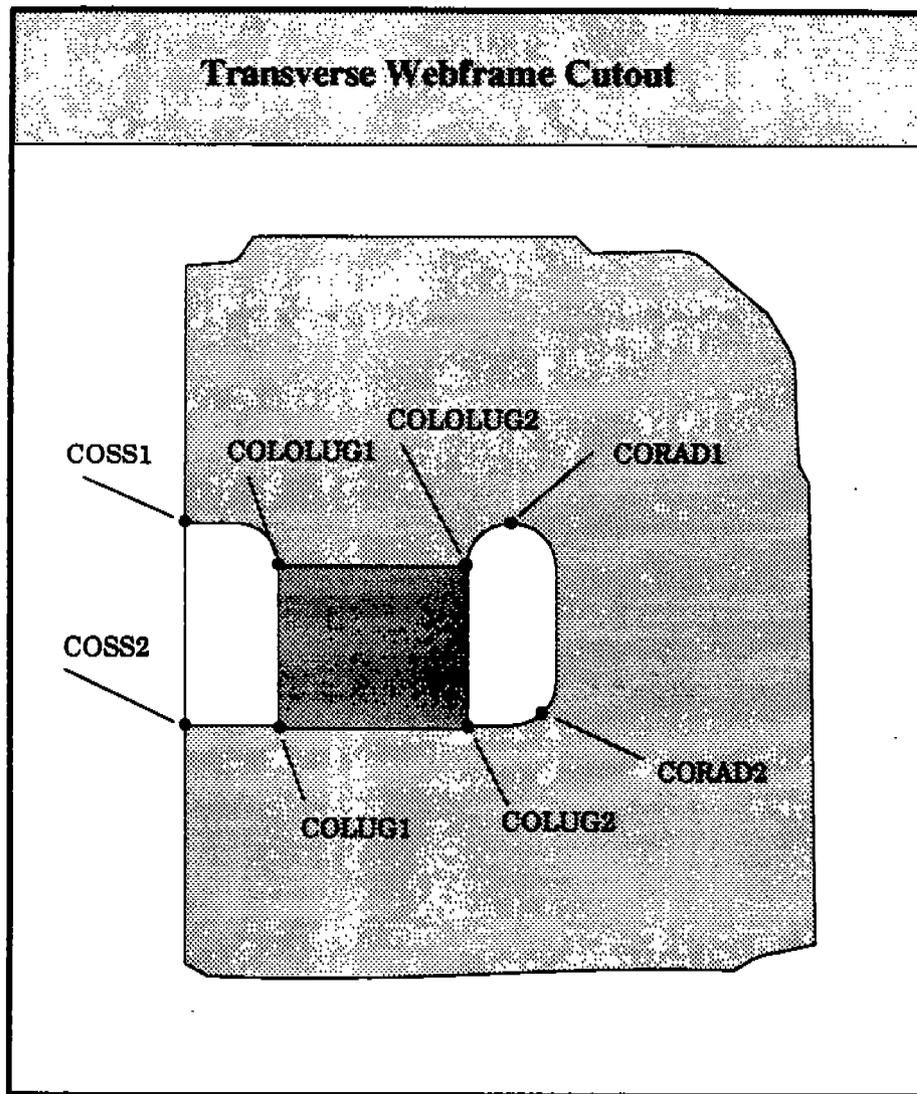
Figure 3.2: Hotspot Definition for Cutout

41

237 27

Definition of Codenames
for Hot-Spots
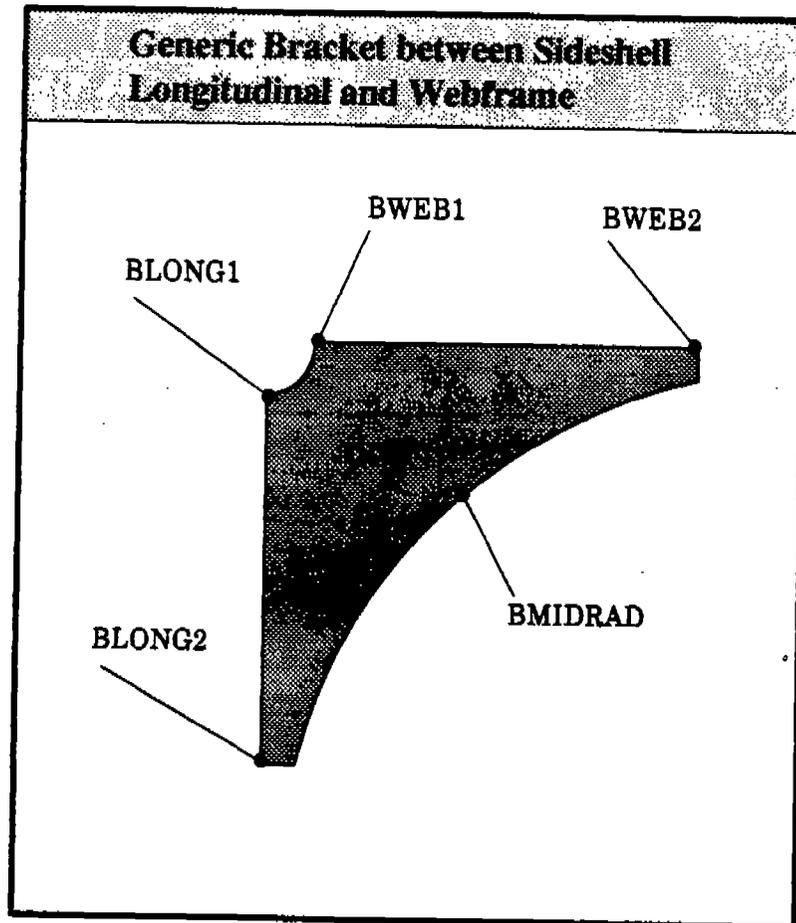
Figure 3.3: Hotspot Definition for Bracket

238

Crack Directions for specified Hot-Spots
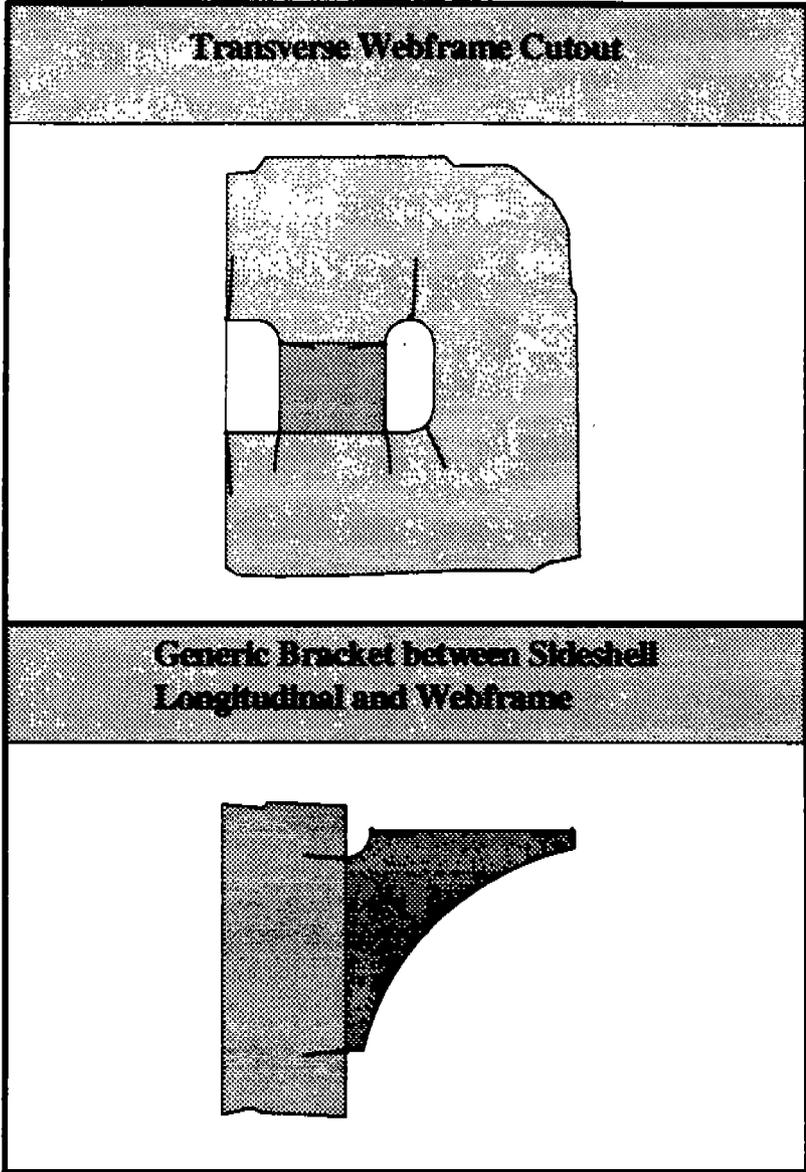
Figure 3.4: Crack Directions for Hotspots

239

Definition of Stress Recovery Locations and Procedures

	Linear Interpolation to Hot-Spot using the last two element stresses
	Stress in Element closest to the Hot-Spot
	Stress at Hot-Spot obtained from TRUSS Element
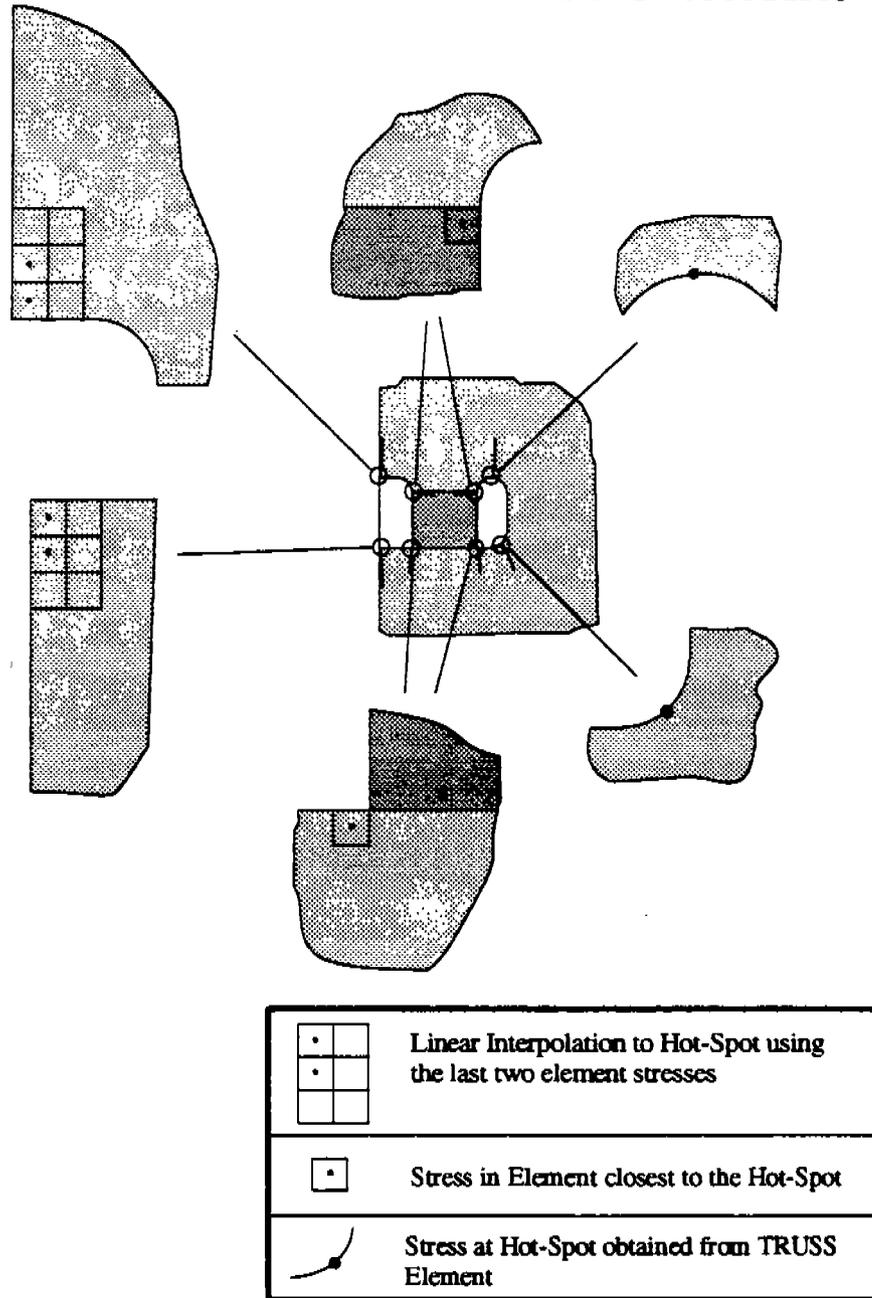
Figure 3.5: Hotspot Stress Recovery Procedures for Cutout

44

Definition of Stress Recovery Locations and Procedures

	Linear Interpolation to Hot-Spot using the last two element stresses
	Stress in Element closest to the Hot-Spot
	Stress at Hot-Spot obtained from TRUSS Element
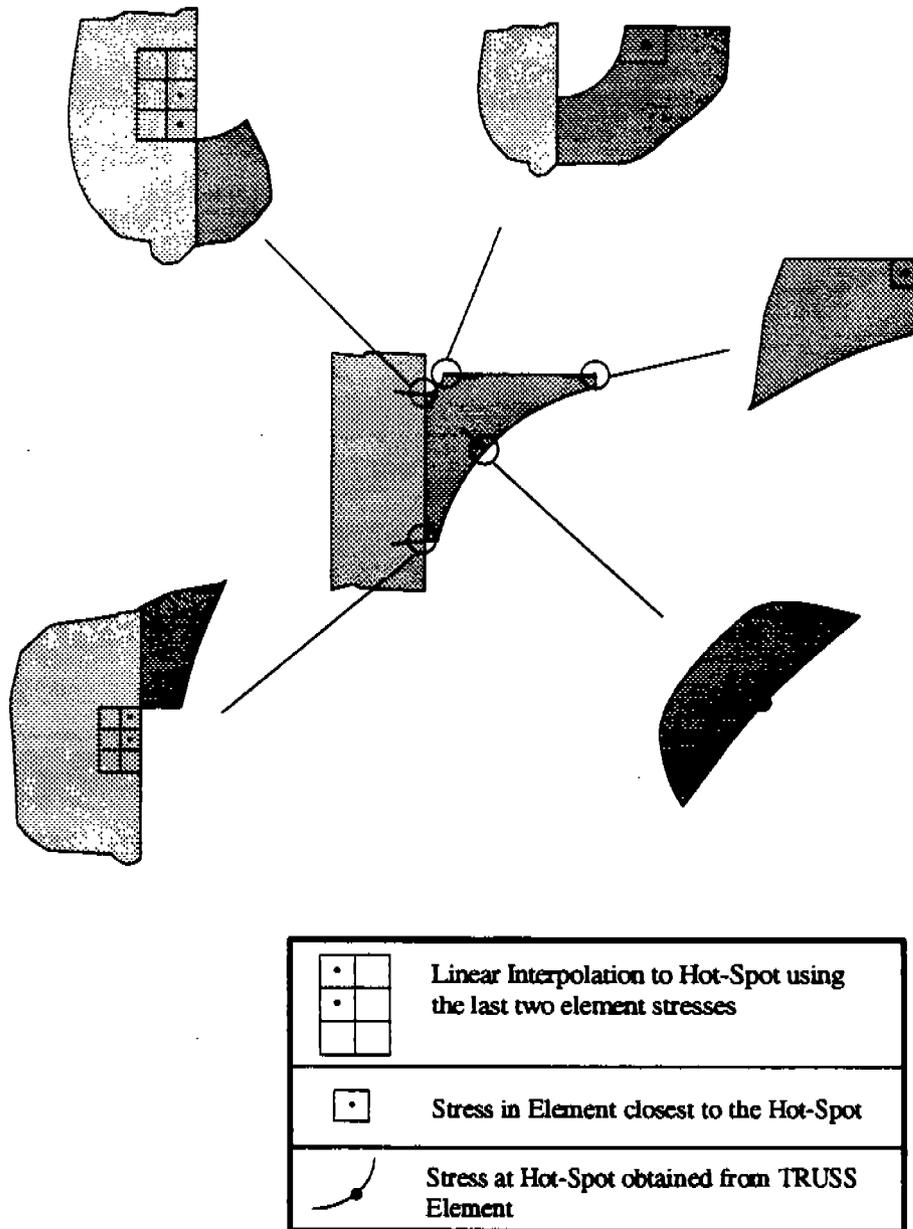
Figure 3.6: Hotspot Stress Recovery Procedures for Bracket

241

Definition of Stress
Interpolation Procedures

Linear Interpolation to Hot-Spot using
the last two element stresses

a - Element Height
   "   Width

approx. equal
to plate thickness

a

a

Hot-Spot

"True" Stress at Hot-Spot

Interpolated Stress
at Hot-Spot
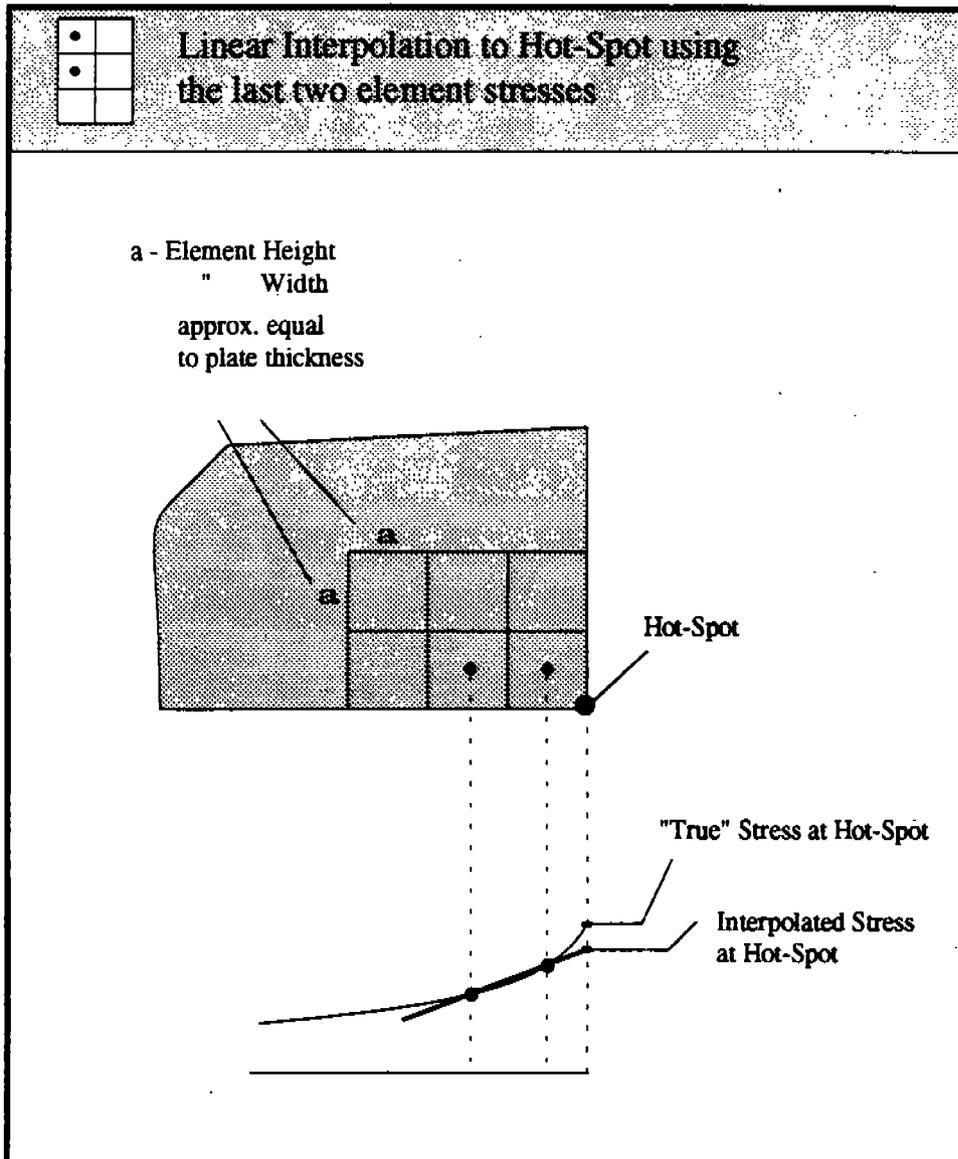
Figure 3.7: Stress Interpolation Procedure

46
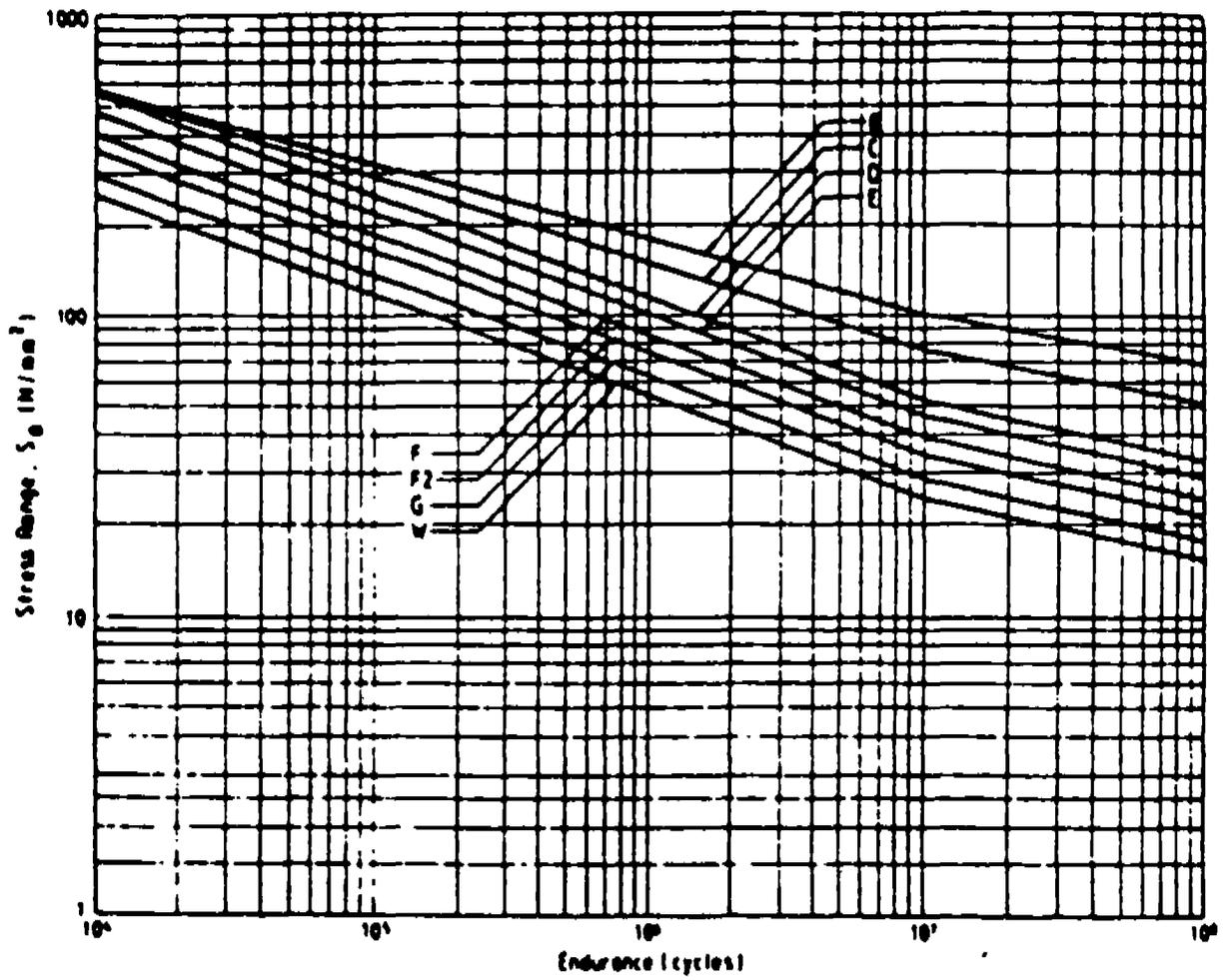
Figure 3.8: UKdeN S-N curves

47

243

Definition of S-N Curves for the defined Hot-Spots

Transverse Webframe Cutout

F

F

C

F
(F2 for Lap Joints)

Generic Bracket between Sideshell Longitudinal and Webframe

F

F
(F2 for
Lap Joints)

C
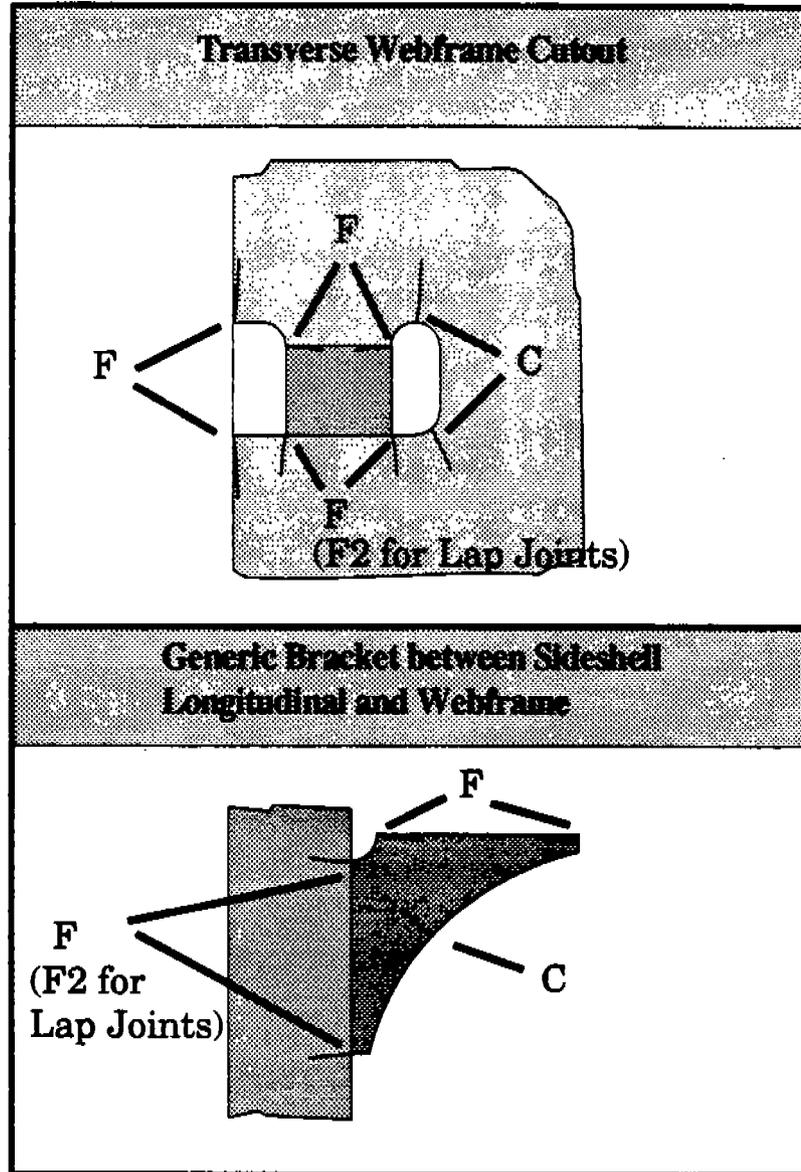
Figure 3.9: S-N Curve Definitions for Hotspots

48

Chapter 4

Loading

4.1 Introduction

The quantification of the response of tanker structures to wave action is crucial for fatigue design purposes. The alternating excitation induced in the marine structures by wave action produces different types of responses such as motions and stresses.

The sea surface of the earth is divided into squares, known as Marsden zones [10]. Each of these zones covers a geographic area over which the wave conditions are fairly uniform. The wave data for each Marsden zone is obtained through observations and measurements, under the assumption of ergodicity. From the worldwide mission profile experienced by the ship, the frequency of occurrence of different sea states over the life time is found, where each sea state is described through significant wave height H_s and zero crossing period T_z. Stationarity is assumed over a short period of time (1~3 hours). The sea elevation is then described as a stationary, relatively narrow-banded, Gaussian random process, where the distribution of wave energy over different frequencies is expressed by a wave spectrum.

Assuming that the ship response to wave excitation is linear, the total response in a seaway can be described by a super-position of the response to all regular wave components that constitute the irregular sea. Given the linearity, the ship response is a stationary, ergodic, but not necessarily a narrow-banded Gaussian process. From the estimated response spectrum, the peak distribution of the response in each stationary short term period is determined using the response spectral moments.

4.2 Environmental Modeling

4.2.1 Sea Condition

From a specified sailing route, the relative time period within each Marsden zone is estimated, and the frequency of occurrence of different sea condi-

49

tions is found as the weighted average of the available wave statistics in the different zones:

$$(H_s, T_z)_{lifetime} = \sum_{i=1}^{N} \mu_i (H_s, T_z)_i \tag{4.1}$$

where $(H_s, T_z)_i$ is the scatter diagram for the i'th Marsden zone, μ_i the fraction of the lifetime within which the ship is in Marsden zone i, and N the total number of zones passed by the ship over its lifetime. The joint distribution of the obtained global discrete scatter diagram is further described by a two dimensional analytical density distribution function, Cramer and Friis-Hansen [6].

4.2.2 Wave Spectrum

For a specified H_s and T_z combination, the wave spectrum describing the distribution of wave energy over different frequencies is estimated under the assumption of stationarity. In the present analysis, a one-sided Gamma wave spectrum is applied:

$$S_\eta(\omega \mid h_s, t_z) = A\omega^{-\xi} \exp(-B\omega^{-\zeta}), \quad \omega > 0 \tag{4.2}$$

The parameter ξ gives the power of the high frequency tail, and the parameter ζ describes the steepness of the low frequency part. A and B are uniquely related to H_s and T_z, leading to a simple description of the wave spectrum for different sea states,

$$A = \frac{1}{16} h_s^2 \zeta \left(\frac{2\pi}{t_z}\right)^{\xi-1} \frac{\Gamma\left(\frac{\xi-1}{\zeta}\right)^{\frac{\xi-3}{2}}}{\Gamma\left(\frac{\xi-3}{\zeta}\right)^{\frac{\xi-1}{2}}} \tag{4.3}$$

$$B = \left(\frac{2\pi}{t_z}\right)^{\zeta} \frac{\Gamma\left(\frac{\xi-1}{\zeta}\right)^{\frac{\zeta}{2}}}{\Gamma\left(\frac{\xi-3}{\zeta}\right)^{\frac{\zeta}{2}}} \tag{4.4}$$

For $\zeta = 4$ and $\xi = 5$, the Gamma spectrum is equivalent to the well known Pierson-Moskowitz spectrum.

4.2.3 Wave Energy Spreading Function

The wave energy spreading function is introduced to account for the energy spreading in different directions for short crested sea. Short crested sea waves are described by a two-dimensional directional spectrum, where the distribution of wave energy from the main wave direction is included in the wave spectrum description. The directional spectrum is, however, difficult

to obtain, and it is commonly assumed that the directional spectrum is approximated by two independent functions,

$$S_\eta(\omega, \overline{\theta}) = S_\eta(\omega) w(\overline{\theta}) \qquad (4.5)$$

where $w(\cdot)$ is the spreading function, and $\overline{\theta} = \theta - \theta_0$ the spreading angle from the main wave component direction. To account for the short-crestedness of the waves, the following spreading function is applied:

$$w(\overline{\theta}) = \begin{cases} k \cos^N(\overline{\theta}) & ; \quad |\overline{\theta}| \le \frac{\pi}{2} \\ 0 & ; \quad |\overline{\theta}| > \frac{\pi}{2} \end{cases} \quad ; \quad k = \frac{1}{\sqrt{\pi}} \frac{\Gamma\left(\frac{N}{2} + 1\right)}{\Gamma\left(\frac{N}{2} + \frac{1}{2}\right)} \qquad (4.6)$$

Here, N is the spreading parameter, typically increasing for higher sea states.

4.3 Wave Response

For the evaluation of the ship response, a linear model is assumed. The response is then described by a super-position of the response of all regular wave components that make up the irregular sea, leading to a frequency domain analysis. The linear model assumption is generally adequate for tanker structures, having high block coefficients.

4.3.1 Transfer Function

The transfer function $H_\sigma(\omega)$, modeling the response due to a sinusoidal wave with a unit amplitude for different frequencies, is usually obtained either from towing tank experiments or from calculations based on the theory of ship motions in potential flow with linearized free surface conditions. The estimated transfer function is, however, only valid for a specified ship velocity V, wave heading angle Θ and loading condition. The loading conditions are typically represented by two discrete cases, full load and ballast load, while a more continuous variation of the parameters V and Θ is to be expected.

4.3.2 Load Combination

In the evaluation of the load response, it is the combined stress response effect on the investigated detail that is sought. The local stress response is a combined effect of different load responses as horizontal and vertical bending moments, external water pressure, and internal cargo inertia forces.

Based on the linear model assumption, a combined local stress response transfer function for all the specified types of stress response can be obtained. This combined transfer function describes the combined directional stress response to a unit wave excitation. The derived combined transfer function

is unique for each investigated detail and for each selected crack growth direction for this detail.

This means that even a non-linear combination of the separate stress responses can be evaluated applying a linear frequency domain analysis by deriving the combined transfer function for the different responses directly.

4.3.3 Response Spectrum

The response spectrum of the ship based on the linear model is directly given by the wave spectrum,

$$S_\sigma(\omega_e \mid h_s, t_z, v, \theta, l) = \mid H_\sigma(\omega_e \mid v, \theta, l) \mid^2 S_\eta(\omega_e \mid h_s, t_z, v, \theta) \qquad (4.7)$$

where ω_e is the encountered wave frequency and $\mid H_\sigma(\omega_e) \mid$ is the modulus of the transfer function. The wave spectrum experienced by the ship, $S_\eta(\omega_e)$, is different from the wave spectrum estimated from the specified sea state, $S_\eta(\omega)$, since the latter wave spectrum is described with respect to a non-moving coordinate system.

The modification of the wave spectrum due to encounter frequency ω_e is based on frequency mapping. The relative velocity between the wave velocity and the ship velocity is given by

$$V_{rel} = V_{wave} - V_{ship} \cos \theta \qquad (4.8)$$

The encountered wave frequency is therefore

$$\omega_e = \mid V_{wave} - V_{ship} \cos \theta \mid k = \mid \omega - k V_{ship} \cos \theta \mid \qquad (4.9)$$

where the wave velocity is expressed as ω/k, $k = 2\pi/\lambda$ is the wave number equal and λ is the wave length.

4.4 Operational Philosophy

In severe sea states, it is a common practice to change the speed and course of the ship in order to reduce the wave induced responses such as slamming and large rolling motions. The long term response distribution is sensitive to the higher sea states, and the effect of maneuvering should therefore be included in the response analysis.

The combined effect of course change (relative to the main wave heading direction) and speed reduction as a function of the significant wave height is modeled as,

$$f_{V\Theta \mid H_s}(v, \theta_0 \mid l, h_s, t_z) = f_{V \mid \Theta H_s}(v \mid \theta_0, l, h_s, t_z) f_{\Theta \mid H_s}(\theta_0 \mid l, h_s, t_z) \qquad (4.10)$$

where $f_{\Theta \mid H_s}$ defines the density function for course selection as a function of significant wave height, and $f_{V \mid \Theta H_s}$ the conditional density of speed. In the following, the proposed procedure in Cramer and Friis-Hansen [6] is applied.

4.4.1 Heading Angle - $f_{\Theta|H_s}$

Under normal wave conditions the ship generally travels independently of the main wave heading angle θ_0. For larger wave heights the captain tries to reduce the wave induced response on the ship by changing the heading direction.

The distribution of ship heading angles relative to the main wave direction in different sea states is modeled as a directional distribution function within specified feasible domains of the heading angle. The feasible domains are given as a function of H_s, where the feasible domain for the ship heading angle is $[0, 2\pi]$ in lower sea states. For severe seas, the feasible interval is continuously decreased as a function of the significant wave height, in the sense that the possibility for beam waves is reduced. In extreme sea states, it is assumed that all the waves are encountered as head waves.

For a short crested sea, the waves are having a spread around the main wave direction given by

$$\theta = \theta_0 + \bar{\theta} \tag{4.11}$$

where the distribution function of the spreading $\bar{\theta}$ is as given in Eqn. 4.6.

4.4.2 Ship Speed - $f_{V|\Theta,H_s}$

The ship is assumed to travel at a specified cruising speed V_C under normal sea conditions. At a certain significant wave height H_1, depending on the wave heading angle, the captain decreases the speed (or changes the heading direction) in order to reduce the wave response. At another higher significant wave height H_2, it is assumed that the wave induced response is so drastic that the captain is forced to reduce the speed to steering speed V_S. In the intermediate phase between H_1 and H_2, a linear reduction of the ship speed with H_s is assumed. The significant wave heights H_1 and H_2 are functions of the main wave heading angle.

4.4.3 Loading Condition - f_L

The ship is assumed to operate solely under two different loading conditions, fully loaded condition and ballast condition. The fraction of the lifetime under full loading condition depends on the type of ship and the sailing route. The loading condition influences the operational philosophy, since the captain makes different decisions with respect to maneuvering, depending on the loading condition (reduction of the ship speed and change of heading angle as a function of the significant wave height).

4.5 Short Term Response Statistics

4.5.1 Peak Distribution

Under the assumption of a stationary, zero mean Gaussian wave elevation process within each short term period, the response process for the linear system is also a stationary zero mean Gaussian process. For a narrow banded response process, the peaks are Rayleigh distributed,

$$F_p(a) = 1 - \exp\left(-\frac{a^2}{2m_0}\right) \tag{4.12}$$

where m_0 is the spectral moment of order zero, equal to the mean square of the response process. The distribution is directly given as functions of the spectral moments of the response spectrum. It should be emphasized that the distribution is conditional on H_s, T_z, v, θ and L.

The number of peaks within each time period is estimated from the rate of peaks ν_p

$$\nu_p = \frac{1}{2\pi}\sqrt{\frac{m_4}{m_2}} \tag{4.13}$$

For a narrow banded process, the rate of peaks is approximated by the rate of zero crossings ν_0,

$$\nu_p \approx \nu_0 = \frac{1}{2\pi}\sqrt{\frac{m_2}{m_0}} \tag{4.14}$$

4.5.2 Stress Range Distribution for Fatigue Analysis

In fatigue analysis, the stress range distribution is of interest. For a zero mean narrow banded process, the stress range is twice the amplitude, leading to the following stress range distribution for a narrow banded process

$$F_{\Delta S}(s) = 1 - \exp\left(-\frac{s^2}{8m_0}\right) \tag{4.15}$$

For increasing bandwidth, the process starts to include both negative and positive maxima. A fatigue analysis based on the narrow-band model ignores the effect of increasing number of small amplitude, high frequency oscillations. In an average sense, this leads to actual smaller peak and stress range values than the narrow band model predicts, and consequently, the narrow-band assumption will generally lead to conservative results.

Wirsching and Light [29] obtained a wide-band correction factor for the narrow band number of peaks. Estimates of this factor were obtained by computing the fatigue damage from a rain-flow analysis by digital simulation. They produced the empirical formula

$$\dot{\nu}_p = \nu_0[a(m) + (1 - a(m))(1 - \epsilon)^{b(m)}] \tag{4.16}$$

where

$$a(m) = 0.926 - 0.033m \quad ; \quad b(m) = 1.587m - 2.323 \qquad (4.17)$$

and ϵ the spectral parameter.

4.6 Long Term Response Statistics

The long term peak distribution of the response effect over the lifetime is obtained by unconditioning the short term distribution,

$$F_p(a) = \int_{H_s} \int_{T_z} \int_L \int_\Theta \int_V \quad \overline{\nu}_{hs,tz,l,\theta,v} F_p(a \mid h_s, t_z, v, \theta, l) f_{V\Theta}(v, \theta \mid l, h_s, t_z) \times$$
$$f_{H_s T_z}(h_s, t_z) f_L(l) \; dv \; d\theta \; dl \; dt_z \; dh_s \qquad (4.18)$$

$\overline{\nu}_{Hs,Tz,v,\theta,L}$ is a weighting factor, which expresses the relative rate of response peaks within each sea state. $f_{V\Theta}(v, \theta \mid l, h_s, t_z)$ accounts for the effect of maneuvering in heavy weather with respect to sailing speed and relative heading angle, $f_L(l)$ is the discrete distribution of loading conditions and $f_{H_s T_z}$ is the two-dimensional description of the sea-state experienced by the ship over the lifetime.

It is not possible to obtain a closed form solution of Eqn. 4.18. Therefore the value of the integral is obtained by Monte Carlo simulation (MCs) as shown in Cramer and Friis-Hansen [6]. However, even with the use of MCs technique, the integral in Eqn. 4.18 is too complex to be applicable directly in a structural reliability analysis. Therefore, an equivalent long term Weibull distribution is calibrated to the simulated outcome of the MC simulation.

For the fatigue analysis, a Weibull distribution is fitted to the long term stress range distribution,

$$F_{Long \; \Delta S}(s) = 1 - \exp(-(s/A)^B) \qquad (4.19)$$

The fitting of the Weibull parameters are based on the 0.95 and 0.99 fractile values, which approximately divides the contribution to the fatigue damage ($E[s^m]$) into three areas of equal magnitude,

$$\ln A = \frac{k \ln a_{0.95} - \ln a_{0.99}}{k - 1} \quad ; \quad B = \frac{\ln(-\ln 0.99)}{\ln a_{0.95} - \ln A} \qquad (4.20)$$

where
$$k = \frac{\ln(-\ln 0.95)}{\ln(-\ln 0.99)}$$

The expression for the m'th moment of the stress range process modeling the fatigue damage is then further,

$$E[\sigma^m] = A^m \Gamma(1 + \frac{m}{B}) = \sigma_N^m (\ln N)^{-m/B} \Gamma(1 + \frac{m}{B}) \qquad (4.21)$$

The average rate of stress cycles over the lifetime is found in the simulation procedure for the evaluation of the long term response distribution

$$\nu_0 = \frac{1}{N} \sum_{i=1}^{N} \nu_{hs,tz,l,\theta,v,i} \qquad (4.22)$$

where $\nu_{hs,tz,l,\theta,v,i}$ is the rate of stress cycles for the specified short term condition i and N is the number of simulations used in evaluating the integral. The number of stress cycles the ship is exposed to in its lifetime T_L is then given by,

$$N_{peak} = \nu_0 r_L T_L \qquad (4.23)$$

where r_L models the fraction of the lifetime the ship is expected to be at sea.

4.7 Direct Load Response Modeling

The estimation of the long-term Weibull stress range distribution applying a long-term frequency domain analysis as described above, is a very computationally costly approach, requiring unconditioning with respect to sea state conditions, ship speeds, wave heading angle and loading condition. Another simplified approach commonly applied to evaluate the long-term stress range distribution is to compute the extreme stress response for a specified extreme environmental condition over a certain time period. The computed extreme stress response is then applied together with a chosen value for the shape parameter B to evaluate the long-term stress range response.

The shape parameter B depends on the type of tanker structure, the sailing route, the maneuvering philosophy, etc., and is difficult to estimate accurately. In general, however, this shape parameter is expected to be in the area of $B = 0.8 \sim 1.0$.

The American Bureau of Shipping has in the "Guide for Fatigue Assessment of Tankers" defined a simplified approach for estimating the B shape parameter, [1]. The shape parameter is here dependent on the ship length and on the type of structure that is of concern, e.g. deck structure, side shells etc..

$$
\begin{aligned}
B &= 1.40 - 0.036\alpha L^{1/2} & for\ 190 < L \leq 305m \qquad (4.24) \\
&= 1.54 - 0.044\alpha L^{1/2} & for\ L > 305m
\end{aligned}
$$

where:

α	$= 1.00$	for deck structures
α	$= 0.93$	for bottom structures
α	$= 0.86$	for side shell and longitudinal bulkhead structures

$$\alpha \quad = 0.80 \quad \text{for transverse bulkhead structures}$$
$$L \quad = \text{ship's length as defined in ABS Steel Vessel Rules}$$

Defining σ_N as the maximum wave induced stress response out of N wave cycles, the scale parameter A in the Weibull distribution is written as,

$$P(\sigma \le \sigma_N) = 1 - \exp(-(\sigma_N/A)^B) = 1 - 1/N \qquad (4.25)$$
$$\Rightarrow \quad A = \sigma_N(\ln N)^{-1/B} \qquad (4.26)$$

The maximum local stress response σ can be found directly from an extreme response analysis, having e.g. a 10^{-4} or 10^{-8} wave extreme condition.

4.8 Load Histograms

Another simplified approach to model the long-term stress range distribution is to describe the distribution of stress ranges directly applying histograms.

Applying histograms, the long-term stress range distribution is described in a discrete manner. The stress range distribution is divided into a discrete number of blocks, where each block is described with a specified stress range level and a relative number of stress cycles.

Further, as above, the total number of stress cycles the investigated detail is exposed, to is expressed as a function of the average number of cycles per time unit, say years, and the the length of the time period.

4.9 Corrosion

A corrosive environment might, in addition to influence the fatigue material parameters in the fatigue model, lead to a general increase in the stress level with time due to a reduction in the steel thickness.

In the fatigue program, the increase in the stress level is expressed as,

$$\bar{S}_{cor}(t) = \frac{z}{z - k_{cor}t} = \frac{z}{z - k_{cor}N_t/(r\nu_0)} \quad , \qquad t < z/k_{cor} \qquad (4.27)$$

where z is the steel thickness, k_{cor} is the corrosion rate and N_t is the number of load cycles at time t. The rate of corrosion will depend on the type of corrosive environment and on the use of cathodic protection in the area where the investigated detail is located. The influence of the thickness reduction on the long-term stress level is then,

$$\sum_{i=1}^{N_T} (\Delta\sigma_i \bar{S}_{cor}(t_i))^m = \sum_{i=1}^{N_T} \left(\Delta\sigma_i \frac{z}{z - k_{cor}(i-1)/(r\nu_0)} \right)^m \qquad (4.28)$$
$$\approx E[\Delta\sigma^m] \sum_{i=1}^{N_T} \left(\frac{z}{z - k_{cor}(i-1)/r\nu_0} \right)^m$$

$$\approx E[\Delta\sigma^m] \int_0^{rt\nu_0} \left(\frac{z}{z - k_{cor}x/(r\nu_0)} \right)^m dx$$

$$= E[\Delta\sigma^m] \frac{zr\nu_0}{k_{cor}(m-1)} \left(\left(\frac{z}{z - k_{cor}t} \right)^{m-1} - 1 \right)$$

The expression is rewritten as,

$$\sum_{i=1}^{N_T} \left(\Delta\sigma_i \hat{S}_{cor}(t) \right)^m = rt\nu_0 E[(\Delta\sigma)^m] \, B_{cor}(t) \qquad (4.29)$$

where,

$$B_{cor}(t) = \frac{z}{k_{cor}t(m-1)} \left(\left(\frac{z}{z - k_{cor}t} \right)^{m-1} - 1 \right) \qquad (4.30)$$

accounts for the effect of increased stress level over time due to corrosion. The derivation is based on the assumption of a stationary stress range process over the lifetime.

4.10 Bias Factors

Soares [26] has conducted an extensive study over the various bias terms effecting the transfer function calculation. Including the bias factors, the transfer function may be rewritten as

$$\hat{H}(\omega) = \psi_L \psi_{SH} H_L(\omega) \qquad (4.31)$$

where ψ_L is a bias factor representing the difference between experiments and the mathematically estimated transfer functions and ψ_{SH} is a non-linear bias factor. When the calculation of the transfer functions is based on the theory of Salvesen, Tuck and Faltinsen [23], the bias factor ψ_L is given as Ref. [26],

$$\psi_L = \begin{cases} -0.005\theta + 0.42F_n + 0.70C_B + 1.25 & ; \quad 90 < \theta \le 180 \\ 0.0063\theta + 1.22F_n + 0.66C_B + 0.06 & ; \quad 0 \le \theta < 90 \end{cases} \qquad (4.32)$$

where F_n is the Froude number and C_B is the block coefficient.

The non-linearity bias factor ψ_{SH} accounts for the difference in sagging and hogging moments, and it is dependent on the accuracy of the assumption of the ship sides being vertical,

$$\psi_S = 1.74 - 0.93C_B \qquad \text{(sagging)} \qquad (4.33)$$

$$\psi_H = 0.26 + 0.93C_B \qquad \text{(hogging)} \qquad (4.34)$$

Note that when applying these non-linearity factors for fatigue analysis, one should apply $(\psi_S + \psi_H)/2 = 1$, implying that the non-linear sagging/hogging effect on the estimated fatigue damage has no influence.

Chapter 5

Reliability Model for Fatigue Life Evaluation

5.1 Introduction

The calculation of the fatigue damage for a structural detail is based on several variables. Each of these variables is to some extent random. In order to account for this randomness implicit and explicit *factors of safety* are widely used. The safety factors are rather subjective measures that are calibrated based on past experience.

Information about the degree of uncertainty of different variables can not be used effectively.

Reliability theory offers a way to include uncertainty information in the fatigue damage calculation. It allows to calculate the *component reliability*, i.e. the probability that a detail has failed at the end of the specified life time.

Using *system reliability* it is possible to evaluate the reliability of a system of structural details.

This chapter documents the reliability model that is used in the *Fatigue Life Evaluation* software. The component reliability model applied is based on the procedures of Wirsching et. al. [28].

5.2 Component Reliability

In this study the S-N curve approach combined with the use of Miner's summation rule is used to calculate fatigue damage. Different methods to account for the randomness in loading are applied.

255

5.2.1 Fatigue Damage Assessment

It is assumed that the curve characterizing fatigue behavior under constant amplitude loading is of the form

$$NS^m = K \tag{5.1}$$

with
- N = Number of cycles to failure
- S = Stress range
- m = Empirical constant
- K = Empirical constant

A second basic assumption is that Miner's rule applies. Fatigue damage is then given by

$$D = \frac{N_T}{K}D(S^m) \tag{5.2}$$

- N_T = Total number of cycles in time T
- T = Time
- D = Damage
- $E(S^m)$ = Expected, mean, or average value of S^m
- S = Stress range (random variable)

To account for the uncertainties in the stress calculation the following relation between the actual stress range in the member, S_A, and the estimated stress range, S is introduced

$$S_a = BS \tag{5.3}$$

Here B is a random variable that quantifies the modeling error.
Defining the average frequency of the stress cycles as

$$f_0 = \frac{N_T}{T} \tag{5.4}$$

the expression for fatigue damage can be rewritten as

$$D = \frac{TB^m\Omega}{K} \tag{5.5}$$

with $\Omega = f_0 E(S^m)$ = Stress parameter

The following methods are currently used to calculate Ω and thus the fatigue damage:

- **The Deterministic Method** A long-term wave histogram is defined in which constant amplitude wave height is tabulated as a function of the number of cycles. A stress range histogram relating stress range to number of cycles can then be constructed for the dynamic response

60

of the structure. Damage for each constant stress blocks can then be calculated using the following formula

$$\Omega = f_0 \sum_i \zeta_i S_i^m \tag{5.6}$$

with f_0 = Average frequency of stresses
S_i = Stress range
ζ_i = Fraction of the total number of cycles S_i is acting

- **Spectral Approach** The long-term fatigue stress process, which is nonstationary, can be modeled by a sequence of several discrete and stationary sea-states with the significant wave height and dominant period is specified for each sea-state. The expected value for a stationary and narrow-banded process can be modified for a wide-band process using a rain-flow correction factor λ. The stress parameter Ω is calculated as follows

$$\Omega = \lambda(m)(2\sqrt{2}^m \Gamma\left(\frac{m}{2}+1\right) \sum_i \gamma_i f_i \sigma_i^m \tag{5.7}$$

with $\lambda(m)$ = Rain-flow correction
$\Gamma(.)$ = Gamma function
$\gamma(.)$ = Fraction of time in i-th sea-state
f_i = Frequency of wave loading in i-th sea-state
σ_i = RMS of stress process in i-th sea-state

- **Weibull Model** Here it is assumed that the long-term distribution of the stress range can be described by the Weibull distribution. The three important parameters in this distribution are S_m, ξ and N_T. The stress parameter can be calculated as follows

$$\Omega = \lambda(m) f_0 S_m^m [\ln N_T]^{-m/\xi} \Gamma\left(\frac{m}{\xi}+1\right) \tag{5.8}$$

with S_m = Largest stress range during the life time
ξ = Stress range parameter (Weibull shape parameter)
N_T = Total number of stress ranges in design life
λ = 1, unless Rayleigh assumption was made in analysis

A thorough description of procedures for derivation of the long-term Weibull stress range distribution is given in the previous Chapter 4.

- **Nolte-Hansford Model** This model is an extension of the Weibull model. It also assumes that the long-term stress distribution of wave

61

heights is the Weibull distribution. Additionally it is assumed that there is a one-to-one correspondence between wave height and stress range with the following relation

$$S = \psi H^\phi \tag{5.9}$$

with
$$H = \text{Wave height}$$
$$\psi = \text{Empirical constant}$$
$$\phi = \text{Empirical constant}$$

This leads to a closed form expression for the stress parameter

$$\Omega = \lambda(m) f_0 \delta^{m\phi} \psi^m \Gamma\left(\frac{m\phi}{\xi} + 1\right) \tag{5.10}$$

with
$$\delta = \text{Weibull scale parameter}$$

Reliability Analysis: Lognormal Format

Wirsching [28] suggests the lognormal format for the probability distributions of all factors of the fatigue damage expressions. This format has been demonstrated to be valid for the variables involved in the fatigue damage analysis, specifically for the variables Δ and K. Miner's rule, which states that failure occurs when the fatigue damage $D \geq 1$, is modified to

$$D \geq \Delta \tag{5.11}$$

where Δ is a random variable denoting damage at failure. This quantifies the modeling errors associated with Miner's rule.

To account for the uncertainties in fatigue strength, the S-N curve parameter K (see equation 5.1) is defined as a random variable.

The time to failure T is then given as

$$T = \frac{\Delta K}{B^m \Omega} \tag{5.12}$$

Since Δ, K, B are random variables, T is also a random variable. The probability of fatigue failure is defined as

$$p_f = P(T \leq T_s) \tag{5.13}$$

with
$$T_s = \text{service life of the structure.}$$

The use of the lognormal format has the advantage that a simple closed form expression for p_f can be found.

$$p_f = \Phi(-\beta) \tag{5.14}$$

62

with Φ = standard normal distribution function and β = safety index.

$$\beta = \frac{\ln(\frac{\tilde{T}}{T})}{\sigma_{\ln T}} \qquad (5.15)$$

$\tilde{T}$ is the median value of T and is equal to

$$\tilde{T} = \frac{\tilde{\Delta}\tilde{K}}{\tilde{B}^m\tilde{\Omega}} \qquad (5.16)$$

The standard deviation of $\ln T$ is given by

$$\sigma_{\ln T} = \sqrt{\ln(1 + C_\Delta^2)(1 + C_K^2)(1 + C_B^2)^{m^2}} \qquad (5.17)$$

The C's denote the coefficients of variation, COV , of each variable.

Statistics for Reliability Model

For a reliability analysis it is necessary to specify the median and the coefficient of variation of K, B and Δ, which are assumed to be lognormally distributed. The median value for K is obtained from least square analysis of the S-N data. The COV of K, C_K is obtained by approximating an equal probability curve with a straight line.

The variables B and Δ are used to quantify the modeling error associated with assumptions made in the stress analysis and the description of fatigue strength. Several sources can contribute to the bias B. Wirsching [28] uses the following 5 contributors

B_M = Fabrication and assembly operations
B_S = Sea state description
B_F = Wave load prediction
B_N = Nominal member loads
B_H = Estimation of hot spot stress concentration factors

In [28] frequently used values for the medians and COV's of the B.'s are listed. Table 5.1 summarizes these values.
Using these 5 bias factors the following representation of B is obtained

$$B = B_M B_S B_F B_N B_H \qquad (5.18)$$

Assuming that each random variable is lognormally distributed the median and the COV of B are, respectively

$$\tilde{B} = \prod_i \tilde{B}_i \qquad i = M, S, F, N, H \qquad (5.19)$$

$$C_B = \sqrt{\prod_i (1 + C_i^2) - 1} \qquad (5.20)$$

63

For the random variable Δ, describing the modeling error associated with Miner's rule, the following values for $\bar{\Delta}$ and C_Δ are widely used. $\bar{\Delta} = 1.0$ and $C_\Delta = 0.30$.

A thorough description of uncertainties involved in the stress analysis on ship structures is given in Nikolaidis and Kaplan [17].

5.3 System Reliability

It has long been recognized that the fatigue reliability of a single joint does not yield a quantitative measure of safety of the structure against fatigue failure. A tanker structure is defined through thousands of fatigue sensitive joints in which possible fatigue crack growth might originate. The fatigue failure probability of not only one single joint is therefore sought, but also the fatigue failure probability of a number of fatigue sensitive joints is of interest.

However, in the evaluation of the system reliability, the system of components to be evaluate in a probabilistic manner must be defined. The defined system must not be so complicated that the probabilistic calculations are getting to tedious. It is not manageable to address the fatigue reliability level of the whole ship in one probabilistic computation, but by considering only smaller sections of the ship, as e.g. a panel section, the effect of different design strategies can be judged.

For the tanker structure, a system is defined from a group of identical joints over the structure, or a section of the structure as e.g. the side shell or bottom panel. The system is modeled as a series system, and the fatigue failure probability of the system is defined as the probability of fatigue failure of one or more of the joints included in the system definition.

An adequate description of the uncertainties is crucial for a satisfactory estimate of the fatigue failure probability. The different sources of uncertainties affecting the fatigue damage model must therefore be identified, quantified, and accounted for in the reliability modeling.

5.3.1 Series System

To properly account for the presence of multiple joints in the evaluation of an acceptable design reliability level, an approach considering the series system effect is applied. This type of modeling is analog to a fail-fail modeling, or a first leakage approach. The fatigue failure probability of the system is then identical to the fatigue failure probability of the weakest of the joints in the system. The modeling of a system of fatigue sensitive joints as a series system gives a conservative estimate of the failure probability of the system.

The estimated fatigue failure of the different joints in the system is not independent due to common uncertainties in the modeling of the fatigue resistance of the different joints and the common stochastic load response

process the joints is exposed to. The correlation in the estimated fatigue failure probability of the different joints must be included in the evaluation of the fatigue failure probability of the system. However, a neglection of this correlation, $\rho = 0$, will lead to conservative results in the estimated system reliability.

The reliability level of the series system is based on the reliability level of the individual joints in the system, the correlation in the fatigue failure probabilities of the different joints and the number of joints in the system. The fatigue failure probability of the series system consisting of n joints is expressed as,

$$
\begin{aligned}
P_{F_s} &= 1 - \Phi_n(\bar{\beta} : \bar{\rho}) \\
&= 1 - \int_{\infty}^{\infty} \phi(t) \prod_{i=1}^{n} \left(\frac{\beta_i - \sqrt{\rho}t}{\sqrt{1-\rho}} \right) \, dt
\end{aligned} \tag{5.21}
$$

where β_i is the reliability index of the individual joints and ρ is the correlation coefficient between any pair of safety margins.

If the series system is defined from identical joints, the expression is simplified to,

$$
P_{F_s} = 1 - \int_{\infty}^{\infty} \phi(t) \left[\left(\frac{\beta_e - \sqrt{\rho}t}{\sqrt{1-\rho}} \right) \right]^n \, dt \tag{5.22}
$$

where β_e is the common reliability index for the identical joints in the series system.

The correlation in the failure probabilities for the different joints in the system can be derived from the reliability calculation of the individual joints, or be defined directly by the user. The correlation coefficient can theoretically have any value in the area of [-1,1]. However, only non-negative values of ρ are realistic. $\rho = 0$ implies independent failure probabilities of the different joints in the system while $\rho = 1$ implies a fully correlated system, where the fatigue failure probability of the system is identical to the fatigue failure probability of the individual joints.

The reliability index for the individual joints can be derived in number of different ways, where the Lognormal approach defined in the previous section is one of them. Another recommended approach, is to apply first order or second order full distribution reliability methods, FORM/SORM.

5.3.2 Target Reliability

The main purpose of applying a probabilistic series system analysis in the evaluation of the fatigue failure probability, is to recommend required reliability levels for the different fatigue sensitive joints over their lifetime. In order to do this, an acceptable target reliability level for the system considered has to be defined.

The value of this acceptable target reliability level depends on several factors, such as the consequence of fatigue failure (leakage, loss of serviceability,

etc.), the ship owners desire for a specified reliability level, or requirements from the classification societies.

To properly account for the effect of multiple fatigue failure locations in the evaluation of the required reliability level for the individual joints, the system effect must be considered. The accepted fatigue failure probability of the system defines then directly the minimum required reliability level for the joints.

Based on a specified minimum reliability level for the system over the lifetime, the minimum required reliability level for each of the joints in the system can be derived as a function of the number of joints in the system and the correlation between these joints.

Defining the largest acceptable fatigue failure probability of the system by, P_{F_a}, the required reliability index for the individual joints in the system, β_R is estimated from the equation,

$$P_{F_a} = 1 - \int_{\infty}^{\infty} \phi(t) \left[\left(\frac{\beta_R - \sqrt{\rho}t}{\sqrt{1-\rho}} \right) \right]^n \, dt \qquad (5.23)$$

where ρ again is the correlation in failure probabilities of the different joints. A neglection of the correlation leads to conservative estimated required fatigue reliability levels for the different joints.

Table 5.1: Summary of Bias and COV of Components of B

Random variables representing sources of uncertainty in fatigue stress estimates	Bias	COV
B_M	0.90 - 1.30	0.10 - 0.30
B_S	0.60 - 1.20	0.40 - 0.60
B_F	0.60 - 1.10	0.10 - 0.30
B_N	0.80 - 1.10	0.20 - 0.40
B_H	0.80 - 1.20	0.10 - 0.50

Bibliography

[1] *Guide for Fatigue Strength Assessment of Tankers.* American Bureau of Shipping (ABS), New York, June 1992.

[2] International Institute of Welding (IIW). *IIW Recommendation on the Application of an Engineering·Critical Assessment in Design, Fabrication and Inspection to Assess the Fitnesss for Purpose of Welded Products*, 1988.

[3] *Offshore Installations: Guidance on Design, Construction and Certification; Section 21:Steel.* U.K. Department of Energy, London, fourth edition edition, January 1990.

[4] A. Almar-Naess. *Fatigue Handbook.* Tapir, Trondheim, 1985.

[5] Yung-kuang Chen. *Fatigue Classification of Ship Structural Details.* Technical Report SMP 1-4, Structural Maintenance for New and Existing Ships, 1992.

[6] E.H. Cramer and P. Friis-Hansen. Stochastic modeling of the longterm wave induced response of ship structures. April 1992. Submitted to Marine Structures.

[7] K. Engesvik. *Life - A Computer Program for Fracture Mechanics Analysis of Crack Growth in Welded Structural Components.* Technical Report No. 5.8, SINTEF - Norwegian Institute of Technology, 1984.

[8] K.M. Engesvik. *Analysis of Uncertainties in the Fatigue Capacity of Welded Joints.* PhD thesis, Division of Marine Structures, The University of Trondheim, The Norwegian Institute of Technology, Trondheim, 1981.

[9] T.R. Gurney. *Fatigue of welded structures.* Cambridge University Press, Cambridge London New York Melbourne, 1979.

[10] N. Hogben. *Global Wave Statistics.* British Maritime Technology Ltd., Feltham, 1986.

264

[11] T.M. Hsu. A simplified method for calculating the remaining fatigue life of cracked structures. In *International Conference on Offshore Mechanics and Arctic Engineering (OMAE)*, Houston, Texas, 1988.

[12] C. Lindley, P.H. Bateson, S.E Webster, B. Lian, and F. Knight. Fatigue endurance under constant and variable amplitude loading of a welded quenched and tempered structural steel. In *Int. Conf. 'Welding -90'*, GKSS Research Center Geesthacht, Germany, 1990.

[13] S. Machida, H. Yajima, and M. Matoba. *On the Use of High Tensile Steels in Marine Structures*. Technical Report Draft, International Ship Ship Structures Comitee (ISSC), 1991.

[14] J.G. Merkle. *A Review of some of the Existing Stress-Intensity Solutions for Part-Through Surface Cracks*. Technical Report ORNL-TM-3983, U.S. Atomic Energy Commision, 1973.

[15] W.H. Munse. *Fatigue Characterization of Fabricated Ship Details*. Technical Report SSC-318, Ship Structure Commitee, 1983.

[16] J.C. Newman. *Predicting Failure of Specimens with either Surface Cracks of Corner Cracks at Holes*. Technical Report TN D-8244, NASA, 1976.

[17] E. Nikolaidis and P Kaplan. *Uncertainties in Stress Analyses on Marine Structures*. Technical Report SSC - 363, Ship Structure Committee, 1991.

[18] International Institue of Welding. Design recommendations for cyclic loaded steel structures. *Welding in the World*, Vol. 20(No. 718), 1982.

[19] P. Paris and F.Erdogan. A critical analysis of crack propagation laws. *Journ. Basic Engng*, 1963.

[20] I.S. Raju and J.C. Newman. An empirical stress intensity factor equation for the surface crack. *Engineering Fracture Mechanics*, Vol. 15, 1981.

[21] H.C. Rhee and M.M. Salama. *Applied Mechanics Review*, chapter Fracture mechanics in offshore industry. ASME, 1988.

[22] S.T. Rolfe and J.M. Barsom. *Fracture and Fatigue Control in Structures*. Prentice Hall, 1977.

[23] N. Salvesen, E.O. Tuck, and O. Faltinsen. Ship motions and sea loads. In *Vol. 78*, pages 250–287, SNAME Transactions, 1970.

$\partial\omega\mathcal{S}$

[24] R. Schulte-Strathaus and R. G. Bea. *Fatigue Database Development and Analysis.* Technical Report SMP 1-1, Structural Maintenance for New and Existing Ships, 1991.

[25] R. Schulte-Strathaus and R. G. Bea. *Verification Study for Tanker CSD Evaluation Software.* Technical Report SMP 1-8, Structural Maintenance for New and Existing Ships, 1992.

[26] C. Guedes Soares. *Probabilistic models for load effects in ship structures.* Technical Report, Marinteknisk Avdeling, Norges Tekniske Høgskole, 1984. Report no UR-84-38.

[27] H.-J. Wessel. *Fracture Mechanics Analysis of Crack Growth in Plate Girders.* PhD thesis, Department of Marine Technology, The University of Trondheim, The Norwegian Institute of Technology, Trondheim, 1986.

[28] P.H. Wirsching. Fatigue reliability for offshore structures. *Journal of Structural Engineering*, Vol. 110(No. 10), 1984.

[29] P.H. Wirsching and M.C. Light. Fatigue under wide band random stresses. *Journal of Structural Division, ASCE*, 106(ST7), July 1980.

STRUCTURAL MAINTENANCE
FOR
NEW AND EXISTING SHIPS

Study 1 - Fatigue Damage Evaluations
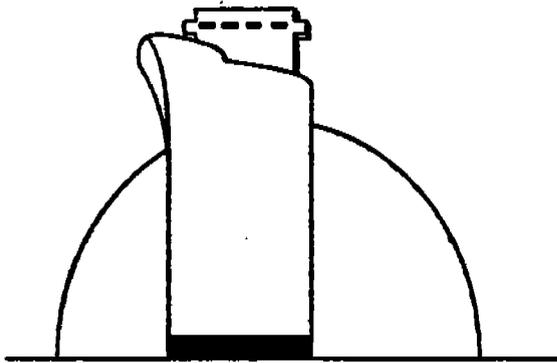
**Fatigue Damage
Evaluation Software:**
Verification Analysis

by
Rolf Schulte-Strathaus
and
Robert G. Bea

Report No. SMP-1-8
September 1992

PREFACE

The two year Joint Industry Research Project "Structural Maintenance for New and Existing Ships" was initiated in 1990 by the University of California at Berkeley Department of Naval Architecture and Offshore Engineering to both develop practical tools and procedures for the analysis of proposed ship structural repairs and to prepare guidelines for the cost-effective design and construction of lower-maintenance ship structures.

This project was made possible by the following sponsoring organizations:

- American Bureau of Shipping
- Amoco Transport Company
- BP Marine
- Bureau Veritas
- Chevron Shipping Company
- Daewoo Shipbuilding & Heavy Machinery Ltd.
- Exxon Company International
- Ishikawajima-Harima Heavy Industries Co. Ltd.

- Jurong Shipyard Ltd.
- Lisnave Estaleiros Navais de Lisboa,S.A.
- Military Sealift Command
- Mitsubishi Heavy Industries Inc.
- Mobil Ship and Transport Company
- National Defense Headquarters (Canada)
- Naval Sea Systems Command
- Newport News Shipbuilding & Dry Dock Co.
- United States Coast Guard

In addition, the following organizations contributed to the project as observers:

- *Germanischer Lloyd*
- *Lloyd's Register of Shipping*
- *West State Inc.*

This project was organized into six studies:

> Study 1 – Fatigue Damage Evaluations
> Study 2 – Corrosion Damage Evaluations
> Study 3 – Interaction of Details with Adjacent Structure
> Study 4 – Fatigue and Corrosion Repair Assessments
> Study 5 – Durability Considerations for New & Existing Ships
> Study 6 – Development of Software and Applications Examples

This report documents results from Study 1 – Fatigue Damage Evaluations whose objective is to develop and verify engineering guidelines for the evaluation of fatigue damage to critical structural components of existing ships.

In particular, the results of the verification analysis for the SMP project are documented in this report. For two classes of ships the integrated software package has been used to analyze the fatigue damage for selected details and to compare the results with statistical fatigue failure rates obtained from data analyses of actual failure data for the two classes of ships.

Contents

270

271

List of Tables

272

List of Figures

273

1 Procedure for Verification Analysis

1.1 Introduction

It is one of the main objectives of the SMP project to develop computer software that can be used as a tool to improve design and maintenance of oil tankers with special emphasis on tankers and Very Large Crude Carriers (VLCC). The main portion of the research effort has been directed to the problems related to internal Critical Structural Details (CSD) of these ships.

Based on the research conducted in the different parts of the SMP project, the following functionality will be provided by the software:

- **Global - Local Interactions:** For different configurations of CSD's finite element (FE) models can be created based on the dimensions of the specific CSD. The response of these models to external and internal loads on the ship hull can then be calculated.

- **Fatigue:** Based on the results of the finite element analyses the fatigue life of an uncracked or cracked CSD can be evaluated using both probabilistic and deterministic methods. It is possible to include safety factors and corrosion effects.

- **Corrosion:** For a given location in the ship the average corrosion rate can be determined based on the developed database of inspection results. Based on plate buckling as the failure criterion, the time until repair can be estimated.

- **Repairs:** A Repair Management System will provide guidance for the appropriate choice of a repair method.

The different software that has been developed to provide the above described functionality has to be thoroughly tested and verified. Since several computer programs have to be combined to produce the final software, it is especially important to test the links between the different programs. The choice of the verification cases is therefore governed by the requirement that all programs can use the same verification case.

Although a limited number of verification analyses could be performed during this project, it is expected that the results will provide useful information with regards to possible systematic bias and uncertainties present in the analysis procedure.

The documented verification cases will also serve as a tutorial for the developed software and will be used for the demonstration of the software.

The following steps have to be performed for each verification case:

- Definition of structural detail and crack location. This definition will be based on the availability of sufficient data in the database.

6

274

- Calculation of actual probability of failure based on the database analysis.

- Calculation of Transfer function for the ship. The transfer functions are calculated for the two load cases *Full Load* and *Ballast* and for several wave headings and ship speeds. The theory and the procedure is defined and documented in [1].

- Calculation of stress concentration factors at the hot-spots based on Unit-loads.

- Estimation of the long-term distribution of the stress range σ at a hot-spot. This estimation is based on a specified *travel route* through given Marsden zones and a specified *maneuvering philosophy*.

1.2 Choice of Verification Cases

Two different classes of VLCC's have been chosen as the two verification cases for the SMP project. Table (1) describes the two classes. The ship used for Verification Case I is a single hull ship with 165,000 DWT and the ship used for Verification Case II is a double bottom ship with 190,000 DWT.

The choice was governed by the availability of fatigue crack data. For these two classes, existing databases containing the complete cracking history for CSD's were available to the SMP project.

With this information it is possible to determine the probability of failure for a given CSD at a given location. This can then be used to verify and calibrate the *fatigue* software. The actual CSD and the location in the ship will be determined based on the availability of crack data.

1.3 Estimation of Probability of Failure from Crack Database

It is the intent of the database analysis to obtain an estimate of the probability of failure (P_f) for a given CSD. This P_f can then be compared with the P_f obtained as a result of the developed computer program.

The terms *Probability of Failure* and *Observation Period (T_0)* are defined as follows:

- **Probability of Failure:** Probability that a Crack has occurred in the Detail at the End of the Observation Period (T_0)

- **Observation Period (T_0 [years]):** Time between Date the Vessel was built and the Date of the last Survey included in the Database

The probability of failure for a detail is estimated based on the database as follows:

$$P_f = \frac{c}{N_0} \tag{1}$$

7

where

c = Number of crack occurrences

N_0 = Number of possible crack locations

The *Annual Probability of Failure* is defined as:

$$P_f(annual) = \frac{P_f}{T_0} \qquad (2)$$

In order to determine the number of possible crack locations it is assumed that there are two crack locations (port and starboard) for each longitudinal to webframe connection. These two locations are multiplied with the number of webframes in the tank and the number of vessels. This gives the number of crack locations for each longitudinal. This number is multiplied by the number of longitudinals that are combined. The *Number of possible crack locations* N_0 can therefore be expressed as:

$$N_0 = N_S \cdot N_W \cdot N_V \cdot N_L \qquad (3)$$

where

N_S = Number of sides (2)

N_W = Number of webframes in tank

N_V = Number of vessels

N_L = Number of longitudinals

It is realized that *all* cracks may not have been discovered during the inspections of these ships. Thus, the failure rates deduced on the basis of data could be interpreted as a lower bound estimate.

1.4 Definition of Travel Routes

The travel routes are defined by the time the vessel spends in the specified *Marsden zones* and the total harbour time. A description of the Marsden zones and a complete listing of the wave statistics for each zone can be found in [2].

The ships used for the verification cases operate almost exclusively on the TAPS trade route between California and Alaska. This route passes through the Marsden zones 6, 7, 13, 14, 22. Fig. (1) shows these Marsden zones and some common courses and destinations.

One Owner/Operator has provided a report summarizing the voyage profile for a particular vessel over 15 years, [3]. This report has been analyzed to obtain the percentage of time the vessel spend in each of the above Marsden zones. Table (2) shows the results of this analysis. The ship spend about 60% of the time at sea and 40% in port.

The calculation of the long-term distribution of the stress ranges is based on the time the ship spend in different Marsden zones and the total harbour time. Background on this procedure can be found in [4].

8

$\partial 7\varphi$

For each of the above Marsden zones the estimated percentage is multiplied by the service life of the ship used for the verification.

$$T_i = \lambda_i T_S \tag{4}$$

where

T_i = Time in Marsden zone i
λ_i = Relative Time in Marsden zone i [%]
T_S = Service life of vessel
i = {6, 7, 13, 14, 22}

The above method to determine the time in each Marsden zone based on the known voyage profile of a specific ship is in general not necessary since the owners/operators that use this program will be able to determine the exact voyage profile for a specific vessel.

1.5 Definition of Maneuvering Philosophy

Information about the ship speed *laden* and *under ballast* is needed to calculate the transfer functions for the ship using a ship motion program. Course changes and speed reductions due to bad weather will also strongly affect the long-term distribution of the ship responses. This information is therefore also required input for the estimation of the long-term distribution of the ship responses.

The following information is required, see also [5], the user manual for the program to determine the long-term distribution:

- Fraction of time in Load case 1

- Steering speed in Load case 1

- Cruising speed in Load case 1

- Fraction of time in Load case 2

- Steering speed in Load case 2

- Cruising speed in Load case 2

- Course change for H_S in head, beam and following sea

- Cruising speed change in head, beam and following sea

- Steering speed change in head, beam and following sea

2 Verification Case I

A VLCC with 165,000 DWT is used as verification Case I . Four ships of this class are included in a crack database released to the SMP study by the operator of the vessels. The overall dimensions are described in Table (1). The general arrangement is shown in Fig. (2). The midship section is shown in Fig. (3).

The ships of this class have experienced extensive cracking problems in the sideshell longitudinal to transverse webframe connections. These connections will therefore be used for the verification case.

2.1 Database Analysis

2.1.1 Distribution of Side Shell Cracks

The database for the 4 ships of verification Case I contains about 1800 records of cracks found during surveys of the vessels. This database, which has been provided to the SMP project by the operator of the vessels, has been included in the *SMP Crack Database*. It contains a total of 1988 records of cracks in the four ships.

For the verification case only cracks in the connection of sideshell longitudinals to transverse webframes are considered. Therefore a total of 557 cracks in sideshell longitudinals are selected for the database analysis.

Fig. (4) shows the distribution of these cracks over the shiplength, which is represented by the frame numbers. Most sideshell cracks are concentrated in two areas of the ship, *frames 29 - 35* and *frames 53 - 57*. These two areas correspond to *tank 1* and *tank 4* respectively.

For each tank the distribution of the sideshell longitudinal cracks over the ship height has been plotted. The ship height is represented by the longitudinal #. The midship section, Fig. (3), shows the location of the longitudinals.

Fig. (5) shows the crack distribution for tank 1. About 90% of a total of 226 cracks are found in *longitudinals 40 - 46*, which is just below the waterline.

Fig. (6) shows the crack distribution for *tank 2*. About 75% of a total of 54 cracks are found in *longitudinals 29 - 31*. These longitudinals are located above the turn of the bilge.

Fig. (7) shows the crack distribution for *tank 3*. About 73% of a total of 57 cracks are found in *longitudinals 29 - 31*. These longitudinals are located above the turn of the bilge.

Fig. (8) shows the crack distribution for tank 4. A total of 212 cracks were found in this tank. About 90% of these cracks occurred in *longitudinals 30 - 36*.

Fig. (9) shows the crack distribution for *tank 5*. Only 18 cracks were

278

found in this tank. Due to this small number no clear pattern can be distinguished from the crack distribution.

2.1.2 Choice of Tank

From the distribution of cracks over the shiplength, Fig. (4), it can be concluded that tank 1 and tank 4 have experienced the most severe cracking problems. For this reason one of these two tanks will be used for the verification case.

In tank 1 most cracks occurred in the 7 longitudinals just below the waterline. In tanks 2, 3, 4 the majority of the cracks occurred above the turn of the bilge. Especially in tank 4 the cracks are concentrated in the 7 longitudinals above the turn of the bilge. It is anticipated that the cracks near the waterline in tank 1 are partly caused by local phenomena such as slamming and wave breaking rather than by low-cycle fatigue loads.

From Fig. (2) it can be seen that tank 4 is located just aft of the mainframe. This reduces the influence of both the local forces near the bow and the stern of the ship. Vibrations caused by the engine and the propeller will also not contribute to the fatigue loads.

Tank 4 has been chosen as the location for the Verification Case I.

The reasons for this decision are summarized in the following:

- Tank 1 and tank 4 have each experience about 38% of the sideshell longitudinal cracks.

- The large number of cracks near the waterline in tank 1 indicates the strong influence of local forces.

- The cracks above the turn of the bilge well below the waterline reduces the influence of local, non-linear loads.

- Tank 4 is located in the middle portion of the ship. This will result in the most reliable estimate of the long-term fatigue loads.

2.1.3 Choice of Vertical Position

After the choice of tank 4 as the location for the verification case the vertical position had to be chosen. It can be seen from Fig. (3) that several different detail designs are used for the connection of side shell longitudinals to the webframe.

Based on the distribution of cracks over the height of the ship for tank 4, shown in Fig. (8), only the longitudinal 30 - 36 have experienced a sufficient number of cracks to be used for the verification.

The longitudinals 30 and 31 will also not be used for the verification since both are located in the double bottom, This violates the definition of

11

$\mathcal{D}79$

the CSD to be used for the verification (Side shell longitudinal connection to webframe).

Side shell longitudinals 32 - 36 have been chosen as the location for the Verification Case I.

2.1.4 Choice of Detail Type

For the 5 longitudinals chosen for the verification 2 different types of detail construction have been used. Fig. (3) shows these two types of detail construction. It can be seen that

- Longitudinals 32, 33, 35 are of the type *Detail 6*

- Longitudinals 34, 36 are of the type *Detail 4*

The construction drawing for *Detail 6* is shown in Fig. (10) and the construction drawing for *Detail 4* is shown in Fig. (11).

In the database that is used to define the verification case keywords are used to define different crack types. For side shell longitudinals 11 different keywords are used to categorize the cracks. Table (3) lists the number of cracks for each keyword and each longitudinal for tank 4. Multiple cracks at the same location and with the same keyword have been discarded since these cracks might represent cracks in repaired details.

Since the keywords are not sufficient to determine the exact location of a crack in a particular detail, the operator of the vessels has provided additional information that allowed it to link some of the keywords to specific crack locations in a side longitudinal to web frame connection.

Three different details have been chosen based on three different keywords. The three details (*Detail A*, *Detail B*, *Detail C*) are shown in Fig. (12). *Detail A* is used in longitudinals 34 and 36. The construction drawing is shown in Fig. (11). *Detail A* is used in longitudinals 32, 33, 35. The construction drawing is shown in Fig. (10). *Detail C*, a webframe cutout is used in longitudinals 32 - 36.

The following three keywords have been related to the three different details:

- **Detail A:** The keyword **L** is related to a crack in the side shell longitudinal at the toe of the bracket.

- **Detail B:** The keyword **LONG** is related to a crack in the side shell longitudinal at the toe of the flatbar. the verification

- **Detail C:** The keyword **WEB** is related to a crack in the cutout of the webframe at the connection with the side shell longitudinal.

With the help of these keywords it has been possible to define the exact crack location for three different details. It is therefore possible to obtain the number of cracks of each type that have been detected during the observation period.

2.1.5 Calculation of the Probability of Failure

Three different details located in tank 4 have been chosen for *Verification Case I.* Using the combination of the crack type keywords and the longitudinal #, it is possible to obtain the number of cracks for each detail from Table (3). The number of cracks for the different details is obtained as follows:

- **Detail A**: Sum of crack occurrences for keyword **L** for longitudinals 34, 36.

- **Detail B**: Sum of crack occurrences for keyword **LONG** for longitudinals 32, 33, 35.

- **Detail C**: Sum of crack occurrences for keyword **WEB** for longitudinals 32 - 36.

In section 1.3 the procedure to obtain the probability of failure for each detail is defined. For each detail the following information is needed to calculate the total probability of failure P_f and the annual probability of failure $P_f(annual)$:

- Number of webframes N_W

- Number of vessels N_V

- Number of longitudinals N_L

- Number of cracks c

P_f and $P_f(annual)$ are calculated using equs. 1, 2 respectively. Table (4) shows the input information and the calculated probabilities for all three verification details.

2.1.6 Summary

Using the crack database containing survey results of 4 vessels provided by the owner and operator three details have been defined that will be used as Verification Case I. For these details the probability of failure has been estimated. These probabilities will be used to verify and calibrate the results of the computer program developed by the *Fatigue Study* of the SMP project.

Fig. (13) shows a summary of **Detail A** including the location of the detail, the crack location and the estimated probability of failure.

13

$\partial \mathcal{S} /$

Fig. (14) shows a summary of **Detail B** including the location of the detail, the crack location and the estimated probability of failure.

Fig. (15) shows a summary of **Detail C** including the location of the detail, the crack location and the estimated probability of failure.

Based on the construction drawings Figs. (11, 10) finite element models will be created using the software developed by the *Global - Local Interactions* study.

2.2 Estimation of Long-term Loading for Case I

2.2.1 Voyage Profile for Service Life Case I

The ship used for Verification Case I travels almost exclusively on the TAPS trade route. Therefore the procedure outlined in (1.4) is used to estimate the time spent in each of the Marsden zones and the total harbour time.

Based on the database analysis failure probability has been estimated for a service life of **15 years**. Table (5) shows the calculated time for each Marsden zone.

2.2.2 Maneuvering Philosophy for Case I

The information about the maneuvering philosophy has been obtained from the operator of the vessel used for Verification Case I. In general, course changes due to bad weather are avoided. Speed reduction is used to prevent damage to the ship in bad weather.

Information about the maneuvering philosophy has been obtained from the operator of the vessel. For the given trade route from California to Valdez and back in general no course changes due to bad weather are made. Speed is reduced only for the worst sea conditions.

Table (6) contains a summary of the information that will be used to describe the maneuvering philosophy for Verification Case I.

2.2.3 Finite Element Analysis

Based on the detail geometry, shown in Figs. (11, 10), two finite element models have been produced using the software developed by the *Global-Local Interactions* study of the SMP project. The general procedure used to built these models is described in [6].

For the estimation of the long-term loading the stress concentration factors at the hot-spot have to be calculated for the following two loadcases:

- Unit axial force in the direction of the sideshell longitudinal

- Unit pressure acting normal to the sideshell

The necessary nodal loads for these two loadcases are automatically generated by the software developed by the *Global-Local Interactions* study of the SMP project. The calculated stress concentration factors for the three details are shown in Table (7). The theory and procedure for the generation of the unit loads are documented in [1].

The software for the estimation of the long-term loading, PROSHIP, uses the calculated stress concentration factors for one location in combination with the transfer functions to calculate the parameters of the Weibull distribution that represents the long-term loading for the specified location.

2.2.4 Results for Case I

Based on the stress concentration factors that have been calculated, the travel route and the maneuvering philosophy, the long-term distribution of the stress range has been calculated for the three details of Case I using the program PROSHIP.

The program calculates for one specified location the two parameters of the Weibull distribution and, in addition, the zero crossing rate (average frequency). These three values are written to a file that is used as an input file for the fatigue life evaluation.

For the three details that have been chosen for the Verification Case I the three calculated parameters are shown in Table 8.

2.3 Probability of Failure Calculation

2.3.1 Overview

For each of the three details that have been selected for Verification Case I, the probability of failure has been calculated using the *Fatigue Evaluation Software* . The program requires the choice of the specific location, the input of the long-term stress distribution and the input of the estimated uncertainties that are involved in the calculation of the long-term stress distribution.

For details about the calculation procedure, see the theory documentation [7]. For documentation of the program input, see the user manual, [8].

Since the uncertainties involved in the estimation of the long-term stress distribution are not known precisely, the calculations are performed for a range of values for both the *median bias* and the *coefficient of variation of the bias*. This allows it to see the influence of these parameters and to compare the results to the estimated *target* probability of failure that has been determined from the database analysis. In the following sections the results are documented for each detail of Verification Case I.

15

283

2.3.2 Description of Uncertainties

The *Fatigue Evaluation Software* requires the definition of the uncertainties involved in the estimation of the long-term stress distribution. These uncertainties account for the total modeling error involved in the calculation. Assuming the uncertainties to be log-normally distributed the uncertainty information can be represented through the two parameters *mean value* and *coefficient of variation.*

The approach used for the evaluation of fatigue damage allows it to specify the different contributors to the modeling error. A very good comprehensive summary of the uncertainties in cumulative fatigue damage is given in [9]. In the chapter on *Fatigue* the various uncertainties that influence fatigue life evaluations are analyzed. Based on available literature estimates for these uncertainties are given. The report suggests a value of 0.8 for the coefficient of variation of the bias.

The combination of the different contributing factors for the modeling error defines the total modeling error or bias. The total coefficient of variation of the modeling error or bias is obtained through a combination of the individual coefficients of variation.

For the evaluation of the fatigue damage for the verification cases only the total modeling error (bias) and its coefficient of variation are varied. These values essentially represent the systematic error and the confidence in the estimation of the long-term stress range distribution.

The verification analysis will calculate the probability of failure for each detail for a range of bias values. This allows a comparison with the *target* probability of failure that gives a good feel for the effects of the different bias values. Two graphs are produced for each detail in each verification case.

- **Graph 1:** The calculated probability of failure is plotted over a range of mean bias values. Four curves are shown for different values of the coefficient of variation of the bias. The *target* probability of failure is shown as a horizontal line.

- **Graph 2:** The calculated probability of failure is plotted over a range of the coefficient of variation. Four curves are shown for different values of the median bias. The *target* probability of failure is shown as a horizontal line.

It is important to determine the appropriate ranges for the median bias and the coefficient of variation of the bias since these ranges are shown in the two graphs and only a realistic choice of these ranges will allow a meaningful interpretation of the results.

The selection of bias values and the coefficients of variation for these values are discussed extensively in [9]. This report summarizes the results

of different studies with regard to the appropriate bias values. Based on this report the following ranges for the *bias* and the *coefficient of variation of the bias* have been selected.

Bias	Range
Median Value	0.5 – 2.0
Coefficient of Variation	0.0 – 1.0

A *median* bias of 1.0 means that the estimated stress range is equal to the true stress range. A value of 2.0 means that the true stress range is twice as large as the estimated value.

A *coefficient of variation* of 0.0 means that the bias value has been determined without any uncertainty. A value of 1.0 symbolizes a large uncertainty in the determination of the median bias and thus the estimated stress value. A value of 0.6 is not uncommon for the coefficient of variation of the bias.

Based on the uncertainty estimates given in [9] and on the method used for the estimation of the long-term loading, the following values for bias and coefficient of variation are assumed to be the most appropriate values:

Bias	Estimate
Median Value	1.2
Coefficient of Variation	0.8

2.3.3 Results: Detail A

The results of the verification analysis for **detail A** are shown in Fig. (16). The following long-term loading has been used for the analysis:

Detail	Parameter A	Parameter B	Zero Crossing Rate
	N/mm^2		$1/s$
Detail A	3.2969	0.7538	0.12041

The *Target Probability of Failure* for a service life of 15 years has been estimated as:

$$Pf_{Target} = 0.13333$$

This means that the probability that the detail has cracked at the end of 15 years is 0.1333 or 13.33 % .

From the first graph in Fig. (16) it can be seen that this target probability is calculated within the range of the median bias for all but the lowest (0.2) coefficient of variation. Similarly for the second graph in Fig. (16) for all but the smallest bias (0.5) the target probability is within the range of the coefficient of variation.

These results indicate that the estimated target probability of failure and the calculated probabilities based on the different combinations of bias

17

and coefficient of variation show good agreement.

2.3.4 Results: Detail B

Detail	Parameter A	Parameter B	Zero Crossing Rate
	N/mm^2		$1/s$
Detail B	3.5716	0.7538	0.12041

The *Target Probability of Failure* for a service life of 15 years has been estimated as:

$$Pf_{Target} = 0.1125$$

This means that the probability that the detail has cracked at the end of 15 years is 0.1125 or 11.25 % .

From the first graph in Fig. (17) it can be seen that this target probability is calculated within the range of the median bias for all but the lowest (0.2) coefficient of variation. Similarly for the second graph in Fig. (17) for all but the smallest bias (0.5) the target probability is within the range of the coefficient of variation.

These results indicate that the estimated target probability of failure and the calculated probabilities based on the different combinations of bias and coefficient of variation show good agreement.

The results for detail **A** and the results for detail **B** are almost identical. This can be expected since the S-N information for the two details is identical. The only difference is in the long-term loading. Here only the Weibull shape parameter is slightly different which does not have a great influence on the calculated probability of failure.

2.3.5 Results: Detail C

Detail	Parameter A	Parameter B	Zero Crossing Rate
	N/mm^2		$1/s$
Detail C	0.6896	0.7538	0.12038

The *Target Probability of Failure* for a service life of 15 years has been estimated as:

$$Pf_{Target} = 0.010$$

This means that the probability that the detail has cracked at the end of 15 years is 0.010 or 1.00 % .

Both graphs in Fig. (18) show that the estimated target probability of failure is much larger than the calculated probabilities. This holds for all combinations of the bias and the coefficient of variation. The reason for the low calculated probability of failure lies both in the selected S-N curve (C-curve for non-welded location) and in the estimated long-term loading.

The Weibull scale parameter is significantly lower than for the other two details, which strongly influences the resulting probability of failure.

Although the target probability of failure is underestimated, the results are acceptable in a qualitative sense. The crack data analysis predicted a low probability of failure and the software estimated a low probability of failure.

3 Verification Case II

A VLCC with 190,000 DWT will be used as verification Case II . Two ships of this class are included in a crack database released to the SMP study by the operator of the vessels. The overall dimensions are described in Table (1). The general arrangement is shown in Fig. (19). The midship section is shown in Fig. (20).

The ships of this class have also experienced extensive cracking problems in the sideshell longitudinal to transverse webframe connections. These connections will therefore be used for the verification case.

3.1 Database Analysis

3.1.1 Distribution of Side Shell Cracks

The database for the 2 ships of verification Case II contains all available records of cracks found during surveys of the vessels. This database, which has been provided to the SMP project by the operator of the vessels, has been included in the *SMP Crack Database*. It contains a total of 609 records of cracks for the two ships.

In this database the location of a crack is represented by its coordinates in a ship specific coordinate system. Only a very global categorization into different crack types is used. Therefore the database analysis has to rely on the crack coordinates to determine details for the verification case.

Since the depth of the webframes is known the cracks that occurred in the webframes and the side shell longitudinals can be determined. Fig. (21) shows the distribution of these cracks over the height and the length of the ship. The length is shown by the frame number and the location of the tanks. The height is given by the longitudinal number. From Fig. (20) it can be seen that longitudinal number *31* is located at the height of the double bottom. The side shell longitudinals have a uniform spacing of $3 ft$.

The majority of cracks is found in tank 2 and tank 5. Tanks 3 and 4 show a smaller number of cracks that are almost all located above the double bottom.

The distribution of sideshell and webframe cracks over the height and the width is shown in Fig. (22). The vertical position of all cracks in the two ships that are located within the depth of the webframe are shown. For reference purposes the positions of the flange of the webframe, the side shell and the extent of the side shell longitudinals are shown. Different longitudinal sizes are used over the height of the ship, which is reflected in the plot.

20

3.1.2 Choice of Tank

For the verification case only cracks in the direct vicinity of the side shell longitudinal to webframe connection are of interest. From Fig. (20) it can be seen that the deepest side shell longitudinals (32, 33, 34, 35) have a height of *21"* or *1.75 ft*. With a half breadth of *83 ft* these longitudinals therefore extent to a *width from centerline = 81.25 ft*.

In order to show only cracks in the side shell longitudinal to webframe connection it is sufficient to include only cracks with a width location > 81 ft. Fig. (23) shows the distribution of these cracks over the length and the height of the ship. This plot shows again that tanks 2 and 5 have experienced most cracks in this area. Only a small number of cracks are found in tanks 3 and 4.

Although it is desirable to have a large number of cracks as the basis for the probability of failure estimation it has been decided that tanks 2 and 5 cannot be used as locations for verification case.

This decision is based on the following considerations:

- From Fig. (19) it can be seen that tank 5 is the aft most tank. The fatigue load conditions for this tank are therefore strongly influenced by the *stern effects* and the vibrations induced by the propulsion system (engine, shaft, propeller).

- Tank 2 is close enough to the bow of the ship that the additional loads due to slamming and other *bow effects* will influence the load distribution in tank 2.

- The determination of the long-term fatigue loads is based on assumptions related to overall hull girder bending. These assumption are best satisfied near the midship section of the ship. Both tank 2 and tank 5 are too far from the midship section to produce reliable long-term load distributions.

Based on the above considerations only tanks 3 and/or 4 can be used for the verification case. Tank 3 has more cracks than tank 4. The use of only a single tank as the basis of the verification case would therefore result in significant differences in the estimated probability of failure. Since there is no logical explanation for such a difference, it has been decided to combine tanks 3 and 4 for the verification case.
Tanks 3 and 4 have been chosen as the location for the Verification Case II.

3.1.3 Choice of Vertical Position

After the choice of tanks 3 and 4 as the location for the verification case the vertical position had to be chosen. The distribution of cracks with *width* >

21

81 ft has been plotted for tanks 3 and 4 only, Fig. (24). This figure shows that only longitudinals 33 - 37 have experienced cracks near the flange of the longitudinal.

From the drawing of the midship section, Fig. (20) it can be seen that 3 different detail designs are used for these longitudinal connections. In addition, longitudinals 32 and 33 are influenced by the bracket connecting the webframe and the inner bottom. Longitudinals 36 and 37 are directly influenced by the horizontal tie connecting the webframe with the frame at the longitudinal bulkhead. Since these specific construction details cannot be accurately represented by the finite element models developed in the *Global - Local Interactions* study these longitudinals will not be used for the verification.

As a result of the above considerations only longitudinals 34 and 35 are available for the verification. Both longitudinals are of the same construction type, *Detail 11-C*. A detailed construction drawing of this type is shown in Fig. (25).

Side shell longitudinals 34 - 35 have been chosen as the location for the Verification Case II.

3.2 Choice of Detail Type

For the chosen location, longitudinals 34 and 35 in tanks 3 and 4, the cracks that occurred near the flange of the longitudinal have to be examined to determine the type of each crack. A total number of 3 cracks are considered to be close enough to the flange of the longitudinal to be used for verification purposes. Table (9) shows the height and width location of these cracks. This information is also shown in Fig. (26).

In order to determine the exact position of these reported cracks, copies of the survey results have been obtained from the owner / operator. Unfortunately, it was not possible to identify the exact crack location.

A relatively large uncertainty is therefore associated with the choice of this verification case. Based on the fact that only one crack incident was available in the middle portion of the vessel, this uncertainty is not critical.

It has been decided to use the crack, whose vertical position is closest to a longitudinal for the verification case. The chosen crack has the coordinates (310.6; 81.1; 24.2). From Fig. (26) it can be seen that this crack is inboard of the flange of the longitudinal. This crack is therefore considered to be a crack at the connection of the flatbar stiffener to the side shell longitudinal and is shown in Fig. (27).

3.2.1 Calculation of the Probability of Failure

One detail located in the middle portion of the tanker (tanks 3 and 4) has been chosen for *Verification Case II*. This choice has been made based on the location of the cracks. The detail has experienced 1 crack.

22

In section 1.3 the procedure to obtain the probability of failure for this detail is defined. The following information is needed to calculate the total probability of failure P_f and the annual probability of failure $P_f(annual)$:

- **Number of webframes** N_W

- **Number of vessels** N_V

- **Number of longitudinals** N_L

- **Number of cracks** c

P_f and $P_f(annual)$ are calculated using equ. 1 and equ. 2 respectively. Table (10) shows the input information and the calculated probabilities for the verification detail. It can be seen that the resulting probability of failure (.893 %) is very small. Considering the fact that this value has been estimated based on one crack occurrence for the location and the detail in question, the estimated probability does not have a high level of confidence.

3.2.2 Summary

Using the crack database containing survey results of 2 vessels provided by the owner and operator one detail has been defined that will be used as Verification Case II. For this detail the probability of failure has been estimated. This probability will be used to verify and calibrate the results of the computer program developed by the *Fatigue Study* of the SMP project.

The exact location of the crack in the detail could not be verified with the available information.

Fig. (28) shows a summary of the Detail including the location of the detail, the crack location and the estimated probability of failure.

3.3 Estimation of Long-term Loading for Case II

3.4 Voyage Profile for Service Life Case II

The ship used for Verification Case II travels almost exclusively on the TAPS trade route. Therefore the procedure outlined in (1.4) is used to estimate the time spent in each of the Marsden zones and the total harbour time.

Based on the database analysis failure probability has been estimated for a service life of **13 years**. Table (11) shows the calculated time for each Marsden zone.

3.5 Maneuvering Philosophy for Case II

The information about the maneuvering philosophy has been obtained from the operator of the vessel used for Verification Case II. In general course

23

changes due to bad weather are avoided. According to the owner/operator speed reduction to prevent damage to the ship in bad weather is only used in extreme conditions since the increased resistance caused by high sea states will automatically result in a reduced speed.

Table (12) contains a summary of the information that will be used to describe the maneuvering philosophy for Verification Case II.

3.5.1 Finite Element Analysis

Based on the detail geometry, shown in Fig. (25, a finite element model has been produced using the software developed by the *Global-Local Interactions* study of the SMP project. The general procedure used to built these models is described in [6].

For the estimation of the long-term loading the stress concentration factors at the hot-spot have to be calculated for the following two loadcases:

- Unit axial force in the direction of the sideshell longitudinal

- Unit pressure acting normal to the sideshell

The necessary nodal loads for these two loadcases are automatically generated by the software developed by the *Global-Local Interactions* study of the SMP project. The calculated stress concentration factors for the detail is shown in Table (13). The theory and procedure for the generation of the unit loads are documented in [1].

The software for the estimation of the long-term loading, PROSHIP, uses the calculated stress concentration factors for one location in combination with the transfer functions to calculate the parameters of the Weibull distribution that represents the long-term loading for the specified location.

3.5.2 Results for Case II

Based on the stress concentration factors that have been calculated, the travel route and the maneuvering philosophy, the long-term distribution of the stress range has been calculated for the detail of Case II using the program PROSHIP.

The program calculates for the specified location the two parameters of the Weibull distribution and, in addition, the zero crossing rate (average frequency). These three values are written to a file that is used as an input file for the fatigue life evaluation.

For the chosen detail for the Verification Case II the three calculated parameters are shown in Table 14. It has to be noted that the calculated zero crossing rate is substantially larger than the respective values for Case I. This value cannot be justified physically. The ships for the two verification cases are very similar in dimensions and the trade routes are identical.

24

Based on these considerations a value for the zero crossing period of about 0.12, is considered realistic. This value has been estimated for verification Case I. Due to time and man-power constraints it has not been possible to positively identify the reasons for the *wrong* value. It is judged that the estimated transfer functions are responsible for the estimation of this value.

In order to conduct the verification case with realistic values, a zero crossing rate of 0.12 has been used. Table 14 shows the original estimates for the long-term loading and the modified values that will be used for the calculation of the probability of failure.

3.6 Probability of Failure Calculation

3.6.1 Overview

For the detail that has been selected for Verification Case II, the probability of failure has been calculated using the *Fatigue Evaluation Software* . The program requires the choice of the specific location, the input of the long-term stress distribution and the input of the estimated uncertainties that are involved in the calculation of the long-term stress distribution.

For details about the calculation procedure, see the theory documentation [7]. For documentation of the program input, see the user manual, [8].

Since the uncertainties involved in the estimation of the long-term stress distribution are not known precisely, the calculations are performed for a range of values for both the *median bias* and the *coefficient of variation of the bias*. This allows it to see the influence of these parameters and to compare the results to the estimated *target* probability of failure that has been determined from the database analysis. In the following sections the results are documented for Verification Case II.

3.6.2 Description of Uncertainties

The *Fatigue Evaluation Software* requires the definition of the uncertainties involved in the estimation of the long-term stress distribution. These uncertainties account for the total modeling error involved in the calculation. Assuming the uncertainties to be log-normally distributed the uncertainty information can be represented through the two parameters *mean value* and *coefficient of variation.*

The approach used for the evaluation of fatigue damage allows it to specify the different contributors to the modeling error. A very good comprehensive summary of the uncertainties in cumulative fatigue damage is given in [9].

The combination of the different contributing factors for the modeling error defines the total modeling error or bias. The total coefficient of varia-

25

tion of the modeling error or bias is obtained through a combination of the individual coefficients of variation.

For the evaluation of the fatigue damage for the verification cases only the total modeling error (bias) and its coefficient of variation are varied. These values essentially represent the systematic error and the confidence in the estimation of the long-term stress range distribution.

The verification analysis will calculate the probability of failure for each detail for a range of bias values. This allows a comparison with the *target* probability of failure that gives a good feel for the effects of the different bias values. Two graphs are produced for each detail in each verification case.

- **Graph 1**: The calculated probability of failure is plotted over a range of mean bias values. Four curves are shown for different values of the coefficient of variation of the bias. The *target* probability of failure is shown as a horizontal line.

- **Graph 2**: The calculated probability of failure is plotted over a range of the coefficient of variation. Four curves are shown for different values of the median bias. The *target* probability of failure is shown as a horizontal line.

It is important to determine the appropriate ranges for the median bias and the coefficient of variation of the bias since these ranges are shown in the two graphs and only a realistic choice of these ranges will allow a meaningful interpretation of the results.

The selection of bias values and the coefficients of variation for these values are discussed extensively in [9]. This report summarizes the results of different studies with regard to the appropriate bias values. Based on this report the following ranges for the *bias* and the *coefficient of variation of the bias* have been selected.

Bias	Range
Median Value	$0.5 - 2.0$
Coefficient of Variation	$0.0 - 1.0$

A *median* bias of 1.0 means that the estimated stress range is equal to the true stress range. A value of 2.0 means that the true stress range is twice as large as the estimated value.

A *coefficient of variation* of 0.0 means that the bias value has been determined without any uncertainty. A value of 1.0 symbolizes a large uncertainty in the determination of the median bias and thus the estimated stress value. A value of 0.6 is not uncommon for the coefficient of variation of the bias.

Based on the uncertainty estimates given in [9] and on the method used for the estimation of the long-term loading, the following values for bias and coefficient of variation are assumed to be the most appropriate values:

26

Bias	Estimate
Median Value	1.2
Coefficient of Variation	0.8

3.6.3 Results: Detail A

The results of the verification analysis for **detail A** are shown in Fig. (29). The following long-term loading has been used for the analysis:

Detail	Parameter A	Parameter B	Zero Crossing Rate
	N/mm^2		$1/s$
Detail A	3.0316	0.67555	0.12

As stated in section 3.5.2, the zero crossing period has been modified to a more plausible value of $0.12[1/s]$. This value is identical to the value used for Verification Case I.

The *Target Probability of Failure* for a service life of 13 years has been estimated as:

$$Pf_{Target} = 0.00893$$

This means that the probability that the detail has cracked at the end of 15 years is 0.00893 or .893 % . From the discussion in section 3.2.2 it is clear that this value is not very precise. It is based on only one crack occurrence in the selected detail and location in 13 years. The level of confidence in this value is therefore very low.

From the first graph in Fig. (29) it can be seen that the probability of failure is over-estimated for most combinations of the bias value and the coefficient of variation. Only for coefficients of variation as small as 0.4 and bias values less than 1.0 the probability of failure is estimated in the range of the *target* probability of failure.

The second graph in Fig. (29) shows the probability of failure over a range of coefficients of variation. Four curves, each for a different median bias value, are shown. Again, the probability of failure is over-estimated for most combinations of median bias and coefficient of variation.

For a median bias of 1.0 and a coefficient of variation of 0.4 the estimated *target* probability and the calculated probability coincide. This coefficient of variation is too small for the given application. Too many uncertainties are involved in the estimation of the long-term loading for this coefficient of variation to be realistic.

Nevertheless, the agreement for this combination of values shows that the calculation procedure is capable of producing results that are in the range of the actual obtained *target* probability. In addition it has to be mentioned that the *target* probability is not accurate enough to be the basis of a qualified judgment of the analysis results.

295

4 Conclusion

Within the Structural Maintenance Project for New and Existing Ships two verification cases have been analyzed with the main purpose of verifying and testing the developed software.

These verification cases are based on an analysis of crack data that is included in the developed database. The details used in the analysis are obtained from owners/operators of the vessels. The long-term loading has been estimated based on the travel routes and maneuvering philosophy. The evaluation of the fatigue life and the probability of failure for a given detail have been performed using the developed *Fatigue Evaluation Software* .

For the first verification case three different detail locations have been analyzed. The results have been compared to the estimated *target* probabilities obtained from the database analysis. For two of the three details the results show very good agreement with the *target* values.

For the third detail the probability of failure is substantially under-estimated. The *target* probability of failure for this detail was estimated to be very low. This places the calculation in the tail end of the probability distributions. Here the influence of parameter approximations and even the chosen calculation model are very strong and differences in the numerical values have to be expected. Nevertheless the calculated results indicate a very low probability of failure, which is in accordance with the estimated *target* value.

Only one detail has been selected for the second verification case due to lack of failure data. Even for the selected detail the available information was not sufficient to obtain a realistic *target* probability of failure. The results over-estimate the probability of failure for most combinations of bias and coefficient of variation. Given the fact that the *target* value is very low and also based on insufficient information, the results of the calculation can be considered to be in reasonable agreement with the estimated *target* values.

In general, the verification analysis has been essential to adjust and calibrate the different components of the developed software. This includes the mesh generation, the development of the FE loads, the estimation of the long-term loading and the calculation of the fatigue life and probability of failure.

The successful completion of the verification cases has shown that the approach of developing an integrated software package for the evaluation of Critical Structural Details (CSD) is very beneficial and will be of great influence for the many design, inspection and maintenance operations.

296

References

[1] Jim Stear. *Structural Analysis and Loadings.* Technical Report SMP 3-1, Structural Maintenance for New and Existing Ships, 1992.

[2] N. Hogben. *Global Wave Statistics.* British Maritime Technology Ltd., Feltham, 1986.

[3] ARCO Marine Inc. Voyage profile of arco 120,000 lt deadweight tankers. In *Structural Fatigue Damae Assessment of ARCO 120,000 deadweight Tankers,* Long Beach, CA, Dezember, 1991.

[4] E.H. Cramer and P. Friis-Hansen. Stochastic modeling of the longterm wave induced response of ship structures. April 1992. Submitted to Marine Structures.

[5] E.H. Cramer, P. Friis-Hansen, and R. Schulte-Strathaus. *PROSHIP: User Manual.* Technical Report SMP 1-10, Structural Maintenance for New and Existing Ships, 1992.

[6] Tao Xu. *Study of Critical Structural Details.* Technical Report SMP 3-2, Structural Maintenance for New and Existing Ships, 1992.

[7] Espen H. Cramer, R. Schulte-Strathaus, and R. G. Bea. *Fatigue Life Evaluation Software: Theory Documentation.* Technical Report SMP 1-5, Structural Maintenance for New and Existing Ships, 1992.

[8] R. Schulte-Strathaus and R. G. Bea. *Fatigue Life Evaluation Software: User Manual.* Technical Report SMP 1-6, Structural Maintenance for New and Existing Ships, 1992.

[9] E. Nikolaidis and P Kaplan. *Uncertainties in Stress Analyses on Marine Structures.* Technical Report SSC - 363, Ship Structure Committee, 1991.

297

	Case I	Case II
Number of Ships	4	2
DWT	165,000	190,000
LOA	274.2 m	290.4 m
LBP	262.1 m	279.5 m
Breadth Molded	52.7 m	50.6 m
Depth Molded	22.9 m	23.8 m
Draft	17.4 m	18.1 m
Construction	Single Hull	Double Bottom

Table 1: Overall Dimensions for both Verification Cases

	% Time
Harbour Time	41.7
Marsden Zone	
6	16.42
7	11.72
13	11.98
14	9.84
22	8.34

Table 2: Voyage Profile for TAPS Trade

30

| Crack Type per Longitudinal | | | | | | | | | | | | |
| Tank 4 only (double entries discarded) | | | | | | | | | | | | |
Crack Type	29	30	31	32	33	34	35	36	37	38	43	48
B	1					1						
BKT												
C												
FP AND WEB		4	1	1	.	1	3	1	1	1		
L		14	13	1	2	3	1	6		4		1
LG		4	3	2	1	1	1	2		1		
LONG	1	4	1	7	5	3	4		1		2	
S		2	1	1	3	1						
S/L	2	7	5	3	5	2	1					
S/L WEB			2	2	2							
WEB	1	6	2	1	1							

Table 3: Crack Type per Longitudinal

Calculation of Probability of Failure			
Number of Webframes			5
Number of Vessels			4
Port and Starboard			2
Number of Crack Locations per Longitudinal			40
Observation Period			15 Years
	Detail A	Detail B	Detail C
Cracktype	LONG	L	WEB
Longitudinal	32,33, 35	34, 36	32 - 36
Number of Longitudinals	3	2	5
Number of Cracks	16	9	2
Number of Crack Locations	120	80	200
P_f	0.13333	0.11250	0.010
$P_f(annual)$	0.00889	0.00750	0.00067

Table 4: Case I: Calculation of Probability of Failure

299

	Time [Years]
Harbour Time	6.255
Marsden Zone	
6	2.463
7	1.758
13	1.797
14	1.476
22	1.251
Service Life	**15**

Table 5: Case I: Voyage Profile for Service Life of 15 years

Information	Input Data
Fraction of time *ballast*	45
Steering speed *ballast*	2.06 m/s
Cruising speed *ballast*	8.23 m/s
Fraction of time *laden*	55
Steering speed *laden*	2.06 m/s
Cruising speed *laden*	7.9 m/s
Course change for H_S in head, beam and following sea	12, 12, 12
Cruising speed change for H_S in head, beam and following sea	9, 8, 9
Steering speed change for H_S in head, beam and following sea	10, 9, 10

Table 6: Case I: Maneuvering Philosophy and Speed Characteristics

Detail	Stress Concentration Factor	
	Axial	Pressure
Detail A	1.2	-2500
Detail B	1.2	-280
Detail C	.25	1030

Table 7: Case I: Stress Concentration Factors

300

Detail	Parameter A	Parameter B	Zero Crossing Rate
	N/mm^2		$1/s$
Detail A	3.2969	0.7538	0.12041
Detail B	3.5716	0.7538	0.12041
Detail C	0.6896	0.7538	0.12038

Table 8: Case I: Long-term Stress Distributions

Crack	Width Loc [ft]	Height Loc [ft]Case II
1	81.1	24.2
2	81.3	25.4
3	81.4	22.2

Table 9: Case II: Coordinates of Cracks considered for Verification

Calculation of Probability of Failure	
Number of Webframes	7
Number of Vessels	2
Tanks 3 & 4	2
Port and Starboard	2
Number of Crack Locations per Longitudinal	**56**
Observation Period	13 Years
	Detail A
Width Location	81.1 ft
Longitudinal	34 - 35
Number of Longitudinals	2
Number of Cracks	1
Number of Crack Locations	112
P_f	**0.00893**
$P_f(annual)$	6.9×10^{-4}

Table 10: Case II: Calculation of Probability of Failure

34

302

	Time [Years]
Harbour Time	5.421
Marsden Zone	
6	2.135
7	1.524
13	1.557
14	1.279
22	1.084
Service Life	13

Table 11: Case II: Voyage Profile for Service Life of 13 years

Information	Input Data
Fraction of time *ballast*	45
Steering speed *ballast*	2.3 m/s
Cruising speed *ballast*	7.9 m/s
Fraction of time *laden*	55
Steering speed *laden*	2.05 m/s
Cruising speed *laden*	7.46 m/s
Course change for H_S in head, beam and following sea	12, 12, 12
Cruising speed change for H_S in head, beam and following sea	10, 9, 10
Steering speed change for H_S in head, beam and following sea	11, 10, 11

Table 12: Case II: Maneuvering Philosophy and Speed Characteristics

Detail	Stress Concentration Factor	
	Axial	Pressure
Detail A	1.2	-2500

Table 13: Case II: Stress Concentration Factors

303

Detail	Parameter A	Parameter B	Zero Crossing Rate
	N/mm^2		$1/s$
Detail **A**	3.0316	0.67555	0.36606

Table 14: Case II: Long-term Stress Distributions

304
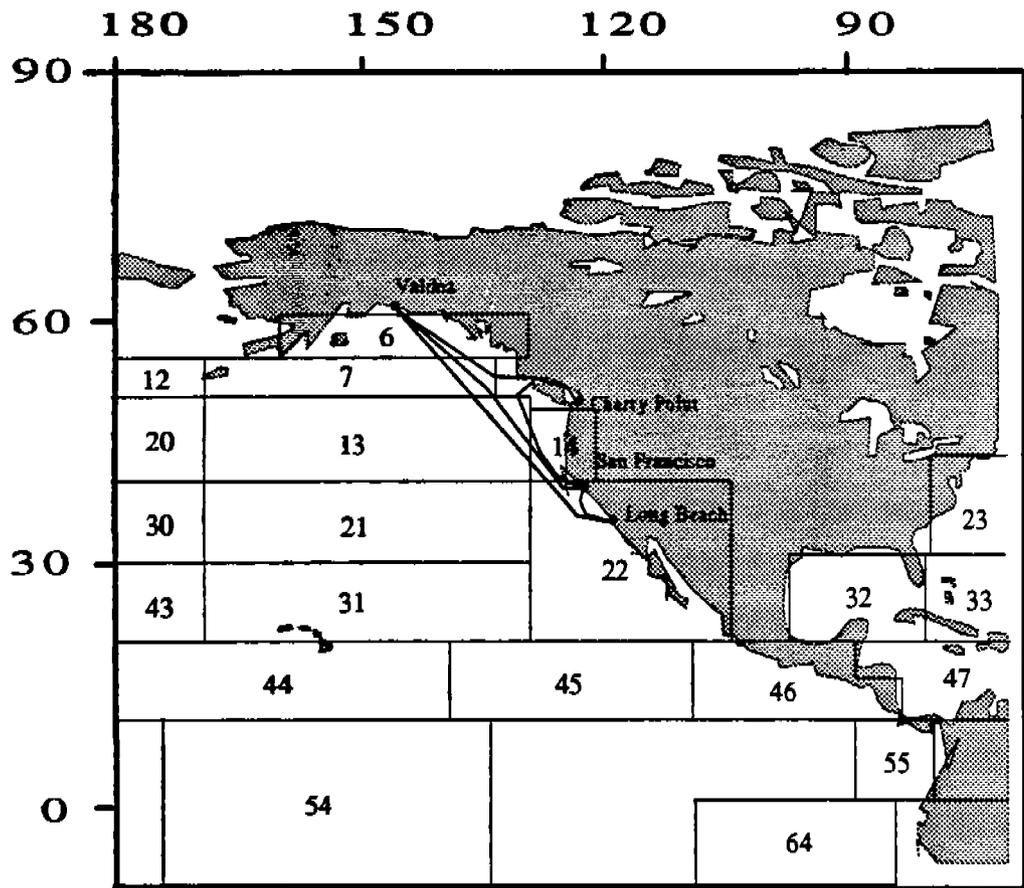
Figure 1: Marsden Zones for North Pacific

37

305

General Arrangement
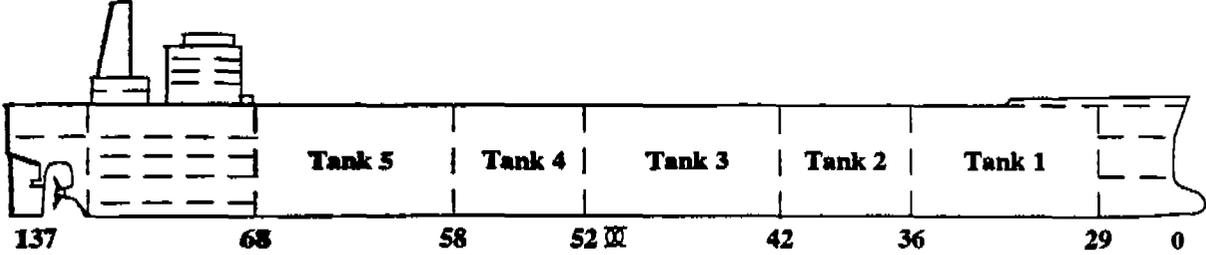
Profile
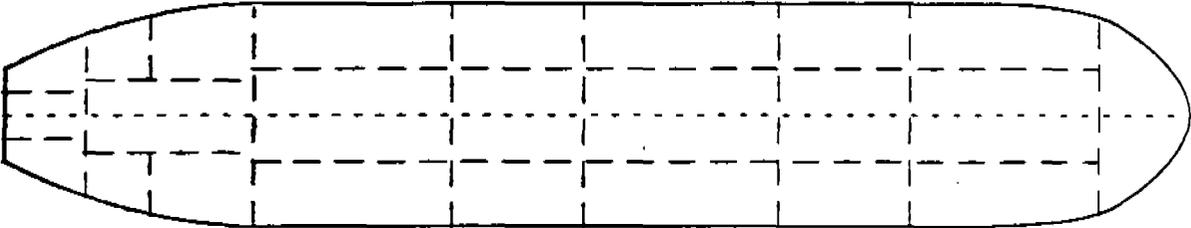
Upper Deck

Figure 2: Case I: General Arrangement

38

306

Midship Section
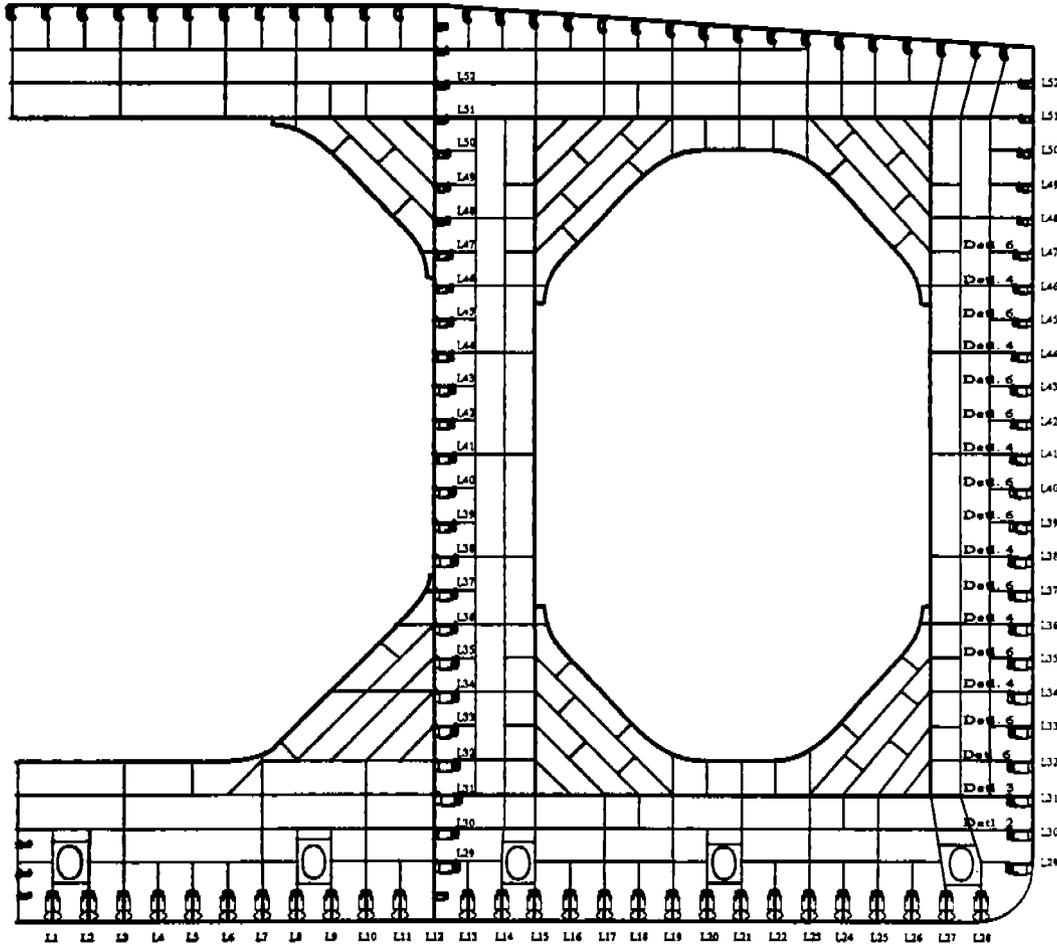
Shell and Longl. Bhd Longitudinals

Shell Longls	Bhd. Longls	Size	Spacing 35"
51, 52	51, 52	10" x .30"/ 2" x .50"	
48, 49, 50	48, 49, 50	12" x .46"/ 4" x .75"	
45, 46, 47	45, 46, 47	15" x .46"/ 4" x .75"	
42, 43, 44	42, 43, 44	17" x .46"/ 4.5" x .75"	
39, 40, 41	39, 40, 41	18" x .46"/ 5.5" x .75"	
36, 37, 38	36, 37, 38	20" x .46"/ 6" x .75"	
33, 34, 35	33, 34, 35	22" x .46"/ 6.5" x .75"	
30, 31, 32	30, 31, 32	23" x .46"/ 6.5" x .75"	
29	29	23" x .46"/ 7" x .75"	

Figure 35 Case I: Midship Section

307

of Cracks over Shiplength

(Side Shell Cracks only)
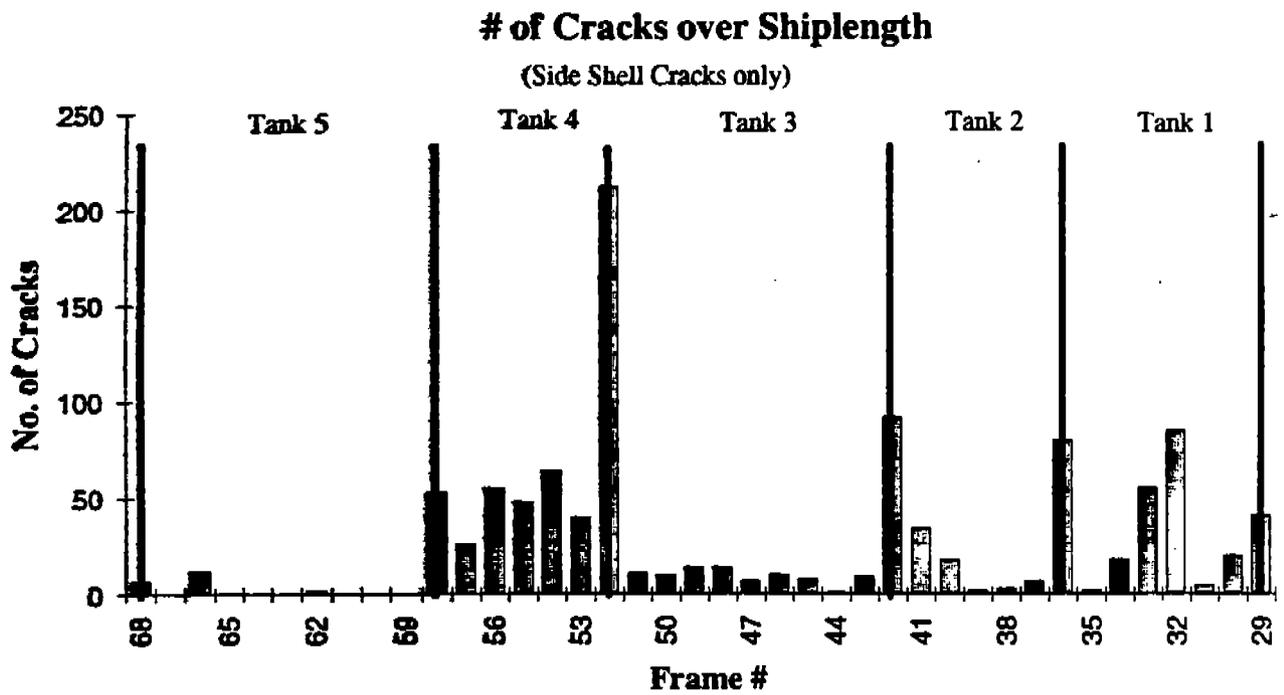
Figure 4: Case I: Number of Sideshell Cracks over Shiplength

40

308

Side-Shell Longitudinal Cracks in Tank1

Total Number of Cracks in Tank 1: 184
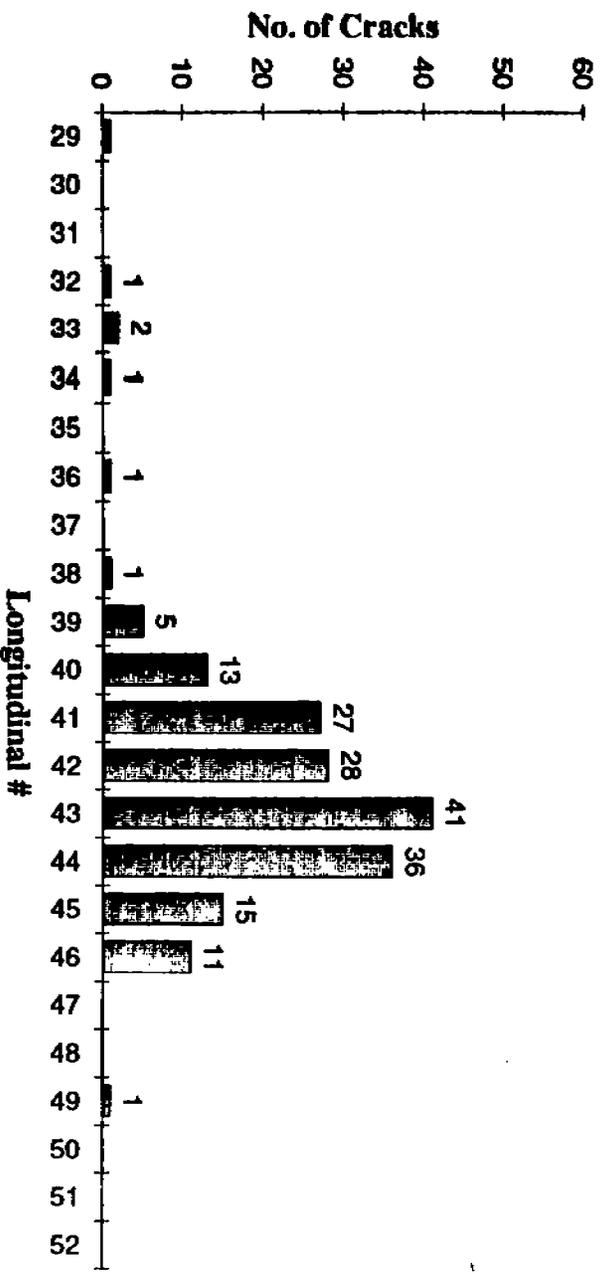
Figure 5: Case I: Side Shell Longitudinal Cracks in Tank 1

41

Side-Shell Longitudinal Cracks in Tank2

Total Number of Cracks in Tank 2: 65
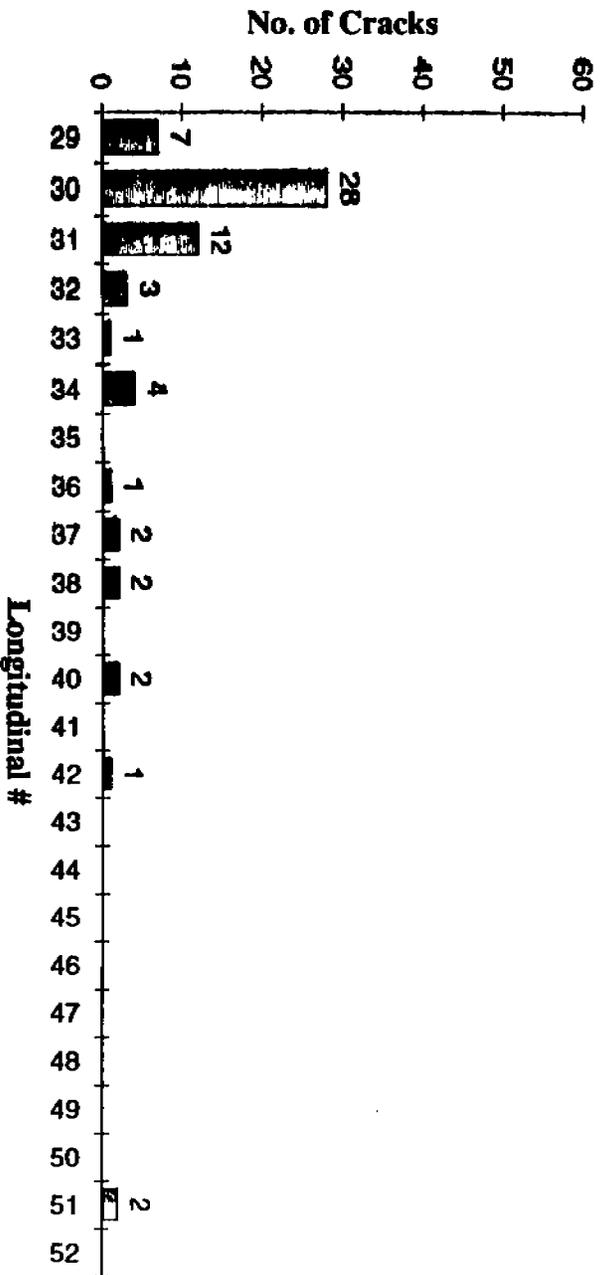
Figure 6: Case I: Side Shell Longitudinal Cracks in Tank 2

310

Side-Shell Longitudinal Cracks in Tank3

Total Number of Cracks in Tank 3: 83
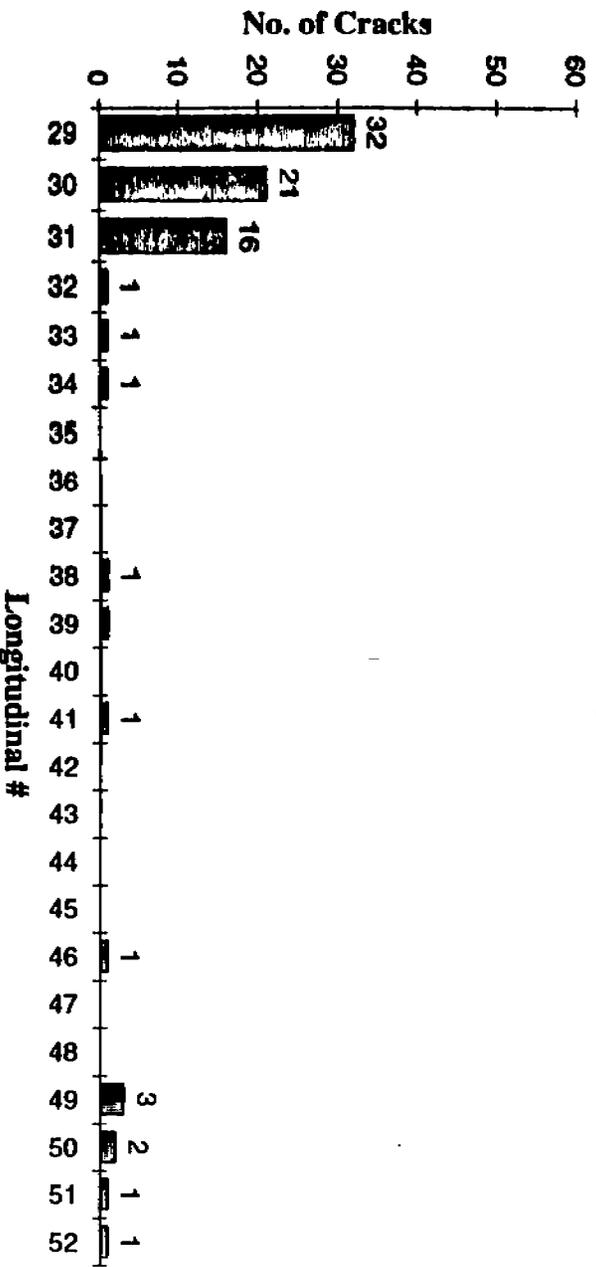
Figure 7: Case I: Side Shell Longitudinal Cracks in Tank 3

Side-Shell Longitudinal Cracks in Tank 4

Total Number of Cracks in Tank 4: 234
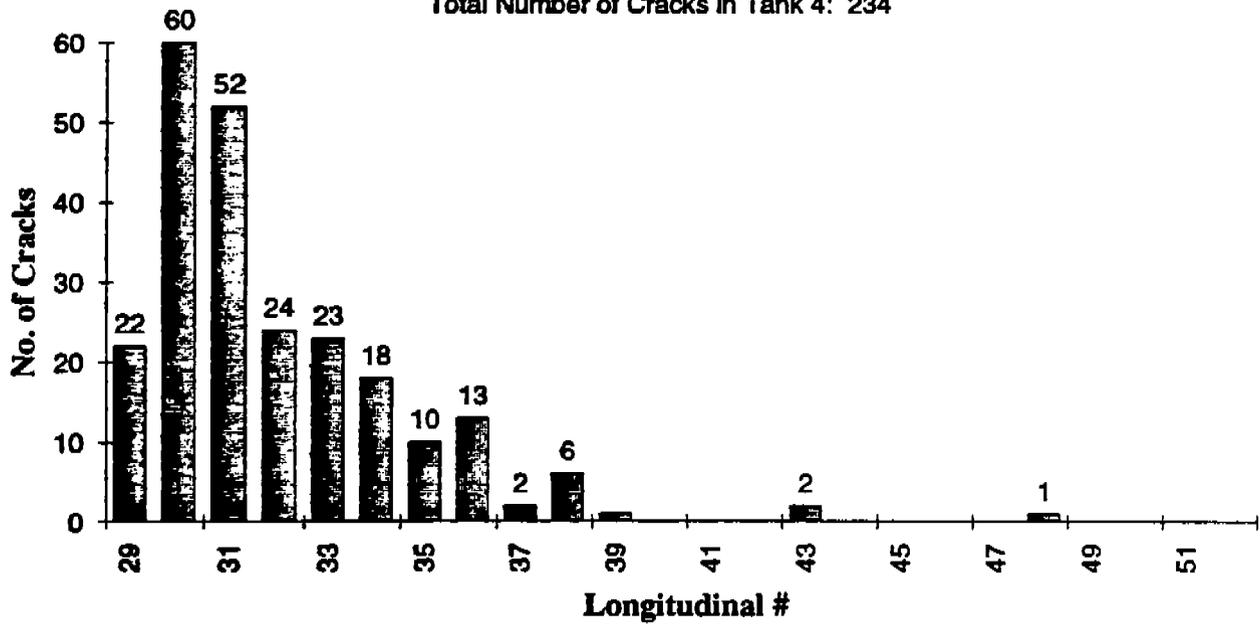
Figure 8: Case I: Side Shell Longitudinal Cracks in Tank 4

44

312
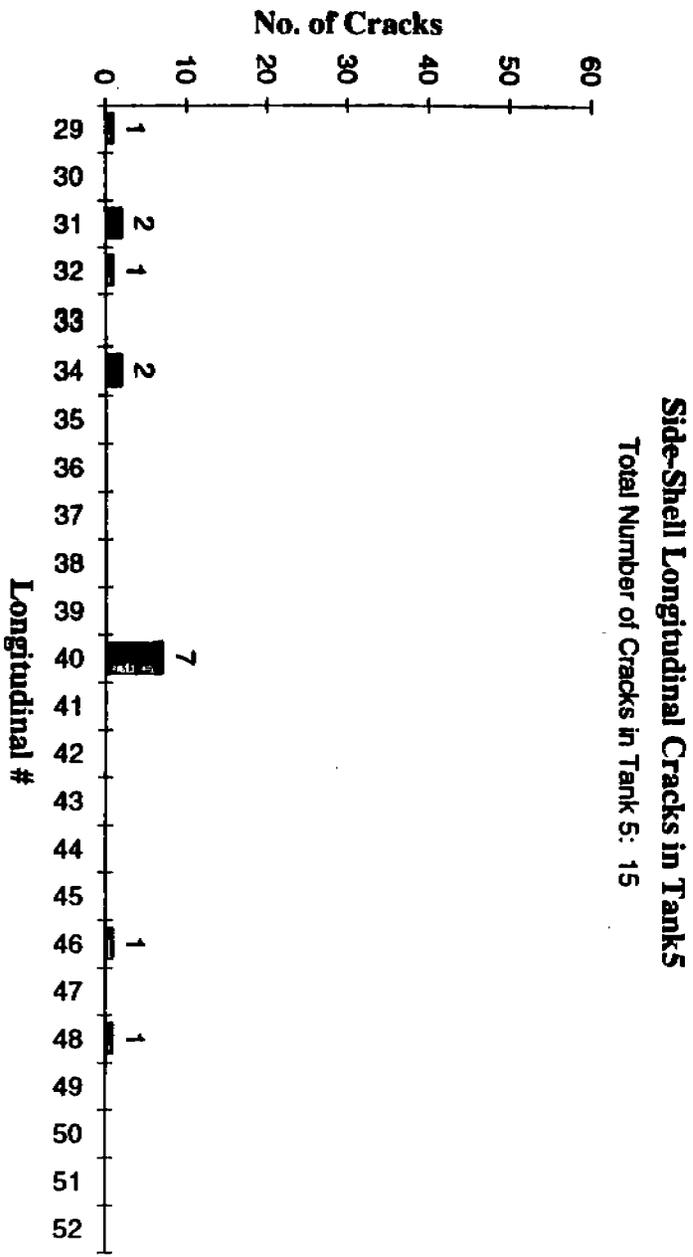
Figure 9: Case I: Side Shell Longitudinal Cracks in Tank 5

45

3/3

Detail Geometry

Detail 6

Figure 10: Case I: Construction Drawing for *Detail 6*
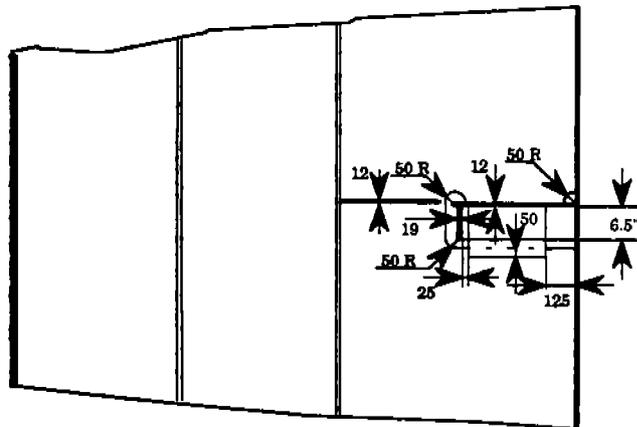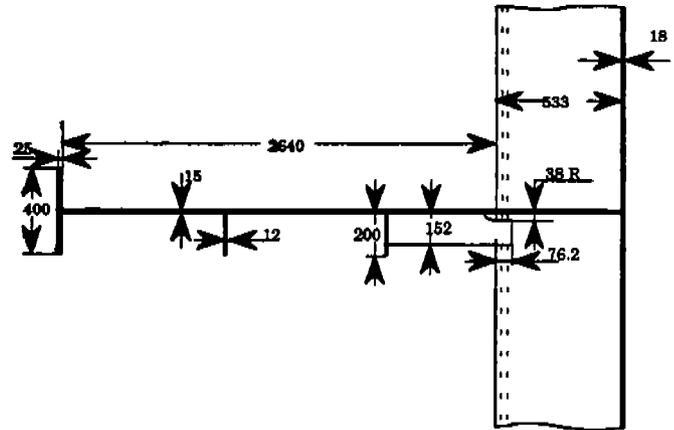
Frame Spacing	5120 mm
Longitudinal Spacing	890 mm

46

314

Detail Geometry
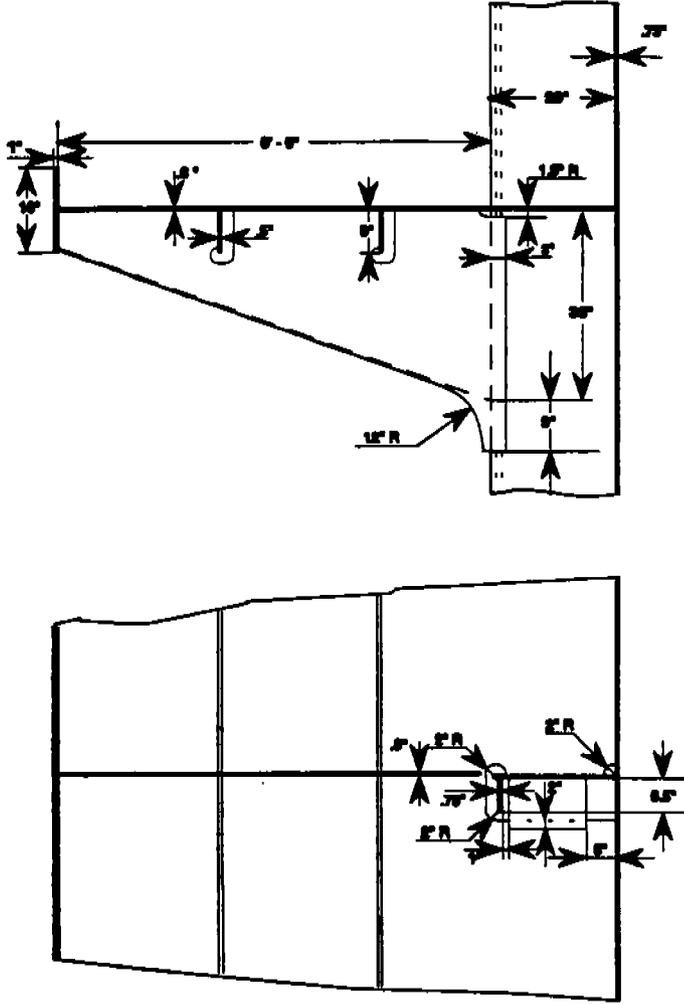
| Frame Spacing | 16.8 ft |
| Longitudinal Spacing | 35 in |

Figure 11: Case I: Construction Drawing for *Detail 4*

315
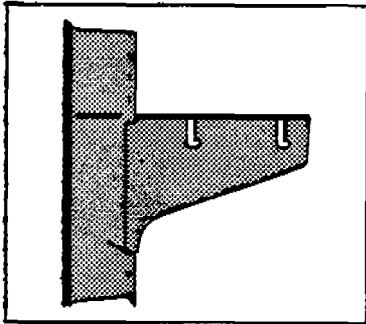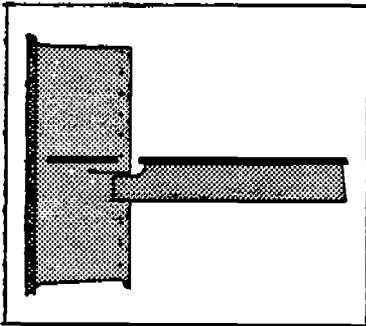
Summary

Detail A

Detail B
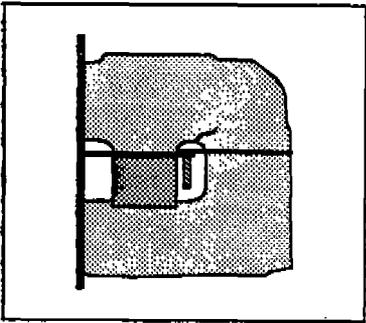
Detail C

Figure 12: Case I: Summary of the three Verification Details

48

316

Detail A

Crack in Longitudinal at the Connection with Bracket
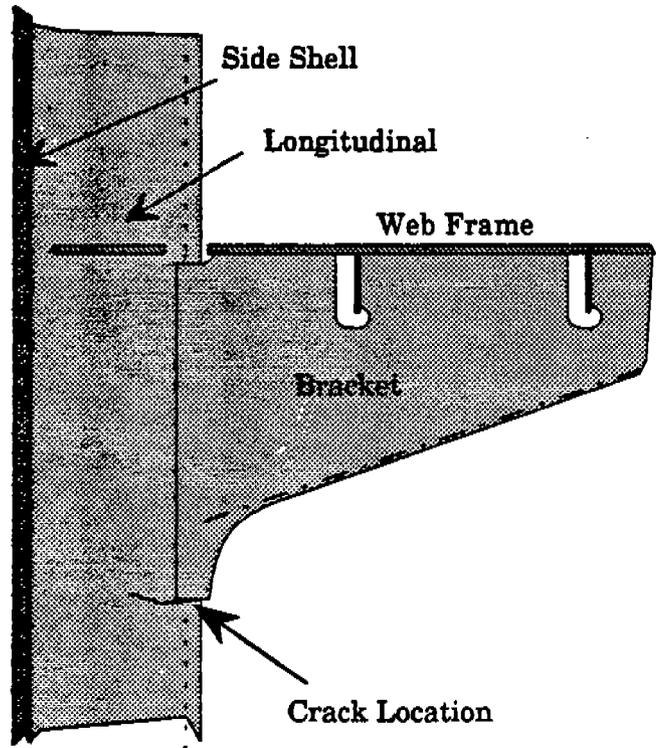
Side Shell

Longitudinal

Web Frame

Bracket

Crack Location

Probability of Failure Calculation

4 Ships of 165 DWT Class

Tank 4 (Port and Starboard)

6 Frames

Longitudinals 34, 36

9 Cracks found
over 15 year period

Number of Details
4 x 2 x 2 x 5 = 80

Pf (15 years) = 0.11250

Pf (annual) = 0.00750

Figure 13: Case I: Summary of Detail A

317

Detail B

Crack in Longitudinal at the Connection with Flatbar Stiffener
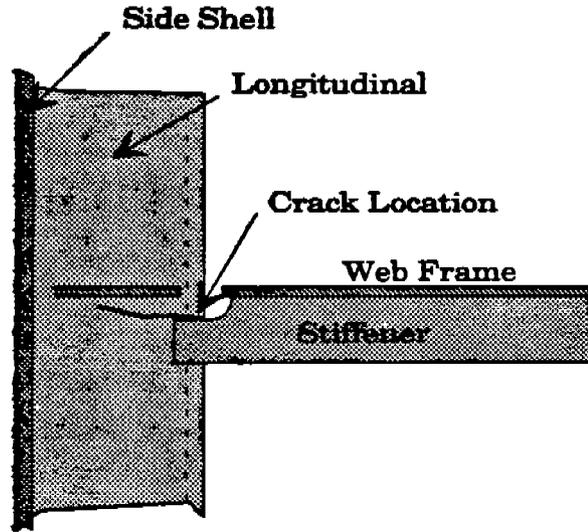
Side Shell

Longitudinal

Crack Location

Web Frame

Stiffener

Probability of Failure Calculation

4 Ships of 165 DWT Class

Tank 4 (Port and Starboard)

5 Frames

Longitudinals 32, 33, 35

16 Cracks found
over 15 year period

Number of Details

4 x 2 x 3 x 5 = 120

Pf (15 years) = 0.1333

Pf (annual) = 0.00889

Figure 14: Case I: Summary of Detail B

50

318

Detail C   Crack in Cutout of Webframe
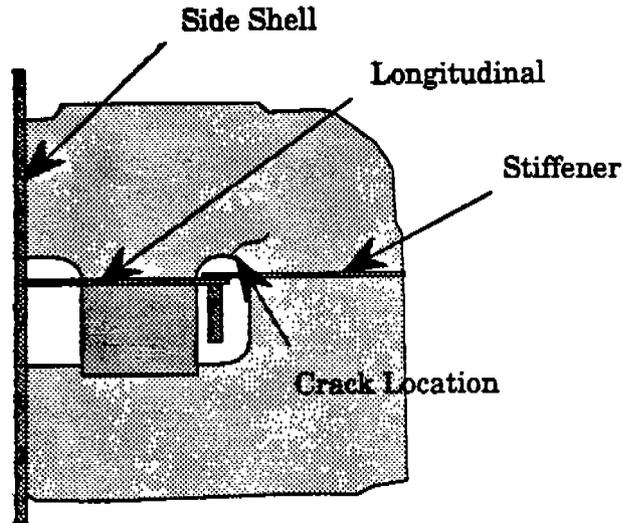
Figure showing Side Shell, Longitudinal, Stiffener, and Crack Location

Probability of Failure Calculation

4 Ships of 165 DWT Class

Tank 4 (Port and Starboard)

5 Frames

Longitudinals 32 - 36

2 Cracks found
over 15 year period

Number of Details
$4 \times 2 \times 5 \times 5 = 200$

Pf (15 years) = 0.010

Pf (annual) = 6.7 x 10^-4

Figure 15: Case I: Summary of Detail C

Case I: Detail A

Weibull Parameters from Loading Program:		
Shape Parameter	Scale Parameter	Zero Crossing Rate
3.2969	0.7538	0.12041

Probability of Failure vs. Bias

Verification Case I: Detail A

Probability of Failure vs. CoV of Bias

Verification Case I: Detail C
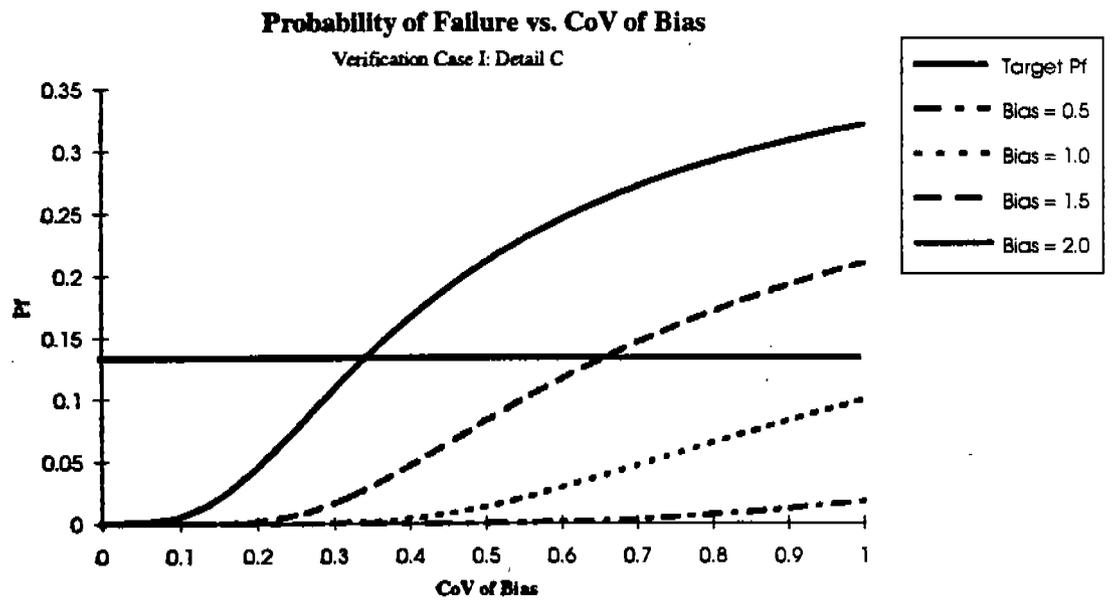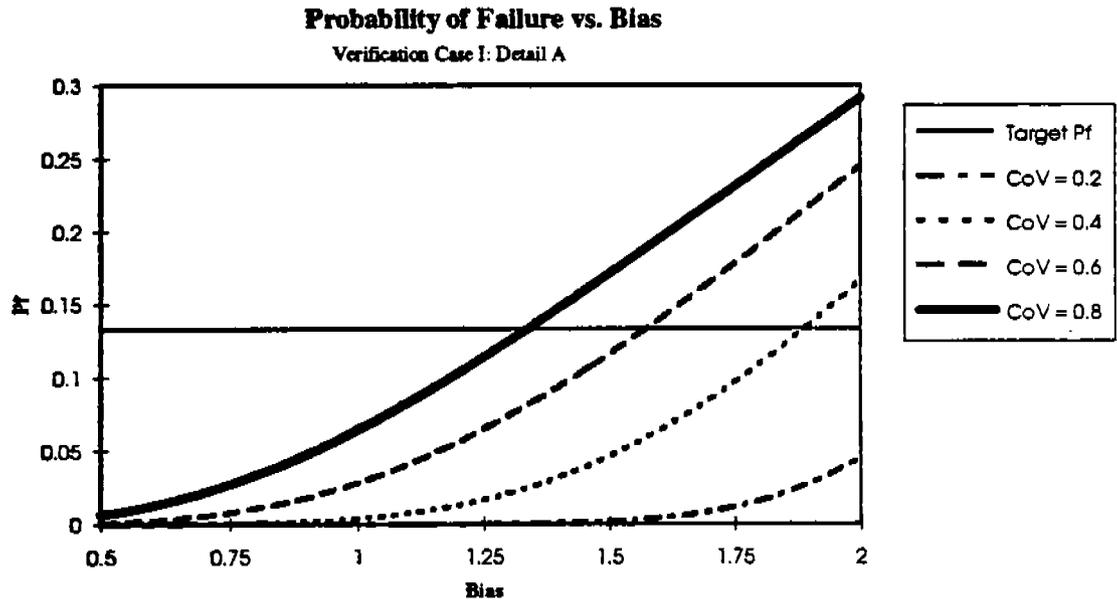
Figure 16: Case I: Results for Detail A

52

320

Case I: Detail B

Weibull Parameters from Loading Program:		
Shape Parameter	Scale Parameter	Zero Crossing Rate
3.5716	0.7538	0.12041

Probability of Failure vs. Bias
Verification Case I: Detail B

Probability of Failure vs. CoV of Bias
Verification Case I: Detail B
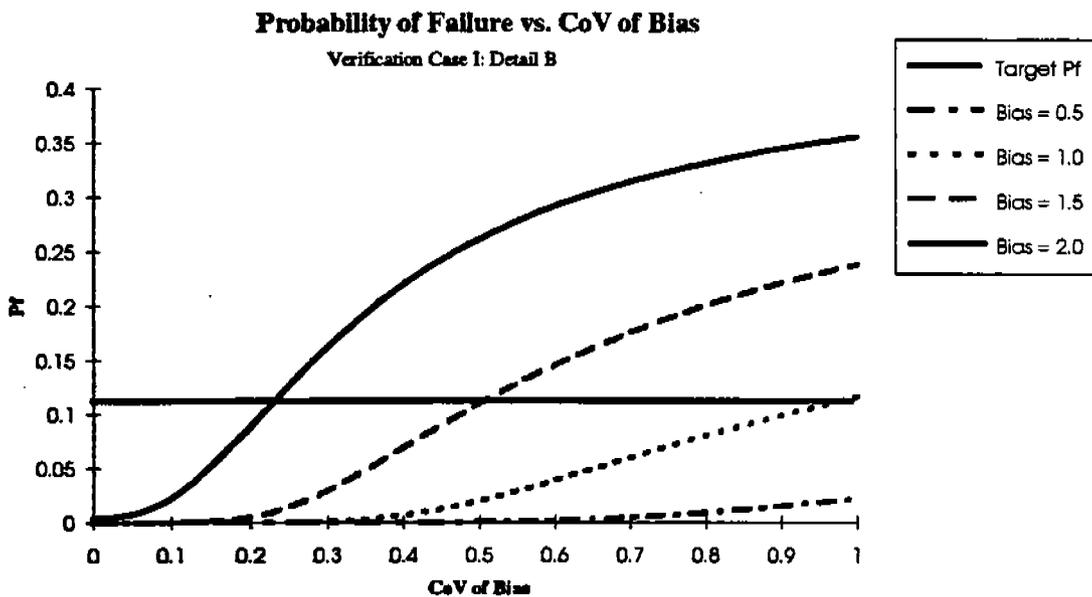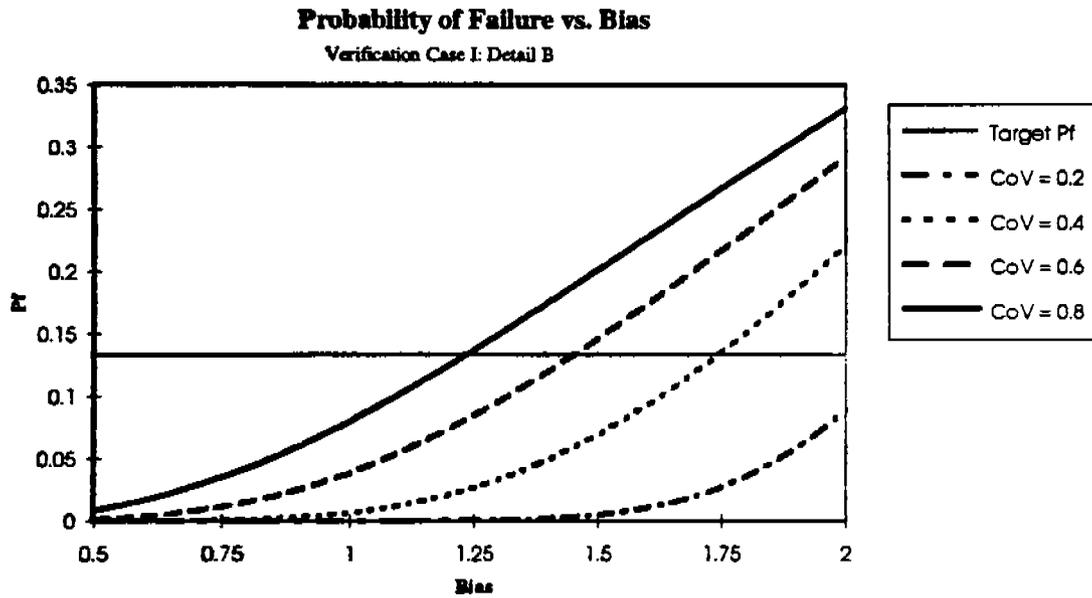
Figure 17: Case I: Results for Detail B

321

Case I: Detail C

Weibull Parameters from Loading Program:		
Shape Parameter	Scale Parameter	Zero Crossing Rate
0.6896	0.7538	0.12038

Probability of Failure vs. Bias

Verification Case I: Detail C

Probability of Failure vs. CoV of Bias

Verification Case I: Detail C
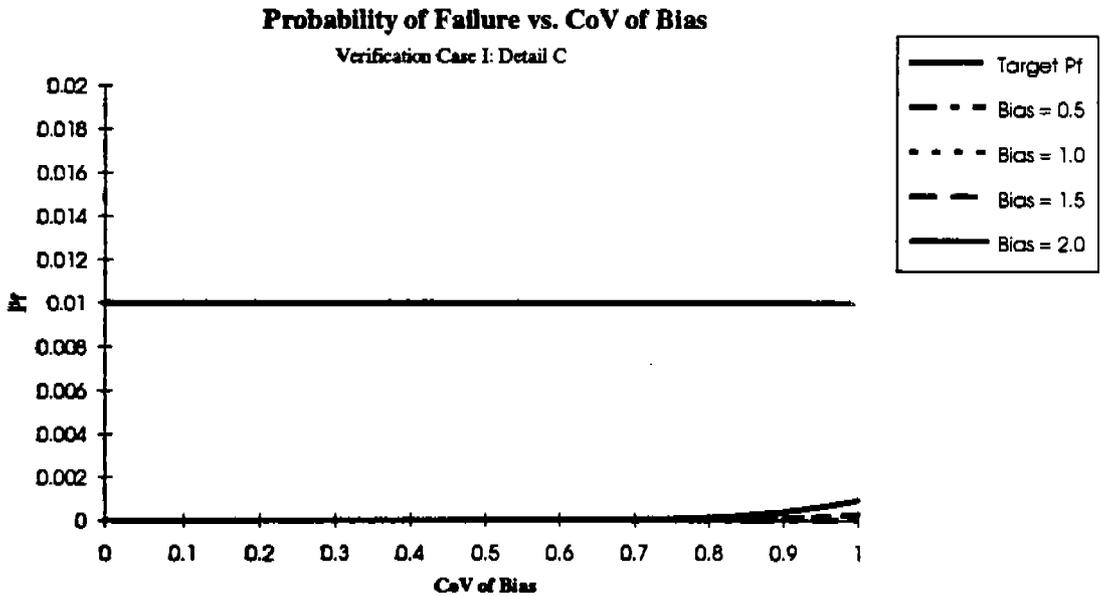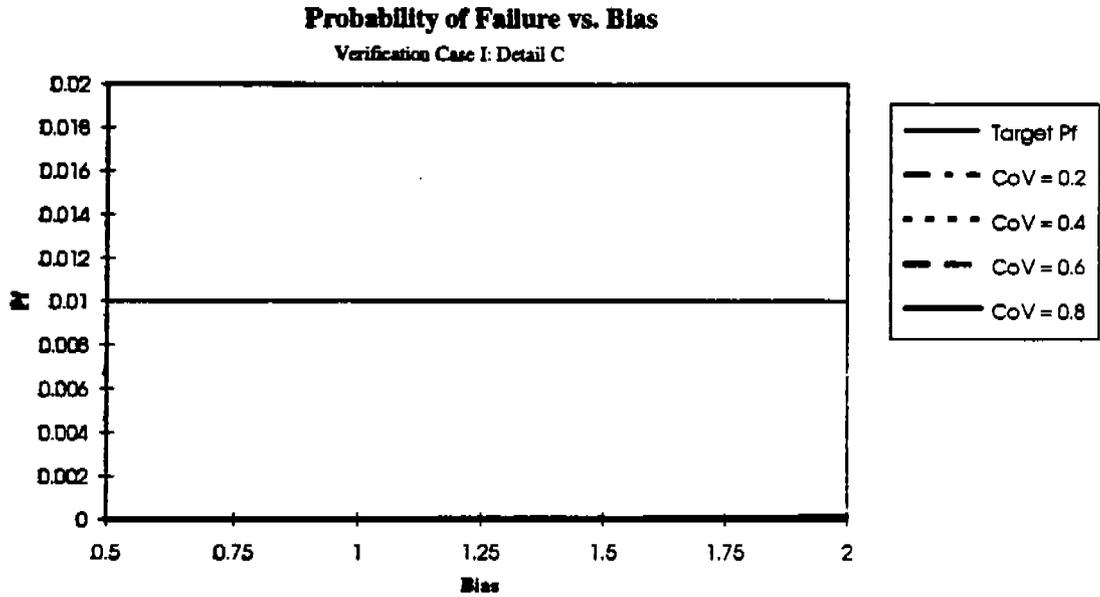
Figure 18: Case I: Results for Detail C

322

General Arrangement

Profile

Upper Deck
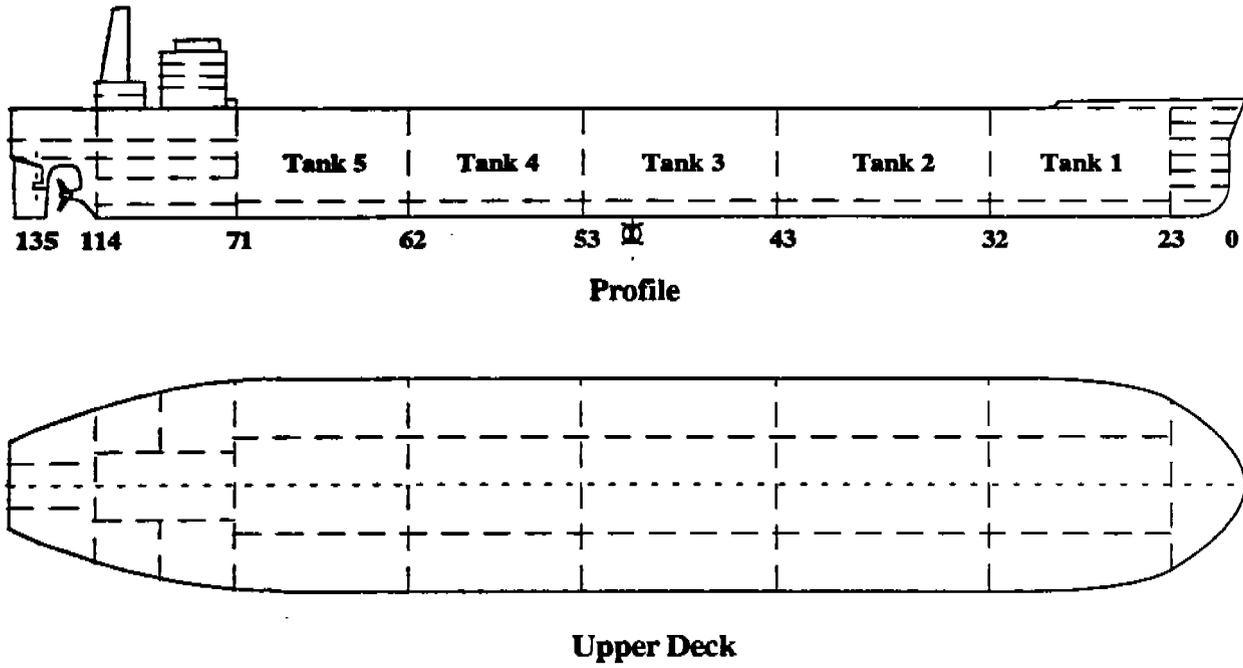
Figure 19: Case II: General Arrangement

323 3

Midship Section
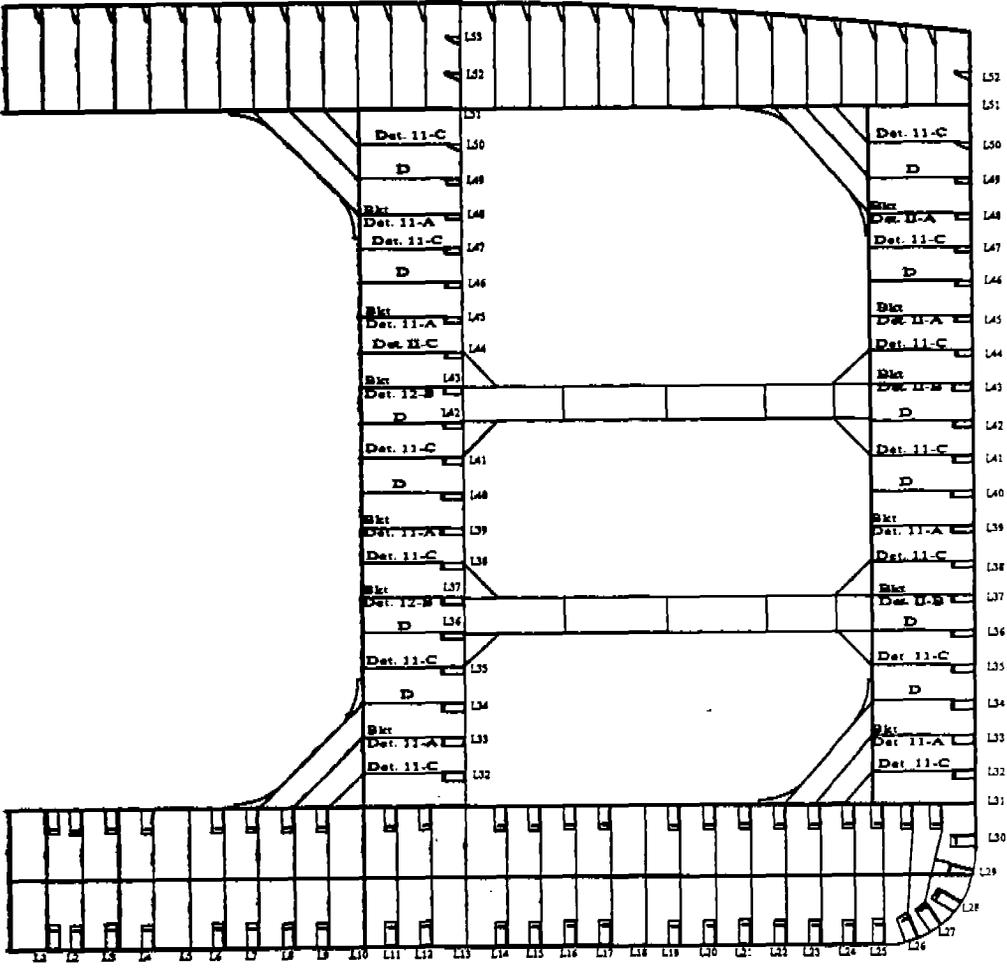
Shell and Longl. Bhd Longitudinals

Shell Longls	Bhd. Longls	Size	Spacing 36"
50, 51, 52	50, 51, 52, 53	12" x 45.9 FB	
47, 48, 49	47, 48, 49	14" x 4" x.5".75"	
46	45, 46	15" x 5" x.5"/.75"	
43, 44, 45	43, 44	16" x 5" x.5"/.75"	
40, 41, 42	39, 40, 41, 42	18" x 6" x.5"/.75"	
36, 37, 38, 39	35, 36, 37, 38	21" x 6" x.5"/.75"	
32, 33, 34, 35	32, 33, 34	21" x 8" x.5"/.75"	

Figure 20: Case II: Midship Section

56

324

Cracks in Sideshell/Webframe Area
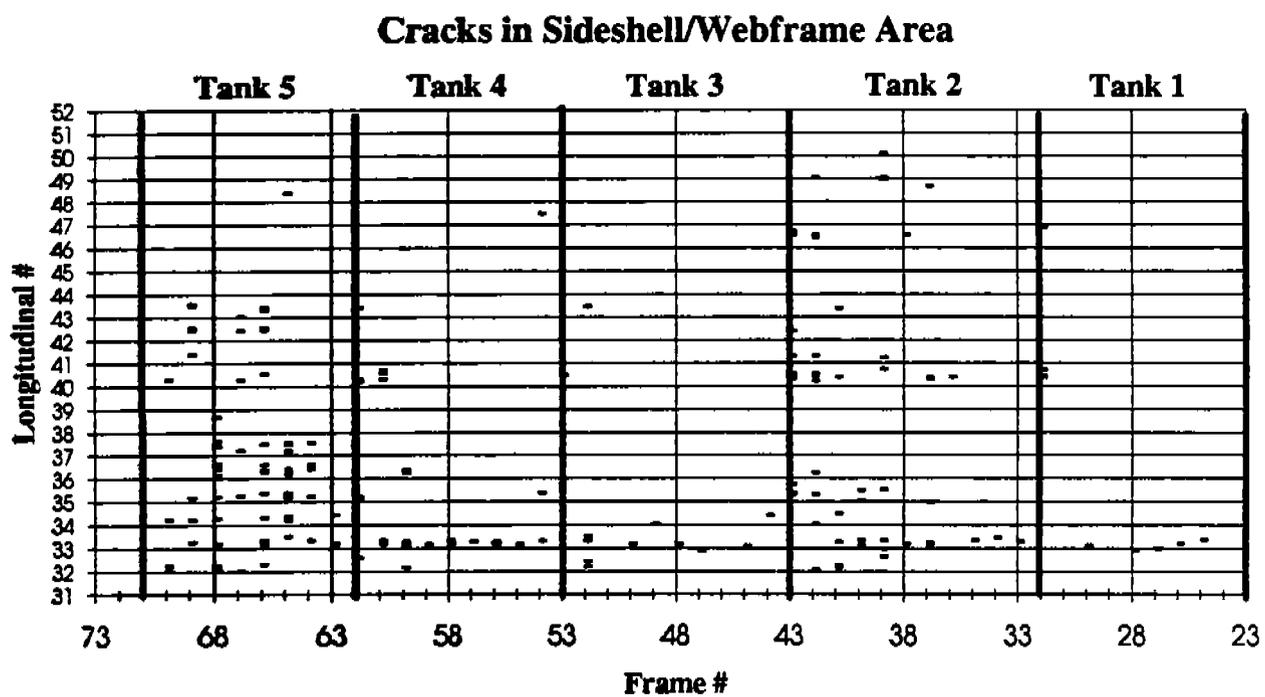
Figure 21: Case II: Crack Distribution (L / H)

325

Crack Distribution Height / Width
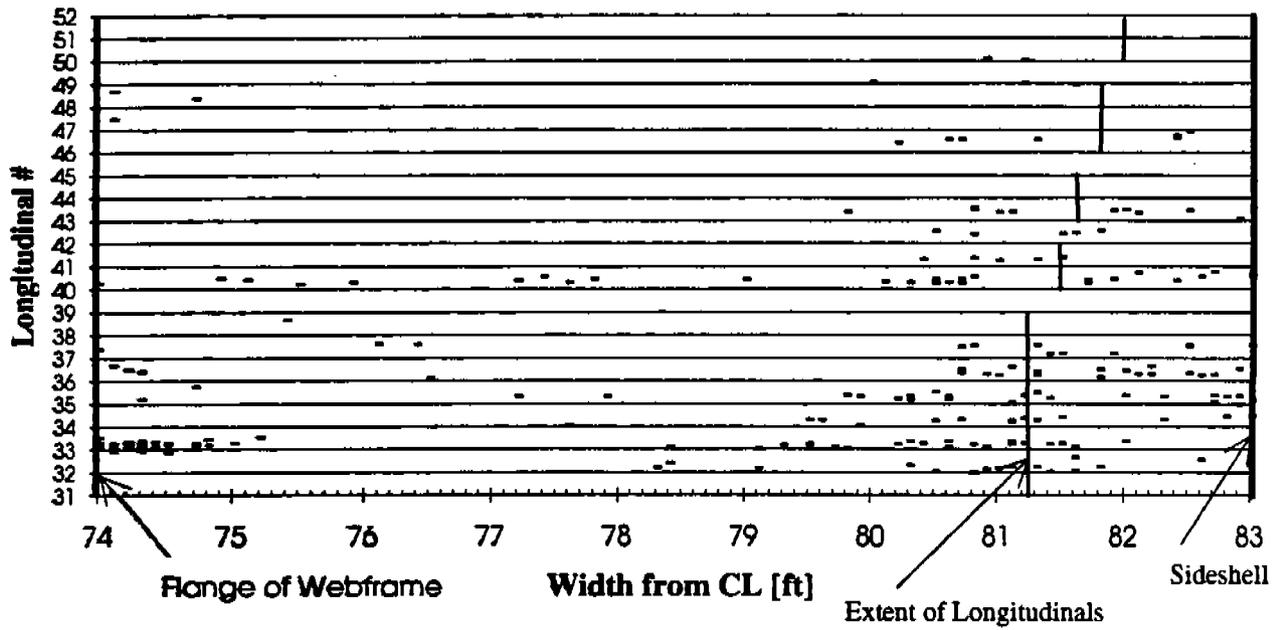
Figure 22: Case II:Crack Distribution (W / H)

326

Cracks in Sideshell/Webframe Area
(for width > 81ft)
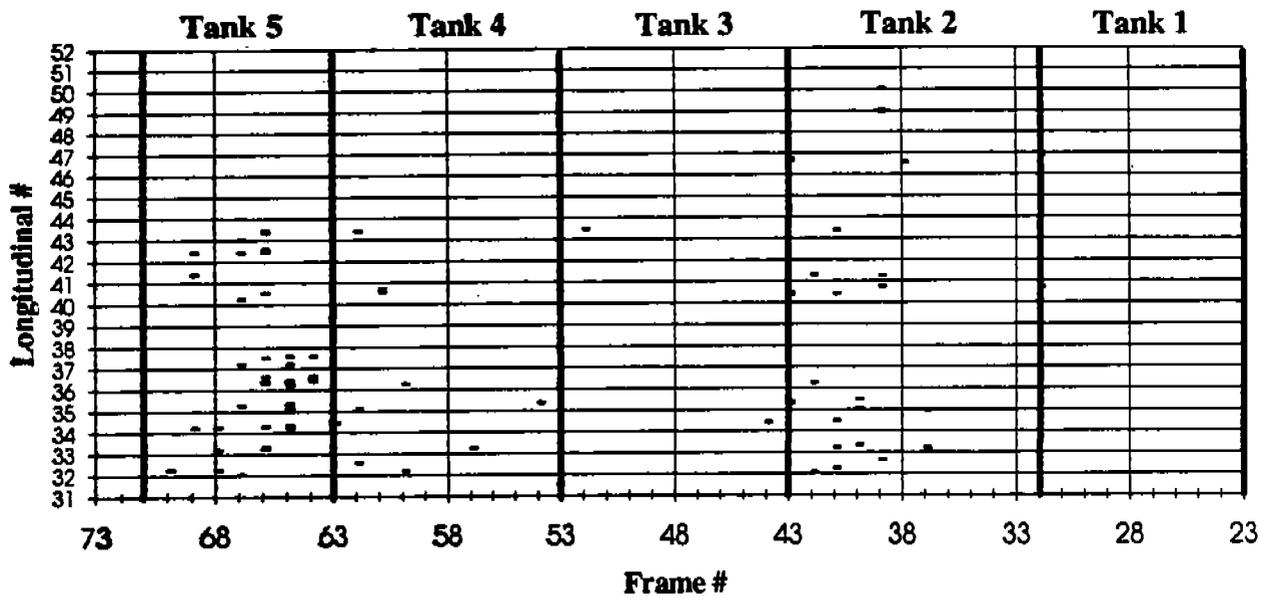
Figure 23: Case II: Crack Distribution (L / H): W > 81 ft only

327

Tanks 3, 4: Crack Distribution Height / Width
(for width > 81ft)
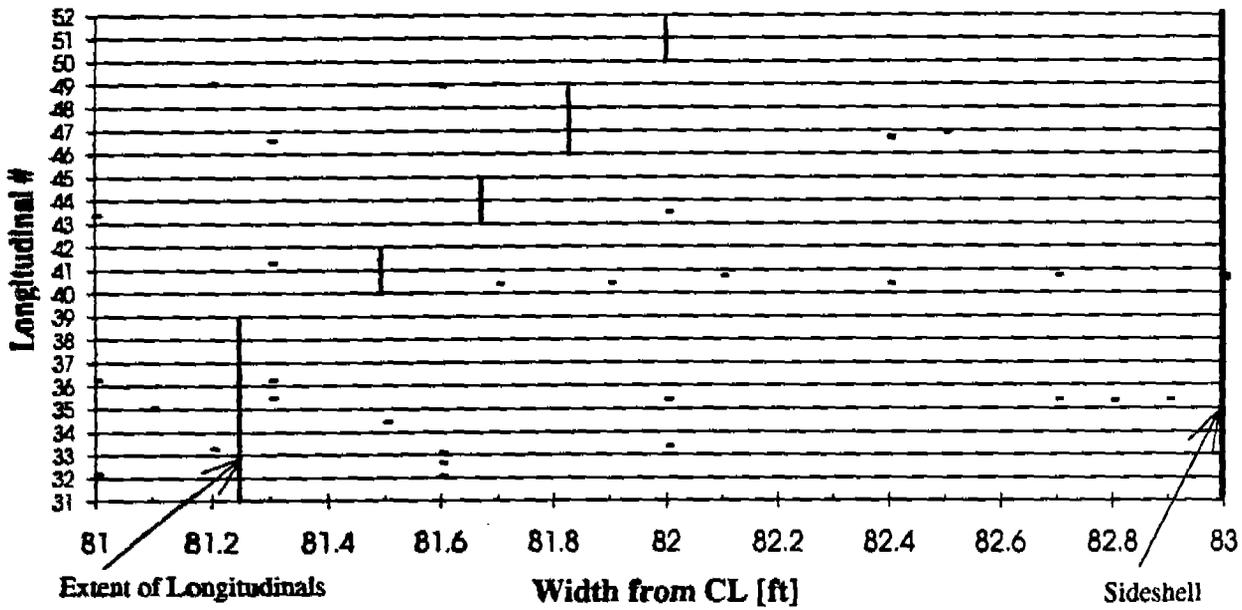
Figure 24: Case II: Crack Distribution in Tanks 3 and 4 (H / W)

60

328

Frame Spacing	15 ft
Longitudinal Spacing	36 in
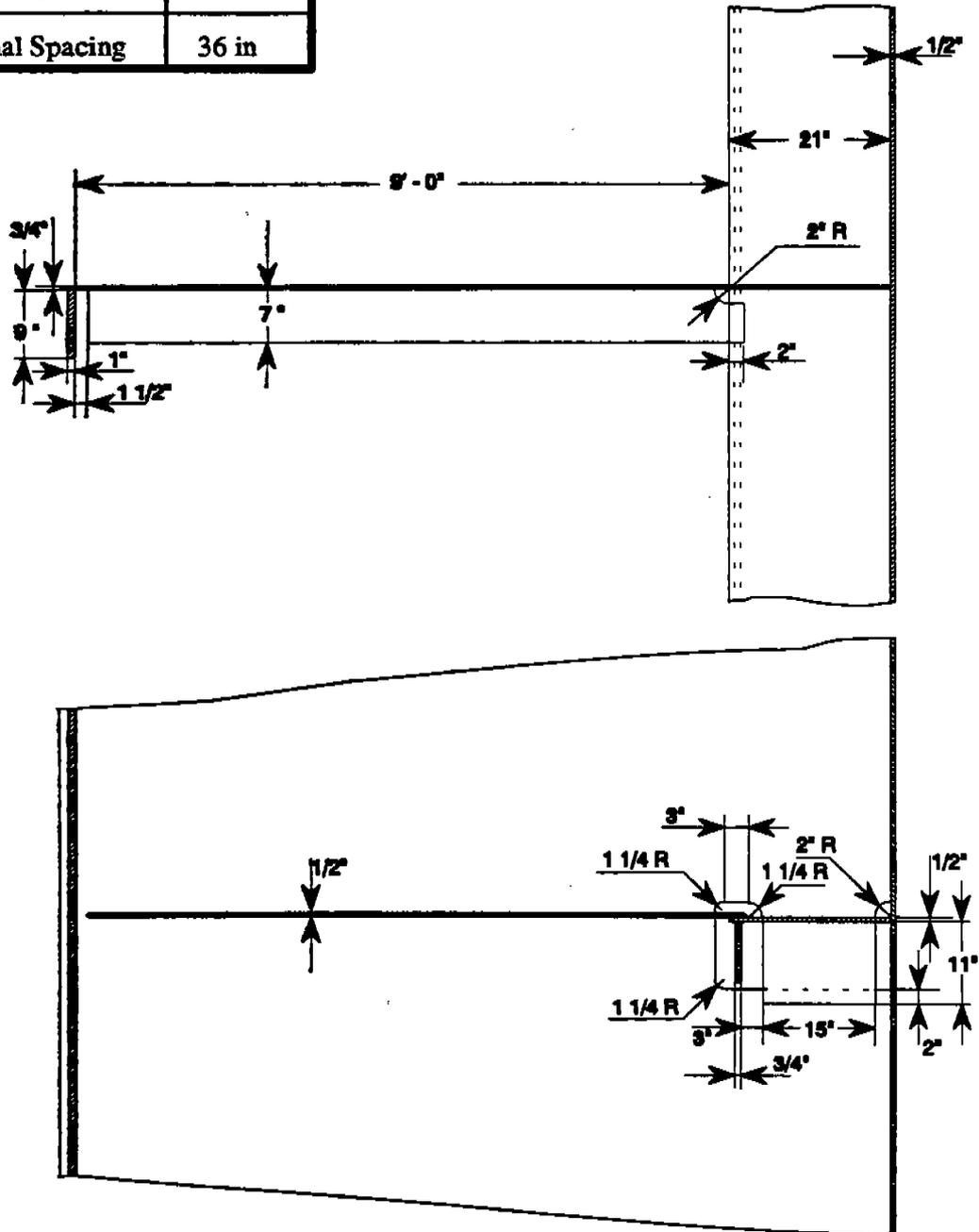
Figure 25: Case II: Construction Drawing for *Detail 11-C*

329

Tanks 3, 4: Crack Distribution Height / Width
(Coordinates of cracks for verification)
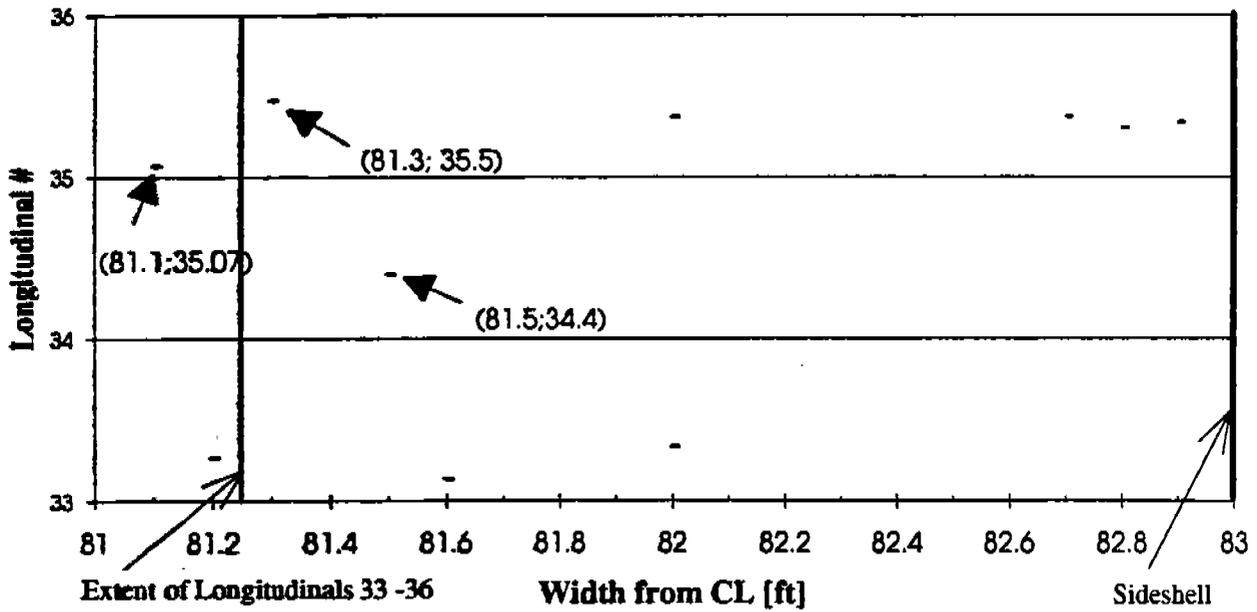
Figure 26: Case II: Coordinates for Cracks considered for Verification

62

330
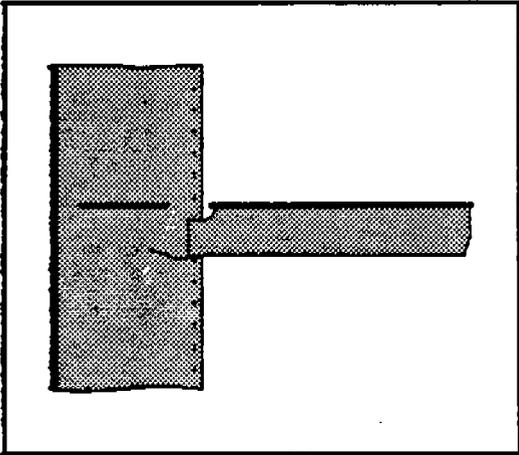
Summary

Detail A

Figure 27: Case II: Summary of the Verification Detail

331

Detail A

Crack in Longitudinal at the Connection with Flatbar Stiffener
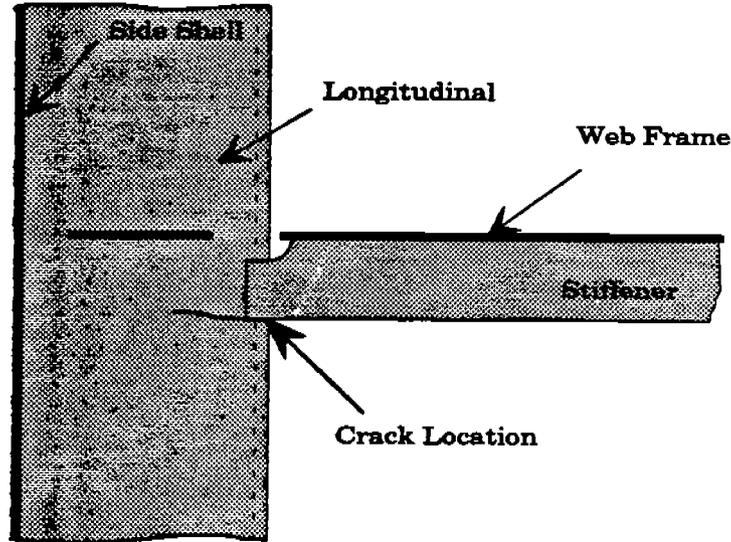
Probability of Failure Calculation

2 Ships of 190 DWT Class

Tanks 3 & 4 (Port and Starboard)

7 Frames

Longitudinals 34 - 35

1 Crack found
over 13 year period

Number of Details

2 x 4 x 7 x 2 = 112

Pf (13 years) = 0.00893

Pf (annual) = 6.9 x 10^-4

Figure 28: Case II: Summary of **Detail A**

64

332

Weibull Parameters from Loading Program:		
Shape Parameter	Scale Parameter	Zero Crossing Rate
3.0316	0.67555	0.12

Probability of Failure vs. Bias
Verification Case II

Legend: Target Pf, CoV = 0.2, CoV = 0.4, CoV = 0.6, CoV = 0.8

Probability of Failure vs. CoV of Bias
Verification Case II

Legend: Target Pf, Bias = 0.5, Bias = 1.0, Bias = 1.5, Bias = 2.0
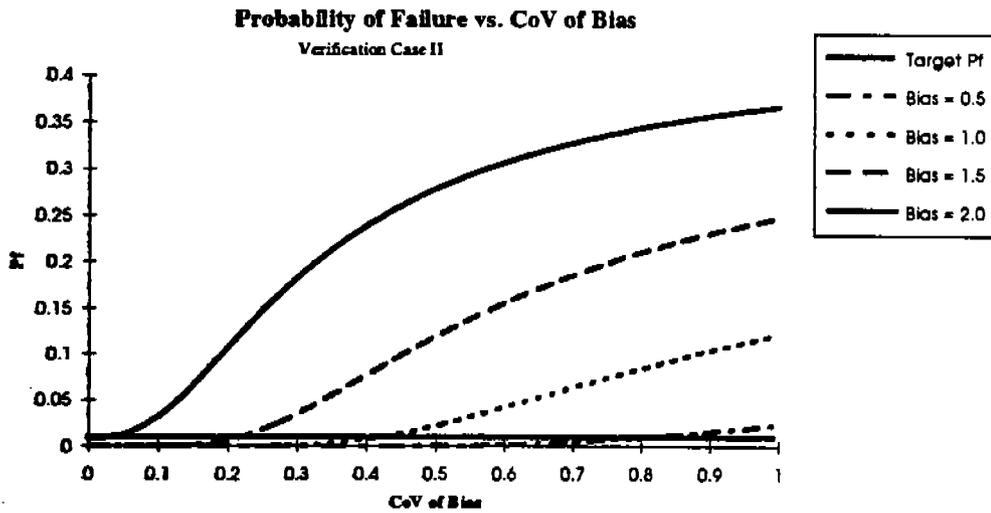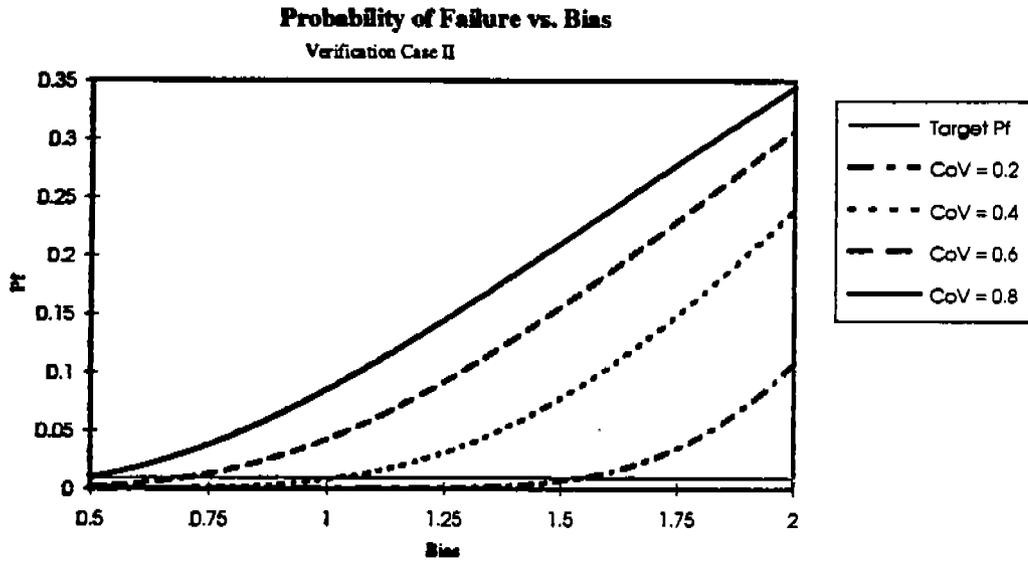
Figure 29: Case II: Results of Detail A